Analysis and evaluation of human thermal comfort conditions for Chinese cities, based on updated Köppen-Geiger classification

Thesis submitted in partial fulfilment of the requirements of the degree Doctor rer. nat. of the Faculty of Environment and Natural Resources, Albert-Ludwigs-Universität Freiburg im Breisgau, Germany

by

Shiqi Yang

Freiburg im Breisgau, Germany
September 2016

Back:
Dean: Prof. Dr. Tim Freytag
First Supervisor: Prof. Dr. Andreas Matzarakis
Second supervisor: Prof. Dr. Rüdiger Glaser
Date of thesis' defence: 30th January 2017

Preface ..... **iv**

Zusammenfassung ..... **v**

Summary ..... **x**

1 Introduction **1**

2 Problem statement **11**

2.1 Efficient information on meso scale 11

2.2 Implementation on macro scale 12

2.3 Application for design on micro scale in different climate types 14

3 State of the art **17**

3.1 Impact factors of human thermal comfort (HTC) 17

3.1.1 Meteorological factors 17

3.1.2 Individual conditions of human beings 21

3.2 Thermal comfort indices 22

3.2.1 Physiologically equivalent temperature (PET) 22

3.2.2 Other applied indices 25

3.3 Correlation between HTC and urban development 27

3.3.1 Urban planning and urban design 28

3.3.2 Tourism 29

3.3.3 Human health 30

3.3.4 Energy consumption 31

3.4 Meteorological analysis on macro scale 32

3.4.1 Köppen-Geiger climate classification updated (KGC) 32

3.4.2 Other popular climate classifications 35

3.5 Meteorological analysis on meso scale 39

3.6 Meteorological analysis on local scale 41

3.7 Meteorological analysis on micro scale 42

3.7.1 Computer simulations in urban areas 42

3.7.2 Analysis through measurements in urban areas 44

3.8 The residential district with high-rise buildings 45

3.9 Community environment design in residential district 46

4 Study areas **50**

5 Data and Methods 54
5.1 Preliminary analysis of HTC on meso scale 54
5.1.1 Selection of study cities 54
5.1.2 Calculation of PET 55
5.1.3 Detection of the daily warmest time 56
5.1.4 Analysis of the HTC conditions 57
5.1.5 Analysis of related meteorological parameters 58
5.2 Implementation of HTC in KGC on macro scale 59
5.2.1 Analysis of parameters in KGC 59
5.2.2 Obtainment of data 59
5.2.3 Linking HTC information with each KGC type 60
5.2.4 Categorisation of data 60
5.2.5 Visualisation of HTC conditions 61
5.3 Application of HTC information for design on micro scale 62
5.3.1 The residential district for simulations 62
5.3.2 Preparation of the input setting 64
5.3.3 Analysis of the 1st round simulations without design elements 64
5.3.4 Design elements for the 2nd round simulations 67
5.3.5 Effects of design elements on HTC conditions 69
6 Results 71
6.1 Preliminary analysis of HTC on meso scale 71
6.1.1 Location of each city in KGC 71
6.1.2 HTC conditions at 8 points in time 72
6.1.3 Monthly and annual HTC conditions 73
6.1.4 Related meteorological parameters 81
6.2 Implementation of HTC in KGC on macro scale 93
6.2.1 HTC conditions of each climate type in KGC 93
6.2.2 Comparison of the entire HTC conditions between climate types 95
6.2.3 Comparison between the opposite extreme months 96
6.2.4 Observed similarities in extreme months 96
6.2.5 Differences in KGC type Dwa 97

6.3 HTC information service for design on micro scale 98
6.3.1 Preparation of input for simulations 98
6.3.2 Estimation of parameters in the 1st round simulation 103
6.3.3 Community environment design 104
6.3.4 Design effects on HTC in each city 118
7 Discussion 136
7.1 Preliminary analysis on meso scale 136
7.1.1 Approach of data analysis 136
7.1.2 Application in different topics 144
7.2 Implementation of HTC in KGC 150
7.2.1 Preliminary description of HTC information in KGC 150
7.2.2 Limitation and orientation in further studies 151
7.2.3 Meaning in application 152
7.3 Application for outdoor design 152
7.3.1 Approach of evaluation on micro scale 153
7.3.2 The effects of direct short wave radiation 156
7.3.3 Analysis and evaluation of the 12 scenarios 157
7.3.4 Limitations in current simulations 169
8 Conclusion and Outlook 171
8.1 Conclusion 171
8.2 Outlook 173
Reference 175
Appendices 188
List of Figures 231
List of Tables 235
List of Abbreviations 237
List of Symbols 239

Preface

My deepest appreciation is given to my first supervisor, Prof. Dr. Andreas Matzarakis, for his highly supports in my whole research progress. Without his supervision, patience, encouragement, and confirmations, the creatively academic ideas in this study would be hard to be completed, neither to be considered in future studies. It is also my pleasure to get the support from my second supervisor, Prof. Dr. Rüdiger Glaser. My highly appreciation is given to him for all of his help on my study, and his excellent advises on my future research. I would like to thank Prof. Dr. Helmut Mayer and PD Dr. Dirk Schindler of the Chair of environmental climate, University of Freiburg, for their supports on my doctoral study. Meanwhile, I wish to express my gratitude to Prof. Ph.D. Tzu-Ping Lin. Without his academic guides related to the biometeorological study, or his introduction to Prof. Dr. Andreas Matzarakis, there would be less chance for me to experience this excited research period.

I also sincerely thank all my colleagues for their kindest help during my study. Thanks to Dr. Dominik Fröhlich who taught me the necessary operations of the models and software which are the fundaments of my research. Thanks to Ph.D. Letizia Martinelli, one of my best friends. She has given me the kindest and the most genuine help not only on my study, but also on the adaptation of the life in Germany. Thanks to Dr. Paul Neuman, Dr. Emmanuel Lubango Ndetto, Dr. Christine Ketterer, Dr. Hyunjung Lee, Dr. Spyridon Paparrizos, Dr. Yung-Chang Chen, M.Sc., Ronja Vitt, M.Sc. and Marcel Valerian Gangwisch, B.Sc., for the warmest and the friendliest help which makes me to concentrate on my work.

I am most grateful to my mother, father and relatives for all kinds of support!

This study is supported by the China Scholarship Council (No. 201206990020).

Zusammenfassung

Weil die Bedingungen des thermischen Komforts von Menschen (HTC) ─ ein Aspekt der Human-Biometeorologie ─ zeigen, wie Menschen die thermische Umwelt wahrnehmen, sowie deren Zufriedenheit mit ihrer thermischen Umwelt, wird die Quantifizierung des HTC einer Region, einer Stadt, oder sogar eines urbanen Raums den Fortschritt der Stadtplanung, des Städtebaus und des Stadtmanagements (urban-PDM) unter Einbeziehung der menschlichen Gesundheit, des Tourismus, sowie des Energieverbrauchs unterstützen. Um die HTC Informationen in urban-PDM anzuwenden, wobei die Skala am Anfang jedes Projekt berücksichtigt werden muss. Hierbei kann das Konzept der Skalen in der Meteorologie als die Referenzen gewählt werden. Auf der Grundlage der Konzepte der Makroskala, der Mesoskala und der Mikroskala, hat diese Studie das Augenmerk auf alle drei Skalen gelegt.

Der erste Teil (die vorläufige Analyse) fokussiert sich auf die Mesoskala. Basierend auf den meteorologischen Daten von 12 Chinesischen Städten in 11 Klimaregionen einer aktualisierten Köppen-Geiger Klimaklassifikation (KGC) wurden die HTC Bedingungen auf der Mesoskala hauptsächlich durch die monatlichen Häufigkeiten der Klassen thermischer Indizes analysiert. Gemäß den monatlichen Häufigkeiten von physiologische äquivalenter Temperatur (PET) um 14 Uhr (dem relativ wärmsten Zeitpunkt eines Tag) sind die Bedingungen des Hintergrund HTC bestimmt worden. Hitzestress herrschte an mehr als 75% der Tagen der Monat von März bis Oktober in Sanya (Aw), und von Mai bis September in Qionghai (Am) und Shenzhen (Cwa). In Kunming (Cwb) sind warme Bedingungen an mehr als 50% der Tage im Sommer aufgetreten. Akzeptable Bedingungen herrschten von Oktober bis April an mehr als 60% der Tage. Die akzeptablen Bedingungen sind in Lhasa (Dwc) von April bis Oktober an mehr als 70% der Tage aufgetreten. In Shanghai (Cfa) herrschte Hitzestress an ca. 80% der Tage im Juli und August. Im Gegensatz dazu herrschte Kältestress von November bis März. Kältestress ist mit großer Häufigkeit jeweils von November bis März in Yuncheng (BSk),

Yinchuan (BWk) und Beijing (Dwa) aufgetreten. Hitzestress herrschte an mehr als 70% der Sommertage in Yuncheng (BSk) und Beijing (Dwa), und an etwa 50–70% der Sommertage in Yinchuan (BWk). Hitzestress war in Dalian (Dwa) von Juni bis September nicht häufig; jedoch gab es häufig Kältestress von Oktober bis April. Es gab in Sommer regelmäßig Hitzestress in Hohhot (Dwb) und häufigen Kältestress von November bis Februar. In Urumqi (Dfb) gab es Hitzestress an rund um 30–40% der Tage im Sommer. Im Gegensatz dazu herrschte Kältestress an fast 100% der Tage im Winter, und von Oktober bis April.

Die Analyse auf der Mesoskala hat die human-biometeorologischen Hintergrundbedingungen beschrieben. Sie kann als Information über deren zeitliche Dimension verstanden werden. Die human-biometeorologischen Langzeitinformationen basierend auf den Analysen in der vorliegenden Studie können in der Stadtplanung, Städtebau und Stadtverwaltung (urban-PDM) unter Einbeziehung der menschlichen Gesundheit, des Tourismus und des Energieverbrauchs angewendet worden. Daher wurde der erste Teil als die Verbesserung des Verfahrens zur human-biometeorologischen Datenanalyse insbesondere für die 12 Chinesischen Städte in dieser Studie betrachtet. Zum Beispiel hat die Angabe der Periode mit Hitzestress gesundheitliche Warnhinweise in jeder Stadt ermöglicht, insbesondere im Sommer. Die komfortablen Bedingungen haben die potenziellen Möglichkeit für den Tourismus in bestimmten Monaten für jede Stadt gezeigt. Die Periode mit Kältestress kann den Energieverbrauch im Winter in nördlichen Städten voraussagen. Zudem ist die Analyse auf der Mesoskala die Grundlage der Downscaling Studien, z.B. der mikroklimatischen Simulationen. Als eine Art der Grundinformation zu einer Stadt wird die Analyse der HTC Bedingungen auf der Mesoskala in dieser Studie dringend empfohlen um bei der Entwicklung der urban-PDM berücksichtigt zu werden. In diesem Teil wurden die HTC Bedingungen in 12 chinesischen Städten in 11 Klimaregionen durch einen Ansatz mit, im Vergleich zu traditionellen meteorologischen Information (z. B. den einzelnen Mittelwerten),

stärkerer Aussagekräftigkeit analysiert. Der Ansatz der monatlichen Häufigkeiten in diesem Teil ist die Grundlage des zweiten und des dritten Teils.

Der zweite Teil (Implementierung der HTC Information in KGC) konzentrierte sich auf die Makroskala. Wegen des Mangels an HTC Information in den Klassen der globalen Klimaklassifizierung hat diese Studie einen Ansatz entwickelt, wie man die HTC-Information zusammen mit der Luftfeuchtigkeit (AH) in Klassen zur Unterscheidung der HTC Bedingungen auf Makroskala beschreiben kann. Der neue Ansatz der HTC Informationen in einer globalen Klimaklassifizierung basiert auf 6 Arten von Häufigkeiten vereinfachter Klassen von PET und Wasserdampfdruck (*VP*), die für jede Klimaregion berechet werden. Die 6 Arten von Häufigkeiten waren die jährliche Häufigkeit von PET-Klassen, die Häufigkeit von PET-Klassen im heißesten Monat, die Häufigkeit von PET-Klassen im kältesten Monat, die jährliche Häufigkeit von *VP*-Klassen, die Häufigkeit von *VP*-Klassen im feuchtesten Monat, und die Häufigkeit von *VP*-Klassen im trockensten Monat.

Dieser Teil der vorliegenden Studie ist der erste Versuch HTC Information in Klassen einer globalen Klimaklassifizierung zu implementieren. Auf der Grundlage der zukünftigen globalen HTC Informationen könnten besser geeignete Baustile ausgewählt, Energieverbrauch (Heizen/Kühlen) präziser prognostiziert, mögliche Krankheitsperioden vorhergesagt und die am besten geeignete touristische Saison in jeder Klimaregion abgeschätzt werden.

Der dritte Teil der vorliegenden Arbeit (Anwendung im Outdoor-Design) konzentrierte sich auf die Mikroskala. In diesem Teil wurde ein Wohnviertel mit Hochhäusern als Examplarischer Ortsteil für die Analyse und die Bewertung von HTC Bedingungen auf der Mikroskala ausgewählt. Innerhalb des Wohnviertels ist die Analyse der HTC Bedingungen und die Bewertung der Auswirkungen des Outdoor-Designs des Wohnviertels (eine Gruppe) unter 12 Sätzen meteorologischer Parameter durchgeführt worden. Entsprechend der Verteilung der simulierten HTC Bedingungen in einem

Wohnviertel in jeder Gruppe ist das Outdoor-Design des Wohnviertels durch Hinzufügen der Design-Elemente (Bäume, Hecken, Gras und Wasserkörper) an bestimmten Positionen individuell angepasst worden. Nach einer zweiten Simulationsrund, wurde die mildernde Wirkung der Design-Elemente (oder des Design-Schemas) durch den Vergleich zwischen den zwei mikroklimatischen Simulationen in jeder Gruppe bewertet.

Die erste Runde der Simulationen zeigten, dass relativ geringe Windgeschwindigkeiten (v) viel häufiger auf der Leeseite als auf der Luvseite aufgetreten sind. Der Vergleich der Verteilung von PET und der Distribution von v zeigte, dass die meisten Zonen mit Hitzestress in der Sonne sowie auf der Leeseite der Gebäudelagen. Aus dem Vergleich zwischen den zwei Simulationen könnten die geringeren PET-Werte in der zweiten Simulationensrunde in den Gitternzellen beobachtet werden, in denen Bäumen, Hecken und Gewässern hinzugefügt worden sind. Im Gegensatz dazu könnten Bäumen und Hecken höhere PET-Werte in der zweiten Simulationsrunde verursacht haben. Die Wirkungen von Gras auf PET ließ sich in der aktuellen Studie auf der Grundlage der Klassen nicht nachweisen. Nach Auswertung der HTC Bedingungen der verschiedenen Outdoor-Designs gibt es mehrere Aspekte, die beachtet werden sollten. Wenn die Bäume zum Outdoor-Design hinzugefügt wurden, sollte wegen der kombinierten Wirkung von Beschattung und Himmelssichtsfaktor (SVF) zunächst der Bereich der Auswirkung des Design-Elements berücksichtigt werden. Zweitens sollte die Art der Bäume unter Berücksichtigung der Höhe des Baumstamms und der Breite des Kronendachs betrachtet werden, um den optimalen thermischen Effekt in dem Outdoor-Design zu erreichen. Darüber hinaus sollte besser identifiziert werden, welche Zonen im Design-Viertel den optimalen Luftstrom ermöglichen, da durch die dichten Bäume und Hecken Windabschattung verursacht werden kann.

Im Hinblick auf die Funktion des Outdoor-Designs der Minderung von thermischem Stress auf Ebene der Mikroskala wurden auf Basis der Analyse der numerischen Simulationen Empfehlung gegeben, wie die digitalen Mikroklimasimulationen

bestmöglich zu nutzen sind. Basierend auf den 24 Szenarien (jeweils ein nicht modifizierts und ein angepassts Design für alle 12 Klimaregionen) könnte die Analyse und Bewertung der HTC Bedingungen vor und nach der Anpassung eines Outdoor-Designs als eine Ansatz betrachtet werden, die HTC Information in der Designpraxis anwenden zu können.

Durch die vorliegende Studie wurden nicht nur die HTC Bedingungen in 12 Chinesischen Städten analysiert und bewertet, sondern auch ein Ansatz zur Anwendung von HTC Information auf verschiedenen Skalen beschrieben. Alle drei Teile dieser Studie zusammen können als Ansatz der Anwendung der human-biometeorologischen Information sowie als eine neue Art der Auswertung der meteorologischen Informationen auf verschiedenen Skalen betrachtet werden. Die Berücksichtigung der HTC Information auf der Makroskala bei der Klassifizierung der weltweiten Regionen und der Definition von deren HTC Bedingungen können die thermischen Anforderungen an Menschen auf globaler Skala veranschaulichen. Die Ergebnisse der Langzeit-Datenanalyse auf der Mesoskala sind grundlegende Informationen, die das Verständnis in urban-PDM und verwandten Disziplinen erleichtern werden. Auf der Mikroskala kann die Anwendung der numerischen Simulation der HTC Bedingungen als einen notwendiger Ansatz betrachtet werden, um das Outdoor-Design in der Zukunft zu verbessern. Schließlich wurde in der vorliegenden Studie der systematische Ablauf der Analyse und der Bewertung der human-biometeorologischen Informationen auf mehreren Skalen beschrieben, was es den verschiedenen Disziplinen erleichtern kann, komfortable thermische Bedingungen zu schaffen.

Summary

As the human thermal comfort (HTC) conditions, one issue in human-biometeorology, reveal how human beings perceive the thermal environment, as well as the satisfaction of the thermal environment, the quantification of HTC information for a region, a city, or even an urban space, will assist the progress of urban planning, urban design and urban management (urban-PDM) which involve the concerns on human health, tourism, as well as energy consumption. In order to apply the HTC information into urban-PDM which consider the scale for each project at the beginning, the concepts of the scales in meteorology can be selected as the reference. Based on the concepts of the macro scale, the meso scale, and the micro scale, this study has paid attention for all three levels.

The Part One (Preliminary analysis) focused on the meso scale. Based on the meteorological data of 12 Chinese cities in 11 climate types from an updated Köppen-Geiger climate classification (KGC), the HTC conditions on meso scale have been analysed mainly through the monthly frequencies of value classes. According to the monthly frequencies of physiologically equivalent temperature (PET) at 14 LST (the relative warmest point in time in one day), the background HTC conditions have been obtained. The heat stress existed with more than 75 % days per month from March to October in Sanya (Aw), and from May to September in Qionghai (Am) and Shenzhen (Cwa), respectively. In Kunming (Cwb), the warm conditions appeared with more than 50 % days per month in summer, and the acceptable conditions lasted since October until April with more than 60 % days per month. The acceptable conditions existed in Lhasa (Dwc) from April to October with more than 70 % days per month. In Shanghai (Cfa), the heat stress appeared with approx. 80 % days in July and August, respectively; in contrast, the cold stress existed since November until March. The cold stress with high frequency lasted from November to March in Yuncheng (BSk), Yinchuan (BWk) and Beijing (Dwa), respectively; however, the heat stress existed with more than 70 % days per month in summer in Yuncheng (BSk) and Beijing (Dwa), and with about 50–70 %

days per month in summer in Yinchuan (BWk). The heat stress, which was not frequent, existed in Dalian (Dwa) from June to September; however, the cold stress appeared frequently since October until April. There were regularly heat stress in Hohhot (Dwb) in summer, and frequent cold stress since November until February. In Urumqi (Dfb), the heat stress appeared with around 30─40 % days per month in summer; in contrast, the cold stress lasted with almost 100 % days per month in winter, and it existed from October to April.

The analysis on meso scale depicted the background conditions of human-biometeorology, and it could be understood as the information on the temporal dimension. Based on the analysis in current study, there are possibilities to apply the temporally human-biometeorological information in urban planning, urban design, and urban management (urban-PDM), which involve the attention on human health, tourism, and energy consumption. Therefore, Part One has been regarded as the improvement of the method on human-biometeorological data analysis, especially for 12 Chinese cities in this study. For instance, the information of the period with heat stress provided the warning information for the issue of human health in each city, especially in summer. The acceptable conditions indicated the potential market of the tourism in certain month for each city. The period with the cold stress preliminarily depicted the requirements of energy consumption in winter in northern cities. Meanwhile, the analysis on meso scale is the fundamental phase of the downscaling study, e.g. microclimatic simulations. As one kind of basic information of a city, the analysis of HTC conditions on meso scale in this study is highly recommended to be considered in the progress of urban-PDM. In this part, the HTC conditions in 12 Chinese cities in 11 climate types have been analysed through an approach with more perspicuous information, compared to the traditionally meteorological information (e.g. the single average values). The approach of the monthly frequencies in this part is the fundament of the Part Two and Part Three.

The Part Two (Implementation of HTC in KGC) concentrated on macro scale. Due to the

lack of the HTC information in the thresholds of world climate classifications, this study has explored an approach on how to describe the HTC information together with air humidity (AH) information in the threshold for distinguishing the HTC conditions on macro scale. The approach of the implementation of HTC information in world climate classification has been obtained, which is achieved through 6 kinds of frequencies of the simplified value classes of PET and vapour pressure (*VP*), respectively, for each climate type. The 6 kinds of frequencies were the annual frequency of PET, the frequency of PET in the hottest month, the frequency of PET in the coldest month, the annual frequency of *VP*, the frequency of *VP* in the wettest month, and the frequency of *VP* in the driest month.

The study in this level is the first attempt on how to implement the HTC information in the threshold of world climate classification. Based on the future global HTC information, more suitable building styles could be selected, more precise energy consumption (heating/cooling) could be budgeted, possible disease periods could be predicted, and the most suitable tourism season could be estimated in each climate type.

The Part Three (Application in outdoor design) was on micro scale. In this part, a residential district with high-rise buildings has been selected as a sample district for the analysis and evaluation of HTC conditions on micro scale. Inside the residential district, the analysis of the HTC conditions before design and the evaluations of effects from community environment design have been performed under 12 groups of meteorological input settings, respectively. According to the distribution of the simulated HTC conditions in the residential district in each group, the community environment design has been provided individually through adding design elements (trees, hedges, grass, and water bodies) in specific positions. Meanwhile, after the 2nd round simulations, the mitigating effects of the design elements (i.e. the design scheme) have been evaluated through the comparison between twice microclimatic simulations in each group.

It could be found in the 1st round simulations that the relative low wind velocity (v) appeared on the lee side much more frequently than that on the wind ward side; comparing

the distribution of PET and the distribution of *v*, most of the areas with heat stress were under the sun, as well as on the lee side of the buildings. From the comparison between twice simulations, it could be found that the lower PET values in the 2nd round simulations could be observed in the same grids, in which trees, hedges and water bodies were added; in contrast, the higher PET values in the 2nd simulations could be caused by the trees and hedges, without water bodies. The effects of grass on the PET has not been detected, based on the value classes in current study. According to the evaluation of HTC conditions in the design, there are several aspects are worthy to be noticed. First of all, when adding trees in the community environment design, the displacement of the efficient mitigation should be taken into account, due to the combined impact from shading and sky view factor (SVF). Secondly, the type of tree with the respect of the height of the trunk and the width of the canopy should be considered, in order to form the ideal thermal environment in the design. Furthermore, it should be better identified which areas in the design district demand the optimal air flow, as the blocking effects were caused by the dense trees and hedges.

Concentrated on the function of the community environment design on the mitigation of HTC conditions on micro scale, the design has been given under the analysis based on the numerical simulation, which has sought a way on how to utilise the digital micro climate simulation. Based on the 12 groups (i.e. comparison between the simulation before adding design elements and the simulation after adding design elements in 12 climate types), the analysis and evaluation of the HTC conditions before and after community environment design could be considered as a set of approaches, by which the HTC information could be applied in the design practice.

Through current study, not only the HTC conditions in 12 Chinese cities have been analysed and evaluated, but also a series of approaches for the application of HTC information on different scales have been obtained. All three parts in this study could be regarded as one kind of the exploration of the application of the human-biometeorological

information, as well as the updated meteorological information on diverse scales. The implementation of the HTC information on macro scale is of importance on the distinguishing and defining the HTC conditions in regions worldwide; and consequently the threshold with HTC information will reveal the thermal requirements of the human beings on global scale. The data analysis on meso scale is one kind of fundamental information in urban-PDM on temporal dimension, which will facilitate the understanding of the related topics. On micro scale, the application of the numerical simulation of the HTC conditions can be regarded as the necessary approach in the future to improve the community environment design. In conclusion, a systematic process of the analysis and evaluation on human-biometeorological information in multiple scales has been presented in current study, and this system would facilitate the diverse topics which are related to forming the comfortable thermal conditions.

1 Introduction

Importance of human thermal comfort

Human thermal comfort (HTC), as a research topic of human-biometeorology, focuses on one kind of basic physiological requirements of human beings, which is the human body's demand on forming thermal comfort environments both indoors and outdoors. The demand of the physiologically thermal comfort can be found in the theory of Maslow's hierarchy of needs (Maslow 1943), and previously it is understood as the need on warmth (please see ***Fig. 1.1.1***) (McLeod 2007; Poston 2009) which is one of the fundamental levels of need at the bottom of the pyramid.

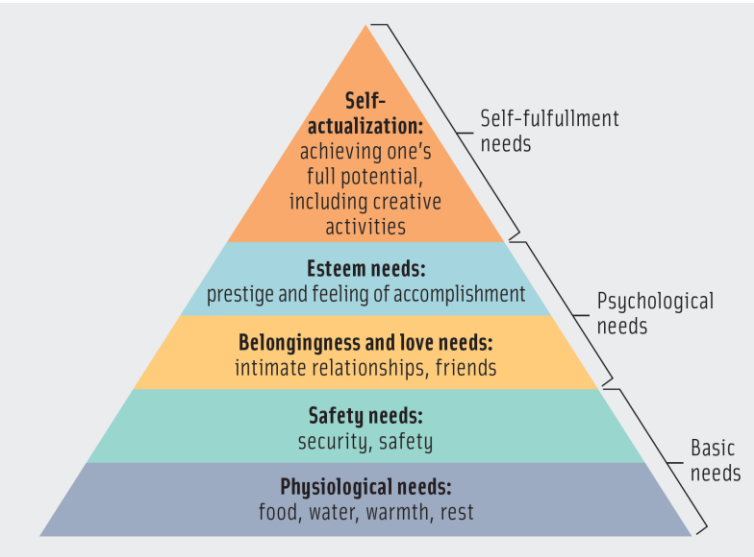

Fig. 1.1.1 Maslow's hierarchy pyramid (from Poston 2009)

HTC is an issue belonging to biometeorology which studies the impacts from meteorological conditions on living organisms (Gosling et al. 2014). Thus, HTC is influenced both by meteorological parameters and individual conditions (Fanger 1973; Höppe 1999; Matzarakis et al. 2007), and HTC conditions describe how human beings perceive their thermal environment (Fanger 1970; ASHRAE 2004). After the development in the last decades, the key achievements have been obtained in the research field on HTC, such as the establishment of the theory (Fanger 1970; Parsons 2014), the methodology of investigation of subjects (Gagge et al. 1967; Fanger 1973; Lin and

Matzarakis 2008; Lai et al. 2014), and the developments of the basic indices (Höppe 1999; Staiger et al. 2012; Jendritzky et al. 2012). Meanwhile, combined with user-friendly model (Matzarakis et al. 2007, 2010) for calculation, thermal comfort indices can be studied based on large data sets (e.g. the 3-hour data in 10 years).

Human health is influenced by HTC conditions (Laschewski and Jendritzky 2002; Patz et al. 2005; Bi et al. 2011); hence, in order to fulfil the requirement of thermal comfort, building construction, energy consumption, clothing manufactures, as well as outdoor space modification have to be performed; and currently, all of the fabrications are mainly based on the resource on the earth (Endy 2005). However, it has no doubt that the amount of the resource on the earth is limited. As HTC conditions can indicate the HTC requirements with the quantified information (i.e. information indicated by a specific thermal index), the analysis and evaluation of thermal comfort possess valuable meaning on predicting the budget of energy consumption (de Dear and Brager 2001; Brager and de Dear 2001), the risk period of human health (Omonijo et al. 2012; Omonijo et al. 2013) and the popular period of tourism (Matzarakis 2007a; Lin and Matzarakis 2008; Li and Chi 2014; Amelung and Viner 2006). Thus, quantification of HTC conditions is an approach on predicting the potential strength of resource consumption, and consequently the quantification can facilitate the sustainable development strategy.

In general, the HTC quantifications for tourism, human health, and energy consumption, can be considered and arranged beforehand in the urban planning, urban design and urban management (urban-PDM) (Law 1993; Corburn 2004; Vanos et al. 2010; Madlener and Sunak 2011). Therefore, the analysis and evaluation of HTC conditions should be regarded as essential components in urban-PDM in coming future.

Scales of meteorological analysis

The scale is an essential concept required in each project of urban planning, urban design, and sometimes even in urban management (Schmidt and Buehler 2007; Ren et al. 2011).

According to the "Boundary Layer Climates" (Oke 2002), there are four meteorological scales in horizontal distance: macro scale (10^5 to 10^8 m), meso scale (10^4 to 2×10^5 m), local scale (10^2 to 5×10^4 m) and micro scale (10^{-2} to 10^3 m) (please see ***Fig. 1.1.2***). As the calculation of HTC indices are related to the meteorological parameters, in order to analyse and evaluate HTC conditions in urban-PDM, it is necessary to clarify on which scale the analysis of the meteorological conditions will be applied.

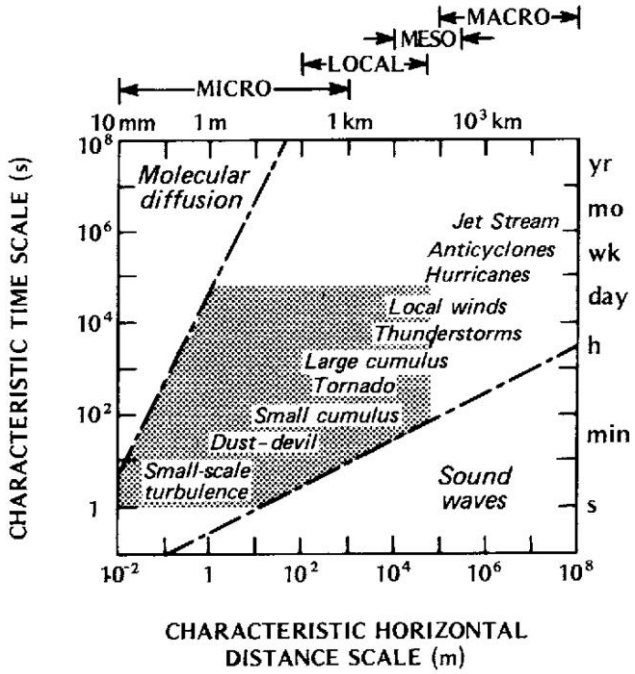

Fig. 1.1.2 Time and space scales of various atmospheric phenomena. The shaded area represents the characteristic domain of boundary layer features (Oke 2002, Smagorinsky 1974)

Based on the concepts of scales, there are some studies for generalising the key meteorological conditions for different spatial scales. The world climate classifications (Kottek et al. 2006; Rubel and Kottek 2010; Peel et al. 2007) can be considered as one kind of generalisation of meteorological conditions on macro scale, which distinguish the main meteorological characteristics between **regions** nationwide or worldwide. Based on the unified thresholds and the meteorological data in different period, a series of world map have been produced (e.g. ***Fig. 1.1.3***).

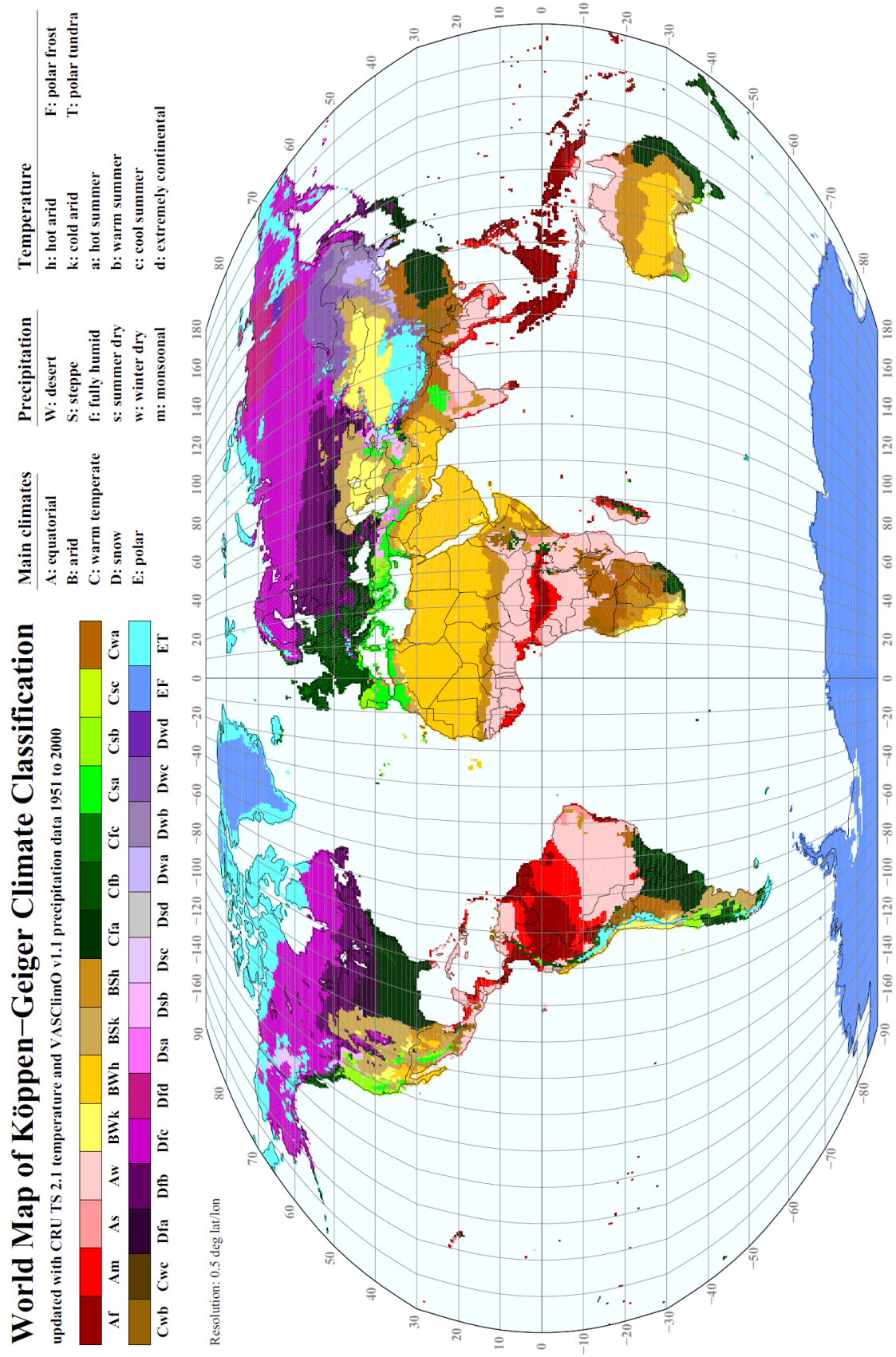

Fig. 1.1.3 World Map of Köppen-Geiger climate classification for the period 1951 to 2000 on a regular 0.5 degree latitude/longitude grid (Kottek et al. 2006)

The meteorological characteristics on meso scale present the key meteorological conditions in smaller areas (such as **cities**) than regions, e.g. the recorded meteorological data from the urban weather stations (Ng 2012; Pantavou et al. 2011; Lin and Matzarakis 2008). Normally, the single values, such as the monthly mean air temperature, the monthly accumulated precipitation, and the monthly highest/lowest air temperature, have been applied to describe the general meteorological conditions of an area; however, there are already visual method innovated for quantifying the large data set with more detailed information (e.g. ***Fig. 1.1.4***).

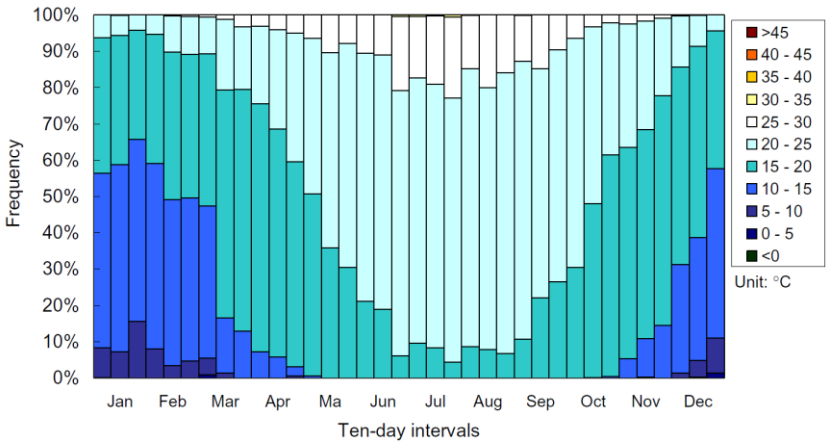

Fig. 1.1.4 Air temperature frequencies for Sun Moon Lake, Taiwan in 10-day units, based on the hourly data from 1996 to 2005 (Lin and Matzarakis 2008)

More elaborately, meteorological analysis on the local scale distinguishes the meteorological conditions between, for example, each **local zone** (i.e. each urban district) in one city (Stewart and Oke 2012; Ren et al. 2012; Matzarakis et al. 2008) (e.g. ***Fig. 1.1.5***).

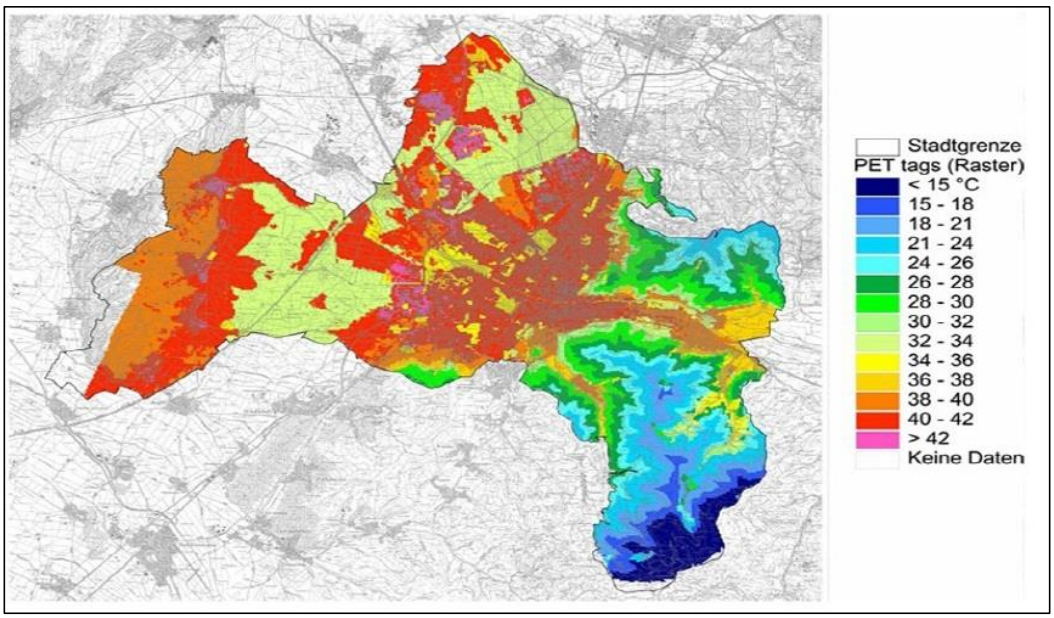

Fig. 1.1.5 Map of the physiologically equivalent temperature (PET) during day time in Freiburg, Germany (Matzarakis et al. 2008)

The specifically meteorological observations and computer simulations of each **urban space** in one local zone, are grouped as the study on micro scale (Matzarakis et al. 2006; Fröhlich and Matzarakis 2013; Ali-Toudert and Mayer 2007b) (e.g. ***Fig. 1.1.6***).

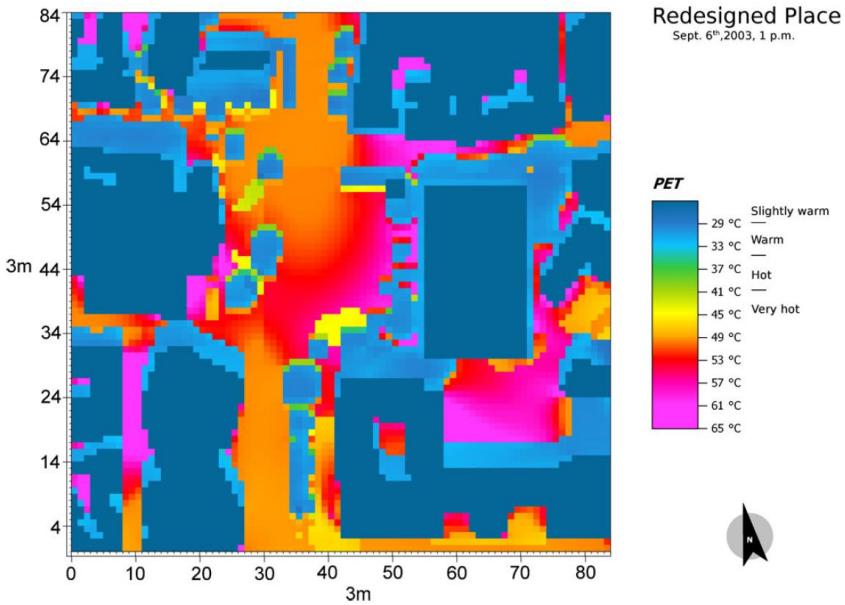

Fig. 1.1.6 Thermal bioclimatic conditions on the redesigned Place of the Old Synagogue as calculated by ENVI-met for the third day of a hot and dry period (Fröhlich and Matzarakis 2013)

Based on the specific meteorological data on each scale, the HTC conditions in each scale can be obtained afterwards. According to the theory on scales, there are followed basic assumptions in the current study:

a. The meteorological data from macro scale to micro scale demands the expressions of the analysis from low resolution to high resolution in horizontal distance.

b. Cities in one region own the similar macro-scale meteorological conditions, as well as the macro-scale HTC conditions. In order to fulfil the ideal urban development, the adaptation on these macro-scale conditions is at the first order.

c. Urban districts (i.e. local climate zones) in one city own the similar meso-scale meteorological conditions, as well as the similar meso-scale HTC conditions. The optimal constructions of the urban district should adapt to these meso-scale conditions, or should better not cause the degeneration of the typical thermal environment.

d. Urban spaces in one local climate zone own the similar local-scale meteorological conditions, as well as the similar local-scale HTC conditions. The small projects in one urban district should adapt to these local-scale conditions, or should better not intensify the thermal stress inside the local climate zone.

e. There are diverse human-biometeorological conditions between different urban spaces on micro scale, i.e. different sorts of spaces inside the urban district. It is helpful for the landscape architectural designers to locate and to identify the differences of these urban spaces in a small-scale project, e.g. the community environment design for a residential district.

f. The differences of human-biometeorology between urban spaces are driven not only by the urban fabric, but also by the background meteorological conditions.

Connection with urban-PDM

The urban-PDM, previously mentioned, is the abbreviation for urban planning, urban design, and urban management in current study. Through the adaptation to climate, human beings had selected general comfortable sites, and settled down in the ancient time. This progress may be the starting of majority villages and cities in the world. In the modern society, due to the human beings' ability on building the living environment, the passive adaptation may have been converted into active construction, and the active construction seems to be more and more intensive as the population keeps increasing. During the rapid urbanisation, there is no doubt that urban-PDM will be one sort of the necessary approaches to guarantee the sustainable development. Under the adaptation of the main meteorological conditions in each region (i.e. in macro scale), urban-PDM can mainly handle the constructions from meso scale (e.g. the development strategy of the whole city) to micro scale (e.g. the precisely projects inside each urban district).

First of all, the human-biometeorological conditions on macro scale, to which the whole city belongs, are the stably periodic conditions. The guidelines of the urban-PDM in one city should be adapted to the climate type. Currently, there are several popular climate classifications describing the periodic conditions, based on the meteorological parameters. The continents have been zoned by the specific meteorological characteristics in climate classifications; however, there is a lack of HTC information as the threshold on the human-biometeorological zoning.

Downscaling, in order to optimise the thermal environment from meso scale to micro scale by urban-PDM, the quantification of the meteorological conditions on meso scale have been considered as the basic information. The popular information is, for example, the mean monthly air temperature, the highest/lowest daily temperature, and the accumulated precipitation in one month, which is understood as the information related to "prevailing" and "critical" in urban-PDM; however, the single average values can be difficultly taken as the precisely reference values in practices (Ng 2012). Meanwhile, the

HTC conditions have not been regarded as the essential information in urban-PDM in China. In recent years, one approach based on frequencies of value classes have been applied to generalise the background meteorological conditions, as well as HTC conditions (Lin and Matzarakis 2008; Pantavou et al. 2011). The information expressed by frequencies of multiple value classes with time series is helpful for the analysis of energy consumption related to the possibly utilised range, the analysis of tourism industry related to the optimal period, and the analysis of human health related to the risk period in cities, due to the relative perspicuity of the HTC conditions. However, the information of frequency on meso scale have not been applied broadly for the analysis and evaluation of HTC conditions in urban-PDM in China. For instance, the national standards for civil building still apply the single monthly average values (GB50352-2005).

Considering the recent construction scope in China, e.g. planning a new town or constructing one building in an urban district, the local-scale and micro-scale meteorological conditions, as well as the HTC conditions, have been influenced, and even been changed, due to the variation of the air movement, radiant conditions and surface roughness (Oke 2002). The residential district with high-rise buildings, as one kind of Local Climate Zones (LCZs) in the theory from Stewart and Oke (2012), is one of the most popular district in Chinese cities. As the residents in China prefer to do daily outdoor sports or communication just nearby home, the community environment of the district acts as the important public space. In order to guarantee the optimal quality of the open space, community environment design has to consider and fulfil the diverse demands which involved HTC. However, the requirements on the comfortable thermal environment have not been paid sufficient attention on micro scale (Wang and Akbari 2015), i.e. currently, the consideration of the HTC in the community environment design has not been regarded as important as the aesthetics, traffic, or financial budget.

According to the concepts of the scale in meteorology, the study on human-biometeorology can be clustered into the same scales. Therefore, based on the necessary data set, the structure of current study has been generalised into the ***Table 1.1.1***. Due to the importance of HTC, the scales of meteorological analysis, as well as the necessary of the application of the HTC information in urban-PDM, this study has been performed in three parts. The related problems have been presented in details in the following section.

Table 1.1.1 Structure of current study, based on the human-biometeorological data

The human-biometeorological data on each horizontal scale			
Macro scale	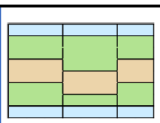	*Deficient implementation*	***Part Two*** Implementation of HTC in KGC
Meso scale	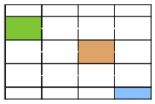	*Less efficient information*	***Part One*** Preliminary analysis of HTC
Local scale	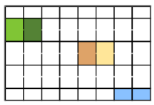	*Inadequate application in urban planning and design*	***Part Three*** Application in outdoor design (in one LCZ and on micro scale)
Micro scale	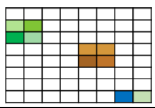		
Concentrated scope of the data, based on the meteorological scale	Sketch map of resolution	***Problem***	Exploration / application in current study

2 Problem statement

2.1 Efficient information on meso scale

In order to generalise the meteorological and human-biometeorological information on meso-scale, the long-term data is helpful. Currently, the normal meteorological information (e.g. mean monthly air temperature, mean monthly accumulated precipitation) is adopted as the main reference in the tourism (e.g. tourists guidebooks), energy consumption (GB50352-2005), human health (Tan et al. 2004), as well as urban-PDM (Ng 2012), of which the operations have been considered on meso scale (i.e. the meteorological conditions in one city are regarded as a homogenous condition). However, in practice, the traditionally meteorological information is relatively less efficient for pointing out the real-time conditions, i.e. it is difficult to get the concrete correspondence between the monthly average values and the actual conditions (Ng 2012). Consequently, the difficulty is more obviously on HTC conditions, which are influenced by multiple meteorological parameters, if the single monthly average values were continually adopted. Therefore, the efficient information on HTC together with the equally meteorological information are required, due to the more practical requirements in different topics on meso scale.

Thus, the first question is what kind of information can be efficient and user-friendly to present the HTC information on meso scale with a series of time labels in one view?

Based on the experience of daily life, the variations of the HTC conditions exist between different seasons, months, days, as well as hours. The general monthly average values seem to be inefficient to distinguish the variations day by day, nor in shorter period. First of all, this omission will lead to the submergence of the extremely thermal uncomfortable conditions (e.g. very hot or very cold) for human beings, which are the actually driving force of the sorts of energy consumption (e.g. cooling demands or heating demands). Meanwhile, during the extreme conditions with heat/cold stress, the human body will be

much weaker on self-protection than that in the thermal comfortable conditions (Laschewski and Jendritzky 2002; Patz et al. 2005; Bi et al. 2011). As a consequence, the health will be threatened. Furthermore, due to the requirements of the quantification of the energy budget (Burkhard et al. 2012), the energy consumption for heating and cooling will exist under a weakly planned situation without the certainly regular pattern of the variation in HTC conditions.

Comparing with a single value for one month (e.g. the mean monthly air temperature), the frequencies of specific value classes at certain points in time of one period can be more efficient, direct and practical for application. The frequencies of specific value classes could be regarded as full-view information, the temporally dynamic values, or multiple averages in one period. Currently, in China, there is still a lack of full-view information on HTC conditions, as well as other related meteorological conditions in most of Chinese cities.

Actually, there are enlightenments existed in other studies which apply the frequencies to describe the HTC conditions. Thus, in order to develop a specific and practical information system to analyse the basic HTC conditions and meteorological conditions of cities on meso-scale, 12 Chinese cities have been selected as samples, based on a world map of Köppen-Geiger climate classification (KGC). This is the ***Part One (Preliminary analysis of HTC)*** of this study: Preliminary analysis of thermal comfort conditions in 12 Chinese cities — Based on KGC. Actually, this part can be regarded as the fundament for summarising information on macro scale, as well as for selecting the typical period of the study on micro scale.

2.2 Implementation on macro scale

HTC conditions have been analysed in different topics, such as tourism (Matzarakis 2007b; Lin and Matzarakis 2008), energy consumption (de Dear and Brager 2001; Wende

et al. 2010; Rijal et al. 2007), human health (Omonijo et al. 2012), as well as urban-PDM (Plumley 1977; Lin et al. 2010a). However, either the studies regarding to HTC are still limited inside the regional scale (i.e. meso scale) (Hyatt et al. 2010; Lin and Matzarakis 2011), or the studies are the general assessment of HTC conditions in global scale (i.e. macro scale) (Matzarakis and Amelung 2008). There is still a lack of the unified threshold of HTC conditions on macro scale, which can describe, and then distinguish the HTC conditions between regions. In other words, the implementation of HTC on macro scale is deficient. To this end, the enlightenment from world climate classifications can be valuable.

At an age when the information and technology have been highly developed, the barrier on the obtainment of the thresholds for regional HTC conditions in macro scale, is neither the data resource, nor the computational technique of the large data sets. The key point is to develop an optimal approach on how to describe the regional HTC conditions, and how to distinguish them.

Currently, the updated Köppen-Geiger climate classification (KGC) (Kottek et al. 2006) has been obtained, and applied broadly (Rubel and Kottek 2011). KGC is based on the forerunner study by Köppen (1884, translated in 2011), which was generalised according to the distribution of vegetation in the world. World climate classifications, which distinguish the main climate types on macro scale, have been existed since last century; however, they cannot indicate the HTC conditions directly in each climate zone. Actually, the two parameters in KGC, air temperature (T_a) and precipitation (*RR*), are highly corresponding to the climate impacts on plants, instead of the impacts directly on human beings. As the problem of that, there is a requirement to implement HTC information in KGC.

Although the air humidity (AH) has been involved in the HTC, AH should be better considered extra, as a transformation of the wet/dry information indicated by *RR* in KGC. Compared with relative humidity (*RH*), vapour pressure (*VP*) is more optimal to indicate

the AH (Nicol 2004).

In order to find a method for the implementation of HTC information together with AH information in world climate classification on macro scale, the ***Part Two (Implementation of HTC in KGC)*** has been performed in this study.

2.3 Application for design on micro scale in different climate types

Due to the growing living requirements of the large population, the residential district with high-rise buildings have been a popularly urban district in mega cities (Reddy 1996). Based on the individually physical properties of this district within the local scale (Oke 2002), the microclimatic conditions inside have been influenced strongly. Community environment design (i.e. landscape architectural design) can modify the thermal environment in the residential district through the design elements (e.g. trees, and hedges); however, the application of the meteorological conditions, as well as HTC conditions are inadequate in practice in China to assist the design.

Considering on the local scale and micro scale, there are numerous research focusing on measuring and simulating the specific areas. Among these studies, different conditions have been concentrated on, for example, the wind conditions (Nikolopoulou and Lykoudis 2006; Mochida and Lun 2008; Blocken et al. 2013), the shading effects (Lin et al. 2010a; Hwang et al. 2011; Makaremi et al. 2012), as well as the HTC conditions (Matzarakis et al. 2009; Shashua‐Bar et al. 2011; Fröhlich and Matzarakis 2013). While most of these studies are operated under one kind of basic meteorological conditions, and the same locations, i.e. the same meteorological conditions on meso scale, or at least in one climate type on macro scale.

Although the atmospheric phenomena on smaller scale present the diversity distribution, they are following the unified physical laws, which are driven by the main climatic conditions regularly. As the better climatic adaptation in each region and city is required,

the background conditions of meteorology should be clarified before giving the community environment design for the residential district. Meanwhile, if possible, this consideration is also necessary for the urban construction on local scale. Thus, there is a necessity to have a comparison of the diversely atmospheric phenomena in one sample area within local scale, which are under different climate types, i.e. one area under different climatic characteristics. Consequently, the suitable design can be obtained for the area in different climate types.

In order to evaluate the HTC conditions on micro scale before a project is really constructed, the numerical simulations based on the physical laws might be a more reliable method, comparing with the empirical analysis. Meanwhile, although the climate types (as well as the HTC conditions) are diverse in China, the HTC conditions have not been developed as the definite reference on micro scale for the construction projects (include community environment design) in the urbanisation.

To this end, there are series of questions emerged due to the interaction between urban constructions and atmosphere. (1) What kind of input data is suitable for the simulation? Will the HTC conditions in this district be distinguished on micro scale through the simulation? (2) For the same building group but located in different cities, and in different climate types, how the HTC conditions outdoors are? (3) Can the outdoor HTC conditions be modified (i.e. through community environment design) for the building group in different climate types? (4) Are there advices can be obtained from the analysis and evaluation of the HTC conditions on micro scale?

With the series of notice, one hypothetically residential district with high-rise buildings (i.e. a typical residential district in China) has been selected to find a way on analysis of the HTC conditions before the community environment design, and evaluation of the effects from the design regarding the modification on HTC conditions. In accordance with the definition of a Local Climate Zones (LCZs), the selected district is in the local scale and roughly equal to a LCZ (Stewart and Oke 2012). The micro-scale analysis and

evaluations are based on the meteorological conditions and basic HTC conditions of the same Chinese cities in 11 climate types in the two parts forwards. This is the ***Part Three (Application for outdoor design)***: analysis and evaluations of HTC conditions in a residential district in different climate types, based on micro-scale numerical simulations.

3 State of the art

3.1 Impact factors of human thermal comfort (HTC)

Human thermal comfort (HTC) describes how comfortable human beings perceive the thermal environment indoors, as well as outdoors (Fanger 1970; Fanger 1973). The study on HTC, a human-biometeorological issue, is of growing importance for human health (Omonijo et al. 2012; Omonijo et al. 2013), energy consumption (de Dear and Brager 2001; Brager and de Dear 2001), tourism (Amelung and Viner 2006; Matzarakis 2007a; Lin and Matzarakis 2008), which are considered in the process of urban planning, urban design, and urban management (urban-PDM) (Law 1993; Corburn 2004; Vanos et al. 2010; Madlener and Sunak 2011). Basically, HTC conditions are directed by meteorological factors and individual factors together, considering the impacts of these factors on heat transfer between human body and the thermal environment (Parsons 2014).

3.1.1 Meteorological factors

Air temperature (T_a), air humidity (AH), wind velocity (v) and the radiant conditions are the four meteorological factors which influence the HTC conditions (Fanger 1973; Höppe 1999; Blazejczyk et al. 2013; Parsons 2014). In previous studies, they have been used, individually or combinatorially, to indicate the thermal perception of human beings.

3.1.1.1 Air temperature (T_a)

Air temperature (T_a) indicates the temperature of air, in which human beings perceive the thermal environment by convective heat exchange (Kántor and Unger 2011), and it is one of the most popular and traditional meteorological parameters. T_a has been applied in the primary and advanced research on HTC as one of the most important variables. For example in a study, the thermal sensation and sensory estimates of comfort have been compared within the ambient temperature (12–48 °C) (Gagge et al. 1967). In this study, it has been found that the thermal comfort and neutral temperature sensations are in the range of 28–30 ℃, which is the physiological thermal neutrality. Meanwhile, according

to the one figure in this research (Hardy and Stolwijk 1966; Gagge et al. 1967), T_a possesses obviously effects on average skin temperature, metabolism, internal body temperature, evaporative loss, average skin conductance and body heating/cooling progresses. In the study of de Dear and Brager (2002), the thermal comfort (based on T_a) has been revised through 21,000 sets of raw data, which is from four continents and in the different climatic zones. Nicol and Humphreys (2002) explored the origin of the differences between the "rational" indices and the results in field survey based on T_a, and the finding is through analysing of the previous studies and the related theories. Meanwhile, this study also attempted to define the adaptive standards for indoor climate, which may be more meaningful for building designers.

3.1.1.2 Air humidity (AH)

Air humidity (AH) in the HTC studies refer to water vapour conditions in the air, which influences the heat capacity of the air parcel. AH conditions can be indicated by several meteorological parameters, in which the vapour pressure (*VP*) and relative humidity (*RH*) have been utilised popular in HTC studies. Meanwhile, *VP* and *RH* can be converted to each other.

Under the equatorial climate in Singapore where is warm, damp and windless, Webb (1959) had developed a Singapore index for indoor climate through a multiple regression equation, in which the *VP* in millimetre (mm) of mercury has been included. In the study under the hot dry weather in Roorkee, India and Baghdad, Iraq (Nicol 1974), *VP* was used to indicate the moisture of the air. The study found that the humidity has no significant effect on the thermal perception. On the other hand, in the study in 2004 (Nicol), the implementation of humidity (based on *VP*) in the suggested modification has been considered in order to improve the thermal comfort standards for indoor climate in the hot-humid tropics. Meanwhile, this study (Nicol 2004) recommended *VP* as a more robust measure than *RH*, because *RH* is a dependent parameter and *VP* is directly associated with the maintaining of skin temperature.

Relative humidity (*RH*) describes the AH conditions with percentage values, i.e. *RH* indicates the relative humid conditions instead of the absolute conditions. According to the investigation in the warm-humid tropics (Ahmed 2003), the conditions with high *RH* combined with high T_a in a typical street section without wind but in shades provide a relative comfortable environment, which proofed by the longer stay (> 120 min) of the subjects. There is another study on indoor humidity on HTC conditions in Malaysia (humid-tropics) (Djamila et al. 2014), which found that the indoor thermal comfort range (27.5 ℃ to 33.5 ℃ on ASHRAE[1] thermal sensation scale) existed in a wide *RH* range (82 % to 63 %) according to the developed equation in this study. In a development of an approach on minimum the energy consumption in central air-condition buildings (Wan et al. 2009), *RH* conditions have been set as one kind of fundamental conditions. It found that the energy consumption decreased when the indoor *RH* increased, under the given HTC conditions.

3.1.1.3 Wind conditions

Wind velocity (*v*) presents the strength of the air flow. In many situations, *v* is utilised together with wind direction (WD). Once, an evaluation of HTC perception has been performed in the high-rise buildings in Singapore, based on the natural ventilation under the utilisation of windows, fans or air-conditionings (Wong et al. 2002). It is found that residents experienced warmer thermal sensation during the hot afternoon, and they required stronger air movement during this period than in morning and at night. Nikolopoulou and Lykoudis (2006) analysed the HTC conditions in outdoor urban spaces in difference European countries, in which the wind conditions had been included as a key parameter for evaluation. Based on the temporal and spatial comparisons, respectively, their research indicated that the effect of wind is strongly dependent on T_a; meanwhile,

---

[1] the American Society of Heating, Refrigerating, and Air-Conditioning Engineers

the discomfort may increase as the strong winds appear in summer, e.g. in Kassel and Sheffield which are in northern climates. Another study in Hong Kong (Cheng et al. 2012), which is in the sub-tropical climate, found that the v and the radiant conditions can influence the thermal sensation obviously.

3.1.1.4 Radiant conditions

Mean radiant temperature (T_{mrt}) (ISO7226 1998; ASHRAE 2009), which indicated one kind of important heat gains of human body in HTC study, presents the radiant conditions in the thermal environment both indoors and outdoors, and the detail information on this parameter have been reviewed by Kántor and Unger (2011). Atmaca et al. (2007) applied Gagge 2-node model to simulate effects of T_{mrt} on 16 body segments, respectively. In this study, the walls and the ceilings have been regarded as the main resource of the radiation indoors for human beings. The study found that the body segments close to the relatively hot walls/ceilings are influenced stronger than other body segments, meanwhile interior surface temperature of these walls and ceilings are raised through the strong radiation outdoors. Based on the application of a radiant heat exchange model (Gan 1994), another indoor research analysed the effects from windows on the T_{mrt} (Gan 2001). This study found that there is significant gradients of T_{mrt} with the respect to the distance from windows; furthermore the thermal discomfort conditions existed nearby the window in the calculation. Besides indoors, T_{mrt} has also been taken into account for the research on HTC outdoors, for example, the study of urban canyons in Freiburg, Germany (Herrmann and Matzarakis 2012). This study revealed that a great variation of T_{mrt} (say higher than 30 ℃) may exist in the urban district due to the diverse urban structures referring to the width, height and orientation of the urban canyons.

In the quantification of radiant conditions in urban climate, a geometric indicator is necessary, and currently, sky view factor (SVF) has been applied broadly (Yamashita et al. 1986; Blennow 1995; Unger 2008; Chapman and Thornes 2004; Matzarakis and Matuschek 2011). SVF is defined as the ratio of radiation received by a planar surface

from the sky to that received from the entire hemispheric radiating environment (Watson and Johnson 1987). The value range of SVF is from 0 to 1 (Chen et al. 2012); for instance, the SVF of 0.31 means that only 31% of the sky up the concentrated location is visible (Matuschek and Matzarakis 2010). Obtainment of SVF of the concentrated location can be performed either through measurement and calculation by taking fish-eye-photo, or through computer simulations (Matzarakis et al. 2007; Matuschek and Matzarakis 2010). SVF has been also regarded as an independent parameter in the studies on urban climate, for instance, the studies on the relationship between SVF and T_a (Svensson 2004; Chen et al. 2012).

3.1.2 Individual conditions of human beings

There may be no doubt that the original function of clothes is to maintain the HTC conditions, and even in the currently fashion trend, the ability of clothes on keeping warm in winter or maintaining cool in summer is the important consideration. The wearing clothes are regarded as the insulated layer(s) which stop the heat transfer between human body and the thermal environment, and the ability of this function is quantified by the clothing insulation (ASHRAE 2004). The unit of clothing insulation is "*clo*" (Toftum 2005). In a certain HTC conditions, human beings can adjust the clothes status by putting on or taking off; however, the gradations and the effects of the adjustments are limited due to the social customs (Parsons 2002). The clothing insulation has been utilised in a study (Newsham 1997) which detected the relationship between clothing adjustments and the energy consumption through a series of simulation. Based on the simulations, in which the modelled occupant adjusted or fixed the clothing conditions during the variation of thermal environment indoors, the study reveals the association between the optimally thermal environment, the clothing insulation and the energy consumption. Currently, in order to evaluate the HTC conditions of a standard clothing condition of a human body, it is popular to set the clothing insulation as a unified condition in HTC indices calculations (e.g. 0.9 *clo* in PET, please see section 3.2.1).

Metabolic rate is the other personal factor, which is influenced by the individual activity and the certain thermal environment (Wissler 1964; Gagge et al. 1969). The physiological mechanism of human metabolism is complex; however the metabolic rates of some typical behaviours have been obtained, and *MET* is the unit for metabolic rate (1 *MET* = 58.2 W/m^2) (ASHRAE 2013; Havenith et al. 2002). In the conception of human body heat balance, metabolic rate is always positive (Höppe 1999). The default metabolic rates are adopted in HTC studies (Höppe 1999; Jendritzky et al. 2012), in order to imitate the common human body conditions.

3.2 Thermal comfort indices

The meteorological factors stated in section 3.1 have been used to describe the HTC conditions individually or complementarily; however, each of them is barely able to indicate the actual perception on the thermal environment. In order to quantify the HTC conditions, many indices have been developed in last decades (Fanger 1973; Staiger et al. 2012; Höppe 1999; Blazejczyk et al. 2013). Some indices have been accepted and applied in various topics.

3.2.1 Physiologically equivalent temperature (PET)

The physiologically equivalent temperature (PET) is defined as "the air temperature at which, in a typical indoor setting (without wind and solar radiation), the heat balance of human body is maintained with core and skin temperatures equal to those under the conditions being assessed (indoors/outdoors)" and the unit of PET is "°C" (Mayer and Höppe 1987; Höppe 1999; Matzarakis et al. 1999). The PET can be calculated based on 4 meteorological parameters (T_a, *VP* (or *RH*), *v*, and T_{mrt}) and 2 the thermal-physiological factors (metabolic rate and clothing insulation) (Höppe 1999; Matzarakis et al. 1999; Matzarakis et al. 2007). Among these parameters, T_{mrt} is related to the radiant conditions (ISO7226 1998; ASHRAE 2009) of the assessed thermal environment, and it can be

estimated by cloud cover, time, and surface situations (Höppe 1999; Matzarakis et al. 2007, 2010). The metabolism of the human body in the definition is 80 (W), and the clothing insulation is 0.9 *clo*. Meanwhile, the *v* utilised for calculation has to be the value at the relevant height (height of human body's core 1.1 m) (Matzarakis et al. 2009).

In the theoretical statement of PET from Höppe (1999), there is an example which is helpful to understand PET in practice. In a warm and sunny outdoor condition (T_a at 30 ℃, T_{mrt} at 60 ℃, *RH* at 50%, and *v* at 1.0 m/s) for a standard human body with 0.5 *clo*, there is a synthesised HTC condition expressed by a PET value at 43 ℃. This value means that a person in a room with 43 ℃ of T_a owns the same thermal perception as the sunny condition outdoors.

Because PET presents the actual HTC conditions, i.e. PET is a real-time value, the analysis of PET normally requires data with high temporal resolution, and consequently, the analysis of the trend or regular patterns is meaningful for the large data sets (e.g. 3-hour data in several years). For all of these analysis, the computerisation of the PET calculation is necessary. RayMan model (Matzarakis et al. 2007, 2010) is an available model which can calculate several popular HTC indices included PET. The calculation is performed by meteorological parameters and the default thermo-physiological conditions (Höppe 1999; VDI 1998; Matzarakis 2007, 2009). The default thermo-physiological conditions for a standard human body assume that it is a 35-year-old man with 1.75 (m) height and 75 (kg) weight. The clothing insulation of this man (as the definition) is 0.9 *clo*, and this man stands with the activity level at 80 (W).

On the purpose of linking the PET values with human body's comfortable level, one set of thermal sensation with 9 value ranges (please see PET [a] in ***Table 3.2.1***) has been introduced by Matzarakis and Mayer (1996). This 9-range thermal sensitivity is based on the investigation in Western/Middle European. As another regional judgement of the thermal sensation in Tropical climate, a varied 9-range thermal sensation (please see PET [b] in ***Table 3.2.1***) has been obtained in Taiwan (Lin and Matzarakis 2008). Meanwhile,

there is also a 9-range sensation (please see PET [c] in ***Table 3.2.1***) obtained in a northern Chinese city (Tianjin) (Lai et al. 2014). Comparing the three sets of thermal sensation, it can be found that the fluctuation of the cool discomfort conditions are large between them, and the range of the cool discomfort conditions are quite different. For example, the cold sensation is related to 4 — 8 ℃ in Western/Middle European, 14 — 18 ℃ in Taiwan, and – 16 — – 11 ℃ in northern China, respectively. In contrast, the warmer sensation presents the much more similar PET value ranges. For example, the hot sensation is related to 35 — 41 ℃ in Western/Middle European, 38 — 42 ℃ in Taiwan, and 36 — 46 ℃ in northern China, respectively.

Table 3.2.1 Thermal sensitivity and Grades of physiological stress based on PET

PET [a] (℃)	PET [b] (℃)	PET [c] (℃)	Thermal sensation [a]	Physiologically thermal stress [a]
Below 4	Below 14	Below –16	very cold	Extreme cold stress
4 — 8	14 — 18	– 16 — –11	cold	Strong cold stress
8 — 13	18 — 22	– 11 — – 6	cool	Moderate cold stress
13 — 18	22 — 26	– 6 — 11	slightly cool	Slightly cold stress
18 — 23	26 — 30	11 — 24	neutral (comfortable)	No thermal stress
23 — 29	30 — 34	24 — 31	slightly warm	Slightly heat stress
29 — 35	34 — 38	31 — 36	warm	Moderate heat stress
35 — 41	38 — 42	36 — 46	hot	Strong heat stress
Above 41	Above 42	Above 46	very hot	Extreme heat stress

a. According to the study in Western/Middle European (Matzarakis and Mayer 1996)
b. According to the study in Taiwan (Lin and Matzarakis 2008)
c. According to the study in Tianjin (Lai et al. 2014)

Beside the studies related to the PET ranges on thermal sensations, PET has also been applied widely on the research on HTC conditions. For example, based on the analysis of PET, the HTC conditions in Qinghai-Tibet Plateau have been demonstrated that the cold stress is main thermal conditions in the whole year (Li and Chi 2014). Through the assessment on thermal comfort in Netherlands, Taleghani et al. (2015) pointed out that the most intense effect in an extreme hot day in summer on HTC conditions is the radiant conditions which depend on the different urban form.

3.2.2 Other applied indices

Predicted mean vote (PMV) (Fanger 1970; Fanger 1973), together with the predicted percentage of dissatisfied (PPD) (Fanger 1973), is an initial thermal comfort index. In practical assessment of thermal environment, subjects can vote for the environment by the following 7 scales (please see ***Table 3.2.2*** on PMV). Although it is developed based on indoor conditions, this index has been applied broadly for the investigations on thermal environments, especially for indoor environment (Nikolopoulou et al. 2001; Humphreys and Nicol 2002; Fanger and Toftum 2002).

Perceived temperature (PT) presents the T_a of the assessed thermal environment based on the application of PMV, and the clothing insulation varies from 0.5 *clo* to 1.5 *clo* in order to achieve the HTC neutral conditions (PMV = 0) (Staiger et al. 2012). The calculation of PT establishes a modelled subject, who is Klima-Michel, as the representative for all human beings. Meanwhile, there is a 9-range PT values related to the thermal sensation (please see ***Table 3.2.2*** on PT). With the respect to mortality in southwest Germany, the relationship between the PT values and mortality rate has been analysed, based on the 30-year meteorological data from 4 weather stations (Laschewski and Jendritzky 2002). In this study, the calculation of PT was performed with the average values of the 4-station data, and the daily value has been utilised.

The Universal Thermal Climate Index (UTCI) is a newly-developed thermal index (Blazejczyk et al. 2013), which is defined as "the T_a of the reference condition causing the same model response as actual conditions". In order to quantify the multi-dimensionally thermal environment into this one-dimensional index, the calculation is expressed through the approximation up to 6th order by a polynomial, which contains T_a, T_{mrt}, v and VP (Blazejczyk et al. 2013). Meanwhile, for the assessment of the thermal stress, 10 scales have been generalised for UTCI combined with physiological responses (please see ***Table 3.2.2*** on UTCI). A study on HTC conditions in Curitiba, Brazil, has applied UTCI to indicate the thermal sensation of the urban area, which is in the sub-

tropical climate (Bröde et al. 2013). This is one kind of application of HTC study in urban planning.

Table 3.2.2 Classes of three applied human thermal indices, respectively

PMV [a]	Thermal sensation	
– 3	cold	
– 2	cool	
– 1	slightly cool	
0	neutral	
+ 1	slightly warm	
+ 2	warm	
+ 3	hot	
PT (℃) [b]	Thermal sensation	Thermo-physiological stress
Below – 39	Very cold	Extreme cold stress
– 39 — – 26	Cold	Great cold stress
– 26 — – 13	Cool	Moderate cold stress
– 13 — 0	Slightly cool	Slightly cold stress
0 — 20	Comfortable	Comfort possible
20 — 26	Slightly warm	Slightly heat stress
26 — 32	Warm	Moderate heat stress
32 — 38	Hot	Great heat stress
Above 38	Very hot	Extreme heat stress
UTCI (℃) [c]		Stress Category
Above 46		Extreme heat stress
38 — 46		Very strong heat stress
32 — 38		Strong heat stress
26 — 32		Moderate heat stress
9 — 26		No thermal stress
0 — 9		Slight cold stress
– 13 — 0		Moderate cold stress
– 27 — – 13		Strong cold stress
– 27 — – 40		Very strong cold stress
Below – 40		Extreme cold stress

a. According to the study on PMV (Fanger 1973)
b. According to the study on PT (Staiger et al. 2012)
c. According to the study on UTCI (Blazejczyk et al. 2013)

3.3 Correlation between HTC and urban development

In modern society, the development of one city, the scale of the urban area, and the function of the urban districts are all guided by urban planning, urban design, and urban management (urban-PDM). Meanwhile, the urban form definitely influences HTC conditions on diverse scales, due to the individual properties of the constructed materials in urban area, as well as the urban form itself (Oke 2002; Stewart and Oke 2012). Therefore, the optimal strategy for urban-PDM will promote the better HTC conditions. The detailed definition of urban planning and urban design can be found in the book from Carmona et al (2010). Urban planning, performed by the agent of the state, controls the production of land for the purpose of capital accumulation and social reproduction; allocates sites for the collective consumption of social goods such as hospitals, schools and religious buildings; and provides space for the production, circulation and eventual consumption of commodities (Carmona et al. 2010). Urban design, as an open system, uses individual architectural elements and ambient space as its basic vocabulary, and focuses on social interaction and communication in the public realm (Carmona et al. 2010). Based on the study from Rakodi (2001), the urban management is understood (ideally) as an integrated system, which deals with health, education, transport, local economic development and infrastructure provision, as well as land use planning.

Urban planning and urban design focus on the plan on the constructions of the urban physical environment, and urban management is highly related to the policy making, based on the physical environment, as well as the local situations regarding population, culture and economy, such as the strategies on tourism, human health and energy consumption, which are the three aspects concerned in current study as the issues in urban management. Meanwhile, the three aspects on planning, design, and management interact to each other. For instance, the urban management is based on the guideline in urban planning and urban design; the urban design is performed under the urban planning; the urban planning and urban design can be modified based on the feedback from urban

management. Finally, as the new consideration, HTC information together with the updated meteorological information will be helpful in urban-PDM.

3.3.1 Urban planning and urban design

Urban planning and design produce the guideline and the scheme for the construction of a city or one urban district, and even the projects in smaller scale, in which the exactly function of the urban space will decided, and the building style will be limited (Berke and Kaiser 2006). Therefore, the meteorological conditions, as well as the HTC conditions in the concerned spaces will be provide information for the process of planning and design, in order to avoid the worse conditions after (re-)constructions. According to research, the morphology or the urban fabric will influence the HTC conditions on micro scale. For example, an investigation in Dhaka, Bangladesh, which took the T_a, globe temperature, *RH* and *v* into account, shows that subjects voted the wide open spaces, which allow breeze to pass through, as comfortable conditions in warm-humid Tropics during the hottest period of the day (Ahmed 2003). In the study related to the T_{mrt} in street canyon in Freiburg, the effects from the height (*H*) and the width (*W*) of the street canyon have be demonstrated (Herrmann and Matzarakis 2012). Within the high-density of the urban area, the wind conditions have been drawn high attention in the Hong Kong Planning Standards and Guidelines in order to improve the HTC conditions (Ng 2009). As the HTC conditions highly correlate with meteorological conditions, the direct concerns of the meteorology in urban planning are related to the HTC conditions. According to the modelling and evaluation of the meteorological environment in Beijing, China (Fang et al. 2004), the relationship between urban planning and meteorological conditions has been simulated on diverse scales. Furthermore, the approach has been suggested as the supplements on the evaluations for urban planning schemes.

3.3.2 Tourism

According to the definition in the Oxford dictionary[2], tourism refers to the commercial organization and operation of holidays and visits to places of interest. With regarding to the tourists attractions, weather conditions are one of the most important aspects, which influence the satisfaction of the tourists. The thermal perception is decided by the factual weather conditions during the travelling period. The analysis of the HTC conditions of one site can provide the information, for example, the popular tourism period. Clarification of the special period is one kind of useful tourism information (Law 1993), thus the HTC analysis can make this process to match the expectation of tourist. In the study of Sun Moon Lake in Taiwan, the HTC conditions has been analysed in 10-day scale which were regarded as a detailed meteorological information for the tourism authorities and tourists (Lin and Matzarakis 2008). The interesting funding is that the most tourists have not arrived the Sun Moon Lake during the most comfort period. Thus, the detailed meteorological and biometeorological information are suggested in this study, which can be helpful to develop the tourism potential. The study on the tourism in the Hunter Region Australia (Shiue and Matzarakis 2011) analysed the popular period of international tourists and domestic tourists, respectively. In the study in Tibet-Qinghai Plateau, it has been found that the tourists flows in Lhasa and Xining, respectively, correlate with the days with PET between 13 and 29 ℃ (Li and Chi 2014). In all of these studies, there is a common section which is related to Climate Tourism Information Scheme (CTIS) (Matzarakis 2007a; Zaninović and Matzarakis 2009). CTIS, as a simplified climatic information with the respect of tourism, focuses on the meteorological characteristics, as well as the remarkable HTC conditions of one concerning place. As the essential component of the biometeorological leaflet, the CTIS brings the reader-friendly information (Zaninović and Matzarakis 2009), which is in the form of frequencies value

---

[2] http://www.oxforddictionaries.com/de/definition/englisch/tourism

in specific periods.

3.3.3 Human health

According to the definition of health from World Health Organisation (WHO), health is a state of complete physical, mental and social well-being and not merely the absence of disease or infirmity (WHO 1948). Under the acceptable thermal environment, human body can adjust the heat storage or release through the thermoregulation process, and consequently the core temperature of human body can be maintained (Stolwijk and Hardy 1966; Benzinger 1969). However, these physiological adjustments will turn to be weaker when the thermal environment change to be extremely hot or cold (Bi et al. 2011; Laschewski and Jendritzky 2002). Therefore, the more detailed HTC information and the related meteorological information will be helpful for identifying the risk period. The research on mortality emphasise the serious situation on the correlation between health and climate, which has been highly addressed by Patz et al. (2005).

It has been demonstrated that the high mortality rate is associated with old people (especially women) under certain weathers (Bi et al. 2011; Vaneckova et al. 2008). German weather service centre (DWD) (Bucher 1993) has provide a series of combined climate conditions, which have either convenient effects, or inconvenient effects on some popular unhealthy conditions (e.g. migraine, hypotension, hypertension, heart attack, asthma and depressions), in which the ambient temperature has been considered together with other climatic parameter, e.g. humidity, and atmosphere pressure[3].

Regarding the correlation specifically between human health and HTC, the consideration of thermal comfort has been recommended as one of the necessary policies in Australia in urban planning with respect to the extreme weather and climate change (Bi et al. 2011). In the moderate climate (Baden-Württemberg, Germany), correlation between the total

---

[3] The information can be found from http://www.dwd.de/DE/leistungen/gefahrenindizesbiowetter/hintergrund.html

mortality and thermal environment has been demonstrated through the statistical analysis of the mortality data and biometeorological data in 30 years (Laschewski and Jendritzky 2002). Omonijo et al. (2013) have analysed the thermal environment with the attention on human health, which is helpful for the improvement of health care interventions.

3.3.4 Energy consumption

In order to maintain a stable thermal environment indoors, energy consumption is necessary in modern society, especially during the very hot or cold period. Whether the heating system or the cooling system inside buildings, currently, almost run via consumption of limited resource (e.g. coal, petroleum or nature gas). At the same time, the chain effects from the energy utilisation on climate is successively occurred, e.g. the heat island effect (Konopacki and Akbari 2002; Rizwan et al. 2008). Studies on the relationship between the maintenance of thermal environment and the energy consumption, can optimise the configuration of energy, e.g. through urban-PDM (Stone Jr and Rodgers 2001; Solecki et al. 2005). One study, which is also based on the subjects and buildings around the world, has demonstrate the association between indoor comfort temperature and the outdoor T_a (de Dear and Brager 2001). Another study (Rijal et al. 2007) formulated the effects of window opening behaviour pattern on comfort conditions indoors, which associated with the energy consumption. Meanwhile, the optimum and acceptable indoor temperature ranges in different regions have been clarified in this study, which is helpful for saving energy in different climate zones. Based on the hourly meteorological data, Zhao et al. (2015) have simulated the energy demands in a typical indoor space located in 18 cities which are in 5 Chinese climate zones (defined by Chinese standards). In this study, seven parameters (e.g. the air infiltration and the orientation), in total, have been considered for the construction of the typical indoor space (i.e. a residential room), and consequently their effects on energy consumption have been analysed.

In conclusion, ***Table 3.3.1*** presents the summarisation of the correlation between human-

biometeorological information and each aspect in urban development.

Table 3.3.1 The significant meaning of HTC information in diverse aspects in urban development

Aspect	**Importance of HTC information for each aspect**
Urban planning Urban design	Avoid to cause the worse human-biometeorological conditions by (re-)constructions
Urban management	Update reference in management
Human health	Highlight the risk period
Tourism	Indicate the thermal comfortable period
Energy consumption	Optimise the configuration of energy

3.4 Meteorological analysis on macro scale

In meteorological analysis, the macro scale in horizontal is defined as the study in the range of 10^5 to 10^8 (m) (Oke 2002). Considering this horizontal scope, global study on climate classification can be one kind of macro-scale studies. Actually, the world climate classification has existed since a long time ago, and it has been updated with many editions (Belda et al. 2014).

3.4.1 Köppen-Geiger climate classification updated (KGC)

Among all of the existed world climate classifications, Köppen-Geiger climate classification updated (KGC) has been produced within a world map through a group of scientists from Austria and Germany (Kottek et al. 2006). This world map is the first digital map of Köppen-Geiger climate classification (Belda et al. 2014), and it is based on the data set in the period of last 50 years in 20th century (please see ***Fig. 1.1.3***). The resolution of this digital map is in a 0.5 ×0.5 degree of latitude and longitude grid. Based on the criteria in ***Table 3.4.1***, there are 31 climate classes (Kottek et al. 2006). Following this digital map, a series of digital maps have been produced by Rubel and Kottek (2010), which applied a 25-year running average to the observed data and projected data. The digital maps can be obtained via internet (http://koeppen-geiger.vu-wien.ac.at/).

The quantitative description (i.e. the threshold) of KGC is completed through the

generalisation of T_a and RR in specific period in one year. Except the threshold related to average values on T_a or RR, the characteristics of each climate type (i.e. KGC type) has been described qualitatively in ***Table 3.4.1***, such as equatorial rainforest and fully humid, warm temperate climate with warm summer, or snow climate with hot summer. These descriptions are helpful information to understand the generally climatic conditions in each region; however, the fundamental threshold are not efficient to indicate the HTC information, based on the parameters applied in KGC at moment.

Table 3.4.1 Climate types and subtypes defined by the Köppen-Geiger climate classification updated (KGC) (modified after Kottek et al. 2006)

Type/ Subtype		Description	Criteria*
A		Equatorial climates	$T_{min} \geq 18$ °C
Af		Equatorial rainforest, fully humid	$P_{min} \geq 60$ mm
Am		Equatorial monsoon	$P_{ann} \geq 25(100 - P_{min})$
As		Equatorial savannah with dry summer	$P_{min} < 60$ mm in summer
Aw		Equatorial savannah with dry winter	$P_{min} < 60$ mm in winter
B		Arid climates	$P_{ann} < 10\ P_{th}$
BS		Steppe climate	$P_{ann} > 5\ P_{th}$
BW		Desert climate	$P_{ann} \leq 5\ P_{th}$
	h	Hot steppe / desert	$T_{ann} \geq 18$ °C
	k	Cold steppe / desert	$T_{ann} < 18$ °C
C		Warm temperate climates	-3°C $< T_{min} < 18$ °C
Cs		Warm temperate climate with dry summer	$P_{smin} < P_{wmin}$, $P_{wmax} > 3P_{smin}$ and $P_{smin} < 40$ mm
Cw		Warm temperate climate with dry winter	$P_{wmin} < P_{smin}$ and $P_{smax} > 10P_{wmin}$
Cf		Warm temperate climate, fully humid	Neither Cs nor Cw
	a	Hot summer	$T_{max} \geq 22$ °C
	b	Warm summer	Not (a) and at least 4 $T_{mon} \geq 10$ °C
	c	Cool summer and cold winter	Not (b) and $T_{min} > -38$ °C
D		Snow climates	$T_{min} \leq -3$ °C
Ds		Snow climate with dry summer	$P_{smin} < P_{wmin}$, $P_{wmax} > 3P_{smin}$ and $P_{smin} < 40$ mm
Dw		Snow climate with dry winter	$P_{wmin} < P_{smin}$ and $P_{smax} > 10P_{wmin}$
Df		Snow climate, fully humid	Neither Ds nor Dw
	a	Hot summer	$T_{max} \geq 22$ °C
	b	Warm summer	Not (a) and at least 4 $T_{mon} \geq 10$ °C
	c	Cool summer and cold winter	Not (b) and $T_{min} > -38$ °C
	d	Extremely continental	like(c) but $T_{min} \leq -38$ °C
E		Polar climates	$T_{max} < 10$ °C
ET		Tundra climate	0 °C $\leq T_{max} < 10$ °C
EF		Frost climate	$T_{max} < 0$ °C

* Monthly precipitations are in mm/month and annual precipitation is in mm/year. T_{ann}: the annual mean near-surface (2 m) temperature; T_{max} and T_{min}: the monthly mean temperatures of the warmest and coldest months, respectively; P_{ann}: accumulated annual precipitation; P_{min}: the precipitation of the driest month; P_{smin}: the lowest monthly precipitation for the summer on the hemisphere considered; P_{smax}: the highest monthly precipitation for the summer on the hemisphere considered; P_{wmin}: the lowest monthly precipitation for the winter on the hemisphere considered; P_{wmax}: the highest monthly precipitation for the winter on the hemisphere considered; P_{th}:a piecewise-defined function of T_{ann}; T_{mon}: mean monthly temperature.

3.4.2 Other popular climate classifications

Köppen climate classification (KCC) is created by Wladimir Köppen (1846–1940), and it is mainly based on the distribution of the vegetation (Köppen 1884, translated in 2011; Köppen 1900). ***Figure 3.4.1*** is the version of the world map in 1884. After the initial version was created, the KCC has been updated, and the threshold of the final KCC has been summarised in ***Table 3.4.2***, which is from the study of Belda et al. (2014). Comparing with the ***Table 3.4.1***, the number of the climate types in KCC (***Table 3.4.2***) is less.

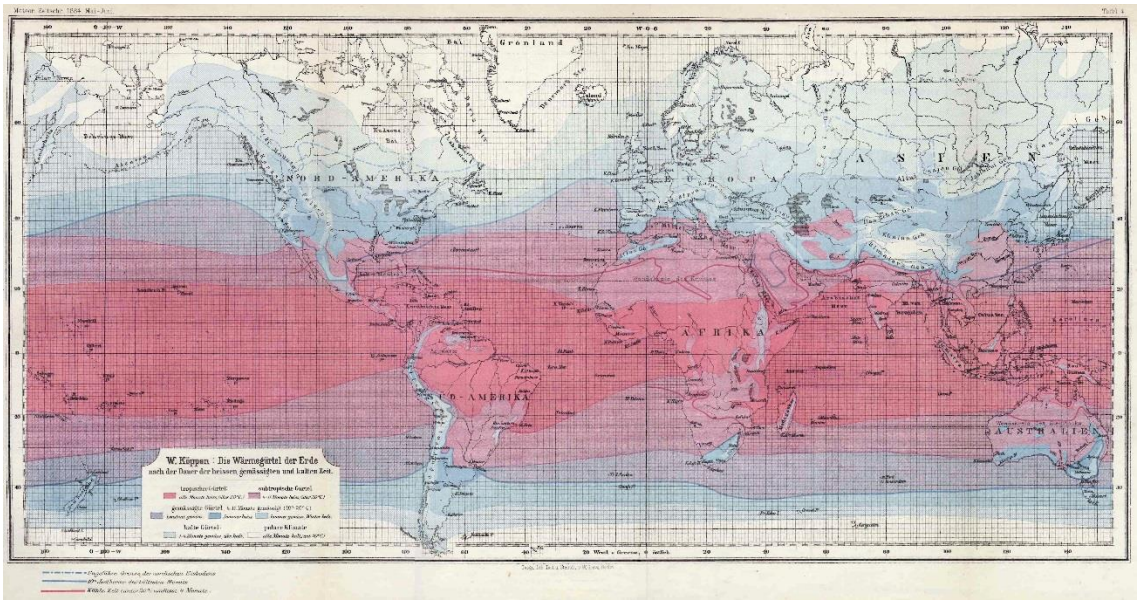

Fig. 3.4.1 The thermal zones of the Earth according to the duration of hot, moderate and cold periods (from Köppen 1884, translated in 2011)

Table 3.4.2 Climate types and subtypes defined by the Köppen climate classification (KCC) (Köppen 1936, from Belda et al. 2014)

Type/ Subtype	Criteria*
A	$T_{cold} > 18$ ℃; P_{mean} above value given for **B**
Af	$P_{mo} \geq 60$ mm for all months
Aw	$P_{mo} < 60$ mm for several months; dry season in low-sun period or winter half-year; annual rainfall insufficient to compensate this enough to allow forest
As	$P_{mo} < 60$ mm for several months; dry season in high-sun period or summer half-year; annual rainfall insufficient to compensate this enough to allow forest (occurs rarely)
Am	$P_{dry} < 60$ mm, rainfall in the rainy season compensates this enough to allow forest
B	P_{max} in summer: $P_{mean} < 2T + 28$; P_{max} in winter: $P_{mean} < 2T$; annual rainfall evenly distributed: $P_{mean} < 2T + 14$
BS	P_{max} in summer: $(2T + 28)/2 < P_{mean} < 2T + 28$ P_{max} in winter: $(2T)/2 < P_{mean} < 2T$ Annual rainfall evenly distributed: $(2T + 14)/2 < P_{mean} < 2T + 14$
BW	P_{max} in summer: $P_{mean} < (2T + 28)/2$ P_{max} in winter: $P_{mean} < (2T)/2$ Annual rainfall evenly distributed: $P_{mean} < (2T + 14)/2$
C	T_{cold} from 18 to −3 °C; $T_{warm} > 10$ ℃; P_{mean} above value given in B
Cs	Summer dry; wettest (winter) month must have more than 3 times the average rainfall of the driest (summer) month; $P_{dry} < 40$ mm
Cw	Winter dry; wettest (summer) month has ≥ 10 times the rainfall of the driest (winter) month
Cf	No dry season
D	$T_{cold} < -3$ °C; $T_{warm} > 10$ ℃; P_{mean} above value given in B
Ds	Summer dry (the same condition as in Cs) (occurs rarely)
Dw	Winter dry (the same condition as in Cw)
Df	No dry season
E	$T_{warm} < 10$ ℃
ET	0 ℃ < T_{warm} < 10 ℃
EF	Mean air temperature of all months < 0 ℃

* P_{max}: masimum annual precipitation rainfall; P_{mo}: monthly precipitation; T: mean annual temperature (℃); T_{mo}: mean monthly temperature (℃); P_{mean}: mean annual rainfall (cm); P_{dry}: monthly rainfall of the driest summer month; T_{cold} (T_{warm}): monthly mean air temperature of the coldest (warmest) month

Another updated Köppen-Geiger climate classification through a research team in Australia (KGC_{AU}) (Peel et al. 2007) is with the highest resolution compared to other classification, which is onto a 0.1 ×0.1 degree of latitude and longitude grid. The data set in KGC_{AU} is mainly in the period from 1909 to 1991 for precipitation and 1923 to 1993 for temperature. Through ***Table 3.4.3***, 30 possible climate types have been defined. The parameters applied in KGC_{AU} are the same with that in KGC, which are T_a and *RR*.

However, the method of the generalisation on the values are slightly different from that in KGC. For example, in the temperate climate zone **C** in ***Table 3.4.3***, T_a in the hottest month is above 10 ℃ and T_a in the coldest month is between 0 ℃ and 18 ℃ in KGC_{AU}; however, the climate zone **C** in KGC (***Table 3.4.1***) is defined as that the T_a in the coldest month is between – 3 ℃ and 18 ℃, which matches the climatic conditions in China better.

Table 3.4.3 Climate types and subtypes defined by the updated Köppen-Geiger climate classification (KGC_{AU}) (modified from Peel et al. 2007)

Type/ Subtype			Description	Criteria*
A			Tropical	$T_{cold} \geq 18$
	f		-Rainforest	$P_{dry} \geq 60$
	m		-Monsoon	Not (Af) &$P_{dry} \geq 100 - MAP/25$
	w		-Savannah	Not (Af) &$P_{dry} < 100 - MAP/25$
B			-Arid	$MAP < 10 \times P_{threshold}$
	W		-Desert	$MAP < 5 \times P_{threshold}$
	S		- Steppe	$MAP \geq 5 \times P_{threshold}$
		h	- Hot	$MAT \geq 18$
		k	- Cold	$MAT < 18$
C			- Temperate	$T_{hot} > 10$ & $0 < T_{cold} < 18$
	s		- Dry Summer	$P_{sdry} < 40$ & $P_{sdry} < P_{wwet}/3$
	w		- Dry Winter	$P_{wdry} < P_{swet}/10$
	f		- Without dry season	Not (Cs) or (Cw)
		a	- Hot summer	$T_{hot} \geq 22$
		b	- Warm Summer	Not (a) & $T_{mon}10 \geq 4$
		c	- Cold Summer	Not (a or b) & $1 \leq T_{mon10} < 4$
D			- Cold	$T_{hot} > 10$ & $T_{cold} \leq 0$
	s		- Dry Summer	$P_{sdry} < 40$ & $P_{sdry} < P_{wwet}/3$
	w		- Dry Winter	$P_{wdry} < P_{swet}/10$
	f		- Without dry season	Not (Ds) or (Dw)
		a	- Hot summer	$T_{hot} \geq 22$
		b	- Warm Summer	Not (a) & $T_{mon10} \geq 4$
		c	- Cold Summer	Not (a, b or d)
		d	- Very Cold Summer	Not (a or b) &$T_{cold} < -38$
E			Polar	$T_{hot} < 10$
	T		- Tundra	$T_{hot} > 0$
	F		- Frost	$T_{hot} \leq 0$

*MAP: mean annual precipitation; MAT: mean annual temperature; T_{hot}: temperature of the hottest month; T_{cold}: temperature of the coldest month; T_{mon10}: number of months where the temperature is above 10; P_{dry}: precipitation of the driest month; P_{sdry}: precipitation of the driest month in summer; P_{wdry}: precipitation of the driest month in winter; P_{swet}: precipitation of the wettest month in summer; P_{wwet}: Precipitation of the wettest month in winter; $P_{threshold}$: varies accoding to the following rules (if 70% of MAP occurs in winter then $P_{threshold} = 2 \times MAT$, if 70% of MAP occurs in summer then $P_{threshold} = 2 \times MAT + 28$, otherwise $P_{threshold} = 2 \times MAT + 14$).

The Köppen-Trewartha climate classification (KTC), as a modification from KCC, is performed by Trewartha at beginning (Belda et al. 2014). It means that KTC's criteria for distinguishing climate types have been modified based on the KCC. According to the study of Belda et al. (2014), the climate type and the characteristics of each climate type in KTC are cited in ***Table 3.4.4***. Meanwhile, the number of the climate types are less than that in KGC and KGC_{AU}.

Table 3.4.4 Climate types and subtypes defined by Köppen-Trewartha climate classification (KTC) (modified from Belda et al. 2014)

Type/Subtype	Criteria*
A	$T_{cold} > 18$ ℃; $P_{mean} \geq R$
Ar	10 to 12 month wet; 0 to 2 month dry
Aw	Winter (low-sun period) dry; > 2 months dry
As	Summer (high-sun period) dry; rare in type Aclimates
B	$P_{mean} < R$
BS	$R/2 < P_{mean} < R$
BW	$P_{mean} < R/2$
C	$T_{cold} < 18$ ℃; 8 to 12 months with $T_{mo} > 10$ ℃
Cs	Summer dry; at least 3 times as much rain in winter half-year as in summer half-year; P dry < 3 cm; total annual precipitation < 89 cm
Cw	Winter dry; at least 10 times as much rain in summer half-year as in winter half-year
Cf	No dry season; difference between driest and wettest month less than required for Cs and Cw; P_{dry} >3 cm
D	4 to 7 months with $T_{mo} > 10$ ℃
Do	$T_{cold} > 0$ ℃ (or > 2 ℃ in some locations inland)
Dc	$T_{cold} < 0$ ℃ (or < 2 ℃)
E	1 to 3 months with $T_{mo} > 10$ ℃
F	$T_{warm} < 10$ ℃
Ft	$T_{warm} > 0$ ℃
Fi	$T_{warm} < 0$ ℃

*T: mean annual temperature (℃); T_{mo}: mean monthly temperature (℃); P_{mean}: mean annual rainfall (cm); P_{dry}: monthly rainfall of the driest summer month; R: Patton's precipitation threshod, defined a $R = 2.3T - 0.64Pw + 41$, where Pw is the percentage of annual precipitation occurring in winter; T_{cold} (T_{warm}): monthly mean air temperature of the coldest (warmest) month

To the end of the section 3.4, ***Table 3.4.5*** summarises five aspects of the difference between the thresholds of the versions upwards. Due to the advantages of KGC which has been mentioned in the introduction of KGC, and in the comparison between KGC and other classifications, KGC has been selected as the reference climate classification in

current study.

Table 3.4.5 Comparison of each version in five aspects of difference

Version	Categories of main type	Levels of subtypes	Amount of all climate type	Parameter	Main data type
KCC	5	2	14	T_a & RR	Average value
KTC	6	2	13		
KGC	5	3	31		
KGC_{AU}	5	3	30		

3.5 Meteorological analysis on meso scale

In meteorological analysis, the atmosphere phenomena on meso scale in horizontal are defined as the phenomena in the range of 10^4 to 2×10^5 (m) (Oke 2002). Regarding the meteorological application, there are both simulated analysis (e.g. regional weather forecast) and measured data at concerning places which are the fundament of the simulation, and other utilisation (e.g. historical analysis).

According to the handbook from World Meteorological Organisation (WMO-No. 8) (Jarraud 2008), the weather and climate are influenced on meso scale by the whole city area; thus, for detection of the accurate meteorological conditions of a city, normally a single station is not appreciate. Under the relative sufficient support of the stations, for instance in the study of urban heat island effect (UHI) in New York City (NYC) (Gedzelman et al. 2003), the UHI has been analysed based on the data from 50 volunteer stations and 25 national weather service stations. As a high developed urban area, the number of the weather station in NYC is not a single one, but has reached to 25 (national level) which formed the meso-scale network for NYC at least 20 years ago, i.e. the analysis concentrated on the scope within meso scale, but the data resource was with higher resolution. Therefore, the data from the network guarantees the more accurate meteorological analysis, comparing with the cities which own much less weather stations. In the modelling meteorological analysis on meso scale regarding the distinguish and forecast atmosphere phenomenon (Pielke Sr 2013), the data from multiple weather

stations are significant for construction of the realistic meteorological conditions (Warner and Seaman 1990; Manobianco et al. 1996; Steinacker et al. 2006); thus, the higher resolution of the data resource will support the more accurate simulation on meso scale.

However, in other cities or larger regions, due to the lack of financial or technical supports, the multiple stations may be not sufficient for forming the similar network as that in NYC. Considering the city with less stations, if the standard meet the requirement of the handbook from WMO , the data analysis based on the first order stations is still acceptable (Jarraud 2008). Hence the data from the single station has been applied in a number of studies related to the basic meteorology and biometeorology in cities or regions. For instance, in the study focusing on the mortality in Shanghai, China, one set of meteorological data from Shanghai Meteorological Bureau has been applied to describe the basic meteorological conditions in Shanghai, which is mainly based on the daily average T_a in summer from 1989 to 1998 (Tan et al. 2004). The measured data from an urban climate station in Freiburg, Germany, which present the background conditions at the urban climate station, has been utilised as the comparison for the effects of the urban configuration (Herrmann and Matzarakis 2012). The data from one station located at the airport climate station of Doha, State of Qatar, has been accepted for the analysis of the hot and windy conditions of the city, which is mainly focus on the sensitivity of the 3 HTC indices under the background meteorological conditions in Doha (Fröhlich and Matzarakis 2015). Currently in China, the data from the national level stations, whose quality is guaranteed, is used for the international data exchange. Through the comparing between National Meteorological Information Centre of China (http://data.cma.cn/) and Ogimet (http://www.ogimet.com/), a free website for Weather Information Service, the same station codes can be found.

3.6 Meteorological analysis on local scale

In meteorological analysis, the local scale in horizontal is defined as the study on the atmosphere phenomena in the range of 10^2 to 5×10^4 (m) (Oke 2002). This scale is applied popularly in the urban climate study, because the meteorological conditions in a whole city has been started to distinguished, for example, between different urban districts.

Inside one city, there are diverse land cover use, such as business centres, residential district, green spaces, and industrial district. According to the classification on Local Climate Zones (LCZs) (Stewart and Oke 2012), the regions ranged from hundreds of meters to several meters have been grouped depending on the uniform surface cover, structure, material and human activity. Following the guidelines, this LCZs system can be applied for urban climate studies in specific urban districts, as each LCZ is assumed with the homogeneous environments in the range of 10^2 to 5×10^4 (m). In order to apply this LCZs system, it is necessary to be familiar with the table on the definitions of LCZs (Stewart and Oke 2012), and the tables on all properties of each LCZ (Stewart and Oke 2012), which include geometric, surface cover, thermal, radiative properties. LCZs will present the homogeneous conditions of the atmospheric phenomena on micro scale in each LCZ.

Based on the local scale, Urban Climate Maps (UCMap) system (Ren et al. 2011) is similar application of the study on this scale. In order to give a full view of the urban climate, the UCMap system contains two parts: the urban climatic analysis maps and the urban climatic recommendation maps (Ren et al. 2012). Based on the Geographic Information System (GIS), for example, the UCMap system has been applied to analyse the urban climate in the Municipality of Arnhem, Netherlands (Ren et al. 2012). The biometeorological analysis in day and at night has applied the mapping method to illustrate the PET distribution, and distinguished the different thermal stress zones in Freiburg, Germany (Matzarakis et al. 2008). This mapping method has also been applied to analyse the HTC conditions (based on PET) in July in Göteborg, Sweden (Svensson et

al. 2003). In this study, the land cover is categorised into urban dense area, multi-family area, single house area, industry area, and green space.

3.7 Meteorological analysis on micro scale

In meteorological analysis, the micro scale in horizontal is defined as the study on the atmosphere activities in the range of 10^{-2} to 10^{3} (m) (Oke 2002). The resolution of the study range is smaller and more precisely than that on local scale. Therefore, the meteorological variations between different positions (e.g. under the canopy of a tree, between buildings, or on the football playground) will be considered in a more sensitive level, especially for the radiant conditions and the air movement.

In order to obtain micrometeorological data for site analysis, computer simulations with high resolution and measurements in certain places are always performed. Depending on different purposes, these two operations could be combined together, or performed separately.

3.7.1 Computer simulations in urban areas

Based on the development of the computational technology, simulation of the micrometeorology has been one momentous approach for meteorological analysis. Currently, there are some models or approaches which have been applied to simulate the micro meteorological conditions, such as RayMan Model, SOLWEIG, CFD, SkyHelios, and ENVI-met.

RayMan Model (Matzarakis et al. 2007, 2010) can estimate the Sky view factor (SVF) with relative easy way on building-layout input, and the model can also calculate thermal indices, as well as the radiant conditions, with necessary input parameters. Matzarakis and Rutz (2005) applied RayMan model to estimate the sun path and SVF of a complex environment in Freiburg, Germany, and to calculate the thermal indices for Athens, Greece for the period of 1955–2001. The more details on building environments

(buildings and trees) and the distribution of shadow based on applications of RayMan model have been completed in another research paper (Matzarakis et al. 2006). Lin et al. (2010a) have done a research especially focused on shading effect on outdoor thermal comfort based on RayMan model. The results in this study indicate that barely shaded conditions in Taiwan cause discomfort in summer, and highly shades conditions cause discomfort in winter.

The Solar Longwave Environmental Irradiance Geometry model (SOLWEIG) focuses on simulating the 3-dimensional (3D) fluxes of long-wave and short-wave radiation of a specific environment, consequently the model can calculate the T_{mrt} (Lindberg et al. 2008). SOLWEIG has been utilised for simulations of 3D radiation fluxes and T_{mrt} in complex urban settings in three European cities, meanwhile T_{mrt} and shadow effects have been estimated through this model (Lau et al. 2014). This research finds that severe heat stress exists in all cities; however the conditions in dense urban structures are milder than the conditions in open areas. The similar application of SOLWEIG for calculation of SVF has been performed by Konarska et al. (2015).

Computational Fluid Dynamics (CFD), which focuses on simulating the fluid flows, is widely applied for the simulations of wind conditions in urban meteorological studies (Hirsch 2007). Based on two different modelling approaches, Gousseau et al. (2011) have applied CFD to evaluate the pollutant dispersion in street valleys for pedestrian, and the two approaches have been also compared. Blocken et al. (2013) have summarised 16 papers in total, which are mostly related to the micro-scale pollutant dispersion based on CFD simulations.

SkyHelios, based on the simulation of continuous SVF and wind, can estimate the radiant environment and wind conditions on micro scale or in complex urban areas (Matzarakis and Matuschek 2011). With the respect to features of the spatial urban climate, SkyHelios has been developed (Matzarakis et al. 2015). SkyHelios can be used as a tool for the quick overview of the SVF (Fröhlich and Matzarakis 2013), and this model has also been

applied to estimate the SVF of one part of Freiburg, Germany, with the resolution of 1 (m) × 1(m) at the height of 1 (m) (Matzarakis et al. 2015).

ENVI-met is a 3D model which combines the simulations on radiant conditions, air flows, vegetation effects, energy balance of soil, as well as thermal indices (Bruse 2004). According to the updated introduction from the homepage of the numerical model (http://www.envi-met.com/), ENVI-met is designed for environment analysis in meteorological aspects. Through the application ENVI-met simulation for the campus of National University of Singapore, the cooling effect of the dense green space has been proofed; meanwhile the weaker cooling effect has been detected in the area with higher building density (Wong et al. 2007). The application of ENVI-met for the evaluation of a redesigning open space in Freiburg, Germany, indicates that the more frequent thermal heat stress will be caused by the less tree cover space; meanwhile, the water body has not shown the cooling effects around itself (Fröhlich and Matzarakis 2013).

From ***Table 3.7.1***, the brief comparison between the 5 models/approaches has been presented, which focuses on the concentrated aspects of each model.

Table 3.7.1 Concentrated aspects of 5 simulation models/approaches in urban climate

Model	**Concentration**
RayMan	Radiant environment, calculation of HTC indices
SOLWEIG	Radiant environment, calculation of T_{mrt}
CFD	Meteorological parameters related to fluid flow on micro scale
SkyHelios	Estimation of SVF, wind conditions and radiant environment of complex urban area, calculation of thermal indices
ENVI-met	Microclimatic parameters of specific urban area

3.7.2 Analysis through measurements in urban areas

Field measurement is another approach to obtain the actual data of the particular conditions. Meanwhile, the collected data can also be used for validation of simulations (Huttner 2012).

In the study of the campus of National University of Singapore (Wong et al. 2007), the field measurements have been carried out in different sites (e.g. bio-information centre, medicine car park and sports field), which present the different T_a values at the same point in time in 15th September 2005. The comparison between the measured near surface temperature and simulated near surface temperature in a study present the better agreement during the daytime (Chow and Brazel 2012).

3.8 The residential district with high-rise buildings

The progress of the construction techniques has conditioned the building style enormously, and the permitted building stories have been increased. According to the General Principles for the design of civil buildings in China (GB 50352-2005), if there are 10 stories or more than 10 stories in the residential building, this building belongs to the high-rise building. The high-rise buildings have turned to be one of the main building styles in a number of cities, especially in the process of urban redevelopment (Reddy 1996). In the last decades, due to the increase of population (related to the high demand of houses), and the development of the economy, the requirements of efficient land use have been complied through the widely construction of high-rise buildings in Asian countries, in which China is included (Niu 2004; Chen et al. 2008). In consequent, the living pattern has been influenced by high-rise buildings, especially in the mega cities in China. In Shenzhen, according to the research of Wai (1994), the high-rise building is one of the basic building style. Meanwhile, the density of population increased dramatically. For example in Shanghai, the urban area has been mainly constructed with high-rise buildings for the past few decades (Tang et al. 2008; Yang et al. 2010), and the density of urban area in Shanghai has reached to 21,283 people/km^2.

Based on the definitions in LCZs system (Stewart and Oke 2012), it can be found that the high-rise building has strong influences on the urban climate. According to the satellite-

based studies on the UHI during day and night, the area with high-rise buildings presents the different thermal environments compared to other land cover (e.g. low rise bungalow residential area, and bus depot) (Nichol 2005). The study of the influence of urban morphology and sea breeze on urban climate points out that the urban structure influence the daytime temperature significantly, and the high ratio of the height of the building to the width of the building can reduce the maximum daily temperature, i.e. the maximum daily temperature can be reduced in the area with high density of buildings; meanwhile, the wind speeds may also be reduced in the area with high density of buildings (Emmanuel and Johansson 2006).

3.9 Community environment design in residential district

Normally, the high-rise buildings for residences are constructed in a group in China, i.e. a residential district. The community environment outdoors is the most important public space of the residential district, where the functions for residents (included daily sport, entertainment, and transport) are supported. Consequently, there is the common idea that the design for community environment should fulfil the residents' needs (Jacobs and Appleyard 1987; Han-fei 2002). Furthermore, an optimal design of the community environment has been regarded as one of the most important parts in the residential real estate. Because of the rapid urbanisation and the decrease of the nature space in urban area, the natural scenic view and the possibility of utilisation of the natural landscape became the important aspect in residential district. According to a study, which is based on the analysis of the transaction for the apartments in high-rise buildings in Hong Kong, where the high-rise buildings were the typical building style for middle-income dwellings (Jim and Chen 2009), the home-buyers would like to pay higher price for the good harbour view; meanwhile, the transaction fee increases, when the distance between the apartment and the preferred natural landscape decreases. The studies in the literature review from Maller et al. (2006) indicates that the nature resource has significant effect

on promoting the public health. Actually, according to opinion of Howard for the garden city, the nature resource has already been regarded as a kind of guarantee for human health (Howard 2010; Frank et al. 2003). As the public space of the residential district is easy reaching, the nature resource in this area is important for the residents, and the quality of the nature resource is decided in the design phase. Therefore, an optimal design of community environment would perform a convenient outdoor space for the residents.

In order to form a liveable community environment, there are a number of popular and necessary elements (e.g. trees, hedges, grass, and water bodies) which are utilised to back the community environment design (Booth 1989). According to the field study in Hong Kong, the increase of the tree cover can mitigate the UHI during daytime, and the shrub cover in this study has more effective cooling effect than tree cover in the certain areas (Giridharan et al. 2008). The cooling effect from trees, for example, has also demonstrated in the study from Shashua-Bar and Hoffman (2000), in which a series of observations were performed along an avenue. In another study (Hamada and Ohta 2010), the cooling effect from green space has been analysed based on seasonal changings, and the spatial changing (i.e. the distance from green space). The effect of grass in microclimate has been detected, based on the comparison between bare ground and grass cover; and the cooling effect has been found, but in a limited height (Champness 1950). Water bodies has been proposed to be placed in the narrow domains in urban area, because the cooling effect has been measured in field studies (Nishimura et al. 1998). Another study through modelling the influence of trees and the water pond on microclimate between buildings, announces that the water bodies should be applied in outdoor space design due to the abilities on improvement of microclimate (Robitu et al. 2006).

However, in a long period, the design principles mainly considered on the aspects of aesthetic and the functions related to the local culture and custom (Rogers 2001); in contrasted, the meteorological impact on the outdoor thermal environment has been considered negligently in practice. Towards the insufficient consideration of HTC

conditions in the community environment design, there are attempts focusing on the analysis and evaluations of the micro climate (Johansson and Emmanuel 2006; Picot 2004; Upmanis et al. 1998). According to LCZs system, there are two LCZs related to high-rise building, which are LCZ 1 and LCZ 4 (Stewart and Oke 2012), which formed the diverse heat transfer patterns related to the radiant conditions, and air flow; and consequently the micro climate inside the district with high-rise buildings are affected synchronously. As the design elements can improve the thermal environment outdoors, the HTC analysis together with the meteorological analysis on micro scale for the certain open space are helpful for landscape architectural designers. The related aspects of the evaluation on the outdoor environment design has been presented in ***Fig. 3.9.1***.

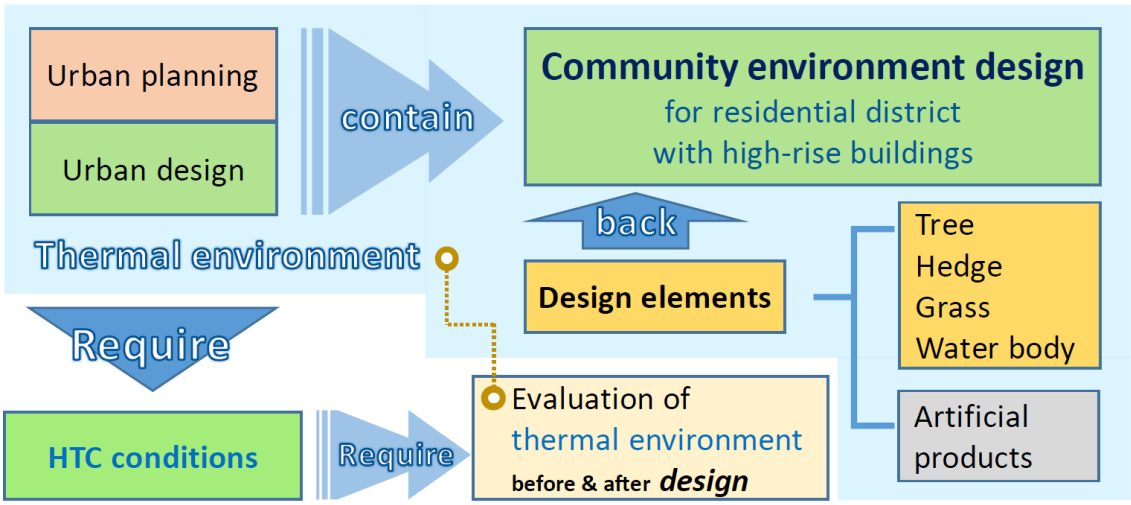

Fig. 3.9.1 Connection between the evaluation of thermal environment and community environment design

The state of art releases the possible correlation between the human-biometeorological information and the different topics (please see ***Table 3.9.1***). The possible correlation indicates the potential of the biometeorological information in serving the sustainable development of cities, regions, and countries.

Table 3.9.1 Overview of state of the art in current study

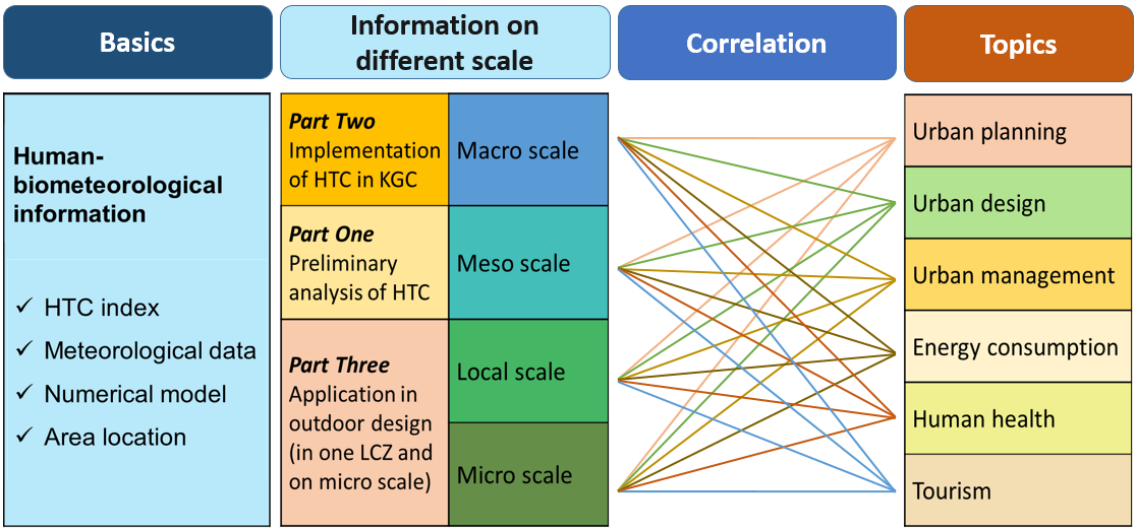

4 Study areas

The 12 Chinese cities introduced below are the study cities in this study. Together with ***Fig. 4.1.1*** and ***Table 4.1.1***, the description mainly focuses on the geographical conditions[4]. According to KGC, the climate type has been added individually after each city in the bracket.

Sanya (Aw) is one of the most famous tourist destination cities in China; it is located at the mountainous southern edge of the Hainan province facing the South China Sea. The terrain slopes slightly from north to south and the main urban area is protected from sea breeze by the hills from the south and southeast.

Qionghai (Am) is a small city, but has been the permanent site of Boao Forum for Asia (BFA). It is located at the eastern edge of Hainan Province and close to the South China Sea. The whole urban area is nearby the coast, and it is encircled by Wanquan River.

Shenzhen (Cwa) is a coast city of Guangdong Province in the south, and it is located at the south of the Tropic of Cancer, as well as at the east bank of Zhujiang River. Connecting to the South China Sea, it faces Mirs Bay and Daya Bay to the east, Shenzhen Bay and Zhujiang River Estuary to the southwest, respectively. It neighbours to Hong Kong to the south. The terrain in the southeast is higher than that in the northwest, but most of the area is formed by low hills and mesas. Only a small part of the terrain is made-up of flat plains.

Kunming (Cwb) is the capital of Yunnan Province and it is surrounded by mountains. The major terrain of the city is a basin, and it is also located on the middle part of Yunnan-Guizhou Plateau. From north to south, the topography becomes lower tier by tier. Dian Lake — the biggest Lake in Yunnan Province — is at the southwest of Kunming.

---

[4] These geographical features are obtained through observation in the online google map and online Baidu map, in which the name of special areas, the altitudes and the coverage of vegetation are available.

Placed inside Lhasa River Valley from east to west, Lhasa (Dwc) is the capital of the Tibet Autonomous Region. It is located in the central Qinghai-Tibet Plateau. The northern area of Lhasa is constituted by the southern edge of the alpine steppe which is the property of the northern Tibet Autonomous Region.

Shanghai (Cfa) lies in the area between the Yangtze Estuary to the north and Hangzhou bay to the south. It borders Jiangsu Province and Zhejiang Province to the west, and faces the East China Sea (Pacific Ocean). The terrain of Shanghai is part of the Yangtze River Delta Fluvial Plain. There are several little hills in the west.

Yuncheng (BSk) is a city surrounded by the Yellow River from west to south, and it is located in the south of Shanxi Province. It is situated along the Lvliang Mountain to the north, and the Zhongtiao Mountain to the east, respectively. Within a flat urban area, there are several salt lakes and salt shoals, of which Xiechi is the largest lake.

At the upper reaches of the Yellow River in the northwest of China, Yinchuan (BWk) lies in the middle of the Ningxia Plain. To the east of the urban area, the Yellow River goes through Yinchuan (BWk) from the southwest to the northeast. The city stretches along the Helan Mountain from north-north-east to south-south-west. The terrain in Yinchuan slopes slightly from southwest to northeast.

Dalian (Dwa) lies at the southern end of Liaodong Peninsula. The northwest side of Dalian faces the Bohai Sea and the southeast side faces the Yellow Sea. There are many rivers flowing through Dalian, which then flow into the Bohai Sea and the Yellow Sea, respectively. A branch of the Changbai Mountain Range is part of Dalian. Most of the terrain is mountainous, except the parts along estuaries, which are flat plains. The elevation in the north is higher than that in the south, and it slopes slightly from the centre to west and east.

Beijing (Dwa), as the capital of China, is located in the North China Plain, as well as in the Bohai Bay Basin. The west and the north of Beijing are mostly flat plains. These two

areas are circled by a branch of the Taihang Mountain Range and by a branch of the Yanshan Mountain Range, respectively. A large area of Beijing is mountainous.

Hohhot (Dwb) is the capital of the Inner Mongolia Autonomous Region, and it is located in the southern part of the centre. The whole area is formed of two types of terrain, which are mountainous in the north (Yin Mountains) and southeast (Manhan Mountain), and flat plain in the south and southwest, respectively. The elevation becomes lower from northeast to southwest. There are three little streams within the urban area.

Situated in the hinterland of the Eurasia Continent, Urumqi (Dfb) is the capital of Xinjiang province. It is located at the northern foot of the Tianshan Mountains and at the south edge of the Zhungeer Basin. The city with partly hilly terrain is surrounded by mountains in three directions—east, south and west. In the north, a small area of the city is flat plain.

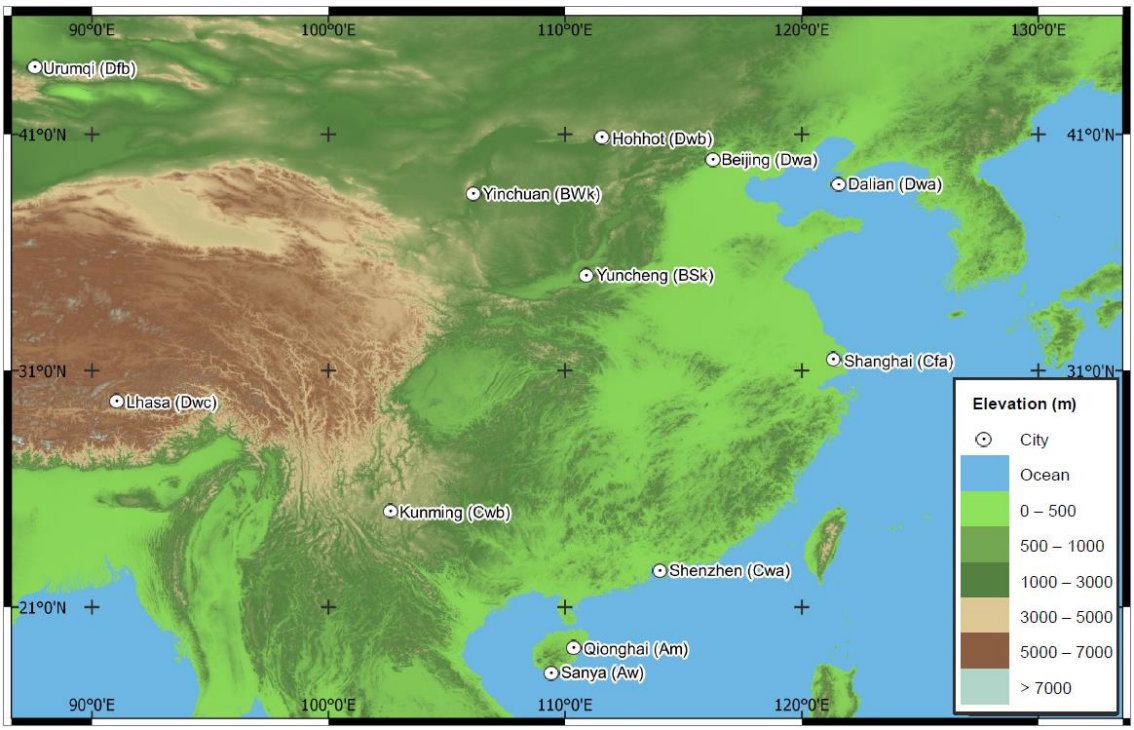

Fig. 4.1.1 Location of 12 Chinese cites (Elevation data from China Geospatial Data Cloud)

Table 4.1.1 Basic information of 12 Chinese cities

City	KGC type	Elevation (m)	Weather Stations' Location	
			Latitude (N)	Longitude (E)
Sanya	Aw	7	18°14'	109°31'
Qionghai	Am	25	19°14'	110°28'
Shenzhen	Cwa	18	22°33'	114°06'
Kunming	Cwb	1892	25°01'	102°41'
Shanghai	Cfa	8	31°24'	121°28'
Dalian	Dwa	97	38°54'	121°38'
Beijing	Dwa	55	39°56'	116°17'
Hohhot	Dwb	1065	40°49'	111°41'
Lhasa	Dwc	3650	29°40'	91°08'
Urumqi	Dfb	919	43°47'	87°37'
Yuncheng	BSk	376	35°02'	111°01'
Yinchuan	BWk	1112	38°29'	106°13'

5 Data and Methods

As the research is comprised of three parts which are associated with each other, there is relevance in the section of data and method. In Part One (Preliminary analysis), the 12 cities were regarded as the cities self; in Part Two (Implementation of HTC in KGC), they were assumed to be the representations of the climate types where they were located in; in Part Three (Application in outdoor design), the meteorological data of the 12 cities are used for preparing the reasonable input of the numerical simulations. Due to the significant of each part, the data and method were considered separately.

5.1 Preliminary analysis of HTC on meso scale

5.1.1 Selection of study cities

In this study, the KGC has been used as the reference on different climate types. 11 climate types in the KGC, which are Aw, Am, Cwa, Cwb, Cfa, Dwa, Dwb, Dwc, Dfb, BSk and BWk, have been chosen for the selection of the study cities. Basically, one city has been selected in each climate type, respectively. As the topographical features are complex in climate type Dwa in China, two cities have been selected in this climate type. The first reason of selecting these cities in each climate type is the high population. Moreover, some of these cities are the capital of a province (Beijing, Hohhot, Kunming, Lhasa, Shanghai, Urumqi and Yinchuan), some of them are the central cities of economy and culture (Dalian, Sanya, Shenzhen and Yuncheng). The area of climate type Am in China is not as large as others, and Qionghai, as a new developing city in this climate type, has been selected. In order to depict the location of each city in each KGC type, the digital map of KGC (1976─2000) has been download (http://koeppen-geiger.vu-wien.ac.at) and edited especially for this study. The resolution of this map is 0.5 degree of latitude and longitude. Based on the application of QGIS, the visualisation of the location has been completed. Therefore, 12 cities in total have been obtained from south to north in China: Sanya (Aw), Qionghai (Am), Shenzhen (Cwa), Kunming (Cwb), Lhasa (Dwc), Shanghai

(Cfa), Yuncheng (BSk), Yinchuan (BWk), Dalian (Dwa), Beijing (Dwa), Hohhot (Dwb) and Urumqi (Dfb).

The 3-hourly meteorological data (with low missing values), together with the location of these weather stations, has been obtained from "OGIMET" (http://www.ogimet.com/). This website collects climatic data mainly from National Oceanic and Atmospheric Administration (NOAA). The points in time of the data set are 2:00, 5:00, 8:00, 11:00, 14:00, 17:00, 20:00 and 23:00 in Local Standard Time (LST). The period of this data set is from 2000 to 2012. Due to the relocation of the weather station of Sanya in 2009, the meteorological data from 2000 to 2008 has been applied in this study for Sanya (Aw).

5.1.2 Calculation of PET

Due to the applications in practice (Svensson et al. 2003; Röckle et al. 2003; Li and Chi 2014; Matzarakis et al. 2008) and broadly research (Höppe 1999; Lin and Matzarakis 2008; Lai et al. 2014), PET has been utilised to quantify the HTC conditions in this study. RayMan model (Matzarakis et al. 2007, 2010) has been applied to calculate PET values which are also with 3-hour resolution from 2000 to 2012. The calculation of PET, which is according to the definition of PET (VDI 1998; Höppe 1999), is based on the default thermo-physiological conditions of a standard human being, and 4 meteorological parameters.

The standard human being is a 35-year-old man with height of 1.75 (m) and weigh of 75 (kg). Meanwhile, this human being is standing with the clothing insulation at 0.9 (*clo*) and activity level at 80 (W).

The 4 meteorological parameters are as following:

Air temperature (T_a)

Vapour pressure (*VP*)

Wind velocity (v) at 1.1 (m)

Mean Radiant Temperature (T_{mrt}) at 1.1 (m)

The original data of wind v is at 10 (m), however, the v at 1.1 (m) can be converted from the v at 10 (m) through a series formulas (Matzarakis et al. 2009) which have been accepted broadly in urban climatic studies.

T_{mrt} can be calculated within the same run of calculation of PET in RayMan model, which obtained reliable results (Matzarakis et al. 2010). The required meteorological data for the calculation of T_{mrt} is T_{a}, VP, v, and cloud cover degree (Matzarakis et al. 2007). The other meteorological parameters, such as wind direction (WD), relative humidity (RH) have been analysed together, due to the importance in HTC study.

The calculation of PET is one kind of complex process, and the data set in current study is large; therefore, the RayMan model (which has been introduced in section 3.7.1) has been regarded as the fundament for the calculation.

5.1.3 Detection of the daily warmest time

Beanplots are a handy method to give a visual distribution of univariate data, especially when there are multiple batches (Kampstra 2008). One beanplot can show every individual value of any parameter with small lines in a one-dimensional scatter diagram. Moreover, beanplots can also show the total average line and the single bean average line. Its feasibility for the application has been proved in the analysis of HTC (Muthers and Matzarakis 2010). In order to detect the warmest point in time in each city, T_a, T_{mrt} and PET have been organised into 8-point-in-time batches, respectively. For example, all 3-hour T_a values in 2000─2012 have been grouped as values at 2:00, 5:00, 8:00, 11:00, 14:00, 17:00, 20:00 and 23:00 in LST, respectively. The distribution of each parameter at each point in time has been directly visualised. T_a, T_{mrt} and PET separately construct the univariate data. Meanwhile, the boxplots, a traditional method in statistic, have been combined with beanplots for presenting the statistical characteristics of each diagram. Afterwards, the relative warmest point in time has been detected, and the HTC conditions have been summarised.

5.1.4 Analysis of the HTC conditions

Based on the selected warmest point in time (which is 14 LST), the monthly HTC conditions have been analysed through monthly frequencies of actual PET at 14 LST in different value classes. The meaning of the data at the warmest point in time (or the warmest period) can be regarded as the possibly alerting time at which the daily extreme heat stress may appear. The value classes for PET (℃) and the associated HTC conditions (please see ***Table 5.1.1***) were based on the classification of thermo-physiological stress for PET from Matzarakis and Mayer (1996) (please see ***Table 3.2.1***). In Part One (Preliminary analysis), the summarised HTC conditions (please see ***Table 5.1.1***) have been applied as additional value classes for analysis, as well as the comparison of data trend in each city. Therefore, in current study, the HTC conditions which are very hot and hot, have been defined as the HTC conditions with heat stress; the HTC conditions which are slightly warm, neutral and slightly cool, have been regarded as the acceptable conditions; and the HTC conditions which are very cold, have been labelled as the HTC conditions with cold stress.

Table 5.1.1 PET value classes and HTC conditions (modified after Matzarakis and Mayer 1996)

PET	**HTC conditions**	**Summarised HTC conditions applied in current study**
Below 0 ℃		Cold stress[+]
Below 4 ℃	Very cold	Cold stress
4 — 8 °C	Cold	
8 — 13 °C	Cool	
13 — 18 °C	Slightly cool	
18 — 23 °C	Neutral (comfortable)	Acceptable conditions
23 — 29 °C	Slightly warm	
29 — 35 °C	Warm	
35 — 41 °C	Hot	Heat stress
Above 41 ℃	Very hot	

Meanwhile, the annual analysis of the HTC conditions in each city has been completed through the statistic of the days with specific HTC conditions at 14 LST. As the extreme cold conditions (i.e. PET < 0 ℃) existed frequently in several cities, e.g. Yinchuan (BWk), Beijing (Dwa), Dalian (Dwa), Hohhot (Dwb) and Urumqi (Dfb), the HTC conditions with cold stress$^+$ (PET < 0 ℃) were applied in this study for the statistic of days, in order to distinguish the HTC conditions between each city. Thus the calculation of the days with heat stress, the acceptable conditions, and cold stress$^+$, was based on the three value classes, which are PET above 35 ℃, PET between 13 ℃ and 29 ℃, and PET below 0 ℃.

5.1.5 Analysis of related meteorological parameters

Due to the effects on HTC conditions, the monthly frequencies of T_a, T_{mrt}, *VP* and *RH* at 14 LST were analysed as the accessorial HTC information. The value classes of T_a and T_{mrt} were the same as that of PET which are 9 value classes, therefore it was easy to compare the variations of the values of these three parameters. The value classes for *VP* (hPa) were modified after the Sun Moon Lake study (Lin and Matzarakis 2008). According to the research related to relative humidity (*RH*), the comfortable *RH* range is from 30% to 60% around 25 ℃ indoors (ASHRAE 1992; Wolkoff and Kjærgaard 2007; Balaras et al. 2007). Then 10% intervals when *RH* was above 30% and 15% intervals when *RH* was below 30% were applied here for aggregating *RH* data. Results of *VP* and *RH* were organized into two tables, in order to describe the days per year of different value ranges in each city, and to compared the AH conditions between cities.

The data with 3-hour resolution has been used to describe the wind conditions at 1.1 (m) in each city, because of the temporal and spatial instability of *v* and WD, respectively. Wind rose with 16 directions has been chosen to show the conditions of wind in each city. The *v* values in wind roses (unit: m/s) have been categorised by 0.5—1.5, 1.5—2.5, 2.5—4.5 and above 4.5. The bar chart of the monthly frequencies of *v* in each city has also been performed. The *v* values in bar chart (unit: m/s) have been categorised by below 0.5, 0.5—1.5, 1.5—2.5, 2.5—3.5, 3.5—4.5 and above 4.5, which are modified after the value

classes in wind rose.

5.2 Implementation of HTC in KGC on macro scale

5.2.1 Analysis of parameters in KGC

First of all, in order to link HTC information with KGC in a corresponding form, the parameters and time scales, which are utilised in the threshold of KGC, have been analysed. Air temperature (T_a) and precipitation (*RR*) are the two parameters used to indicate hot/cold climatic conditions and wet/dry climatic conditions in KGC, respectively. Due to the characteristics of PET (which indicates human thermal conditions) and *VP* (which can indicate AH conditions), hot/cold conditions can be described by PET, and wet/dry conditions can be described by *VP*. Meanwhile, the time scales in KGC are mainly the annual period, the warmest month, the coldest month and the driest month. Therefore, the thermal comfort conditions can be organised with the similar time scales in KGC, which are the annual period, the hottest month, the coldest month, the wettest month, and the driest month.

5.2.2 Obtainment of data

In this study, 12 Chinese cities (***Fig. 4.1.1*** and ***Fig. 6.1.1***) have been continually utilised as the preliminary representations of 11 KGC types, respectively. Two cities, i.e. Beijing and Dalian, have been regarded as the two representations for the KGC type Dwa as comparisons, due to the complex topographical situation in this climate type in China. The 11 KGC types (12 cities) are Aw (Sanya), Am (Qionghai), Cwa (Shenzhen), Cwb (Kunming), Cfa (Shanghai), Dwa (Beijing), Dwa (Dalian), Dwb (Hohhot), Dwc (Lhasa), Dfb (Urumqi), BSk (Yuncheng) and BWk (Yinchuan). In order to fulfil the new requirements of information on macro scale, the data of 11 KGC types (12 cities), i.e. 3-hour PET and 3-hour *VP* in 2000─2012 (2000─2008 in Sanya), has been analysed.

5.2.3 Linking HTC information with each KGC type

Quantification of the HTC conditions for each KGC type is the key step in this study. According to the quantifications of PET and *VP*, which associate to T_a and *RR*, respectively, the HTC conditions of each KGC type will be described by distribution of data. As data with 3-hour resolution in a long-term period for each KGC type is one kind of large data set, frequencies can better present the actual distribution of the data set. Therefore, the linking phase will be achieved by adding specific frequencies of PET and *VP* to 11 KGC types.

5.2.4 Categorisation of data

Three-hour PET values and *VP* values of each KGC type have been categorised by frequencies of 3-value classes and 4-value classes, respectively. The 3-value classes for PET are ≤ 8 °C, 8—35 °C, and > 35 °C. It is a modification of the classification of thermo–physiological stress for PET (Matzarakis and Mayer 1996). The 4-value classes for *VP* are ≤ 6 hPa, 6—12 hPa, 12—18 hPa, and > 18 hPa. This category is based on the Sun Moon Lake study (Lin and Matzarakis 2008).

Meanwhile, these frequencies have been grouped by 5 time scales: the annual period, the hottest month, the coldest month, the wettest month and the driest month. The annual period can present the entire HTC conditions throughout the whole year. The last 4 time scales can present the extreme conditions (i.e. the hottest, the coldest, the wettest, and the driest) in one year for each climate type.

The final frequencies of PET and *VP* will be calculated according to the ranges from the value classes and the time scales. Therefore, 6 kinds of frequencies will be added to each climate type: (1) **annual** frequencies of **PET** within 3-value classes (**PET_a**), (2) frequencies of **PET** in the **hottest** month within 3-value classes (**PET_h**), (3) frequencies of **PET** in the **coldest** month within 3-value classes (**PET_c**), (4) **annual** frequencies of ***VP*** within 4-value classes (**VP_a**), (5) frequencies of ***VP*** in the **wettest** month within 4-

value classes (**VP_w**), and (6) frequencies of ***VP*** in the **driest** month within 4-value classes (**VP_d**).

5.2.5 Visualisation of HTC conditions

Visualisation of numerical information can always help readers to directly gain the key message. Therefore, in order to obtain a visual form of the HTC conditions for each climate type, bar graphs have been used to present these frequencies. Twelve groups of bar graphs have been created for Aw (Sanya), Am (Qionghai), Cwa (Shenzhen), Cwb (Kunming), Cfa (Shanghai), Dwa (Beijing), Dwa (Dalian), Dwb (Hohhot), Dwc (Lhasa), Dfb (Urumqi), BSk (Yuncheng) and BWk (Yinchuan), respectively. Each bar-graph group was composed of 6 horizontal bar graphs. These 6 bar graphs represent **PET_a**, **PET_h**, **PET_c**, **VP_a**, **VP_w** and **VP_d** in an order from top to bottom. Due to the 3-value classes of PET and the 4-value classes of *VP*, 3 colours have been utilised to display the frequencies of PET in bar graphs, and 4 colours have been utilised to display the frequencies of *VP*, respectively. Therefore, the quantification of HTC conditions has been displayed in a visual form. Meanwhile, the approach on implementation of the HTC information in KGC has been preliminary obtained. The example of the quantitative description for each climate type has been depicted in ***Fig. 5.2.1***.

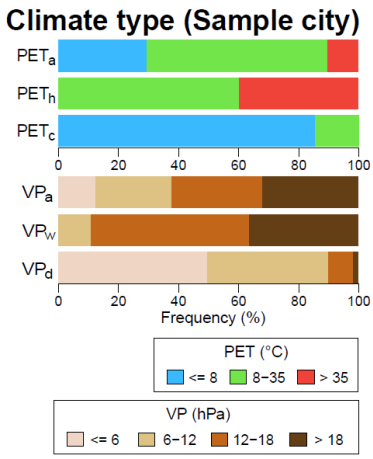

Fig. 5.2.1 The example of the HTC conditions in one climate type (sample city)

5.3 Application of HTC information for design on micro scale

In order to apply HTC information in community environment design, there are four steps in general, which are (1) the 1st simulation of HTC conditions, (2) the analysis of HTC conditions, (3) the possible design for modification of the HTC conditions, (4) and the comparison between the 1st simulation and the 2nd simulation for evaluation of the effects on HTC from the design. The simulations, which were short-term, have been accomplished through the application of the ENVI-met 3.0 model (Bruse 2004; Bruse and Fleer 1998; Huttner et al. 2008), which has been introduced in section 3.7.1. This part has selected one unified urban district as the simulation area based on the 12 meteorological scenarios, i.e. meteorological conditions in the 12 cities which were selected in Part One (Preliminary analysis). In order to specify the simulated period and evaluate the distribution of the extreme HTC conditions, the meteorological conditions in the hottest month of each city have been used to calculate the input data, which can be regarded as the representative situation of the hottest month. Based on the results in Part One (Preliminary analysis), the hottest month has been chosen for each city. According to the meteorological data from 12 cities, 12 scenarios input data have been prepared for the 2-round simulations. Afterwards, 24 (i.e. 12 ×2) sets of results have been obtained.

5.3.1 The residential district for simulations

First of all, a hypothetical residential district (***Fig. 5.3.1)*** with high-rise buildings has been selected as a unified physical environment for the 1st round simulations in 12 scenarios, respectively. In this district, the main building style ─ the high-rise building ─ was 66 (m) high (i.e. 22 stories). The other building height is 10 (m), such as the buildings along the street valley in ***Fig. 5.3.1***. The street valley of this district is formed by the regular distribution of buildings, and the distribution of the 4 buildings in the top of ***Fig. 5.3.1*** is irregular, i.e. they were arranged neither into one row, nor into one column. The cover materials of the street in street valley was asphalt, and the pavements at the sides of this street were paved by red brick. The paths in between buildings were paved by asphalt,

and the other area in this district was bare soil. The orientation and the scope, which were indicated by north arrow and the scale bar, respectively, were based on the actual conditions in practice. The valid simulation area was 340 ×340 m^2 in horizontal; however, the real size of this district was a little bit smaller than the valid area, in order to avoid blocking the air flow along the border of simulation area.

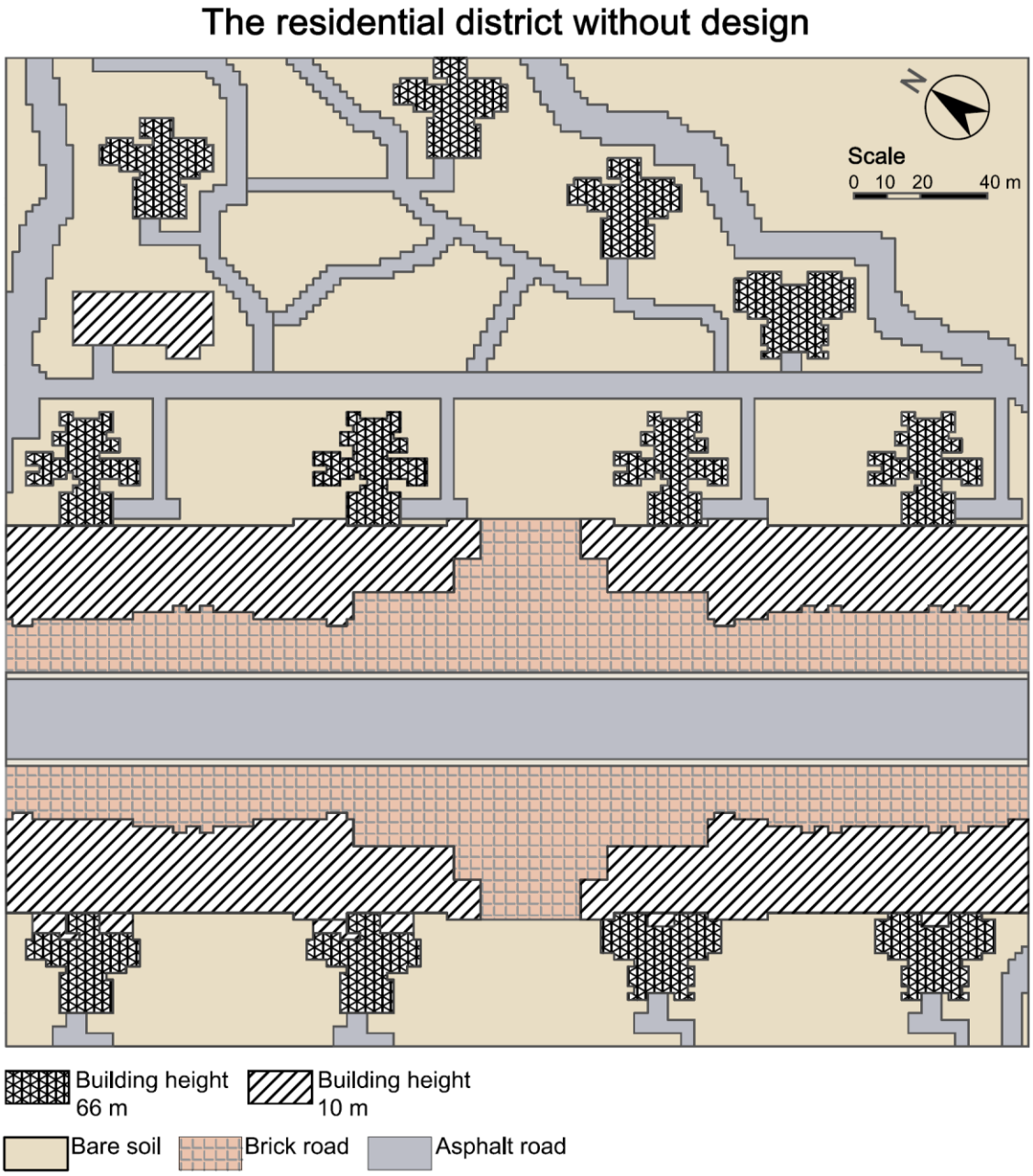

Fig. 5.3.1 The unified residential district without community environment design in the 1st round simulations

5.3.2 Preparation of the input setting

As the long-term meteorological data (3-hour resolution in 2000─2012, or 2000─2008) of each city has been analysed in Part One (Preliminary analysis), and the hottest month in each city has been identified, based on the monthly frequencies of T_a (dominant) and PET (reference). The basic input settings were the abbreviation of each scenario, the latitude and longitude, v, WD, atmospheric pressure (ATM), dew point (DWPT) and specific humidity (SH). Each of the meteorological value has been assigned the average value of the hottest month, respectively, except v which has been given the annually average value. Due to the instability of the monthly average v in each year, the annually average value has been chosen to present the general conditions in each city.

The advanced input data were the hourly T_a and hourly RH in one day (i.e. 24 hours). These values were used to form the initialisation of the atmospheric conditions for the 48-hour simulation. The hourly T_a values and hourly RH values have been calculated through the weighted mean values based on the 3-hour data in the hottest month, respectively.

The scope of the 3D simulation has been set within 340 × 340 (m^2) horizontally, and 100 (m) vertically. Two-meter resolution has been set in the horizontal direction, and labelled by x and y, respectively. Three-meter resolution has been set in the vertical direction, and labelled by z. Buildings and the different cover materials have been draw into the model as the features introduced in section 5.3.1.

5.3.3 Analysis of the 1st round simulations without design elements

Hourly meteorological parameters of this residential district in each scenario have been obtained through a 48-hour simulation in ENVI-met 3.0 model, respectively. In order to calculate PET in this district, hourly meteorological parameters, which were T_a, T_{mrt}, v, and SH, have been used in calcPET[5]. Due to the users' experience, the first 24-hour

[5] CalcPET is a plug-in module in ENVI-met. Currently, it has not been offered publicly.

simulation has been utilised to form a stable atmospheric environment, and the second 24-hour simulation has been selected for analysis. Finally, hourly *x-y* cut figures at z = 0─3 (m) on PET values, as well as other meteorological parameters, have been obtained from the simulation.

Currently, the formulas either in ENVI-met or in calcPET are not open source (i.e. the formulas are inaccessible for analysis). However, as there were several variables involved for PET calculations, it is necessary to estimate the impact of each parameters on PET values, in order to find the reasonable analysis to facilitate the design phase. Thus, the multiple linear regression through R language has been applied to examine the interaction between the parameters (i.e. predictor variables) related to PET (i.e. the response variable) calculation. As the formulas of ENVI-met 3.0 has not been 100% open to the user, the correlation of the parameters related to the calculation of the PET cannot be analysed in details. However, based on the basic knowledge, the multiple liner regressing has been applied to give an estimation of the possible correlation in the simulation. The script in R language is as following, which is an example in the examination for the scenario of Sanya (Aw) in the 1st round simulation:

$$\mathbf{lm}\ (\text{formula} = \mathbf{PET} \sim \boldsymbol{T_a} + \boldsymbol{RH} + \boldsymbol{v} + \boldsymbol{T_{mrt}} \times \boldsymbol{v} \times \boldsymbol{K_{di}} \times \boldsymbol{K_{fs}} \times \boldsymbol{K_{rf}} \times \boldsymbol{L_{en}} \times \mathbf{SVF} \times \boldsymbol{T_s} \times \boldsymbol{T_a} \times \boldsymbol{RH}, \text{data} = \mathbf{SYB})$$

The "+" means that predictor variables (i.e. $\boldsymbol{T_a}$, $\boldsymbol{RH}$, and $\boldsymbol{v}$) influence the response variable individually; and the "×" means there are interaction between each predictor variable (i.e. $\boldsymbol{T_{mrt}}$, $\boldsymbol{v}$, $\boldsymbol{K_{di}}$, $\boldsymbol{K_{fs}}$, $\boldsymbol{K_{rf}}$, $\boldsymbol{L_{en}}$, **SVF**, $\boldsymbol{T_s}$, $\boldsymbol{T_a}$, and $\boldsymbol{RH}$), and they possess the diverse impacts on the response variable under the different combinations. Meaning of each abbreviation in the formula of the multiple liner regression:

lm()	Calling the function of the multiple linear regression in R language
PET	Column name of the values on PET (℃)
$\boldsymbol{v}$	Column name of the values on v (m/s)
$\boldsymbol{T_a}$	Column name of the values on T_a (℃)
$\boldsymbol{RH}$	Column name of the values on RH
$\boldsymbol{T_{mrt}}$	Column name of the values on T_{mrt} (℃)
$\boldsymbol{K_{di}}$	Column name of the values on direct short wave radiation flux density (W/m^2)
$\boldsymbol{K_{fs}}$	Column name of the values on diffuse short wave radiation flux density (W/m^2)

K_{rf}	Column name of the values on reflected short wave radiation flux density (W/m^2)
L_{en}	Column name of the values on long wave radiation flux density from environment (W/m^2)
SVF	Column name of the values on SVF
T_s	Column name of the values on surface temperature (℃)
SYB	Data set from the 1st simulation on Sanya (Aw) without the data in building grids

The estimate of the single parameter and the R^2 in each scenario from the multiple liner regression, have been summarised into one table. R^2 indicates how close the data are to the fitted regression line. The estimate of each parameter indicates the strength of impact of each parameter (and each combination of parameters) on PET value. SVF and *v* have been found with the strongest effects on PET after comparison; therefore the conditions of *v* and the conditions of SVF have been used to partially explain and analyse the conditions of PET.

According to the analysis of distribution of PET at each hour in the 1st round simulations, the point in time with the most frequent thermally stress (heat stress) in each city has been selected. PET values and *v* values of each scenario at this point in time have been illustrated into a 2D figure (i.e. a map) with a new set of value classes (compared to the value classes in Part One), respectively. The new value classes of PET present a warmer distribution than that in the classification of thermal sensitivity for moderate climates. The value classes (unit: °C) have been categorised by below 18, 18─23, 23─29, 29─35, 35─41, 41─47, 47─54, 54─60 and above 60. The new value classes of *v* present a more finely distribution than that in the wind roses and bar charts in Part One (Preliminary analysis). The *v* value classes (unit: m/s) have been categorised by below 0.2, 0.2─0.6, 0.6─1, 1─1.5, 1.5─2, 2─2.5, 2.5─3, 3─3.5 and above 3.5. The conditions of SVF are the same in all of the 1st round simulations. Therefore, one figure has been used to depict the SVF values in all 12 scenarios in the 1st round simulation. The value classes of SVF have been categorised by below 0.1, 0.1─0.3, 0.3─0.5, 0.5─0.7, 0.7─0.8, 0.8─0.9 and above 0.9. Based on the horizontal distribution of the PET values (dominate), the SVF values (reference) and the *v* values (reference) in the district in the vertical space of 0─3 (m) up ground, the undesirable HTC areas at the selected point in time in the district have been

detected for each scenario, and this information will be the reference for adding design elements in specific areas.

5.3.4 Design elements for the 2nd round simulations

In order to control the variables, the same input settings in the 1st round simulations have been given to the 2nd round simulations of the 12 scenarios, respectively. However, based on the diverse HTC conditions, the various design strategies with the similar design elements have been added to each scenario in the 2nd round simulations. Firstly, the position of the design elements must follow the user behaviour, e.g. the tree will not appear on the asphalt road. The design elements were consist of trees, hedges, grass and water bodies, which were introduced in ***Table 5.3.1***. The type of the tree, which will be applied in the 2nd simulations, was selected in the typical trees in each city. The unified type of the hedge, the grass, as well as the stable and deep water body has been applied in the 2nd round simulations for 12 scenarios, respectively. All the characteristics of the elements are according to the default settings in ENVI-met 3.0, and the difference between each vegetation (indicated by certain code in ENVI-met 3.0) is described through the individual leaf area density (LAD) and the individual root area density (RAD) at different vertical level.

Table 5.3.1 Typical tree in each city and the input code of the tree, the hedge and grass, respectively

City	Typical tree	MO*	sk*	sc*	sm*	bs*	h*	gb*
Sanya (Aw)	*Cocos nucifera* L.	√						
Qionghai (Am)	*Cocos nucifera* L.	√						
Shenzhen (Cwa)	*Litchi chinensis* Sonn.		√					
Kunming (Cwb)	*Magnolia denudata* Desr.		√					
Shanghai (Cfa)	*Platanus orientalis* L.			√				
Beijing (Dwa)	*Sophora japonica* L.				√		√	√
Dalian (Dwa)	*Sophora japonica* L.				√			
Hohhot (Dwb)	*Pinus tabulaeformis* Carr.					√		
Lhasa (Dwc)	*Populus* L.					√		
Urumqi (Dfb)	*Ulmus laevis* Pall.			√				
Yuncheng (BSk)	*Sophora japonica* L.				√			
Yinchuan (BWk)	*Sophora japonica* L.				√			

***MO**: Tree with 20 (m) height, dense; **sk**: Tree with 15 (m) height, very dense; **sc**: Tree with 20 (m) height, very dense; **sm**: Tree with 20 (m) height, very dense, canopy lower than sc; **bs**: Tree with 20 (m) height, dense; **h**: Hedge with 2 (m) height dense; **gb**: Grass with 0.5 (m) height, dense

Table 5.3.2 Adding strength of each design element for the specific areas in each city

Element	Adding strength* in the area with specific HTC conditions			
	Above 54 ℃	41–54 °C	29–41 °C	Below 29 ℃
Tree*	☆☆☆☆☆	☆☆☆	☆	☆
Hedge*	☆☆☆	☆☆☆☆☆	☆☆☆	☆
Grass	In the same areas in 12 scenarios			
Water body	In the same areas in 12 scenarios			

*More stars (☆), more intense

Based on the distribution of PET values in the 1st simulation of each scenario at the point in time with the most frequent thermally stress (heat stress), the design elements were added to the specific areas. The adding rules were presented in ***Table 5.3.2***, which was the adding strength of each design element for the specific areas in the district. The adding strength in this study was a quality definition, instead of the exactly quantified definition.

In order to present how the design is based on the PET distribution in each scenario, the drawings of the design elements have been combined with the PET distribution into one figure. Meanwhile, one coloured example of the community environment design, which was in Yinchuan (BWk), has been displayed individually at the end of section 6.3.3.

5.3.5 Effects of design elements on HTC conditions

The effects of elements in the community environment design have been analysed through the differences between the 1st round simulation and the 2nd simulation in each scenario. In the 2nd round simulations, the distributions of PET, SVF and *v*, which were at the same point in time in each scenario, have been selected to compare with the conditions in the 1st round simulations. The difference in PET of each scenario has been calculated through the PET values in the1st simulation minus the PET values in the 2nd simulation. The same operation has been applied to examine the difference in SVF and the difference in *v*, respectively. Afterwards, the effects of the design elements on the HTC conditions in each scenario have been depicted through the figures on the difference in PET, in SVF, and in *v*, respectively. Based on the analysis of the values on the difference in PET, in SVF, and in *v*, and the purpose on distinguishing the distribution of the changes (i.e. the difference in each parameter), the individual value classes have been selected for the difference in PET, the difference in SVF, and the difference in *v*, respectively. The value classes for difference in PET (unit: K) were below – 10, – 10 — – 5, – 5 — – 2, – 2 — 2, 2 — 5, 5 — 10, 10 — 15, 15 — 25, and above 25. The exactly meaning of each value class has been explained in ***Table 5.3.3***. The value classes for difference in SVF were below 0.05, 0.05 — 0.15, 0.15 — 0.25, 0.25 — 0.35, 0.35 — 0.45, 0.45 — 0.55, and above 0.55. The value classes for difference in *v* (unit: m/s) were below 0.25, 0.25 — 0.5, 0.5 — 0.75, 0.75 — 1, 1 — 1.25, 1.25 — 1.5, 1.5 — 1.75, 1.75 — 2, and above 2.

Table 5.3.3 The meaning of each value class for the difference in PET (the same for 12 scenarios)

Colour	**Colour name**	**Difference in PET** (K)	**Meaning of the value range (appeared in each grid in the Appendix 5) between the twice simulations**
	Black blue	below – 10	PET in the 1st simulation is at least 10 K lower than that in the 2nd simulation.
	Dark blue	– 10 — – 5	PET in the 1st simulation is 5 — 10 K lower than that in the 2nd simulation.
	Blue	– 5 — – 2	PET in the 1st simulation is 2 — 5 K lower than that in the 2nd simulation.
	Green	– 2 — 2	PET in the 1st simulation is at most 2 K higher/lower than that in the 2nd simulation.
	Light green	2 — 5	PET in the 1st simulation is 2 — 5 K higher than that in the 2nd simulation.
	Yellow	5 — 10	PET in the 1st simulation is 5 — 10 K higher than that in the 2nd simulation.
	Orange	10 — 15	PET in the 1st simulation is 10 — 15 K higher than that in the 2nd simulation.
	Red	15 — 25	PET in the 1st simulation is 15 — 25 K higher than that in the 2nd simulation.
	Purplish red	above 25	PET in the 1st simulation is at least 25 K higher than that in the 2nd simulation.

6 Results

6.1 Preliminary analysis of HTC on meso scale

In this part, the meteorological data from national-level weather station in each city was used to represent the meteorological conditions for the whole city, and it was regarded as the background information on meso scale. Meanwhile, the analysis and evaluation were based on the meteorological data from 2000 to 2012, except the data of Sanya, which was from 2000 to 2008.

6.1.1 Location of each city in KGC

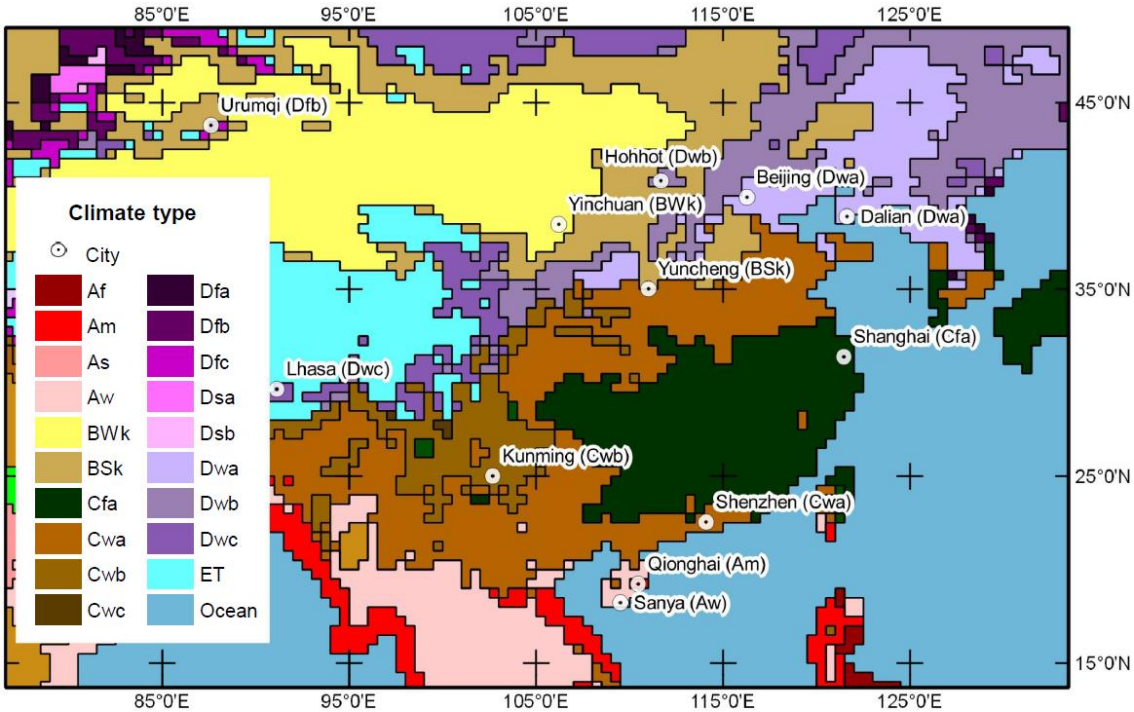

Fig. 6.1.1 Location of each city in the map of Köppen–Geiger climate classification (KGC: 1976–2000) (modified after Rubel and Kottek 2010)

The area of each climate type (i.e. KGC type) in China and the location of the 12 selected cities in each climate type were depicted in ***Fig. 6.1.1***. The details of the topographical information of each city was presented in ***Table 4.1.1***. Meanwhile, a brief introduction of each city was given in the chapter of Study areas, which focused on the basic topographical features.

6.1.2 HTC conditions at 8 points in time

Beanplots (combined with boxplots) of T_a, T_{mrt} and PET, respectively (please see ***Fig. A1.1—A1.12*** in Appendix A1), depicted the values of these parameters in a full view, i.e. the distribution of the value density was examined graphically. Based on these Beanplots and boxplots, the relative warmest point in time was detected.

For instance, in Sanya (Aw) (***Fig. A1.1***), the fluctuation of T_a was limited in between 10 ℃ and 40 ℃. Comparing the shape of the beanplot and quartiles in the boxplot at each point in time (2 LST, 5 LST, 8 LST, 11 LST, 14 LST, 17 LST, 20 LST and 23 LST), the warmest conditions indicated by T_a appeared at 14 LST, and the coolest conditions indicated by T_a were at 5 LST. The T_{mrt} was above 0 ℃ and below 65 ℃. The relative strongest thermally radiant conditions appeared at 11 LST and 14 LST (slightly greater), and the relative weakest thermally radiant conditions were at 23 LST, 2 LST and 5 LST (slightly greater). The fluctuation of PET was limited in between 5 ℃ and 50 ℃. The relative warmest conditions indicated by PET were at 11 LST and 14 LST, and the relative coolest conditions indicated by PET appeared at 5 LST. The individual distributions of T_a value, T_{mrt} value and PET value existed in other 11 cities and the generalised peak values of the 12 cities were summarised into ***Table 6.1.1***. The most frequent point in time with the warmest HTC conditions was 14 LST, based on the information in each city in ***Table 6.1.1***.

Table 6.1.1 Summarised information from beanplots and boxplots of 12 cities

City		Point in time (LST) and the fluctuation (℃)					
		T_a High	T_a Low	T_{mrt} High	T_{mrt} Low	PET High	PET Low
Sanya (Aw)	LST	14	5	14	5	11, 14	5
	℃	10–40		0–65		5–50	
Qionghai (Am)	LST	14	2, **5***	14	5	14	2, **5**
	℃	5–40		0–65		0–55	
Shenzhen (Cwa)	LST	14	5	11, **14**	5	14	5
	℃	0–40		– 10–65		– 5–55	
Kunming (Cwb)	LST	14, **17**	**5**, 8	14	5	14	5
	℃	–5–35		– 5–60		– 10–50	
Lhasa (Dwc)	LST	17	8	14	2, **5**, 8	14	**5**, 8
	℃	– 15–30		– 30–55		– 25–45	
Shanghai (Cfa)	LST	14	5	11	5	11, **14**	5
	℃	–10–40		– 25–65		– 15–50	
Yuncheng (BSk)	LST	14	5	14	5	14	5
	℃	– 15–45		– 30–65		– 25–55	
Yinchuan (BWk)	LST	14, **17**	5	14	5	14	5
	℃	– 25–40		– 40–60		– 35–55	
Dalian (Dwa)	LST	14	5	**11**, 14	23, 2, **5**	**11**, 14	5
	℃	–20–35		– 35–60		– 30–50	
Beijing (Dwa)	LST	14	5	14	5	14	5
	℃	– 20–35		– 35–65		– 30–55	
Hohhot (Dwb)	LST	14, **17**	5	14	5	14	5
	℃	– 30–40		– 40–60		– 35–50	
Urumqi (Dfb)	LST	14, **17**	8	14	5	14	5
	℃	– 30–45		– 40–60		– 40–50	

* Bold numbers refer to the point in time with slightly higher/lower distribution of the value in each parameter, compared with other numbers listed together.

6.1.3 Monthly and annual HTC conditions

As the warmest HTC conditions appeared frequently at 14 LST in 12 cities, in this section, the monthly frequencies of PET in different value classes at 14 LST have been analysed. Meanwhile, the summarisation of the annual HTC conditions were presented into ***Table 6.1.2***, as the analysis of the HTC conditions in each year.

6.1.3.1 Monthly frequencies of PET

The monthly frequencies of each PET value class (i.e. PET value class in ***Table 5.1.1***) in 12 cities have been presented in ***Fig. 6.1.2***, which depict the HTC conditions at 14 LST in each city. The frequency could be also regarded as the percentage of days with specific

HTC conditions in one month, since only one PET value (i.e. one certain HTC condition) per day was counted.

At 14 LST in Sanya (Aw), there were the hot and the very hot conditions together (i.e. the heat stress) in every month in Sanya (Aw). The heat stress appeared monthly with a high frequency (more than 80 %) from March to October. Meanwhile, there were at least 50% days in a month with the very hot conditions in May, June and July, respectively. The heat stress in winter (December, January and February) was not as intense as them in other months. Although there were some days with non-heat stress, such as the days with the slightly warm conditions, the frequency was not high. Furthermore, there was no day with PET below 18 ℃ at 14 LST in Sanya (Aw).

According to the HTC conditions in Qionghai (Am) in ***Fig. 6.1.2***, there was the heat stress in every month at 14 LST. There were more than 80 % days in a month with the heat stress in May, June, July, August and September, respectively. From November to March, the HTC conditions were less intense, and there were more than 60% days in each month with PET below 35 ℃; however, there was no PET below 8 ℃ at 14 LST in Qionghai (Am).

The heat stress with a high frequency (more than 75 % days in a month) existed at 14 LST from May to September in Shenzhen (Cwa). The frequencies of days with the hot conditions in these months were 40─60 %, respectively. The frequencies of days with the very hot conditions in July and August were approximate 50 %, respectively. From November to March, the monthly frequencies of PET below 29 ℃ were more than 50 %, respectively. There was heat stress almost in every month in Shenzhen (Cwa); however, there was a rare condition with PET below 8 ℃ at 14 LST.

The cool, the slightly cool, the comfortable and the slightly warm conditions together dominated the HTC conditions at 14 LST in the whole year in Kunming (Cwb). And even the slightly warm, the comfortable, and the slightly cool conditions together (i.e. the

acceptable conditions) existed with high frequencies of days (more than 60 %) from October to April, respectively. The heat stress appeared in summer (June, July and August) with frequencies less than 20 %, and the most frequent HTC conditions in summer were the warm conditions, which existed with more than 50 % days in each month. In contrast, the most frequent HTC conditions at 14 LST in winter were the slightly cool conditions, which were also in more than 50 % days in each month. At 14 LST in Kunming (Cwb), there was heat stress from May to September with low frequencies, and cold stress in the half of a year also with low frequencies.

According to the results, the acceptable conditions occurred with relative high frequencies (more than 70 %) in Lhasa (Dwc) at 14 LST from April to October. Although the heat stress existed in these months, it was less intense: the hot conditions happened less than 7 % days even in August. The cold stress at 14 LST existed since November until March. The highest frequency of the cold stress at 14 LST was in January, which was more than 30 % days in this month.

The period in Shanghai (Cfa) with the most frequent heat stress was July and August, in which the frequency was around 80 % days in each month. Relative high frequencies (more than 50 %) of the acceptable conditions were found in March, April, May, October and November more than 50 % of days, respectively. In winter, the frequency of the very cold, the cold and the cool conditions together was around 80─90 % days in each month. The most frequent cold stress was in January, in which there was around 40 % days. At 14 LST, the heat stress appeared from April until October, and the cold stress appeared from November until March.

In Yuncheng (BSk) at 14 LST, the heat stress existed in summer in 70─90 % days in each month. Furthermore, there was almost 60 % days in July with the very hot conditions. Relative high frequencies (more than 50 %) of the acceptable conditions existed in March, April, October and November, respectively. The comfortable conditions existed in every month; however, the highest frequency in a month was less than 30 %.The cold stress

appeared in January and December with relative high frequencies of days (40─50 %), respectively. In Yuncheng (BSk) at 14 LST, the obvious existence of the heat stress was from April until October, the cold stress lasted from November until March.

The heat stress in Yinchuan (BWk) was less intense than that in Yuncheng (BSk). In summer, the frequencies of the heat stress were between 50 % days and 70 % days in each month. The relative high frequencies of days (around 50─80 %) with the acceptable conditions were in April, May, September and October, respectively. The cold stress existed with high frequencies of days (more than 90 %) in December and January, respectively. At 14 LST, the heat stress appeared from April until October, the acceptable conditions existed from February until November, and the cold stress appeared from November until March in Yinchuan (BWk).

The heat stress seemed to be not intense in Dalian (Dwa), and it lasted from June to September. In summer, the frequency of the hot conditions was lower than 30 % days in each month, and the very hot conditions were rare. The warm and the slightly warm conditions dominated June, July, August and September with more than 60 % days, respectively. Around 70 % days in May and October were with the acceptable conditions, respectively. The cold stress was found since October until April, and it existed within the more than 90 % days in January.

Although Beijing (Dwa) is located in the same climate type as Dalian, the HTC conditions in Beijing were different, especially in summer. The heat stress was existed with high frequencies in summer, which was more than 70 % days in each month. Furthermore, the very hot conditions existed more than 20 % days in each month in summer. The acceptable conditions appeared with high frequency (approximate 80 %) in April and October. The cold stress dominated the whole winter, and it happened in about 90 % days in January. At 14 LST, the cold stress existed since November until March, and the heat stress existed since May until September.

In Hohhot (Dwb) at 14 LST, the obvious heat stress existed in summer. The month with the highest frequency of the heat stress was July, which was approximate 60 % days. Approximate 60 % days in April, May, September and October were with the acceptable conditions. However, the cold stress existed since October until April. The most frequent cold stress was found in December and January, respectively, in which there was more than 90 % days, respectively. Meanwhile, there was also relative high frequency of days (about 60 %) with the cold stress in November and February, respectively.

The trend of HTC conditions in Urumqi (Dfb) seemed similar to that in Hohhot (Dwb), but the HTC conditions were colder than that in Hohhot (Dwb). During summer, the heat stress existed at 14 LST with 30─40 % days in each month. The most frequent conditions in April, May and September were the acceptable conditions, respectively, which existed in approximated 60 % days in each month. In winter, the cold stress existed with quite high frequencies of days (almost 100 %) in each month. The cold stress appeared at 14 LST in Urumqi (Dfb) since October, and maintained until April.

Comparing all 12 cities, the difference of HTC conditions at 14 LST between these cities could be summarised as following. The warm, the hot and the very hot conditions together existed on more than 80 % days in the 12 months in Sanya (Aw), in 7 months in Qionghai (Am), in 6 months in Shenzhen (Cwa), in 3 months in Yuncheng (BSk), Yinchuan (BWk) and Beijing (Dwa), respectively. The very hot conditions were rare in Kunming (Cwb), Lhasa (Dwc) and Dalian (Dwa). The HTC conditions in Kunming (Cwb) presented the most frequent acceptable conditions through the whole year, and the HTC conditions in Lhasa (Dwc) followed. However, the relative high frequency of the acceptable conditions lasted from October to April in Kunming (Cwb), and from April to October in Lhasa (Dwc). In Yinchuan (BWk), Dalian (Dwa), Beijing (Dwa), Hohhot (Dwb) and Urumqi (Dfb), the dominated HTC conditions were the very cold conditions. There were relative stable HTC conditions in Sanya (Aw) and Qionghai (Am), and relative unstable HTC conditions in other cities except Shenzhen (Cwa) and Kunming (Cwb).

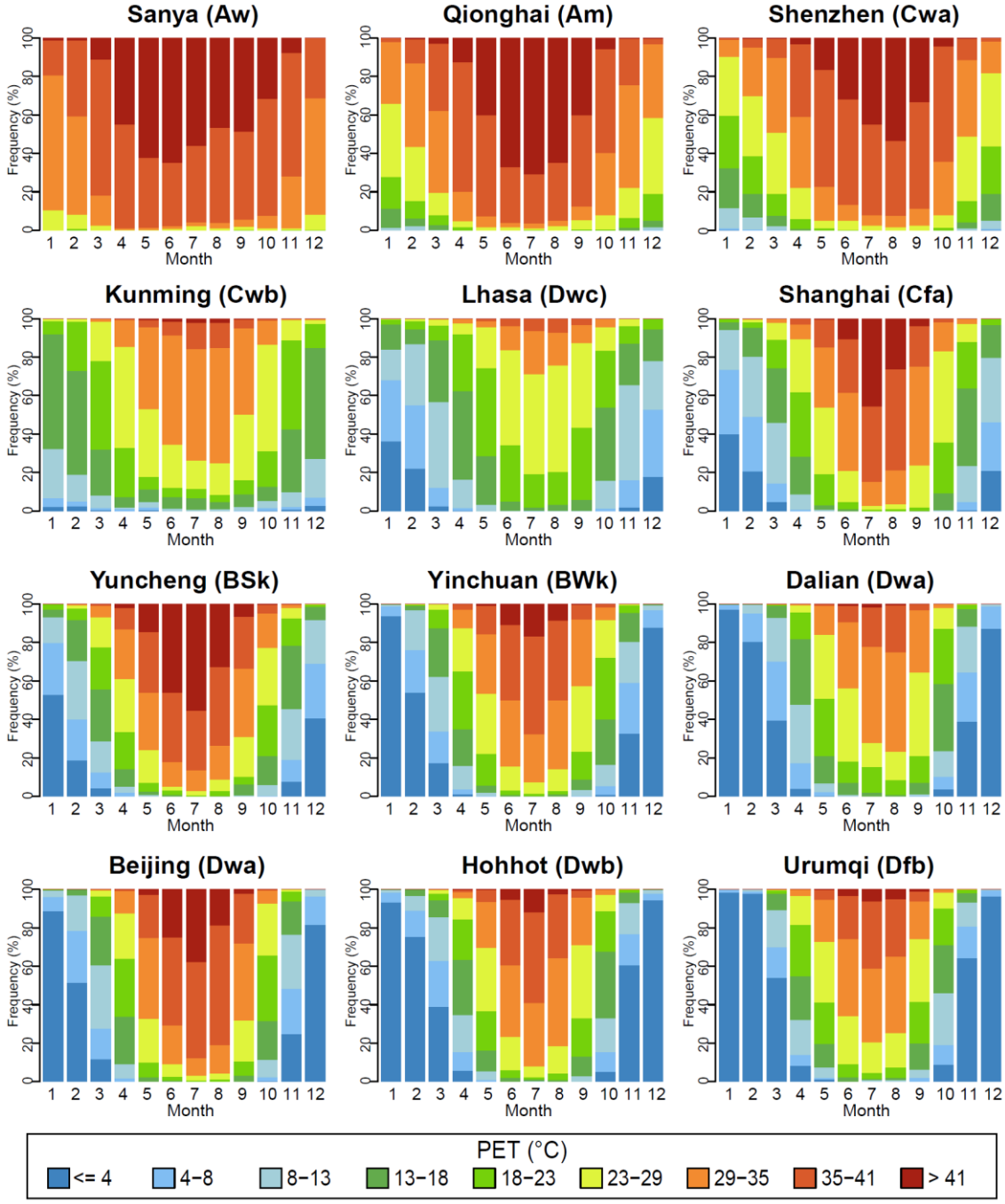

Fig. 6.1.2 Monthly frequencies of different PET value classes at 14 LST in 12 cities in 2000–2012 (Sanya: 2000–2008)

6.1.3.2 Annual HCT conditions

The HTC conditions at 14 LST in each year were summarised in ***Table 6.1.2***. From 2000 to 2004, the days with heat stress in Sanya (Aw) were more than 220, and from 2005 to 2008 the days with heat stress increased to more than 258. The increment may be caused

by the accumulated impacts from urbanization. There was no cold stress+ in Qionghai (Am) at this point in time, but heat stress appeared more than 160 days in every year, particularly in 2012 with more than 200 days. The days within acceptable conditions varied between 72 and 113. The number of days with heat stress was similar to that with acceptable conditions in Shenzhen (Cwa), which were 143.5 days and 128 days, respectively. Meanwhile, the cold stress+ never occurred.

In Kunming (Cwb) at 14 LST, the average number of days with acceptable conditions was 246.2 days. Even though there was heat stress or cold stress+, the HTC conditions lasted for a tiny number of days. In Lhasa (Dwc), the number of days with acceptable conditions was the most prominent conditions in every year at 14 LST, which was 199.6 days on average. The average days with heat stress and cold stress+ were 6.9 and 10.5, respectively. There were 137.9 days on average with acceptable conditions every year at 14 LST in Shanghai (Cfa). Meanwhile there were 60.3 days with heat stress and 11 days with cold stress+ on average.

In Yuncheng (BSk), the days with acceptable conditions were at least 100 days per year except in 2012 (90 days), meanwhile the days with heat stress were more than 86 except in 2003 and 2011. At 14 LST, the cold stress+ happened in 22.7 days on average. The number of days with acceptable conditions was the highest in the past 13 years with an average value of 113.2 in Yinchuan (BWk).

In Dalian (Dwa), the days with acceptable conditions and cold stress+ were by far more numerous than the days with heat stress. The average values of acceptable conditions, cold stress+ and heat stress were 130.8 days, 86.1 days and 8.8 days, respectively. In Beijing (Dwa), for the moment, the average number of days with heat stress was 71.3, while acceptable conditions were 96.8 days, and cold stress+ were in 56.8 days. It seemed that 2007 was warmer than other years, as the highest number of days with heat stress and the lowest number of days with cold stress+ existed in this year.

Table 6.1.2 Days per year with the heat stress (PET > 35 ℃), the cold stress⁺ (PET < 0 ℃) and acceptable conditions (PET in 13─29 °C) in the 12 cities at 14 LST, respectively

Days/year	2000	2001	2002	2003	2004	2005	2006	2007	2008	2009	2010	2011	2012	Means
Sanya(Aw)														
> 35 ℃*	221	229	229	232	220	258	283	278	258	—	—	—	—	245.3
13 ─ 29 °C	23	31	28	30	29	27	15	11	27	—	—	—	—	24.6
< 0 ℃	0	0	0	0	0	0	0	0	0	—	—	—	—	0
Qionghai(Am)														
> 35 ℃	165	165	175	176	168	176	189	172	174	180	185	168	208	177
13 ─ 29 °C	105	113	99	96	106	98	80	88	94	76	76	104	72	92.8
< 0 ℃	0	0	0	0	0	0	0	0	0	0	0	0	0	0
Shenzhen(Cwa)														
> 35 ℃	149	154	154	160	153	171	123	131	133	137	129	128	143	143.5
13 ─ 29 °C	134	139	120	116	110	117	138	139	129	134	133	140	115	128
< 0 ℃	0	0	0	0	0	0	0	0	0	0	0	0	0	0
Kunming(Cwb)														
> 35 ℃	23	9	11	7	5	4	2	1	5	5	3	6	4	6.5
13 ─ 29 °C	227	213	248	264	256	257	268	255	244	228	236	238	266	246.2
< 0 ℃	3	3	1	0	0	0	0	1	0	0	0	2	1	0.8
Lhasa(Dwc)														
> 35 ℃	7	11	4	9	0	3	10	7	10	16	6	4	3	6.9
13 ─ 29 °C	197	209	209	189	201	191	191	199	214	193	214	200	188	199.6
< 0 ℃	17	8	10	14	14	17	2	10	11	6	9	9	9	10.5
Shanghai(Cfa)														
> 35 ℃	60	39	49	67	58	66	75	65	59	55	67	62	62	60.3
13 ─ 29 ℃	129	157	149	128	150	130	148	130	142	123	141	134	132	137.9
< 0 ℃	12	12	5	10	9	17	9	2	16	10	11	14	12	10.7
Yuncheng(BSk)														
> 35 ℃	85	98	101	60	81	100	89	92	86	80	83	77	86	86
13 ─ 29 °C	101	115	108	98	121	107	121	118	111	100	109	111	90	108.5
< 0 ℃	28	19	15	24	22	29	18	9	35	28	19	28	21	22.7
Yinchuan(BWk)														
> 35 ℃	29	39	41	30	33	47	44	40	57	49	43	60	60	44
13 ─ 29 °C	110	116	115	115	126	115	112	120	116	110	106	107	103	113.2
< 0 ℃	75	82	51	79	61	91	78	59	68	69	64	70	81	71.4
Dalian(Dwa)														
> 35 ℃	12	8	9	4	11	14	10	8	5	14	8	7	5	8.8
13 ─ 29 °C	103	129	132	151	135	134	125	124	140	137	121	142	128	130.8
< 0 ℃	92	100	79	83	75	100	81	56	80	88	88	94	103	86.1
Beijing(Dwa)														
> 35 ℃	88	75	64	51	58	68	72	90	61	69	82	75	74	71.3
13 ─ 29 °C	78	92	90	105	109	108	103	88	105	104	76	109	91	96.8
< 0 ℃	63	77	40	56	44	77	47	34	54	57	60	54	75	56.8
Hohhot(Dwb)														
> 35 ℃	31	36	35	27	19	38	24	32	24	26	38	33	28	30.1
13 ─ 29 °C	93	100	97	96	131	113	112	103	115	117	89	102	106	105.7
< 0 ℃	106	94	76	88	85	108	94	97	96	98	103	96	114	96.5
Urumqi(Dfb)														
> 35 ℃	14	18	18	14	27	29	27	21	32	14	30	22	29	22.7
13 ─ 29 °C	104	114	116	116	115	105	116	115	101	136	104	118	111	113.2
< 0 ℃	142	117	116	122	120	113	113	105	99	116	116	132	128	118.4

* The row marked with grey refers to the relative popular HTC conditions at 14 LST in each city, due to the highest average days with specific HTC conditions per year.

In Hohhot (Dwb) at 14 LST, heat stress occurred with a relatively stable number in each

year, say, 30.1 days on average. In contrast, the number of days with cold stress+ and acceptable conditions were both around 100 days in each year. They were much higher than the number of days with heat stress. The cold stress+ happened in much more than 100 days in each year in Urumqi (Dfb) at 14 LST, except for 2008 in 99 days. The average number of days with acceptable conditions was 113.2, which was a little bit lower than that of cold stress+. Heat stress happened with a stable number of days per year, say, 22.7 days on average.

6.1.4 Related meteorological parameters

The monthly frequencies of T_a, T_{mrt}, *VP*, *RH*, and *v* have been calculated and visualised, respectively. Wind rose, as the traditional approach for presenting wind conditions, has been also built for each city, based on the 3-hour data. Meanwhile, the days with different AH conditions (*VP* and *RH*) in the whole period have been calculated for each city.

6.1.4.1 Conditions of air temperature (T_a)

Figure 6.1.3 pointed out the air temperature (T_a) conditions at 14 LST in each city by the monthly frequencies of days with different T_a value classes (i.e. the same value classes for monthly frequencies of PET). The conditions of T_a above 41 ℃ did not exist in all 12 cities. There was almost no condition of T_a above 35 ℃ in Sanya (Aw). In Kunming (Cwb), and Lhasa (Dwc) at 14 LST, there was almost no condition of T_a above 29 ℃.

Actually, the conditions of T_a in 35─41 °C were not frequent in other cities, and the highest frequency of days (approximate 20 %) in a month existed in Shanghai (Cfa) in July, and in Yuncheng (BSk) in June and July, respectively. The conditions of T_a in 29─35 °C were found as the main conditions (monthly frequencies of days more than 60 %) in Sanya (Aw) from April to October, in Qionghai (Am) from April to September, in Shenzhen (Cwa) from June to September, respectively. The conditions of T_a in 29─41 °C were the main conditions in the July and the August of Shanghai (Cfa), in the June and the July of Yuncheng (BSk), and in the summer of Beijing (Dwa).

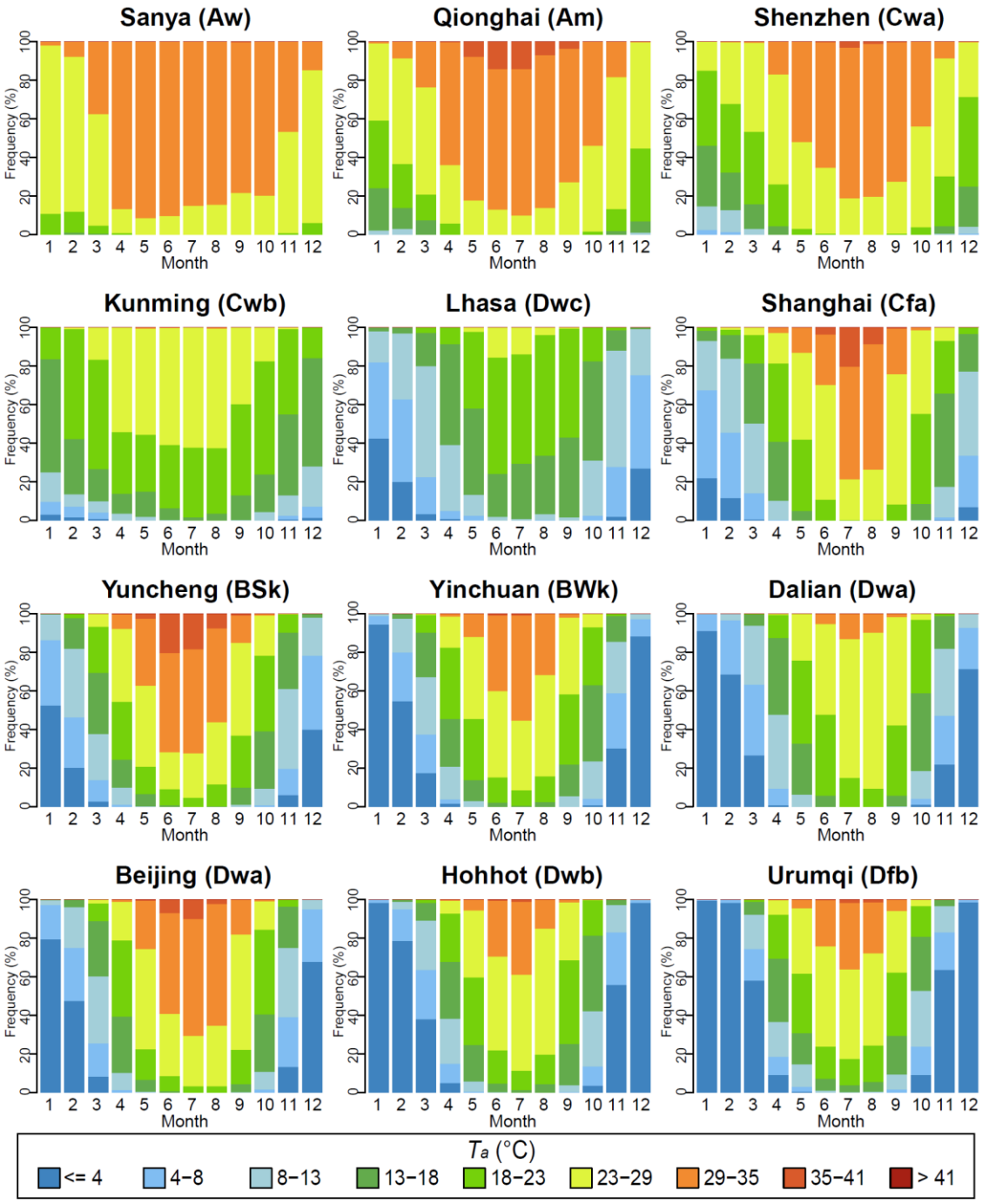

Fig. 6.1.3 Monthly frequencies of different T_a value classes at 14 LST in 12 cities in 2000—2012 (Sanya: 2000—2008)

The conditions of T_a in 23—29 °C were the main conditions in the winter of Sanya (Aw), in the summer of Kunming (Cwb), in the June and September of Shanghai (Cfa), and in the July and August of Dalian (Dwa). In addition, the conditions of T_a in 13—29 °C were

also the main conditions in Qionghai (Am) from November to March; in Shenzhen (Cwa) from November to April; in Lhasa (Dwc) from April to October; in September, October, and spring in Yuncheng (BSk); from April to June, and from August to October in Yinchuan (BWk); in April, May, September, and October in Beijing (Dwa); and in Urumqi (Dfb) from April to September.

The conditions of T_a below 13 ℃ with high frequencies of days in a month (more than 70 %) existed in Lhasa (Dwc) from November to March; in winter in Shanghai (Cfa); in winter in Yuncheng (BSk); in Yinchuan (BWk) from November to February; in Dalian (Dwa) from November to March; in Beijing (Dwa) from November to February; in Hohhot (Dwb) from November to March; and in Urumqi from November to March.

Comparing the conditions of T_a with the conditions of PET, the similar changing trends could be found in each city. However, based on the same value classes, PET indicated more various conditions in each month than T_a did. This is because that PET presents the perception of human beings on the thermal environment more sensitively.

6.1.4.2 Conditions of mean radiant temperature (T_{mrt})

The monthly frequencies of mean radiant temperature (T_{mrt}) at 14 LST were presented by ***Fig. 6.1.4***, based on the T_{mrt} value classes, which were the same as the value classes for monthly frequencies of PET. T_{mrt} above 41 ℃ was the main conditions for all 12 cities in at least five months (which are around summer), especially in Sanya (Aw) and Qionghai (Am), where there were more 80─100 % days in every month, respectively. Except Kunming (Cwb), Lhasa (Dwc) and Urumqi (Dfb), the intense of T_{mrt} in each city decreased from South to North (compared with the latitude in ***Fig. 6.1.1*** and ***Table 4.1.1***). The exception in Kunming (Cwb), Lhasa (Dwc) and Urumqi (Dfb) might be due to the significant difference in longitude (***Table 4.1.1***). As T_{mrt} indicates a temperature which is based on the environmentally radiant conditions, T_{mrt} revealed much more intense thermal conditions compared with PET did in ***Fig. 6.1.2***.

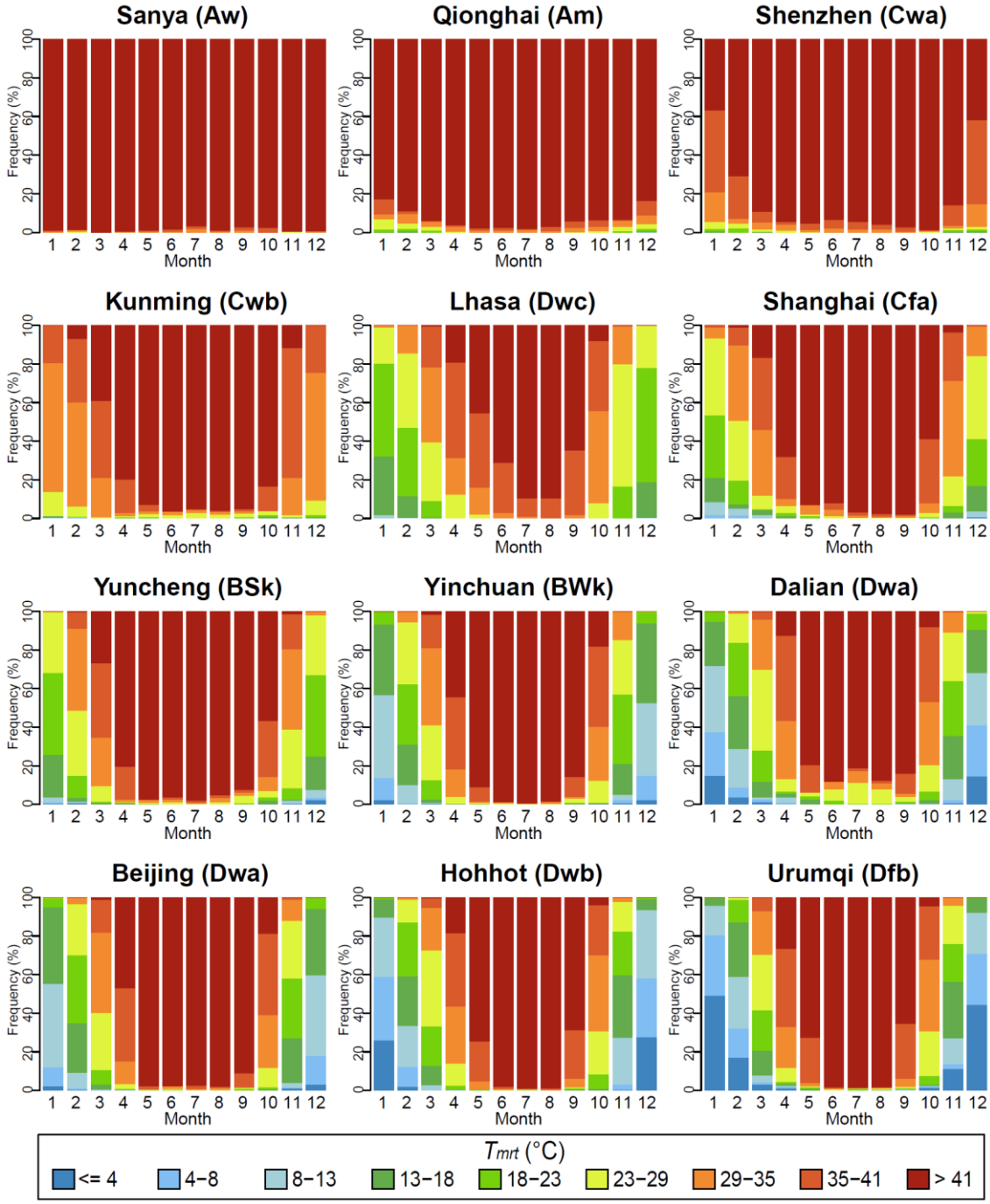

Fig. 6.1.4 Monthly frequencies of different T_{mrt} value classes at 14 LST in 12 cities in 2000–2012 (Sanya: 2000–2008)

6.1.4.3 Air humidity (AH) conditions

The monthly frequencies of vapour pressure (*VP*) value classes at 14 LST were presented in ***Fig. 6.1.5***. The most humid conditions in each city existed in summer, and the driest

conditions in each city happened in winter. However, comparing each city, the humid conditions were not the same. ***Table 6.1.3*** showed the days per year of each *VP* value class at 14 LST in each city. *VP* conditions occurred more than or equal to 33 days, currently, were regarded as the main AH conditions in each city. Combining ***Fig. 6.1.5*** with ***Table 6.1.3***, the humid conditions indicated by *VP* values in each city were analysed individually.

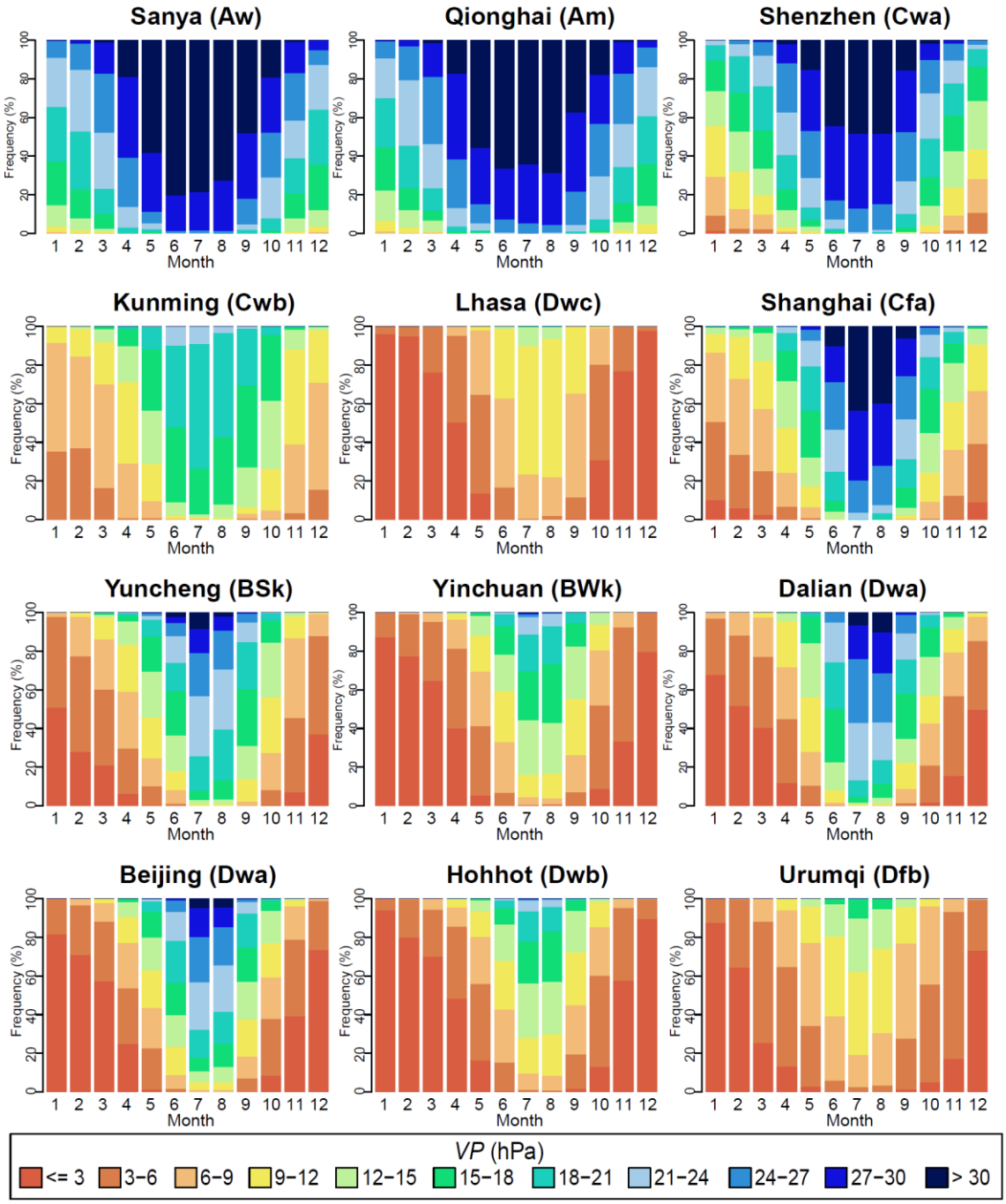

Fig. 6.1.5 Monthly frequencies of different *VP* value classes at 14 LST in 12 cities in 2000─2012 (Sanya: 2000─2008)

VP in Sanya (Aw) and Qionghai (Am) was normally above 18 hPa, while in Shenzhen (Cwa), it was above 12 hPa. In Kunming (Cwb), *VP* conditions were between 3 hPa and 21 hPa, while in Lhasa (Dwc) *VP* conditions were below 12 hPa. There were two main *VP* conditions in Shanghai (Cfa): between 3 hPa and 15 hPa and between 27 hPa and 30 hPa. *VP* was always below 15 hPa in Yuncheng (BSk) and Yinchuan (BWk), it was below

9 hPa in Dalian (Dwa) and Beijing (Dwa), and it was below 12 hPa in Hohhot (Dwb) and Urumqi (Dfb), respectively. If *VP* conditions were compared with the topography information in ***Table 4.1.1***, it seemed that *VP* decreased when latitude increased. Although there seemed to be exceptions in this rule, such as Lhasa (Dwc), Dalian (Dwa) and Beijing (Dwa), the conditions can be explained by the altitude. In fact, Lhasa (Dwc) with the quite low *VP* value classes was the highest city compared with other 11 cities. Although the main AH conditions of Dalian (Dwa) and Beijing (Dwa) presented lower *VP* distributions, there were obviously more days with high *VP* (less than 33 days) in Dalian (Dwa) and Beijing (Dwa), than in Hohhot (Dwb) and Urumqi (Dfb), of which the last two are located at higher altitudes.

Table 6.1.3 Days per year of each *VP* value class in 12 cities at 14 LST in 2000─2012 (Sanya: 2000─2008)*

City	Below 3 hPa	3─6 hPa	6─9 hPa	9─12 hPa	12─15 hPa	15─18 hPa	18─21 hPa	21─24 hPa	24─27 hPa	27─30 hPa	Above 30 hPa
Sanya (Aw)	0	0	1	3	10	25	39	51	47	73	115
Qionghai (Am)	0	0	1	5	14	22	34	50	58	80	101
Shenzhen (Cwa)	1	8	20	28	36	38	39	37	45	60	54
Kunming (Cwb)	0	33	89	64	42	66	64	7	0	0	0
Lhasa (Dwc)	162	71	61	65	5	0	0	0	0	0	0
Shanghai (Cfa)	9	42	58	47	36	29	27	24	29	33	31
Yuncheng (BSk)	46	81	52	37	33	30	30	27	17	7	4
Yinchuan (BWk)	120	85	42	35	36	26	16	5	1	0	0
Dalian (Dwa)	72	74	44	32	27	28	21	26	23	12	5
Beijing (Dwa)	108	69	36	30	28	22	23	22	16	8	3
Hohhot (Dwb)	143	78	42	38	32	19	10	3	0	0	0
Urumqi (Dfb)	88	116	79	54	22	5	0	0	0	0	0

* The number of days more than or equal to 33 in each city has been marked with grey.

The monthly frequencies of relative humidity (*RH*) value classes in each city were depicted in ***Fig. 6.1.6***. Compared to *VP* conditions, the most humid conditions did not always appear in summer in each city, e.g. in Qionghai (Am) and Urumqi (Dfb).

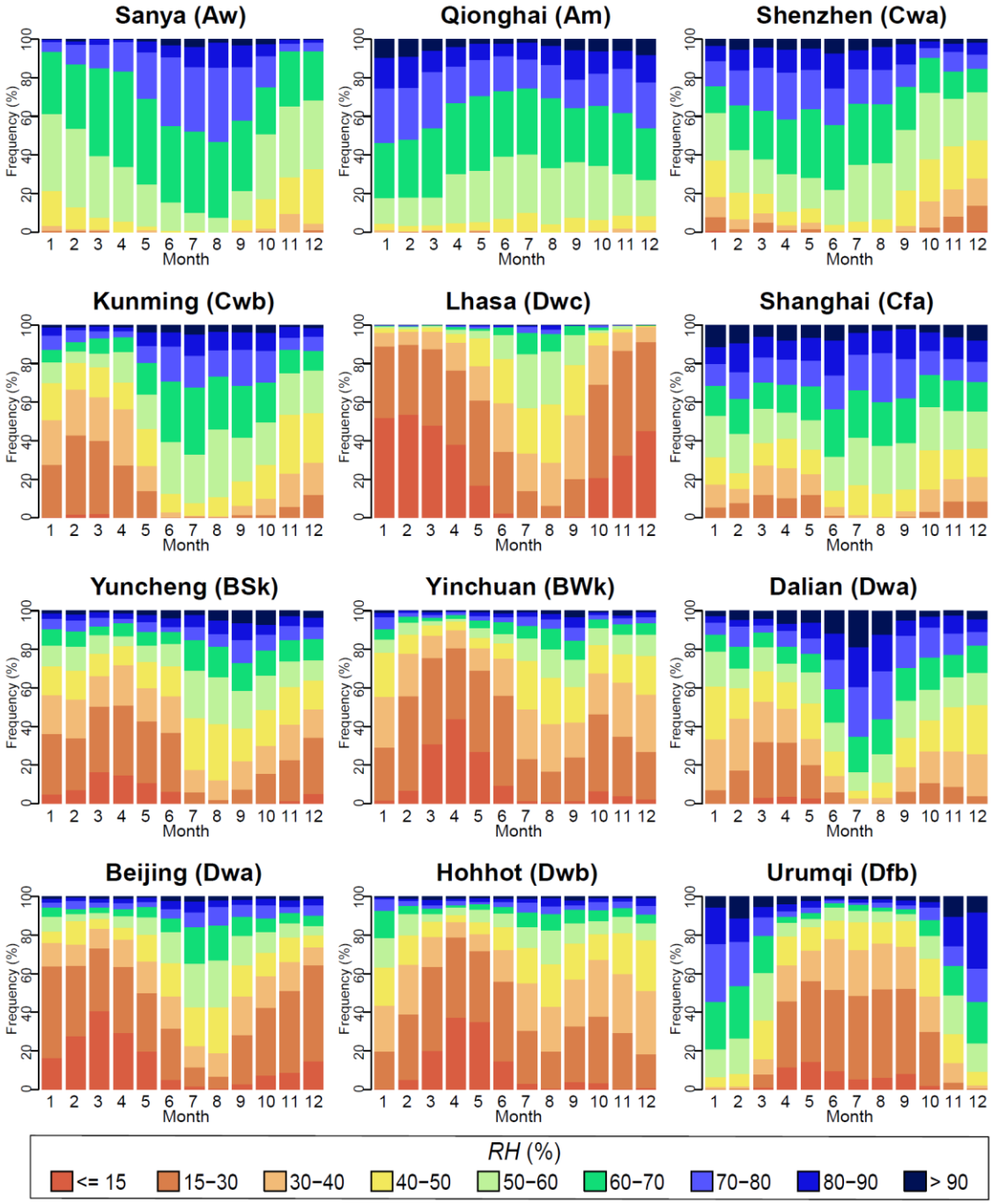

Fig. 6.1.6 Monthly frequencies of different *RH* value classes at 14 LST in 12 cities in 2000─2012 (Sanya: 2000─2008)

Table 6.1.4 presented the days per year of *RH* conditions at 14 LST in the 12 selected cities. However, the AH conditions indicated by *RH* values were the relative conditions. In order to describe *RH* conditions briefly, the *RH* conditions existed more than or equal to 40 days were considered as the main conditions in each city. In Sanya (Aw), *RH* varied between 50% and 80%, in Qionghai (Am) between 50% and 90%, in Shenzhen (Cwa)

between 40% and 80%, and in Shanghai (Cfa) between 40% and 90%, respectively. This was a group of cities with humid environments, as they are located near to the sea and they were only weakly influenced by the dry wind from the north. *RH* varied between 15% to 70% in Kunming (Cwb) and Urumqi (Dfb), between 15% and 60% in Yuncheng (BSk), and between 15% and 80% in Dalian (Dwa), respectively. Most of these cities were situated in inland China, where the influences of the monsoons was weak. However, these cities are close to relative huge water bodies like rivers, lakes or the sea, which might be regarded as the one kind of the locally water-vapour resource. The last group of cities are Lhasa (Dwc), Yinchuan (BWk), Beijing (Dwa) and Hohhot (Dwb) with *RH* conditions always below 50% at 14 LST. The urban areas of these cities were mainly influenced by dry wind, and the distribution of vegetation around these cities were limited. This situation results in a dry environment for human beings.

Table 6.1.4 Days per year of each *RH* value class in 12 cities at 14 LST in 2000─2012 (Sanya: 2000─2008)*

City	below 15%	15─30%	30─40%	40─50%	50─60%	60─70%	70─80%	80─90%	above 90%
Sanya (Aw)	0	1	6	34	96	134	69	19	5
Qionghai (Am)	0	0	2	20	86	119	76	42	19
Shenzhen (Cwa)	1	12	22	47	89	88	57	35	14
Kunming (Cwb)	2	51	49	59	71	63	38	23	9
Lhasa (Dwc)	94	126	59	42	29	10	3	1	0
Shanghai (Cfa)	0	21	33	49	73	68	55	44	23
Yuncheng (BSk)	20	82	60	63	51	37	22	17	12
Yinchuan (BWk)	41	122	75	53	30	20	12	8	4
Dalian (Dwa)	3	41	57	60	53	49	46	32	25
Beijing (Dwa)	53	114	50	46	40	28	18	11	5
Hohhot (Dwb)	38	113	80	56	34	20	12	8	4
Urumqi (Dfb)	18	89	52	45	42	40	33	30	17

* The number of days more than or equal to 40 in each city has been marked with grey.

6.1.4.4 Conditions of wind

The distributions of wind direction (WD) and wind velocity (*v*) of each city by wind roses with 3-hour data were depicted in ***Fig. 6.1.7***. The monthly frequencies of different *v* value classes in each city were presented in ***Fig. 6.1.8***. According to the information in these tow figures, the wind conditions in all 12 cities were mainly with *v* values below 2.5 m/s. However, there were distinguished conditions in each city, not only on the *v* values and directions, but also on the temporal distributions.

The main *v* values in Sanya (Aw) and Lhasa (Dwc) were between 0.5 and 1.5 m/s, and the main WD in these two cities were the east. The relative low *v* values (compared to other cities) may be because that hills (at the south and southeast in Sanya (Aw)) or mountains (at the north and south in Lhasa (Dwc)) prevent the strong wind from blowing into these two cities. The *v* values in 0.5─1.5 m/s and 1.5─2.5 m/s were the main conditions in Yuncheng (BSk), Yinchuan (BWk) and Hohhot (Dwb). The altitude of Yinchuan (BWk) and Hohhot (Dwb) is higher than 1000 (m), and the wind resource was from north. Because of the mountains is along the north side of Yinchuan (BWk), and along the north side and southeast side in Hohhot (Dwb), the wind was blocked in these directions in these two cities. The wind in Yuncheng (BSk) was blocked by the mountains at the north side and east side, respectively. The *v* values in 1.5─ 2.5 m/s appeared with the high frequencies in Qionghai (Am), Shenzhen (Cwa), Kunming (Cwb), Shanghai (Cfa), Dalian (Dwa), Beijing (Dwa) and Urumqi (Dfb); meanwhile there was also a number of days with *v* above 2.5 m/s in Kunming (Cwb), Shanghai (Cfa) and Dalian (Dwa). This group of cities is mostly circled by discontinuous mountains which can block the strong wind partially. Wind velocity of 2.5─4.5 m/s occurred with the relatively high frequency in Kunming (Cwb), Shanghai (Cfa), and Dalian (Dwa). In fact, two cities in this group are coastal cities, i.e. Shanghai (Cfa) and Dalian (Dwa). It might be that the sea wind can influence these cities directly without too many obstacles. For Kunming (Cwb), the main strong wind came from the direction where there is Dian Lake neighbour

to Kunming (Cwb) at the southwest. The possible reason might be related to the heat convection between the land and the large water body.

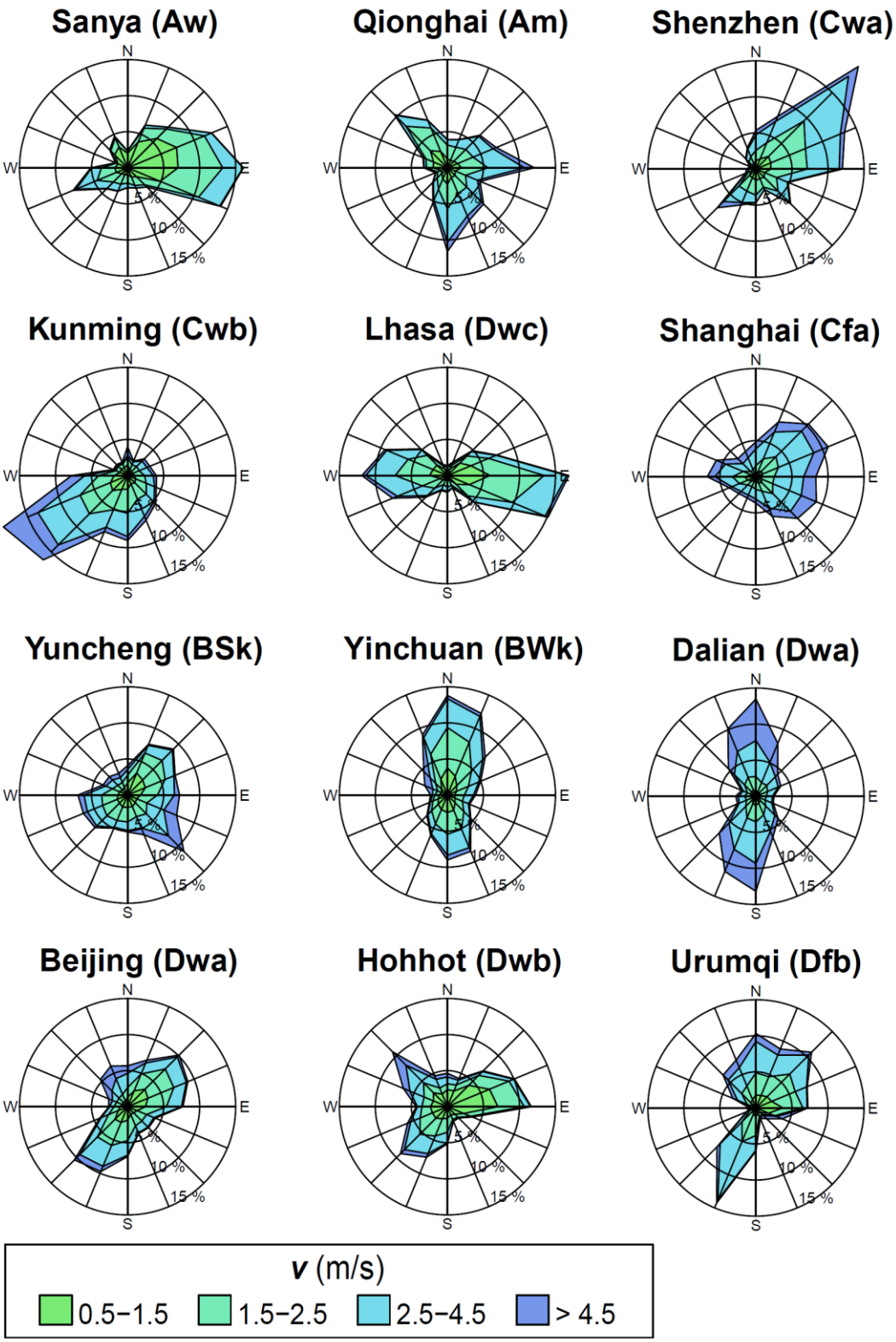

Fig. 6.1.7 Wind roses of 12 cities based on the data at 8 points in time in 2000─2012 (Sanya: 2000─2008)

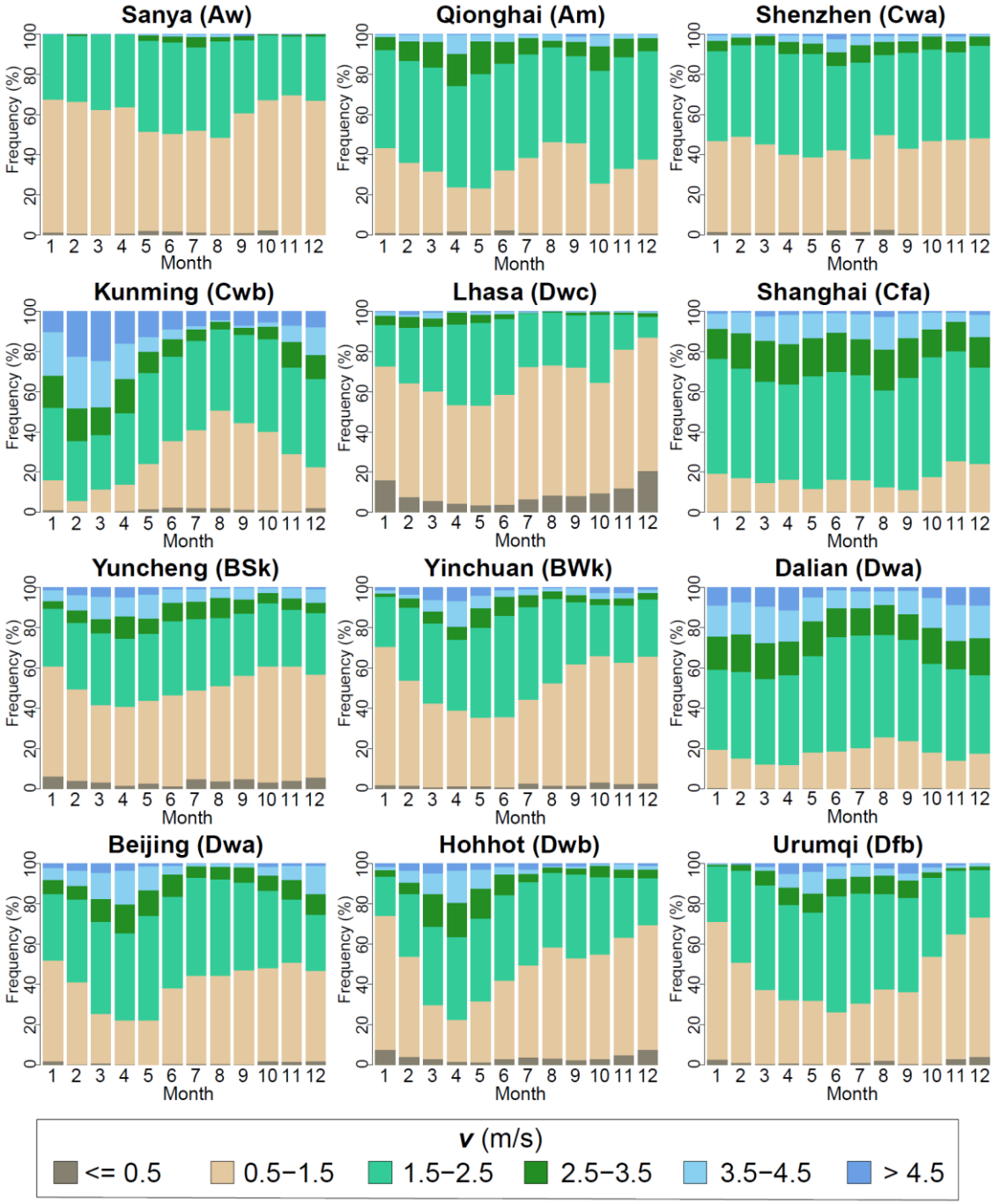

Fig. 6.1.8 Monthly frequencies of different *v* value classes at 8 points in time in 12 cities in 2000—2012 (Sanya: 2000—2008)

The variations of the monthly frequencies of different *v* value classes were not drastically in Sanya (Aw), Shenzhen (Cwa), Lhasa (Dwc), Shanghai (Cfa), and Yuncheng (BSk). The most frequent high *v* values (above 2.5 m/s) were in summer in Sanya (Aw) and Shenzhen (Cwa), in April and May in Lhasa (Dwc), in August and September in Shanghai (Cfa)

and in spring in Yuncheng (BSk), respectively. With the obviously seasonal changings, the most frequent high *v* values (above 2.5 m/s) existed in spring in Yinchuan (BWk), Beijing (Dwa) and Hohhot (Dwb), respectively. The most frequent high *v* values existed in May in Urumqi (Dfb). The most frequent high *v* values appeared in April and October in Qionghai (Am), where there was fluctuant distributions of *v* values through the whole year. The most frequent high *v* values appeared in March and December in Dalian (Dwa), where there was also fluctuant distributions of *v* values through the whole year. The most frequent high *v* values existed in February in Kunming (Cwb), where there were the most drastically variations of the *v* values through the whole year, compared to other 11 cities.

6.2 Implementation of HTC in KGC on macro scale

Under the assumption that the selected cities were the representation of each KGC type on macro scale, the HTC information together with the AH information has been implemented in 11 KGC types. Meanwhile, according to the information, the HTC conditions in each KGC type, with the respect of fluctuation, the differentiation, as well as the similarity, have been analysed and compared with the considerations on macro scale.

6.2.1 HTC conditions of each climate type in KGC

The thermal conditions of each KGC type were represented through 12 groups of figures in ***Fig. 6.2.1***: Aw (Sanya), Am (Qionghai), Cwa (Shenzhen), Cwb (Kunming), Cfa (Shanghai), Dwa (Beijing), Dwa (Dalian), Dwb (Hohhot), Dwc (Lhasa), Dfb (Urumqi), BSk (Yuncheng) and BWk (Yinchuan). These figures are based on the frequencies of PET in 3-value classes and the frequencies of *VP* in 4-value classes. Each group consists of 6 bar graphs corresponding to the annual frequencies of PET (**PET_a**), frequencies of PET in the hottest month (**PET_h**), frequencies of PET in the coldest month (**PET_c**), annual frequencies of *VP* (**VP_a**), frequencies of *VP* in the wettest month (**VP_w**) and frequencies

of *VP* in the driest month (**VP_d**). PET has been used to indicate the hot/cold conditions, and *VP* has been used to indicate the wet/dry conditions.

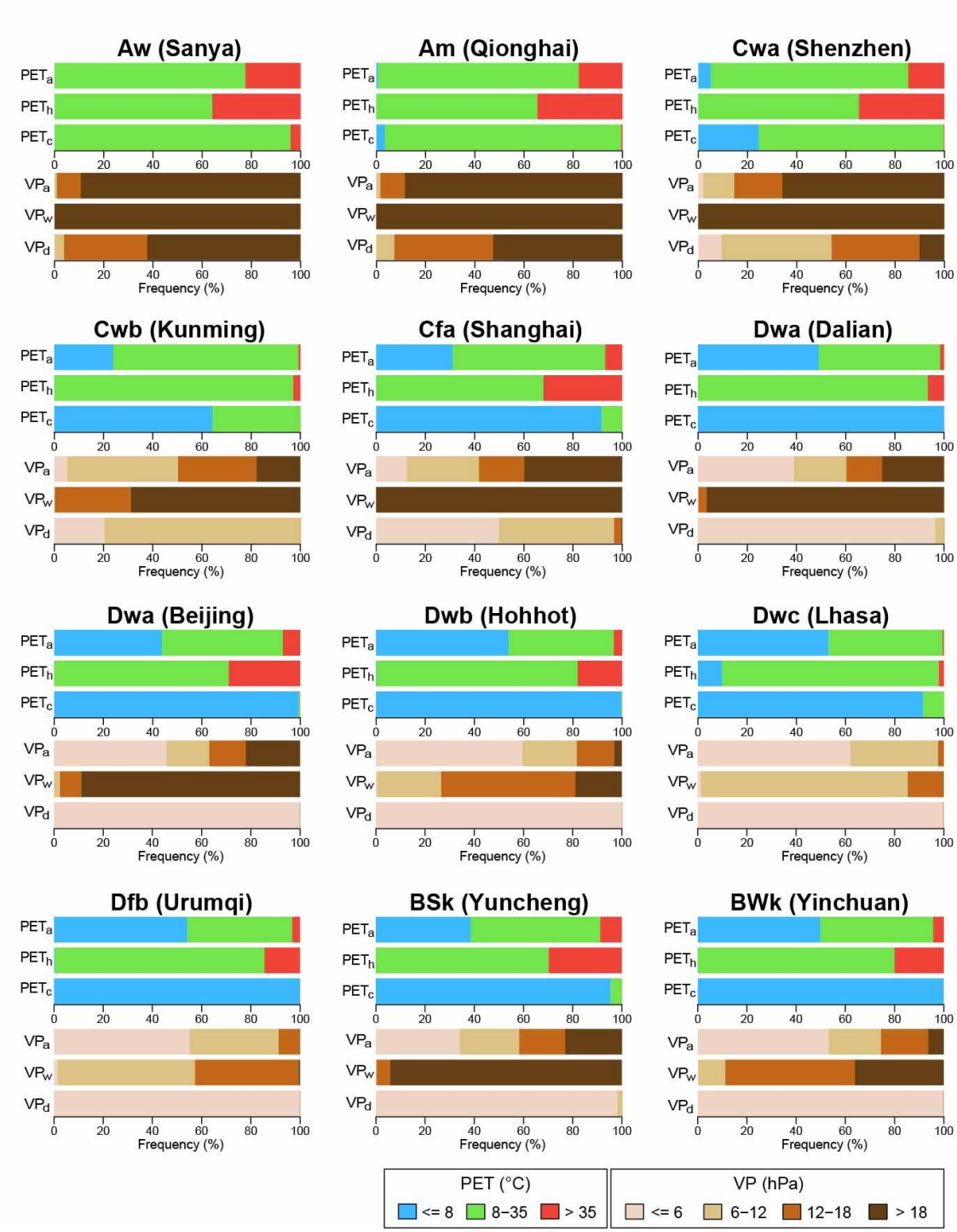

Fig. 6.2.1 The quantification of HTC conditions in 11 climate types in KGC in China (**PET_a**: **annual** frequencies of **PET**; **PET_h**: frequencies of **PET** in the **hottest** month; **PET_c**: frequencies of **PET** in the **coldest** month; **VP_a**: **annual** frequencies of ***VP***; **VP_w**: frequencies of ***VP*** in the **wettest** month; **VP_d**: frequencies of ***VP*** in the **driest** month)

In relation to the climate type Cwa (Shenzhen), the results of the annual analysis shows that the frequency of PET below 8 ℃ was approx. 5% points in time, while for approx. 80 % of the points in time of a year, PET was ranged between 8 ℃ and 35 ℃ and 15 % exceeded the 35 °C. In the hottest month, there was no condition of PET ≤ 8 °C, but there were 65 % of the points in time in the month with PET between 8 ℃ and 35 ℃, and approx. 35 % of the time with PET above 35 ℃. During the coldest month, PET conditions below 8 ℃ reached 25% points in time in the month, and approx. 75 % of the time were 8 °C < PET ≤ 35 °C. Finally, a frequency of 0.5 % depicted PET above 35 ℃ in the coldest month. The annual frequencies of *VP* below 6 hPa, *VP* between 6 hPa and 12 hPa, *VP* between 12 hPa and 18 hPa, and *VP* above 18 hPa in Cwa (Shenzhen) were approx. 2 %, 13 %, 20 % and 66 % points in time of one year, respectively. The frequency of *VP* above 18 hPa dominated with 100 % points in time in the wettest month. The approx. frequencies of the points in time in the driest month of *VP* were approx. 9 %, 45 %, 36 % and 10 % for *VP* below 6 hPa, *VP* between 6 hPa and 12 hPa, *VP* between 12 hPa and 18 hPa, and *VP* above 18 hPa, respectively. Assessment of each other climate type follows the same methodology as conducted for Cwa (Shenzhen).

6.2.2 Comparison of the entire HTC conditions between climate types

According to the 12 bar graphs of $\mathbf{PET_a}$ depicted in ***Fig. 6.2.1***, there were the most frequently thermal stress conditions in the KGC type Aw (Sanya): PET in 78 % points in time of the year was ranged between 8 ℃ and 35 ℃, while PET in 22 % of the time is higher than 35 ℃. Dwa (Beijing), Dwb (Hohhot), Dwc (Lhasa) and Dfb (Urumqi) presented the similar annual frequencies of PET. However, in Dwc (Lhasa), due to the fact that the value class of PET > 35 ℃ rarely exists (less than 0.5 %), the climate type Dwc (Lhasa) has the lowest frequent of the heat stress.

In relation to $\mathbf{VP_a}$ in ***Fig. 6.2.1***, the wettest conditions existed in the KGC type Aw (Sanya), where approx. 1 % points in time of one year possess *VP* between 6 hPa to 12 hPa, almost 10 % points in time was between 12 hPa to 18 hPa and 89 % points in time,

which is the highest among the others, was presented with *VP* > 18 hPa. The driest conditions existed in the KGC type Dwc (Lhasa) (where at 62 % points in time of one year *VP* was below 6 hPa, and at 36 % *VP* ranged between 6 hPa and 12 hPa) and Dfb (Urumqi) (where at 55 % points in time of one year *VP* was below 6 hPa, and at 36 % points in time *VP* ranged between 6 hPa and 12 hPa).

6.2.3 Comparison between the opposite extreme months

The oppositely extreme months refer to the hottest month versus the coldest month, and the wettest month versus the driest month. The hot/cold conditions of each KGC type shifted between the conditions regarding to the hottest month and the coldest month. The wet/dry conditions of each KGC type shifted between the conditions in the wettest month and the driest month. For example, in Cwa (Shenzhen) for 65 % points in time of PET ranged between 8 ℃ and 35 ℃, while for 35 % PET exceeded 35 ℃, regarding the hottest month. On the other hand, during the coldest month, PET presented values lower than 8 ℃ for a frequency of 25 % points in time, while 75 % points in time of the month indicated by PET ranged between 8 ℃ and 35 ℃. Thus, the frequency of PET above 35 ℃ in each other month in Cwa (Shenzhen) will be equal to or less than 35 %, and the frequency of PET below 8 ℃ in each other month will be equal to or less than 25 %. During the wettest month, the frequency of *VP* above 18 hPa reached to 100% points in time. Additionally, during the driest month, approx. 9 % points in time was with *VP* below 6 hPa, approx. 45 % was with *VP* between 6 hPa and 12 hPa, approx. 36 % was with *VP* between 12 hPa and 18 hPa, and approx. 10 % was with *VP* above 18 hPa. Therefore, the frequency of *VP* above 18 hPa in each other month in Cwa (Shenzhen) will be equal to or less than 100 %, while the frequency of *VP* ≤ 6 hPa in each other month will be equal to or less than 9 %.

6.2.4 Observed similarities in extreme months

According to the current value classes for PET and *VP*, similarities were shown regarding

the HTC conditions that existed in extreme months, in several KGC types. In the KGC types Dwa (Dalian), Dwb (Hohhot), Dfb (Urumqi) and BWk (Yinchuan), the frequencies of PET presented with values equal to or less than 8 ℃ were **100 %**, regarding the coldest month. In the KGC types Aw (Sanya), Am (Qionghai), Cwa (Shenzhen) and Cfa (Shanghai), the frequencies of *VP* in the wettest month presented with values above 18 hPa, was also **100 %**. Furthermore, the frequencies of *VP* presented with values below 6 hPa was **100 %** for the driest month in the KGC types Dwa (Beijing), Dwb (Hohhot), Dwc (Lhasa), Dfb (Urumqi) and BWk (Yinchuan).

Due to the fact that one month was approx. 1/12 of one year, the annual frequency of the points in time of one month was approx. 8 % (≈ 1/12). However, the annual frequency of specific condition (**PET_a** or **VP_a**) was considerably higher than 8 %, due to the existence of the same condition in the other 11 months. For instance, in Cwa (Shenzhen), 100 % of the month is presented with a condition of *VP* > 18 hPa for the wettest month. Thus there was 8 % points in time in the annual frequency of this condition from the wettest month. According to the bar graph of **VP_a** in Cwa (Shenzhen), the annual frequency of *VP* above 18 hPa was 66 %. Therefore, the annual frequency of *VP* above 18 hPa in the other 11 months is 58 % (= 66 % – 8 %).

6.2.5 Differences in KGC type Dwa

Although Dwa (Beijing) and Dwa (Dalian) belong to the same KGC type (i.e. Dwa) in the world map version of 1976–2000 (please see ***Fig. 6.1.1***), according to ***Fig. 6.2.1***, the HTC conditions of Dwa (Beijing) and Dwa (Dalian) were presented with some differentiations. For instance, the analysis on the hottest month presented the biggest differentiations. The **PET_h** in Dwa (Beijing) were 71 % points in time and 29 % points in time for PET between 8 ℃ and 35 ℃, and PET above 35 ℃, respectively. In contrast, the **PET_h** in Dwa (Dalian) were 93 % and 7 % for PET between 8 ℃ and 35 ℃, and PET above 35 ℃, respectively. This can be explained due to the fact that Dalian is a coastal city, while Beijing is an inland city; therefore, the background meteorological conditions

(as well as the HTC conditions) of these two study sites are different.

6.3 HTC information service for design on micro scale

The service for environment community design, based on the evaluation of HTC information on micro scale in current study, was supported by both the representative input data (i.e. long-term meteorological data analysis), and the simulated output results (i.e. short-term micrometeorological simulations). In general, there were two sections of services relating to the analysis on HTC conditions before design, and the evaluation on the mitigation after design. The entire process of the evaluation on the HTC conditions for community environment design in each scenario has been generalised in ***Fig. 6.3.1***. In the process, the figures on the distribution of PET, the distribution of SVF, and the distribution of *v* in each scenario, can be checked in Appendix A2, Appendix A3, and Appendix A4, respectively. The figures on the difference in PET, the difference in SVF, and the difference in *v* in each scenario, can be checked in Appendix A5, Appendix A6, and Appendix A7, respectively. Due to the essential preparations, the decisions on simulations, and the service for design, the results have been divided into four progressions.

6.3.1 Preparation of input for simulations

The hottest month and the wettest month in each city have been detected (***Table 6.3.1***), according to the analysis of the monthly frequencies of the conditions of T_a and the conditions of *VP* in Part One (Preliminary analysis). The hottest month has been selected as the reference period for simulation in each scenario, as T_a is the direct input data. Thus, the input data was prepared through the utilisation of the meteorological data in the selected month for each scenario, i.e. Sanya (Aw), Qionghai (Am), Shenzhen (Cwa), Kunming (Cwb), Shanghai (Cfa), Beijing (Dwa), Dalian (Dwa), Hohhot (Dwb), Lhasa (Dwc), Urumqi (Dfb), Yuncheng (BSk) and Yinchuan (BWk), in the twice simulations.

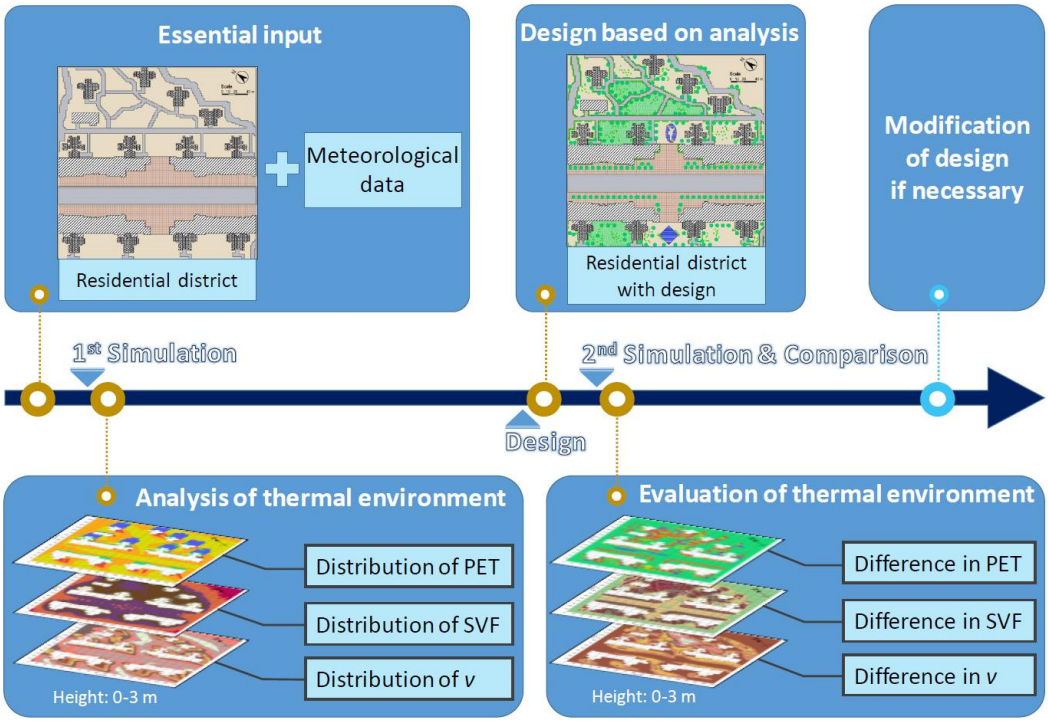

Fig. 6.3.1 The process of the evaluation on the human thermal comfort for community environment design

Table 6.3.1 The hottest month and the wettest month in each city

Scenario	Hottest month (T_a)	Month with the most intense heat stress (PET)	Wettest month (*VP*)	Relative wettest month (*RH*)
Sanya (Aw)	June	June	June	August
Qionghai (Am)	July	July	June	January
Shenzhen (Cwa)	July	August	July	June
Kunming (Cwb)	July	August	July	July
Shanghai (Cfa)	July	July	July	June
Beijing (Dwa)	July	July	July	July
Dalian (Dwa)	August	July	August	July
Hohhot (Dwb)	July	July	July	January
Lhasa (Dwc)	July	July	July	July
Urumqi (Dfb)	July	July	July	January
Yuncheng (BSk)	July	July	July	September
Yinchuan (BWk)	July	July	July	September

Table 6.3.2 presented the basic configuration for the input settings in the twice rounds simulations, i.e. the 1st round simulations (without design elements), and the 2nd round simulations (with design elements).

Table 6.3.2 Basic input settings of twice round simulations for 12 scenarios, based on the long-term data in the hottest month in each city

Scenario	Abbreviation*	Lat. (°)	Long. (°)	Hottest month	*v* (m/s)	WD	ATM (hPa)	DWPT (℃)	SH (g/kg)
Sanya (Aw)	SY**B** (1st) SY**E** (2nd)	18.23	109.52	Jun.	1.5	E	982	24.6	19.8
Qionghai (Am)	QH**B** (1st) QH**E** (2nd)	19.23	110.47	Jul.	2	E	1000	24.6	19.5
Shenzhen (Cwa)	SZ**B** (1st) SZ**E** (2nd)	22.55	114.1	Jul.	2.4	NE	997	24.3	19.2
Kunming (Cwb)	KM**B** (1st) KM**E** (2nd)	25.02	102.68	Jul.	2.3	WSW	807	16.4	14.5
Shanghai (Cfa)	SH**B** (1st) SH**E** (2nd)	31.4	121.47	Jul.	3.1	ENE	1002	23.9	18.6
Beijing (Dwa)	BJ**B** (1st) BJ**E** (2nd)	39.93	116.28	Jul.	2.3	SW	999	19.9	14.6
Dalian (Dwa)	DL**B** (1st) DL**E** (2nd)	38.90	121.63	Aug.	3.4	S	997	20.6	15.0
Hohhot (Dwb)	HH**B** (1st) HH**E** (2nd)	40.82	111.68	Jul.	1.7	E	888	12.1	9.9
Lhasa (Dwc)	LS**B** (1st) LS**E** (2nd)	29.07	91.13	Jul.	1.7	E	652	7.4	9.9
Urumqi (Dfb)	UR**B** (1st) UR**E** (2nd)	43.78	87.62	Jul.	2.5	SSW	904	8.9	7.9
Yuncheng (BSk)	YC**B** (1st) YC**E** (2nd)	35.03	111.02	Jul.	2.2	SE	962	19.9	15.2
Yinchuan (BWk)	YCn**B** (1st) YCn**E** (2nd)	38.48	106.22	Jul.	2.2	N	882	14.3	11.6

* **B** in the abbreviations means there are just buildings in the 1st round simulations, and **E** means there are design elements in the 2nd round simulations; **Lat.**: latitude; **Long.**: longitude; ***v***: wind velocity; **WD**: wind direction; **ATM**: atmospheric pressure; **DWPT**: dew point; **SH**: specific humidity; Simulation date: 02.07.2012 and 03.07.2012; Reference time zone: GMT+8; cloud cover: 0/8.

Figure 6.3.2 is the visualised information on the hourly T_a and *RH* in one simulated day, in which the data at 2 LST, 5 LST, 8 LST, 11 LST, 14 LST, 17 LST, 20 LST and 23 LST was calculated based on the 3-hourly meteorological data in the individual cities, respectively. According to the data set, the hottest point in time is at 14 LST in Sanya (Aw), Qionghai (Am), Shenzhen (Cwa), Shanghai (Cfa), Beijing (Dwa) and Dalian (Dwa), and the hottest point in time is at 17 LST in Kunming (Cwb), Hohhot (Dwb), Lhasa (Dwc), Urumqi (Dfb) and Yinchuan (BWk). From 14 LST to 17 LST is the hottest period in Yuncheng (BSk). The coldest point in time is at 5 LST in most of the cities, except Lhasa (Dwc) and Urumqi (Dfb), where it is at 8 LST. For example in Shanghai (Cfa) in July, the

highest T_a (31.9 ℃) appears at 14 LST, and the lowest T_a (27.1 ℃) appears at 5 LST; and in Urumqi (Dfb) in July, the highest T_a (28 ℃) appears at 17 LST, and the lowest T_a (20.4 ℃) appears at 8 LST.

In contrast, the peak value and the valley value of *RH* appear with the opposite pattern in ***Fig. 6.3.2***: the highest *RH* is found at 5 LST in most of cities, except Lhasa (Dwc) and Urumqi (Dfb), in which it is found at 8 LST; the lowest *RH* appears at 14 LST in Sanya (Aw), Qionghai (Am), Shenzhen (Cwa), Shanghai (Cfa), Beijing (Dwa) and Dalian (Dwa), and at 17 LST in other 6 cities. For example in Shanghai (Cfa), the maximum *RH* (83 %) is at 5 LST, and minimum *RH* (64 %) is at 14 LST; and in Urumqi (Dfb), the maximum *RH* (53 %) is at 8 LST, and the minimum *RH* (31 %) is at 17 LST. Generally, the highest T_a combines with the lowest *RH*, and the lowest T_a combines with the highest *RH* in each scenario.

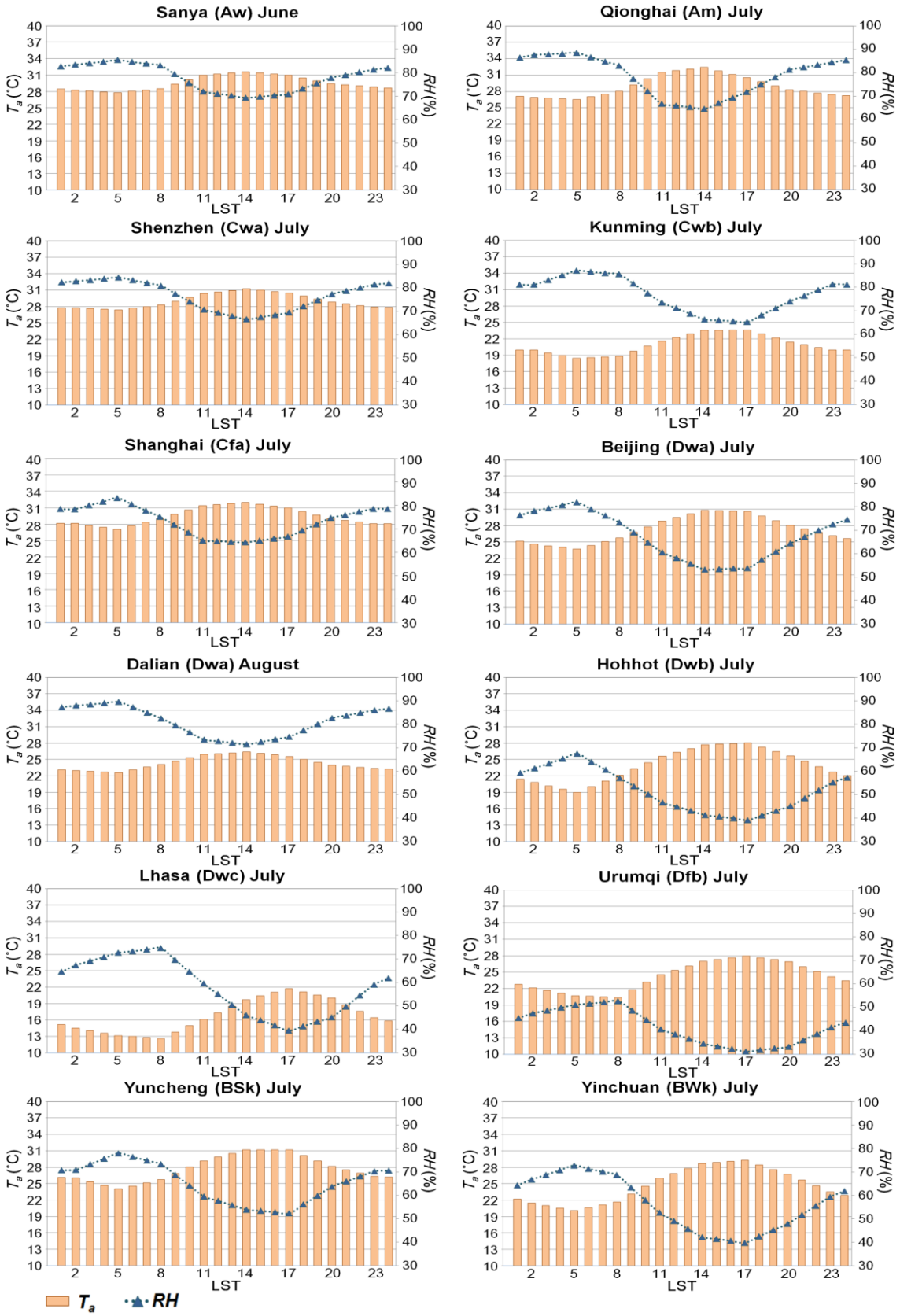

Fig. 6.3.2 Hourly average values of T_a and *RH* in one day in the hottest month

6.3.2 Estimation of parameters in the 1st round simulation

Under the objectives on the detection of the interaction of the related parameters, the effects of these parameters on PET values, as well as the concentration of the possibly modified parameters, the partial results from the multiple linear regression have been arranged into ***Table 6.3.3***, which presented the highest estimates in the test for each scenario.

Table 6.3.3 Partial estimates of 10 parameters, respectively, on PET values in 12 simulations, based on multiple linier regression function in R language

E. *	SY**B**	QH**B**	SZ**B**	KM**B**	SH**B**	BJ**B**	DL**B**	HH**B**	LS**B**	UR**B**	YC**B**	YCn**B**
Int.	4.0 $\times 10^7$	4.6 $\times 10^7$	-2.4 $\times 10^7$	-1.8 $\times 10^6$	4.1 $\times 10^7$	-3.1 $\times 10^6$	-7.9 $\times 10^6$	-1.9 $\times 10^7$	2.7 $\times 10^6$	-5.0 $\times 10^5$	4.2 $\times 10^6$	4.6 $\times 10^6$
v	-2.9 $\times 10^7$	-5.0 $\times 10^6$	-2.1 $\times 10^6$	3.1 $\times 10^6$	2.1 $\times 10^6$	-7.2 $\times 10^6$	-2.0 $\times 10^6$	3.8 $\times 10^6$	-1.0 $\times 10^6$	-7.8 $\times 10^4$	-2.2 $\times 10^6$	-7.6 $\times 10^6$
T_a	-1.1 $\times 10^6$	-1.1 $\times 10^6$	5.7 $\times 10^5$	7.9 $\times 10^4$	-9.5 $\times 10^5$	2.1 $\times 10^4$	2.3 $\times 10^5$	3.3 $\times 10^5$	-1.0 $\times 10^6$	2.7 $\times 10^5$	-6.7 $\times 10^5$	2.9 $\times 10^5$
RH	-1.6 $\times 10^5$	-1.6 $\times 10^5$	-9.3 $\times 10^3$	-9.1 $\times 10^3$	-2.3 $\times 10^5$	1.6 $\times 10^4$	4.5 $\times 10^4$	1.4 $\times 10^5$	-3.1 $\times 10^5$	5.4 $\times 10^4$	-4.0 $\times 10^4$	4.0 $\times 10^4$
T_{mrt}	-5.6 $\times 10^5$	1.5 $\times 10^5$	-4.5 $\times 10^4$	3.5 $\times 10^4$	-4.3 $\times 10^3$	1.7 $\times 10^4$	-7.0 $\times 10^4$	1.5 $\times 10^5$	-1.1 $\times 10^5$	8.8 $\times 10^3$	-4.0 $\times 10^4$	-7.8 $\times 10^4$
K_{di}	-1.1 $\times 10^4$	-1.2 $\times 10^5$	4.3 $\times 10^4$	-4.7 $\times 10^3$	-1.8 $\times 10^4$	-4.7 $\times 10^3$	-2.8 $\times 10^3$	2.8 $\times 10^4$	9.1 $\times 10^2$	-1.9 $\times 10^3$	-3.0 $\times 10^4$	1.1 $\times 10^4$
K_{fs}	-1.1 $\times 10^5$	3.9 $\times 10^5$	7.1 $\times 10^4$	7.0 $\times 10^4$	-1.5 $\times 10^5$	2.7 $\times 10^5$	1.3 $\times 10^5$	-8.2 $\times 10^4$	-3.4 $\times 10^4$	3.5 $\times 10^4$	5.1 $\times 10^3$	-1.8 $\times 10^5$
K_{rf}	2.1 $\times 10^5$	1.0 $\times 10^5$	1.1 $\times 10^5$	-1.7 $\times 10^5$	5.2 $\times 10^5$	2.4 $\times 10^5$	-5.5 $\times 10^4$	-8.5 $\times 10^3$	-4.5 $\times 10^4$	1.7 $\times 10^4$	-8.8 $\times 10^3$	-1.0 $\times 10^5$
L_{en}	-1.1 $\times 10^5$	-1.2 $\times 10^5$	7.2 $\times 10^4$	2.3 $\times 10^4$	-1.1 $\times 10^5$	-1.4 $\times 10^3$	3.0 $\times 10^4$	4.4 $\times 10^4$	-6.5 $\times 10^3$	-3.0 $\times 10^3$	-1.2 $\times 10^4$	-9.8 $\times 10^3$
SVF	-3.9 $\times 10^7$	-4.5 $\times 10^7$	2.5 $\times 10^7$	2.5 $\times 10^6$	-4.1 $\times 10^7$	1.9 $\times 10^6$	7.6 $\times 10^6$	1.9 $\times 10^7$	-2.6 $\times 10^6$	3.3 $\times 10^5$	-2.9 $\times 10^6$	-4.2 $\times 10^6$
T_s	1.6 $\times 10^5$	-8.8 $\times 10^5$	1.1 $\times 10^6$	3.4 $\times 10^4$	-1.6 $\times 10^6$	3.4 $\times 10^5$	5.1 $\times 10^5$	6.3 $\times 10^4$	3.3 $\times 10^5$	-4.3 $\times 10^4$	1.5 $\times 10^5$	-2.4 $\times 10^5$
Omit	---	---	---	---	---	---	---	---	---	---	---	---
M. R^2	0.9538	0.963	0.9556	0.9829	0.9674	0.9505	0.9588	0.9712	0.9932	0.9851	0.9475	0.9566
A. R^2	0.9536	0.9628	0.9555	0.9828	0.9673	0.9503	0.9586	0.9711	0.9931	0.9851	0.9472	0.9564

*** E.**: estimate; **B.**: the 1st round simulations (with buildings, but without design elements); **Int.**: intercept; v: estimate on wind velocity (m/s) individually; T_a: estimate on air temperature (℃) individually; RH: estimate on relative humidity individually; T_{mrt}: estimate on mean radiant temperature (℃) individually; K_{di}: estimate on direct short wave radiation (W/m^2) individually; K_{fs}: estimate on diffuse short wave radiation (W/m^2) individually; K_{rf}: estimate on reflected short wave radiation (W/m^2) individually; L_{en}: estimate on long wave radiation from environment (W/m^2) individually; **SVF**: estimate on sky view factor individually; T_s: estimate on surface temperature (℃) individually; **M.**: multiple; **A.**: adjusted; **Omit**: the lower estimates of other crossing impacts (hundreds of rows) are omitted.

First of all, the high R^2 (above 0.9) indicates that the parameters involved in the multiple liner regression have been well considered in the calculation of PET in ENVI-met 3.0. Meanwhile, the impact from each parameter on PET, which depends on the formula system in ENVI-met 3.0, was described through the estimate of the individual parameter on PET values. According to the first two highest estimates (in most of the scenario except LSB and URB in ***Table 6.3.3***; please see the grey rows), *v* and SVF almost contribute the highest effects to the PET values in simulations. In the scenarios of Lhasa (Dwc) (i.e. LS**B**) and Urumqi (Dfb) (i.e. UR**B**), the estimate of T_a is as high as that of *v*, or a little bit higher than that of *v*.

6.3.3 Community environment design

The residential district with high-rise buildings were depicted in ***Fig. 5.3.1***. The materials (i.e. input settings, in the legend in ***Fig. 5.3.1***) in the 1st round simulations have been maintained in the 2nd round simulations.

Before adding the design elements for the 2nd simulations, the conditions of SVF (please see ***Fig. A3.1*** in Appendix A3) in this residential district were the same for 12 scenarios. Based on the value classes, the figure depicts that the distributions of the lower SVF were nearby buildings, and the distributions of the higher SVF were farther from buildings. Meanwhile, the most of the areas concentrated in community environment design were with SVF in between 0.3 and 0.8. In the street valley, the SVF from 0.8 to 0.9 appears infrequently, and no SVF above 0.9 exists in the street valley.

Although the distributions of the PET were not associated with the distributions of SVF directly in the figures (please see the PET distributions in Appendix A2, and the SVF distribution in Appendix A3), SVF influences the radiant conditions greatly, especially on the incoming of short wave radiation in the concentrated area (i.e. the grid in the simulation area). Due to the difference of each scenario (i.e. the different location of each city on the earth), the direct short wave radiation incoming in one area was also changed

city by city, even with the same SVF conditions in the simulations. Meanwhile, according to the multiple liner regression, SVF has the strongest effect on the simulated PET in each scenario.

All the figures on the distribution of values, which were from simulations, presented the conditions in the residential district in the height of z = 0—3 (m) up from the ground. According to the previously visualised analysis of the HTC conditions at each point in time, the point in time with PET presenting the most frequently emerged heat stress was selected as the represented HTC conditions in each scenario (please see ***Table 6.3.4***). Meanwhile, the PET distribution of each scenario has been depicted in to a figure, which was individually combined with the community environment design (i.e. the CAD drawing, please see Appendix A2). Following the basic design rules and the adding strength in ***Table 5.3.2***, trees, hedges, grass and water bodies were applied in the design, and they were attached to the areas, where there were specific HTC conditions in each scenario. Furthermore, the distribution of v at the same point in time in each scenario has also been presented (please see Appendix A4), which will be used to analyse the distribution of PET, as the high impacts of SVF and v were both detected through the multiple liner regression in section 6.3.2.

Table 6.3.4 The point in time with the most frequently heat stress in each scenario

Scenario	**The point in time**
Sanya (Aw)	**14** LST
Qionghai (Am)	**15** LST
Shenzhen (Cwa)	**15** LST
Kunming (Cwb)	**16** LST
Shanghai (Cfa)	**14** LST
Beijing (Dwa)	**14** LST
Dalian (Dwa)	**14** LST
Hohhot (Dwb)	**15** LST
Lhasa(Dwc)	**17** LST
Urumqi (Dfb)	**16** LST
Yuncheng (BSk)	**15** LST
Yinchuan (BWk)	**15** LST

6.3.3.1 Sanya (Aw)

The most frequently heat stress appeared at 14 LST in the 1st simulation in Sanya (Aw). PET distribution at 14 LST in Sanya (Aw) was depicted in ***Fig. A2.1***, and the distribution of *v* at 14 LST in Sanya (Aw) was in ***Fig. A4.1***.

In this district in Sanya (Aw), there was no area with PET below 29 ℃ at 14 LST. The areas with PET below 41 ℃ were located in the shade areas of buildings, and all the non-shaded areas of this district were with PET above 41 ℃. Areas with PET between 41 ℃ and 54 ℃ existed as the basic HCT conditions in this district, which were roughly in the zone of x = (80—95) and y = (0—110), the zone of x = (35—60) and y = (95—170), the zone of x = (0—170) and y = (50—65), and the zone of x = (100—170) and y = (120—170). Comparing with the simulation input in ***Table 6.3.2*** (i.e. WD from E), the simulated wind firstly arrived the zone of x = (100—170) and y = (120—170).

According to ***Fig. A4.1***, the relative low *v* conditions (below 0.6 m/s) appeared on the lee side much more frequently than that on the windward side. The areas with relative high *v* (above 2 m/s) were in between the buildings in the E-W direction.

Comparing with the distribution of *v* in ***Fig. A4.1***, and the input WD (i.e. E) in Sanya (Aw) (please see ***Table 6.3.2***), the areas with specific HTC conditions (***Fig. A2.1***) presented the orientational dependence, i.e. the distribution of specific HTC conditions associated with the distribution of *v* conditions, which was in the E-W direction. Meanwhile, the position of PET above 54 ℃ was corresponding with the position of *v* below 1 m/s, especially with the position of *v* below 0.2 m/s. In comparison, the position of PET in between 41 ℃ and 54 ℃ was corresponding with the position of *v* above 1 m/s. Furthermore, comparing ***Fig. A2.1*** and ***Fig. A4.1***, most of the areas with PET above 54 ℃ were on the sunny side of the buildings, as well as on the lee side (i.e. the W side).

6.3.3.2 Qionghai (Am)

The most frequently heat stress appeared at 15 LST in the 1st simulation in Qionghai (Am).

PET distribution at 14 LST in Qionghai (Am) was depicted in ***Fig. A2.2***, and the distribution of *v* at 15 LST in Qionghai (Am) was in ***Fig. A4.2***.

In this district in Qionghai (Am), there was no area with PET below 29 ℃ at 15 LST. The areas with PET below 41 ℃ were located in the shade areas of buildings, and all the non-shaded areas of this district were with PET above 41 ℃. The areas with PET between 41 ℃ and 47 ℃ were rare. Areas with PET between 47 ℃ and 54 ℃ existed as the basic HCT conditions in this district, which were roughly in the zone of x = (80─90) and y = (0─110), the zone of x = (40─55) and y = (90─150), the zone of x = (0─170) and y = (45─65), and the zone of x = (120─170) and y = (120─170). The simulated wind firstly arrived the last zone.

According to ***Fig. A4.2***, the relative low *v* conditions (below 1 m/s) appeared on the lee side much more frequently than on the windward side. The areas with relative high *v* (above 2 m/s) were in between the buildings in the E-W direction.

Comparing with the distribution of *v* in ***Fig. A4.2***, and the input WD (i.e. E) in Qionghai (Am) (please see ***Table 6.3.2***), the areas with specific HTC conditions (***Fig. A2.2***) presented the orientational dependence, i.e. the distribution of specific HTC conditions associated with the distribution of *v* conditions, which was in the E-W direction. Meanwhile, the position of PET above 54 ℃ was corresponding with the position of *v* below 1 m/s, the position of PET above 60 ℃ was corresponding with the position of *v* below 0.2 m/s, even around the shade area. The position of PET in between 47 ℃ and 54 ℃ was not corresponding with the distribution of other *v* value classes. Furthermore, comparing ***Fig. A2.2*** and ***Fig. A4.2***, most of the areas with PET above 54 ℃ were on the sunny side of the buildings, as well as on the lee side (i.e. the W side).

6.3.3.3 Shenzhen (Cwa)

The most frequently heat stress appeared at 15 LST in the 1st simulation in Shenzhen (Cwa). PET distribution at 15 LST in Shenzhen (Cwa) was depicted in ***Fig. A2.3***, and the

distribution of *v* at 15 LST in Shenzhen (Cwa) was in ***Fig. A4.3***.

In this district in Shenzhen (Cwa), there was no area with PET below 29 ℃ at 15 LST. The areas with PET below 41 ℃ were located in the shade areas of buildings, and all the non-shaded areas of this district were with PET above 41 ℃. The areas with PET between 41 ℃ and 47 ℃ were rare. Areas with PET between 41 ℃ and 54 ℃ existed as the basic HCT conditions in this district, which were roughly in the zone of x = (75—100) and y = (0—110), the zone of x = (35—65) and y = (90—150), the zone of x = (120—170) and y = (140—170). The simulated wind firstly arrived the NE side of the district.

According to ***Fig. A4.3***, the relative low *v* conditions (below 1.5 m/s) appeared on the lee side much more frequently than on the windward side. The areas with relative high *v* (above 2.5 m/s) were in between the buildings in the NE-SW direction.

Comparing with the distribution of *v* in ***Fig. A4.3***, and the input WD (i.e. NE) in Shenzhen (Cwa) (please see ***Table 6.3.2***), the areas with specific HTC conditions (***Fig. A2.3***) presented the orientational dependence, i.e. the distribution of specific HTC conditions associated with the distribution of *v* conditions, which was in the NE-SW direction. Meanwhile, the position of PET above 54 ℃ was corresponding with the position of *v* below 1 m/s, and the position of PET above 60 ℃ was corresponding with the position of *v* below 0.2 m/s. The position of PET in between 47 ℃ and 54 ℃ was not corresponding with the distribution of other *v* value classes. Furthermore, comparing ***Fig. A2.3*** and ***Fig. A4.3***, most of the areas with PET above 54 ℃ were on the sunny side of the buildings, as well as on the lee side (i.e. the SW side).

6.3.3.4 Kunming (Cwb)

The most frequently heat stress appeared at 16 LST in the 1st simulation in Kunming (Cwb). PET distribution at 16 LST in Kunming (Cwb) was depicted in ***Fig. A2.4***, and the distribution of *v* at 16 LST in Kunming (Cwb) was presented in ***Fig. A4.4***.

In this district in Kunming (Cwb), there was no area with PET below 18 ℃ at 16 LST.

The areas with PET between 18 ℃ and 29 ℃ were located in the shade areas of buildings, and all the non-shaded areas of this district were with PET above 29 ℃. The areas with PET between 29 ℃ and 35 ℃ were rare. Areas with PET between 35 ℃ and 47 ℃ existed as the basic HCT conditions in this district, which were roughly in the zone of x = (75—95) and y = (0—130), the zone of x = (30—60) and y = (95—160), the zone of x = (0—50) and y = (55—70), the zone of x = (80—140) and y = (55—70), the zone of x = (110—170) and y = (140—170), and the zone of x = (0—170) and y = (0—30). The simulated wind firstly arrived the last zone.

According to ***Fig. A4.4***, the relative low v conditions (below 0.6 m/s) appeared on the lee side (i.e. the ENE side) much more frequently than on the windward side (i.e. the WSW side). The areas with relative high v (above 2 m/s) were in between the buildings in the WSW-ENE direction.

Comparing with the distribution of v in ***Fig. A4.4***, and the input WD (i.e. WSW) in Kunming (Cwb) (please see ***Table 6.3.2***), the areas with specific HTC conditions (***Fig. A2.4***) presented the orientational dependence, i.e. the distribution of specific HTC conditions associated with the distribution of v conditions, which was in the WSW-ENE direction. Meanwhile, the position of PET above 47 ℃ was corresponding with the position of v below 0.6 m/s, the position of PET above 54 ℃ was corresponding with the position of v below 0.2 m/s. In comparison, the position of PET in between 35 ℃ and 41 ℃ was corresponding with the position of v above 2 m/s. Furthermore, comparing ***Fig. A2.4*** and ***Fig. A4.4***, most of the areas with PET above 47 ℃ were on the lee side (i.e. the ENE side) in the non-shaded areas.

6.3.3.5 Shanghai (Cfa)

The most frequently heat stress appeared at 14 LST in the 1st simulation in Shanghai (Cfa). PET distribution at 14 LST in Shanghai (Cfa) was depicted in ***Fig. A2.5***, and the distribution of v at 14 LST in Shanghai (Cfa) was presented in ***Fig. A4.5***.

In this district in Shanghai (Cfa), there was no area with PET below 29 ℃ at 14 LST. The areas with PET below 41 ℃ were located in the shade areas of buildings, and all the non-shaded areas of this district were with PET above 41 ℃. Areas with PET between 41 ℃ and 54 ℃ existed as the basic HCT conditions in this district, which were roughly in the zone of x = (70—95) and y = (0—110), the zone of x = (30—60) and y = (90—170), the zone of x = (0—170) and y = (0—30), and the zone of x = (90—170) and y = (140—170). The simulated wind firstly arrived the last zone (i.e. the ENE side).

According to ***Fig. A4.5***, the relative low v conditions (below 0.6 m/s) appeared on the lee side (i.e. the WSW side) much more frequently than on the windward side (i.e. the ENE side). The areas with relative high v (above 2.5 m/s) were in between the buildings in the ENE-WSW direction.

Comparing with the distribution of v in ***Fig. A4.5***, and the input WD (i.e. ENE) in Shanghai (Cfa) (please see ***Table 6.3.2***), the areas with specific HTC conditions (***Fig. A2.5***) presented the orientational dependence, i.e. the distribution of specific HTC conditions associated with the distribution of v conditions, which was in the ENE-WSW direction. Meanwhile, the position of PET above 54 ℃ was corresponding with the position of v below 0.6 m/s, the position of PET above 54 ℃ was corresponding with the position of v below 0.2 m/s. Furthermore, comparing ***Fig. A2.5*** and ***Fig. A4.5***, most of the areas with PET above 54 ℃ were on the sunny side of the buildings, as well as on the lee side (i.e. the WSW side).

6.3.3.6 Beijing (Dwa)

The most frequently heat stress appeared at 14 LST in the 1st simulation in Beijing (Dwa). PET distribution at 14 LST in Beijing (Dwa) was depicted in ***Fig. A2.6***, and the v distribution at 14 LST in Beijing (Dwa) was presented in ***Fig. A4.6***.

In this district in Beijing (Dwa), there was no area with PET below 29 ℃ at 14 LST. The areas with PET below 41 ℃ were located in the shade areas of buildings, and all the non-

shaded areas of this district were with PET above 41 ℃. Areas with PET between 41 ℃ and 54 ℃ existed as the basic HCT conditions in this district, which were roughly in the zone of x = (75—95) and y = (0—140), the zone of x = (30—60) and y = (95—170), the zone of x = (0—170) and y = (60—75), the zone of x = (110—170) and y = (130—170), and the zone of x = (0—170) and y = (0—30). The simulated wind firstly arrived the last zone (i.e. the SW side).

According to ***Fig. A4.6***, the relative low v conditions (below 0.6 m/s) appeared on the lee side (i.e. the NE side) much more frequently than on the windward side (i.e. the SW side). The areas with relative high v (above 2 m/s) were in between the buildings in the SW-NE direction.

Comparing with the distribution of v in ***Fig. A4.6***, and the input WD (i.e. SW) in Beijing (Dwa) (please see ***Table 6.3.2***), the areas with specific HTC conditions (***Fig. A2.6***) presented the orientational dependence, i.e. the distribution of specific HTC conditions associated with the distribution of v conditions, which was in the SW-NE direction. Meanwhile, the position of PET above 54 ℃ was corresponding with the position of v below 0.6 m/s, the position of PET above 60 ℃ was corresponding with the position of v below 0.2 m/s. In comparison, the position of PET in between 41 ℃ and 47 ℃ was corresponding with the position of v above 2.5m/s. Furthermore, comparing ***Fig. A2.6*** and ***Fig. A4.6***, most of the areas with PET above 54 ℃ were on the lee side (i.e. the NE side) in the non-shaded areas.

6.3.3.7 Dalian (Dwa)

The most frequently heat stress appeared at 14 LST in the 1st simulation in Dalian (Dwa). PET distribution at 14 LST in Dalian (Dwa) was depicted in ***Fig. A2.7***, and the v distribution at 14 LST in Dalian (Dwa) was presented in ***Fig. A4.7***.

In this district in Dalian (Dwa), there was no area with PET below 18 ℃ at 14 LST. The areas with PET between 18 ℃ and 35 ℃ were located in the shade areas of buildings,

and all the non-shaded areas of this district were with PET above 35 ℃. Areas with PET between 35 ℃ and 47 ℃ existed as the basic HCT conditions in this district, which were roughly in the whole district.

According to ***Fig. A4.7***, the relative low *v* conditions (below 1.5 m/s) appeared on the lee side (i.e. the N side) much more frequently than on the windward side (i.e. the S side). The areas with relative high *v* (above 3 m/s) were in between the buildings in the N-S direction.

Comparing with the distribution of *v* in ***Fig. A4.7***, and the input WD (i.e. N) in Dalian (Dwa) (please see ***Table 6.3.2***), the areas with specific HTC conditions (***Fig. A2.7***) presented the orientational dependence, i.e. the distribution of specific HTC conditions associated with the distribution of *v* conditions, which was in the N-S direction. Meanwhile, the position of PET above 47 ℃ was corresponding with the position of *v* below 0.6 m/s, the position of PET above 54 ℃ was corresponding with the position of *v* below 0.2 m/s. Furthermore, comparing ***Fig. A2.7*** and ***Fig. A4.7***, most of the areas with PET above 47 ℃ were on the lee side (i.e. the N side) in the non-shaded areas.

6.3.3.8 Hohhot (Dwb)

The most frequently heat stress appeared at 15 LST in the 1st simulation in Hohhot (Dwb). PET distribution at 15 LST in Hohhot (Dwb) was depicted in ***Fig. A2.8***, and the *v* distribution at 15 LST in Hohhot (Dwb) was presented in ***Fig. A4.8***.

In this district in Hohhot (Dwb), there was no area with PET below 23 ℃ at 15 LST. The areas with PET between 23 ℃ and 35 ℃ were located in the shade areas of buildings, and all the non-shaded areas of this district were with PET above 35 ℃. Areas with PET between 41 ℃ and 54 ℃ existed as the basic HCT conditions in this district, which were roughly in the whole district.

According to ***Fig. A4.8***, the relative low *v* conditions (below 0.6 m/s) appeared on the lee side (i.e. the W side) much more frequently than on the windward side (i.e. E the side).

The areas with relative high *v* (above 1.5 m/s) were in between the buildings in the E-W direction.

Comparing with the distribution of *v* in ***Fig. A4.8***, and the input WD (i.e. E) in Hohhot (Dwb) (please see ***Table 6.3.2***), the areas with specific HTC conditions (***Fig. A2.8***) presented the orientational dependence, i.e. the distribution of specific HTC conditions associated with the distribution of *v* conditions, which was in the E-W direction. Meanwhile, the position of PET above 54 ℃ was corresponding with the position of *v* below 0.2 m/s. In comparison, the position of PET in between 41 ℃ and 47 ℃ was corresponding with the position of *v* above 1.5 m/s. Furthermore, comparing ***Fig. A2.8*** and ***Fig. A4.8***, most of the areas with PET above 54 ℃ were on the sunny side of the buildings, as well as on the lee side (i.e. the W side).

6.3.3.9 Lhasa (Dwc)

The most frequently heat stress appeared at 17 LST in the 1st simulation in Lhasa (Dwc). PET distribution at 17 LST in Lhasa (Dwc) was depicted in ***Fig. A2.9***, and *v* distribution at 17 LST in Lhasa (Dwc) was presented in ***Fig. A4.9***.

In this district in Lhasa (Dwc), the areas with PET below 29 ℃ were located in the shade areas of buildings, and all the non-shaded areas of this district were with PET above 29 ℃. Areas with PET between 29 ℃ and 41 ℃ existed as the basic HCT conditions in this district. The areas with PET above 54 ℃ were rare.

According to ***Fig. A4.9***, the relative low *v* conditions (below 0.6 m/s) appeared on the lee side (i.e. the W side) much more frequently than on the windward side (i.e. the E side). The areas with relative high *v* (above 1.5 m/s) were in between the buildings in the E-W direction.

Comparing with the distribution of *v* in ***Fig. A4.9***, and the input WD (i.e. E) in Lhasa (Dwc) (please see ***Table 6.3.2***), the areas with specific HTC conditions (***Fig. A2.9***) presented the orientational dependence, i.e. the distribution of specific HTC conditions

associated with the distribution of *v* conditions, which was in the E-W direction. Meanwhile, the position of PET above 41 ℃ was corresponding with the position of *v* below 1 m/s, the position of PET above 47 ℃ was corresponding with the position of *v* below 0.6 m/s. Furthermore, comparing ***Fig. A2.9*** and ***Fig. A4.9***, most of the areas with PET above 41 ℃ were on the sunny side of the buildings, as well as on the lee side (i.e. the W side).

6.3.3.10 Urumqi (Dfb)

The most frequently heat stress appeared at 16 LST in the 1st simulation in Urumqi (Dfb). PET distribution at 16 LST in Urumqi (Dfb) was depicted in ***Fig. A2.10***, and the *v* distribution at 16 LST in Urumqi (Dfb) was presented in ***Fig. A4.10***.

In this district in Urumqi (Dfb), there was no area with PET below 23 ℃ at 16 LST. The areas with PET between 23 ℃ and 35 ℃ were located in the shade areas of buildings, and all the non-shaded areas of this district were with PET above 35 ℃. Areas with PET between 41 ℃ and 47 ℃ existed as the basic HCT conditions in this district. The areas with PET between 35 ℃ and 41 ℃, and the areas with PET above 54 ℃ were rare.

According to ***Fig. A4.10***, the relative low *v* conditions (below 1.5 m/s) appeared on the lee side (i.e. the NNE side) much more frequently than on the windward side (i.e. the SSW side). The areas with relative high *v* (above 2 m/s) were in between the buildings in the SSW-NNE direction.

Comparing with the distribution of *v* in ***Fig. A4.10***, and the input WD (i.e. E) in Urumqi (Dfb) (please see ***Table 6.3.2***), the areas with specific HTC conditions (***Fig. A2.10***) presented the orientational dependence, i.e. the distribution of specific HTC conditions associated with the distribution of *v* conditions, which was in the SSW-NNE direction. Meanwhile, the position of PET above 47 ℃ was corresponding with the position of *v* below 1.5 m/s. Furthermore, comparing ***Fig. A2.10*** and ***Fig. A4.10***, there were areas with PET above 47 ℃ in the non-shaded zone, on the lee side, and on the windward side (i.e.

the SSW side).

6.3.3.11 Yuncheng (BSk)

The most frequently heat stress appeared at 15 LST in the 1st simulation in Yuncheng (BSk). PET distribution at 15 LST in Yuncheng (BSk) was depicted in ***Fig. A2.11***, and the *v* distribution was presented in ***Fig. A4.11***.

In this district in Yuncheng (BSk), there was no area with PET below 29 ℃ at 15 LST. The areas with PET between 29 ℃ and 41 ℃ were located in the shade areas of buildings, and all the non-shaded areas of this district were with PET above 41 ℃. The areas with PET between 41 ℃ and 47 ℃ were rare. Areas with PET between 47 ℃ and 54 ℃ existed as the basic HCT conditions in this district.

According to ***Fig. A4.11***, the relative low *v* conditions (below 0.6 m/s) appeared on the lee side (i.e. the NW side) much more frequently than on the windward side (i.e. the SE side). The areas with relative high *v* (above 2 m/s) were in between the buildings in the SE-NW direction.

Comparing with the distribution of *v* in ***Fig. A4.11***, and the input WD (i.e. SE) in Yuncheng (BSk) (please see ***Table 6.3.2***), the areas with specific HTC conditions (***Fig. A2.11***) presented the orientational dependence, i.e. the distribution of specific HTC conditions associated with the distribution of *v* conditions, which was in the SE-NW direction. Meanwhile, the position of PET above 54 ℃ was corresponding with the position of *v* below 0.6 m/s. Furthermore, comparing with ***Fig. A2.11***, most of the areas with PET above 54 ℃ were on the lee side (i.e. the NW side) in the non-shaded areas.

6.3.3.12 Yinchuan (BWk)

The most frequently heat stress appeared at 15 LST in the 1st simulation in Yinchuan (BWk). PET distribution at 15 LST in Yinchuan (BWk) was depicted in ***Fig. A2.12***, and the *v* distribution at 15 LST in Yinchuan (BWk) was presented in ***Fig. A4.12***.

In this district in Yinchuan (BWk), there was no area with PET below 23 ℃ at 15 LST. The areas with PET between 23 ℃ and 41 ℃ were located in the shade areas of buildings, and all the non-shaded areas of this district were with PET above 41 ℃. Areas with PET between 41 ℃ and 54 ℃ existed as the basic HCT conditions in this district.

According to ***Fig. A4.12***, the relative low *v* conditions (below 1 m/s) appeared on the lee side (i.e. the S side) much more frequently than on the windward side (i.e. the N side). The areas with relative high *v* (above 2 m/s) were in between the buildings in the N-S direction.

Comparing with the distribution of *v* in ***Fig. A4.12***, and the input WD (i.e. N) in Yinchuan (BWk) (please see ***Table 6.3.2***), the areas with specific HTC conditions (***Fig. A2.12***) presented the orientational dependence, i.e. the distribution of specific HTC conditions associated with the distribution of *v* conditions, which was in the N-S direction. Meanwhile, the position of PET above 54 ℃ was corresponding with the position of *v* below 0.2 m/s. Furthermore, comparing ***Fig. A2.12*** and ***Fig. A4.12***, most of the areas with PET above 54 ℃ were on the sunny side of the buildings, as well as on the lee side (i.e. the S side).

As one example for the community environment design, the final scheme for the residential district in Yinchuan (BWk) was presented in ***Fig. 6.3.3***, which depicted the position and simplified characteristics of each design element more reader-friendly, compared to the combined figures (e.g. ***Fig. A2.12***). Meanwhile, the modified community environment in the residential district, i.e. the example in Yinchuan (BWk) in ***Fig. 6.3.3***, could be clearly compared with the non-design district, i.e. the residential district in ***Fig. 5.3.1***.

With a summary of section 6.3.3 at the end, there are several common aspects between 12 scenarios. First of all, the relative low *v* conditions appeared on the lee side much more frequently than that on the wind ward side, and the relative high *v* conditions were in

between the buildings (please see the Appendix A4). Secondly, comparing the distribution of *v* (please see Appendix A4) and the input WD (please see ***Table 6.3.2***), the areas with relative high PET values presented the orientational dependence, i.e. the distribution of specific HTC conditions associated with the distribution of *v* conditions. Furthermore, comparing the distribution of PET (please see Appendix A2) and the distribution of *v* (please see Appendix A4), most of the areas with heat stress were under the sun, as well as on the lee side of the buildings.

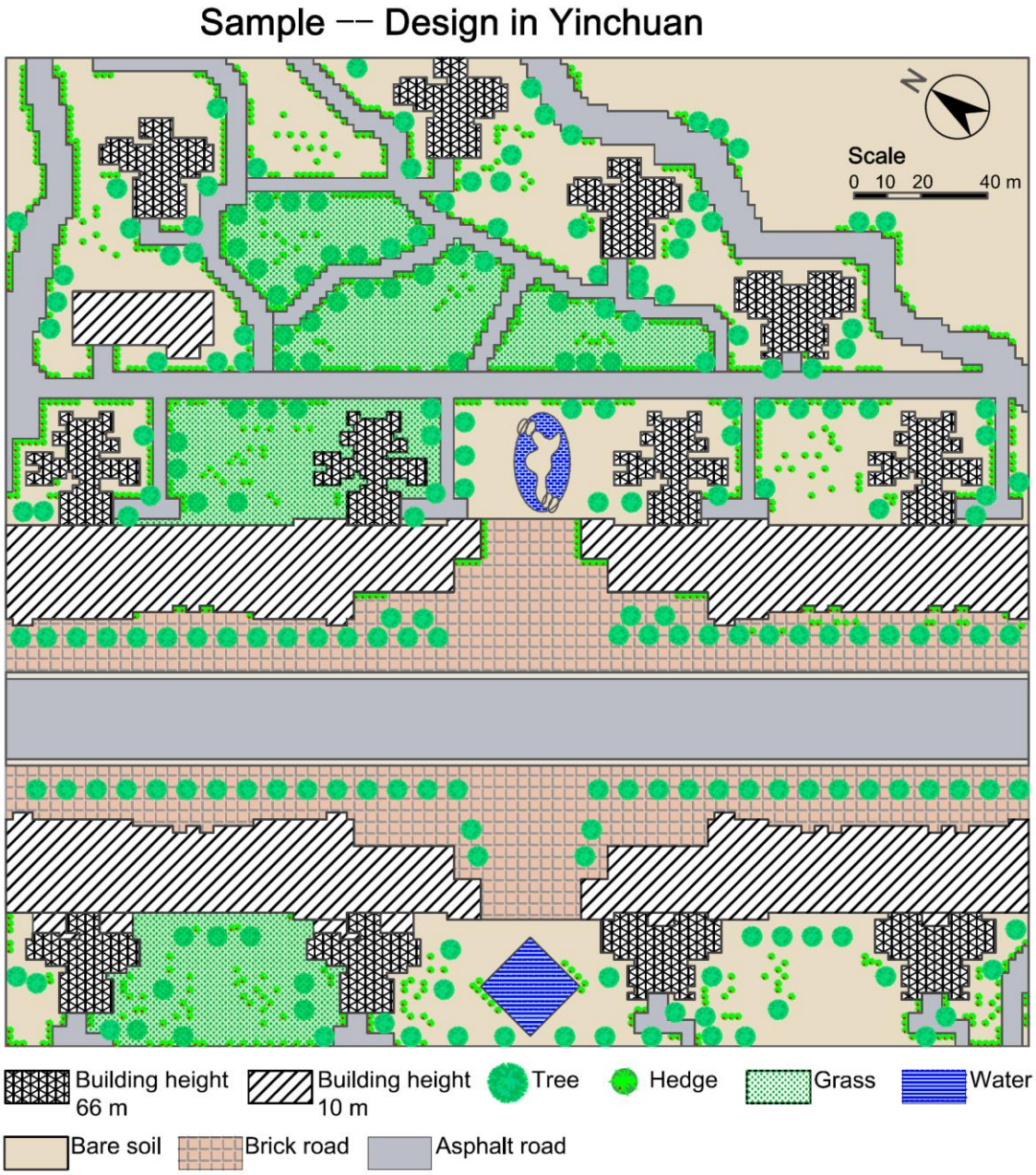

Fig. 6.3.3 The residential district with design elements in Yinchuan (BWk) (example)

6.3.4 Design effects on HTC in each city

The 2nd round simulations were completed, after adding the design elements into the residential district in each scenario. The design effects on HTC conditions in each scenario were presented through the difference in PET, SVF and *v* between twice simulations, respectively. The differences were the conditions at the same point in time selected in each city in the analysis of the 1st round simulations, which were the points in time with the most frequently emerged heat stress in each city. The difference in PET, SVF and *v* have been depicted in figures, respectively (please see Appendix A5, Appendix A6, and Appendix A7, respectively). Since the difference in PET, the difference in SVF, and the difference in *v*, were the values in the 1st round simulation minus that in the 2nd round simulations, respectively, the negative values mean the simulated data in 1st round simulations in a grid was lower than that in the 2nd round simulations in the same grid, and the positive values mean the simulated data in 1st round simulations in a grid was greater than that in the 2nd round simulations in the same grid (please see ***Table 5.3.3***).

6.3.7.1 Sanya (Aw)

The difference in PET between the 1st simulation and the 2nd simulation in Sanya (Aw) was presented in ***Fig. A5.1***, which was the conditions at 14 LST. There was no difference in PET below – 10 K (black blue areas in ***Fig. A5.1***), i.e. PET values in the 2nd simulation would not increase more than 10 K, comparing with the PET values in the 1st simulation. Meanwhile, the position of – 10 ─ – 2 K (the dark blue and blue areas in ***Fig. A5.1***) is between the trees and hedges in ***Fig. A2.1***, especially in the zone of x = (10─100) and the zone of y = (110─150). The most frequent areas in the district were the areas with the difference in PET between – 2 K and 2 K (green areas in ***Fig. A5.1***), where there was grassland in some parts, but no tree, hedge, or water body in ***Fig. A2.1***. Partial areas with difference in 5 ─ 10 K (partial yellow areas in ***Fig. A5.1***) appeared in the areas with water bodies in ***Fig. A2.1***. The other areas with difference in 5 ─ 10 K (partial yellow areas in ***Fig. A5.1***) were always combined with the areas, where there was the difference in 2 ─

5 K (light green areas in ***Fig. A5.1***) or the difference in 10 ─ 15 K (orange areas in ***Fig. A5.1***). According to the position of design elements in ***Fig. A2.1***, the position of the yellow and light green areas was associated with the areas, where there were trees, and the position of the yellow and orange areas was associated with the areas, where there were trees and hedges together. The areas with difference in PET above 10 K (orange, red and purplish red areas in ***Fig. A5.1***) were mainly the areas, where there were hedges (please see ***Fig. A2.1***), e.g. the orange and red areas around the yellow areas in ***Fig. A5.1*** at the position of water bodies. While partially orange, red and purplish red areas in ***Fig. A5.1*** (difference above 10 K) were associated the areas, around which there were hedges and trees together (please see ***Fig. A2.1***), e.g. in the zone of x = (30─50) and y = (25─30).

The difference in SVF between the 1st simulation and the 2nd simulation in Sanya (Aw) was depicted in ***Fig. A6.1***. The most area of the district was the areas with the difference in SVF below 0.05, where there was rare impact from the added vegetation in the 2nd simulation. The areas with the difference in SVF above 0.35 was highly associated with the areas in ***Fig. A2.1***, where there were hedges inside and trees around. The areas with difference in SVF between 0.15 and 0.25 was mainly associated with the areas in ***Fig. A2.1***, where there were trees inside or nearby. Comparing with the difference in PET in ***Fig. A5.1***, the distribution of the difference in PET above 5 K was associated with the distribution of the difference in SVF above 0.15, and the distribution of the difference in PET above 15 K was associated with the distribution of the difference in SVF above 0.35.

The difference in v between the 1st simulation and the 2nd simulation in Sanya (Aw) was depicted in ***Fig. A7.1***, which was the conditions at 14 LST. The most frequent areas of the district were the areas with the difference in v below 0.25 m/s. The main areas with difference in v above 0.75 m/s in ***Fig. A7.1*** were in the zone of x = (35─55) and y = (95─145), zone of x = (65─90) and y = (110─150), zone of x = (75─85) and y = (15─25), zone of x = (100─110) and y = (110─135), zone of x = (125─140) and y = (90─120),

and zone of x = (150─165) and y = (5─30). These zones were located in the zones in ***Fig. A4.1***, which were with the relative high v values (above 1.5 m/s). Comparing the distribution of the difference in PET, the distribution of dark blue and blue areas in ***Fig. A5.1*** was associated with the distribution of the difference in v above 0.5 m/s. Comparing with the design in ***Fig. A2.1***, the areas with difference in v above 0.5 m/s was associated with the areas, where there were trees or hedges around, by which the wind (E) was blocked. Furthermore, the difference in v above 1.25 m/s was associated with the areas, where there was more intensive vegetation.

6.3.7.2 Qionghai (Am)

The difference in PET between the 1st simulation and the 2nd simulation in Qionghai (Am) was presented in ***Fig. A5.2***, which was the conditions at 15 LST. There was no difference in PET below – 10 K (black blue in ***Fig. A5.2***), i.e. PET values in the 2nd simulation would not increase more than 10 K, comparing with the PET values in the 1st simulation. Meanwhile, the position of the dark blue and blue areas is between the trees and hedges in ***Fig. A2.2***, especially in the zone of x = (10─60) and y = (120─150). The most frequent areas in the district were the areas with the difference in PET between – 2 K and 2 K (green areas in ***Fig. A5.2***), where there was grassland in some parts, but no tree, hedge or water bodies in ***Fig. A2.2***. Partial areas with difference in 5─10 K (partial yellow areas in ***Fig. A5.2***) appeared in the areas with water bodies in ***Fig. A2.2***. The other areas with difference in 5─10 K (partial yellow areas in ***Fig. A5.2***) and the areas with difference in 2─5 K (light green areas in ***Fig. A5.2***) were associated with the areas where there were trees in ***Fig. A2.2***. The areas with difference in PET above 10 K (orange, red and purplish red areas in ***Fig. A5.2***) were mainly the areas, where the hedges were gave in the 2nd simulation (comparing with ***Fig. A2.2***), e.g. in the zone of x = (155─160) and y = (10─25).

The difference in SVF between the 1st simulation and the 2nd simulation in Qionghai (Am) was in ***Fig. A6.2***. The main area of the district was the areas with the difference in SVF below 0.05, where there was rare impact from the added vegetation in the 2nd simulation.

The areas with the difference in SVF above 0.35 was highly associated with the areas in ***Fig. A2.2***, where there were hedges inside and trees around. The areas with difference in SVF between 0.15 and 0.25 was mainly associated with the areas in ***Fig. A2.2***, where there were trees inside or nearby. Comparing with the difference in PET in ***Fig. A5.2*** the areas with the difference in PET above 5 K and the partial areas with the difference in PET between – 10 K and – 2 K were associated with the areas with the difference in SVF above 0.15, and the areas with the difference in PET above 15 K were associated with the areas with the difference in SVF above 0.45.

The difference in *v* between the 1st simulation and the 2nd simulation in Qionghai (Am) was depicted in ***Fig. A7.2***, which was the conditions at 15 LST. The most frequent areas of the district were the areas with the difference in *v* below 0.25 m/s. The rough areas with difference in *v* above 0.75 m/s in ***Fig. A7.2*** were in the zone of x = (10—15) and y = (135—160), zone of x = (35—60) and y = (95—160), zone of x = (60—95) and y = (105—135), zone of x = (85—110) and y = (100—130), zone of x = (120—140) and y = (90—120), zone of x = (75—85) and y = (10—20), and zone of x = (150—160) and y = (10—20). These zones were located roughly in the zones with the relative high *v* values (above 2 m/s) in ***Fig. A4.2***. Comparing the distribution of the difference in PET, the distribution of dark blue and blue areas in ***Fig. A5.2*** was associated with the distribution of the difference in *v* above 0.5 m/s in ***Fig. A7.2***. Comparing with the design in ***Fig. A2.2***, the difference in *v* above 0.5 m/s was associated with the areas, where there were trees or hedges (especially hedges), by which the wind (E) was blocked. Furthermore, the difference in *v* above 1.25 m/s was associated with the areas, where there was more intensive vegetation.

6.3.7.3 Shenzhen (Cwa)

The difference in PET between the 1st simulation and the 2nd simulation in Shenzhen (Cwa) was presented in ***Fig. A5.3***, which was the conditions at 15 LST. Although the black blue areas were small in the whole district, it indicated the strongest increase of the thermal

stress in the 2nd simulation in these areas. Comparing with ***Fig. A2.3***, the black blue areas were located on the asphalt road and between trees and hedges, e.g. in the zone of x = (40─60) and y = (110─115) and the zone of x = (15─20) and y = (60─70). The most frequent areas in the district were the areas with the difference in PET between – 2 K and 2 K (green areas in ***Fig. A5.3***), where there was grassland in some parts, but no tree, hedge or water bodies in ***Fig. A2.3***. Partial areas with difference in 5─10 K (partial yellow areas in ***Fig. A5.3***) appeared in the areas with water bodies in ***Fig. A2.3***. The other areas with difference in 5─10 K (partial yellow areas in ***Fig. A5.3***) and the areas with difference in 2─5 K (light green areas in ***Fig. A5.3***) did not appeared frequently, and normally they accompanied the areas where there was difference in PET above 15 K. The areas with difference in PET above 10 K (orange, red and purplish red areas in ***Fig. A5.3***) were mainly the areas, where trees were given in the 2nd simulation (comparing with ***Fig. A2.3***), e.g. the zone of x = (10─160) and y = (50─80). In some of these areas (difference above 10 K) in Shenzhen (Cwa), the decrease of the PET values was caused by the combined effects of hedges and trees (comparing with ***Fig. A2.3***).

The difference in SVF between the 1st simulation and the 2nd simulation in Shenzhen (Cwa) was in ***Fig. A6.3***. The main area of the district was the areas with the difference in SVF below 0.05, where there was rare impact from the added vegetation in the 2nd simulation. The areas with the difference in SVF between 0.05 and 0.15 were also frequent in the whole district. The areas with the difference in SVF above 0.45 were mainly associated with the areas in ***Fig. A2.3***, where there were trees inside or nearby. Partial areas with the difference in SVF above 0.45 was associated with the areas in ***Fig. A2.3***, where there were hedges inside or nearby, e.g. in the zone of x = (140─155) and y = (110─125). Comparing with the difference in PET in ***Fig. A5.3*** the distribution of the difference in PET above 10 K was associated with the distribution of the difference in SVF above 0.35.

The difference in v between the 1st simulation and the 2nd simulation in Shenzhen (Cwa)

was depicted in ***Fig. A7.3***, which was the conditions at 15 LST. The most frequent areas of the district were the areas with the difference in *v* below 0.25 m/s. The rough areas with difference in *v* above 0.75 m/s in ***Fig. A7.3*** were in zone of *x* = (0—170) and *y* = (0—20), zone of *x* = (10—100) and *y* = (50—160), and the zone of *x* = (105—165) and *y* = (90—140). These zones were associated with the zones in ***Fig. A4.3***, where there were relative high *v* values (above 2 m/s). Comparing with the design in ***Fig. A2.3***, the difference in *v* above 1 m/s was associated with the areas, where there were trees or hedges, by which the wind (NE) was blocked. Furthermore, the difference in *v* above 1.5 m/s was highly associated with the areas, where there was the more intensive vegetation.

6.3.7.4 Kunming (Cwb)

The difference in PET between the 1st simulation and the 2nd simulation in Kunming (Cwb) was presented in ***Fig. A5.4***, which was the conditions at 16 LST. There was no difference in PET below – 10 K (i.e. black blue areas in ***Fig. A5.4***), i.e. PET values in the 2nd simulation would not increase more than 10 K, comparing with the PET values in the 1st simulation. The position of the dark blue and blue areas is on the asphalt road (high frequent) and between the hedges in ***Fig. A2.4***, e.g. in the zone of *x* = (40—60) and *y* = (105—130). The most frequent areas in the district were the areas with the difference in PET between – 2 K and 2 K (green areas in ***Fig. A5.4***), where there was grassland in some parts, but no tree, hedge or water bodies in ***Fig. A2.4***. The areas with difference in PET between 2 K and 5 K (light green areas in ***Fig. A5.4***) and the areas with difference in PET above 25 K (purplish red areas in ***Fig. A5.4***) were rare. Partial areas with difference in 5—10 K (partial yellow areas in ***Fig. A5.4***) appeared in the areas with water bodies in ***Fig. A2.4***. The other areas with difference in 5—10 K (partial yellow areas in ***Fig. A5.4***) always existed around the areas, where there was difference in 10—25 K (orange and red areas in ***Fig. A5.4***). According to the position of design elements in ***Fig. A2.4***, trees and hedge were added around these areas, e.g. in the zone of *x* = (10—165) and *y* = (50—75).

The difference in SVF between the 1st simulation and the 2nd simulation in Kunming (Cwb) was in ***Fig. A6.4***. The most parts of the district were the areas with the difference in SVF below 0.05, where there was rare impact from the added vegetation in the 2nd simulation. The areas with the difference in SVF between 0.05 and 0.15 existed also frequently, however, there was no trees or hedges, comparing with the design in ***Fig. A2.4***. The areas with the difference in SVF above 0.45 was highly associated with the areas in ***Fig. A2.4***, where there were hedges inside and trees around. Comparing with the difference in PET in ***Fig. A5.4***, the distribution of the difference in PET above 15 K was associated with the distribution of the difference in SVF above 0.35.

The difference in *v* between the 1st simulation and the 2nd simulation in Kunming (Cwb) was depicted in ***Fig. A7.4***, which was the conditions at 16 LST. The most frequent areas of the district were the areas with the difference in *v* below 0.25 m/s. The main areas with difference in *v* above 0. 5 m/s in ***Fig. A7.4*** were in zone of x = (40─65) and y = (105─170), and the zone of x = (70─105) and y = (105─140). These zones were located in the zones in ***Fig. A4.4***, where there were the relative high *v* values (above 1.5 m/s). Comparing the distribution of the difference in PET, the distribution of dark blue and blue areas in ***Fig. A5.4*** was associated with the areas with difference in *v* above 0.5 m/s. Comparing with the design in ***Fig. A2.4***, the difference in *v* above 0.5 m/s was associated with the areas, where there were trees or hedges, by which the wind (WSW) was blocked.

6.3.7.5 Shanghai (Cfa)

The difference in PET between the 1st simulation and the 2nd simulation in Shanghai (Cfa) was presented in ***Fig. A5.5***, which was the conditions at 14 LST. The areas with difference in PET below – 10 K (black blue in ***Fig. A5.5***) was rare, i.e. PET values in the 2nd simulation would not increase frequently more than 10 K, comparing with the PET values in the 1st simulation. The position of the dark blue and blue areas is on the asphalt road and between the trees or hedges in ***Fig. A2.5***, e.g. in the zone of x = (10─160) and y = (60─70). The most frequent areas in the district were the areas with the difference in PET

between – 2 K and 2 K (green areas in ***Fig. A5.5***), where there was grassland in some parts, but no tree, hedge or water bodies in ***Fig. A2.5***. Partial areas with difference in 5─10 K (partial yellow areas in ***Fig. A5.5***) appeared in the areas with water bodies in ***Fig. A2.5***. The areas with difference in 2─10 K (light green and the other part of yellow areas in ***Fig. A5.5***) were associated with the areas, where there were trees and hedge around ***Fig. A2.5***. The areas with difference in PET above 10 K (orange, red and purplish red areas in ***Fig. A5.5***) were mainly the areas, where the trees and hedges were gave in the 2nd simulation nearby (comparing with ***Fig. A2.5***), e.g. in the zone of x = (10─160) and y = (50─80).

The difference in SVF between the 1st simulation and the 2nd simulation in Shanghai (Cfa) was in ***Fig. A6.5***. The areas with the difference in SVF below 0.05 were the areas where there was rare impact from the added vegetation in the 2nd simulation. The areas with the difference in SVF above 0.45 was highly associated with the areas in ***Fig. A2.5***, where there were trees inside and nearby, and this difference was partially from the added hedges. Comparing with the difference in PET in ***Fig. A5.5*** the distribution of the difference in PET above 15 K was associated with the distribution of the difference in SVF above 0.25.

The difference in v between the 1st simulation and the 2nd simulation in Shanghai (Cfa) was depicted in ***Fig. A7.5***, which was the conditions at 14 LST. The most frequent areas of the district were the areas with the difference in v below 0.25 m/s. The main areas with difference in v above 1.5 m/s in ***Fig. A7.5*** were in zone of x = (40─110) and y = (90─160). These zones were located in the zones in ***Fig. A4.5***, where there were the relative high v values (above 2.5 m/s). Comparing with the design in ***Fig. A2.5***, the difference in v above 2.5 m/s was associated with the areas, where there were the intensive trees or hedges n, by which the wind (ENE) was blocked.

6.3.7.6 Beijing (Dwa)

The difference in PET between the 1st simulation and the 2nd simulation in Beijing (Dwa)

was presented in ***Fig. A5.6***, which was the conditions at 14 LST. There was no difference in PET below – 10 K (i.e. black blue areas in ***Fig. A5.6***), i.e. PET values in the 2nd simulation would not increase more than 10 K, comparing with the PET values in the 1st simulation. The position of the dark blue and blue areas is on the asphalt road and between the trees and hedges in ***Fig. A2.6***, e.g. in the zone of x = (10─35) and y = (60─70). The most frequent areas in the district were the areas with the difference in PET between – 2 K and 2 K (green areas in ***Fig. A5.6***), where there was grassland in some parts, but no tree, hedge or water bodies. Partial areas with difference in 5─10 K (partial yellow areas in ***Fig. A5.6***) appeared in the areas with water bodies in ***Fig. A2.6***. The other areas with difference in 5─10 K (partial yellow areas in ***Fig. A5.6***) were always combined with the areas, where there was the difference above 10 K (orange, red and purplish areas in ***Fig. A5.6***). The areas with difference in PET above 10 K were mainly the areas, where the trees and hedges were gave in the 2nd simulation (comparing with ***Fig. A2.6***), e.g. in the zone of x = (65─120) and y = (10─20).

The difference in SVF between the 1st simulation and the 2nd simulation in Beijing (Dwa) was in ***Fig. A6.6***. The frequent areas of the district was that with the difference in SVF below 0.05, where there was rare impact from the added vegetation in the 2nd simulation. The areas with the difference in SVF above 0.35 was highly associated with the areas in ***Fig. A2.6***, where there were trees and hedges inside and around. Comparing with the difference in PET in ***Fig. A5.6*** the distribution of the difference in PET above 10 K was associated with the distribution of the difference in SVF above 0.45.

The difference in v between the 1st simulation and the 2nd simulation in Beijing (Dwa) was depicted in ***Fig. A7.6***, which was the conditions at 14 LST. The most frequent areas of the district were the areas with the difference in v below 0.25 m/s. The main areas with difference in v above 0.75 m/s in ***Fig. A7.6*** were in the zone of x = (40─95) and y = (100─170), the zone of x = (60─80) and y = (40─65), and the zone of x = (140─160) and y = (85─130). These zones were located in or nearby the zones in ***Fig. A4.6***, where

there were the relative high *v* values (above 2.5 m/s). Comparing with the design in ***Fig. A2.6***, the areas with the difference in *v* above 0.25 m/s was associated with the areas, where there were trees or hedges, by which the wind (SW) was blocked. Furthermore, the areas with the difference in *v* above 1.25 m/s was associated with the areas, where there was more intensive vegetation.

6.3.7.7 Dalian (Dwa)

The difference in PET between the 1st simulation and the 2nd simulation in Dalian (Dwa) was presented in ***Fig. A5.7***, which was the conditions at 14 LST. There was rare difference in PET below – 10 K (i.e. black blue areas in ***Fig. A5.7***), i.e. PET values in the 2nd simulation would rarely increase more than 10 K, comparing with the PET values in the 1st simulation. The position of the dark blue and blue areas is on the asphalt road and between the trees and hedges in ***Fig. A2.7***, e.g. in the zone of x = (40─90) and y = (110─160). The most frequent areas in the district were the areas with the difference in PET between – 2 K and 2 K (green areas in ***Fig. A5.7***), where there was grassland in some parts, but no tree, hedge or water bodies. Partial areas with difference in 5─10 K (partial yellow areas in ***Fig. A5.7***) appeared in the areas with water bodies in ***Fig. A2.7***. The other areas with difference in 5─10 K (partial yellow areas in ***Fig. A5.7***) were always combined with the areas, where there was the difference above 10 K (orange, red and purplish red areas in ***Fig. A5.7***). The areas with difference in PET above 10 K (orange, red and purplish red areas in ***Fig. A5.7***) were mainly the areas, where trees, or hedges were gave in the 2nd simulation (comparing with ***Fig. A2.7***), e.g. in the zone of x = (90─100) and y = (110─120).

The difference in SVF between the 1st simulation and the 2nd simulation in Dalian (Dwa) was in ***Fig. A6.7***. The frequent areas of the district were the areas with the difference in SVF below 0.05, where there was rare impact from the added vegetation in the 2nd simulation. The areas with the difference in SVF above 0.35 was mainly associated with the areas in ***Fig. A2.7***, where there were trees and hedges inside or nearby. Comparing

with the difference in PET in ***Fig. A5.7*** the distribution of the difference in PET above 10 K was associated with the distribution of the difference in SVF above 0.35.

The difference in *v* between the 1st simulation and the 2nd simulation in Dalian (Dwa) was depicted in ***Fig. A7.7***, which was the conditions at 14 LST. The most frequent areas of the district were the areas with the difference in *v* below 0.25 m/s. The main areas with difference in *v* above 0.75 m/s in ***Fig. A7.7*** were in the zone of x = (0—160) and y = (10—25), the zone of x = (0—140) and y = (50—60), and the zone of x = (0—160) and y = (100—165). These zones were located in or nearby the zones in ***Fig. A4.7***, where there were the relative high *v* values (above 2.5 m/s). Comparing with the design in ***Fig. A2.7***, the difference in *v* above 0.25 m/s was associated with the areas, where there were trees or hedges, by which the wind (S) was blocked. Furthermore, the difference in *v* above 1.25 m/s was associated with the areas, where there was the more intensive vegetation.

6.3.7.8 Hohhot (Dwb)

The difference in PET between the 1st simulation and the 2nd simulation in Hohhot (Dwb) was presented in ***Fig. A5.8***, which was the conditions at 15 LST. There was rare difference in PET below – 10 K (i.e. black blue areas in ***Fig. A5.8***), i.e. PET values in the 2nd simulation would rarely increase more than 10 K, comparing with the PET values in the 1st simulation. The position of the dark blue and blue areas is mainly between the trees and hedges in ***Fig. A2.8***, especially in the zone of x = (35—60) and y = (125—160), and the zone of x = (70—85) and y = (125—145). The most frequent areas in the district were the areas with the difference in PET between – 2 K and 2 K (green areas in ***Fig. A5.8***), where there was grassland in some parts, but no tree, hedge or water bodies. The areas with difference in 5—10 K (most of the yellow areas in ***Fig. A5.8***) appeared in the areas with water bodies in ***Fig. A2.8***. The other areas with difference in 5—10 K (the small part of yellow areas in ***Fig. A5.8***) were always combined with the areas, where there was the difference above 10 K (orange, red and purplish red areas in ***Fig. A5.8***). The areas with difference in PET above 10 K (orange, red and purplish red areas in ***Fig. A5.8***) were

mainly the areas, where the trees and hedges were gave in the 2nd simulation (comparing with ***Fig. A2.8***), e.g. in the zone of x = (40─70) and y = (115─155).

The difference in SVF between the 1st simulation and the 2nd simulation in Hohhot (Dwb) was in ***Fig. A6.8***. The most parts of the district was the areas with the difference in SVF below 0.05, where there was rare impact from the added vegetation in the 2nd simulation. The areas with the difference in SVF above 0.25 was highly associated with the areas in ***Fig. A2.8***, where there were trees and hedges inside or around. Comparing with the difference in PET in ***Fig. A5.8***, the distribution of the difference in PET above 10 K was associated with the distribution of the difference in SVF above 0.25.

The difference in v between the 1st simulation and the 2nd simulation in Hohhot (Dwb) was depicted in ***Fig. A7.8***, which was the conditions at 15 LST. The most frequent areas of the district were the areas with the difference in v below 0.25 m/s. The main areas with difference in v above 0.75 m/s in ***Fig. A7.8*** was in the zone of x = (35─145) and y = (90─160). These areas were located in or nearby the areas in ***Fig. A4.8***, where there were the relative high v values (above 1.5 m/s). Comparing with the design in ***Fig. A2.8***, the difference in v above 0.25 m/s was associated with the areas, where there were trees or hedges, by which the wind (E) was blocked. Furthermore, the difference in v above 1.25 m/s was associated with the areas, where there was the more intensive vegetation.

6.3.7.9 Lhasa (Dwc)

The difference in PET between the 1st simulation and the 2nd simulation in Lhasa (Dwc) was presented in ***Fig. A5.9***, which was the conditions at 17 LST. There was no difference in PET below – 10 K (i.e. black blue areas in ***Fig. A5.9***), i.e. PET values in the 2nd simulation would not increase more than 10 K, comparing with the PET values in the 1st simulation. The position of the dark blue and blue areas is around the hedges in ***Fig. A2.9***, e.g. in the zone of x = (120─140) and y = (100─115). The most frequent areas in the district were the areas with the difference in PET between – 2 K and 2 K (green areas in

Fig. A5.9), where there was grassland in some parts, but no tree, hedge or water bodies in ***Fig. A2.9***. Partial areas with difference in 5—10 K (partial yellow areas in ***Fig. A5.9***) appeared in the areas with water bodies in ***Fig. A2.9***. The other areas with difference in 5—10 K (partial yellow areas in ***Fig. A5.9***) were always combined with the areas, where there was the difference above 10 K (orange, red and purplish red areas in ***Fig. A5.9***). The areas with difference in PET above 10 K (orange, red and purplish red areas in ***Fig. A5.9***) were mainly the areas, where the trees and hedges were gave in the 2nd simulation (comparing with ***Fig. A2.9***), e.g. in the zone of x = (60—70) and y = (125—155).

The difference in SVF between the 1st simulation and the 2nd simulation in Lhasa (Dwc) was in ***Fig. A6.9***. The frequent areas of the district was the areas with the difference in SVF below 0.05, where there was rare impact from the added vegetation in the 2nd simulation. The areas with the difference in SVF above 0.25 was mainly associated with the areas in ***Fig. A2.9***, where there were trees and hedges inside or nearby. Comparing with the difference in PET in ***Fig. A5.9***, the distribution of the difference in PET above 10 K was associated with the distribution of the difference in SVF above 0.15.

The difference in v between the 1st simulation and the 2nd simulation in Lhasa (Dwc) was depicted in ***Fig. A7.9***, which was the conditions at 17 LST. The most frequent areas of the district were the areas with the difference in v below 0.25 m/s. The main areas with difference in v above 0.25 m/s in ***Fig. A7.9*** were in the zone of x = (35—140) and y = (90—140). These zones were located in or nearby the zones in ***Fig. A4.9***, where there were the relative high v values (above 1.5 m/s). Comparing with the design in ***Fig. A2.9***, the difference in v above 0.25 m/s was associated with the areas, where there were trees or hedges, by which the wind (E) was blocked.

6.3.7.10 Urumqi (Dfb)

The difference in PET between the 1st simulation and the 2nd simulation in Urumqi (Dfb) was presented in ***Fig. A5.10***, which was the conditions at 16 LST. There was no difference

in PET below – 10 K (i.e. black blue areas in ***Fig. A5.10***), i.e. PET values in the 2nd simulation would not increase more than 10 K, comparing with the PET values in the 1st simulation. The position of the dark blue and blue areas is mainly around the hedges in ***Fig. A2.10***, e.g. in the zone of x = (30─70) and y = (140─160).The most frequent areas in the district were the areas with the difference in PET between – 2 K and 2 K (green areas in ***Fig. A5.10***), where there was grassland in some parts, but no tree, hedge or water bodies. Partial areas with difference in 5─15 K (partial yellow, orange areas in ***Fig. A5.10***) appeared in the areas with water bodies in ***Fig. A2.10***. The other areas with difference in 5─15 K (partial yellow, orange areas in ***Fig. A5.10***) were always combined with the areas, where there was the difference above 15 K (red and purplish red areas in ***Fig. A5.10***). The areas with difference in PET above 15 K were mainly the areas, where the trees and hedges were gave in the 2nd simulation (comparing with ***Fig. A2.10***), e.g. in the zone of x = (10─160) and y = (50─60).

The difference in SVF between the 1st simulation and the 2nd simulation in Urumqi (Dfb) was in ***Fig. A6.10***. The most part of the district was the areas with the difference in SVF below 0.05, where there was rare impact from the added vegetation in the 2nd simulation. The areas with the difference in SVF above 0.35 was mainly associated with the areas in ***Fig. A2.10***, where there were trees inside or nearby. Comparing with the difference in PET in ***Fig. A5.10***, the distribution of the difference in PET above 10 K, except the areas in the zone of x = (80─90) and y = (15─30), was associated with the distribution of the difference in SVF above 0.35.

The difference in v between the 1st simulation and the 2nd simulation in Urumqi (Dfb) was depicted in ***Fig. A7.10***, which was the conditions at 16 LST. The most frequent areas of the district were the areas with the difference in v below 0.25 m/s. The main areas with difference in v above 1 m/s in ***Fig. A7.10*** were in the zone of x = (30─90) and y = (100─170). These zones were located in or nearby the zones in ***Fig. A4.10***, where there were the relative high v values (above 2.5 m/s). Comparing with the design in ***Fig. A2.10***,

the difference in *v* above 1 m/s was associated with the areas, where there were trees or hedges, by which the wind (SSW) was blocked.

6.3.7.11 Yuncheng (BSk)

The difference in PET between the 1st simulation and the 2nd simulation in Yuncheng (BSk) was presented in ***Fig. A5.11***, which was the conditions at 15 LST. There was rare difference in PET below – 10 K (i.e. black blue areas in ***Fig. A5.11***), i.e. PET values in the 2nd simulation would rarely increase more than 10 K, comparing with the PET values in the 1st simulation. The position of the dark blue and blue areas is between the trees and hedges in ***Fig. A2.11***, especially in the zone of x = (80─90) and y = (95─125). The most frequent areas in the district were the areas with the difference in PET between – 2 K and 2 K (green areas in ***Fig. A5.11***), where there was grassland and water body in some parts, but no tree, or hedge. Partial areas with difference in 5─10 K (partial yellow areas in ***Fig. A5.11***) appeared in the areas with water bodies in ***Fig. A2.11***. The other areas with difference in 5─10 K (partial yellow areas in ***Fig. A5.11***) were always combined with the areas, where there was the difference above 10 K (orange, red and purplish red areas in ***Fig. A5.11***). The areas with difference in PET above 10 K were mainly the areas, where the trees and hedges were gave in the 2nd simulation (comparing with ***Fig. A2.11***), e.g. in the zone of x = (40─70) and y = (120─160).

The difference in SVF between the 1st simulation and the 2nd simulation in Yuncheng (BSk) was in ***Fig. A6.11***. The frequent areas of the district was the areas with the difference in SVF below 0.05, where there was rare effect from the added vegetation in the 2nd simulation. The areas with the difference in SVF above 0.35 was mainly associated with the areas in ***Fig. A2.11***, where there were trees and hedges inside or nearby. Comparing with the difference in PET in ***Fig. A5.11***, the distribution of the difference in PET above 15 K was associated with the distribution of the difference in SVF above 0.25.

The difference in *v* between the 1st simulation and the 2nd simulation in Yuncheng (BSk)

was depicted in ***Fig. A7.11***, which was the conditions at 15 LST. The most frequent areas of the district were the areas with the difference in *v* below 0.25 m/s. The main areas with difference in *v* above 0.75 m/s in ***Fig. A7.11*** were in the zone of *x* = (0—140) and *y* = (50—70), the zone of *x* = (0—140) and *y* = (90—140), and the zone of *x* = (0—60) and *y* = (150—160). These zones were located in or nearby the zones in ***Fig. A4.11***, where there were the relative high *v* values (above 2 m/s). Comparing with the design in ***Fig. A2.11***, the difference in *v* was associated with the areas, where there were trees or hedges, by which the wind (SE) was blocked.

6.3.7.12 Yinchuan (BWk)

The difference in PET between the 1st simulation and the 2nd simulation in Yinchuan (BWk) was presented in ***Fig. A5.12***, which was the conditions at 15 LST. There was rare difference in PET below – 10 K (i.e. black blue areas in ***Fig. A5.12***), i.e. PET values in the 2nd simulation would rarely increase more than 10 K, comparing with the PET values in the 1st simulation. The position of the dark blue and blue areas is on the asphalt road between the trees and hedges in ***Fig. A2.12***, e.g. in the zone of *x* = (75—90) and *y* = (110—130). The most frequent areas in the district were the areas with the difference in PET between – 2 K and 2 K (green areas in ***Fig. A5.12***), where there was grassland in some parts, but no tree, hedge or water bodies. Partial areas with difference in 5—10 K (partial yellow areas in ***Fig. A5.12***) appeared in the areas with water bodies in ***Fig. A2.12***. The other areas with difference in 5—10 K (partial yellow areas in ***Fig. A5.12***) were always combined with the areas, where there was the difference above 10 K (orange, red and purplish red areas in ***Fig. A5.12***). The areas with difference in PET above 10 K were mainly the areas, where the trees and hedges were gave in the 2nd simulation (comparing with ***Fig. A2.12***), e.g. in the zone of *x* = (10—160) and *y* = (50—60).

The difference in SVF between the 1st simulation and the 2nd simulation in Yinchuan (BWk) was in ***Fig. A6.12***. The most part of the district was the areas with the difference in SVF below 0.05, where there was rare impact from the added vegetation in the 2nd

simulation. The areas with the difference in SVF above 0.35 was mainly associated with the areas in ***Fig. A2.12***, where there were trees and hedges inside or nearby. As ***Fig. A6.12*** depicted the conditions in 0─3 (m) above ground, the crown of the tress is large, and the densely leaves of the hedge in ENVI-met 3.0 was uniform in 0─2 (m) above ground, the simulated radiation arrived in these areas was reduced sharply. Comparing with the difference in PET in ***Fig. A5.12***, the distribution of the difference in PET above 15 K was associated with the distribution of the difference in SVF above 0.25.

The difference in *v* between the 1st simulation and the 2nd simulation in Yinchuan (BWk) was depicted in ***Fig. A7.12***, which was the conditions at 15 LST. The most frequent areas of the district were the areas with the difference in *v* below 0.25 m/s. The main areas with difference in *v* above 0.75 m/s in ***Fig. A7.12*** were in the zone of x = (30─140) and y = (90─160). These zones were located in or nearby the zones in ***Fig. A4.12***, where there were the relative high *v* values (above 2 m/s). Comparing with the design in ***Fig. A2.12***, the difference in *v* was associated with the areas, where there were trees or hedges, by which the wind (N) was blocked.

Based on the comparison between the 1st simulation and the 2nd simulation in each scenario, there are several common aspects could be recognised from the difference in PET (please see ***Fig. A5.1 ─ A5.12***), the difference in SVF (please see ***Fig. A6.1 ─ A6.12***), and the difference in *v* (please see ***Fig. A7.1 ─ A7.12***). Regarding the difference in PET, there was rare difference in PET below – 10 K in each scenario, i.e. PET values in the 2nd simulation would rarely increase more than 10 K, comparing with the PET values in the 1st simulation. Meanwhile, the most frequent areas in the district were the areas with the difference in PET between – 2 K and 2 K (green areas in ***Fig. A5.1 ─ A5.12***), where there was grassland in some parts, but no tree, hedge or water bodies. Furthermore, the specific changes in PET associated with the position of the added design elements; thus the distribution of the difference in PET is not unified in all scenarios. Regarding with the

difference in SVF, the areas with the obvious changes in SVF was mainly associated with the areas, where there were trees and hedges inside or nearby. With the respect of the difference in *v*, the zones with obvious changes in *v* were located in or nearby the zones in ***Fig. A4.1 —A4.12***, where there were the relative high *v* values, meanwhile, there were added design elements in the 2nd round simulations.

7 Discussion

This study analysed and evaluated the HTC conditions in 12 Chinese cities located in different climate type regarding the different spatial scales. In order to support the urban-PDM in an optimal level through the meteorological and biometeorological analysis, the suitable scale and data regarding the specific project in urban-PDM should be considered thoughtfully.

7.1 Preliminary analysis on meso scale

The detailed HTC conditions together with the meteorological conditions have been presented in Part One (Preliminary analysis), which focus on the conditions at the relative warmest point in time of one day in 12 Chinese cities. On meso scale, this kind of biometeorological information is of importance on updating approach of data analysis, and application in relevant topics (e.g. energy consumption, and architecture).

7.1.1 Approach of data analysis

In order to analysis the regular patterns of the actual HTC conditions in each city, the historically long-term data is necessary. In this study, the 3-hour data from 2000 to 2012 has been analysed for each city. The analysis of the long-term data provides not only the background HTC conditions on meso scale, but also the enlightenments for description and distinguish of the HTC conditions on macro scale, as well as the reference information for the input data sets in the simulation on micro scale. Therefore, the preliminary analysis of HTC conditions on meso scale can be understood as a bridge for other studies in different scales.

7.1.1.1 Comparison based on beanplots and boxplots

According to the series of beanplots and boxplots related to T_a, T_{mrt} and PET in each city, i.e. visualisation of data distribution at 8 points in time, there are possibilities to detect the points in time with relative extreme HTC conditions and the conditions of T_a and T_{mrt} for each city. The boxplot is popular in analysis of HTC conditions and the meteorological

conditions; however, the beanplot is relative new for this field. The beanplots have been applied to detect the sensitivity of the common thermal indices (Fröhlich and Matzarakis 2015), in which the distributions of three HTC indices have been distinguished briefly. The advantage of the beanplot is that the more details of data distribution can be depicted. The advantage of the boxplot is that the values in one cluster can be checked quickly by quartiles. Compared with the boxplots, the beanplots can also depict the quartile lines at the same time, but the visualisation is a little bit messier than that of boxplot. Therefore, the combination of beanplots and boxplots in this study (i.e. ***Fig. A1.1 — A1.12***) could present the key information at the same time, and will simplify the process of figure reading.

Due to the beanplots and the boxplots at 14 LST which possess the relative highest distribution of values, 14 LST was selected as the relative warmest point in time in each city. According to the study (Wong et al. 2002), which mentioned that the stronger v is required during the hot afternoon in Singapore (in KGC type Af), it also demonstrated that the HTC conditions at afternoon demands more notification than that in other period in one day. Therefore, the selected point in time in current study (i.e. 14 LST), at which the data presents the actual HTC conditions, could be the representative conditions in one day with the most frequent heat stress. The HTC conditions at this point in time can be regarded as the possibly alert HTC conditions on meso scale in one day, regarding the heat stress in each city. Based on the data at 14 LST, the bar graphs of monthly frequencies of PET and other parameters[6] are recommended for HTC analysis in each city (***Fig. 6.1.2 — 6.1.18***).

Although the HTC conditions in the whole day are worth to be analysed, current study has mainly concentrated on the information at 14 LST, which has been regarded as the warmest threshold in each day. Meanwhile, because the human beings activities (e.g.

---

[6] Wind roses were presented by annual frequencies in ***Fig. 6.1.7***.

working, doing sport, studying) during day time are much more frequent than that during night, the analysis at 14 LST (i.e. the point in time with frequent heat stress) provides information on the period, in which the heat stress should be careful. The more detailed information regarding the point in time with the most frequent cold stress (around 5 LST according to ***Fig. A1.1 — A1.12***) can be also selected and analysed through the same method in further studies, due to the importance in different topics, e.g. human health, and energy consumption.

Meanwhile, ***Fig. A1.1 — A1.12*** pointed out that the range of PET values were higher than that of T_a values in each city. In a study of quantification of the T_a and HTC conditions in Croatia (Brosy et al. 2014), the beanplots have been applied to detect the data distribution in four seasons at 1400 central European time (14 CET) in the period between 1981 and 2010. This study also found that the distribution of PET values are wider than that of T_a values, which indicates that PET is more sensitive than T_a in the quantification of thermal environment.

7.1.1.2 Monthly frequencies based on value classes

In ***Fig. 6.1.2 — 6.1.4***, the value classes of PET, T_a and T_{mrt} used for the monthly frequencies are currently based on the value classes from the study in Western/Middle European (Matzarakis and Mayer 1996) located in the Cfb climate type in KGC. There is no doubt that the considerations of the other value classes (e.g. the other two sets of value classes in ***Table 3.2.1***) are helpful to indicate the thermal perception for local inhabitants in further studies. However, as the original study for distinguishing the thermal perception in a temperate climatic zone, it is still reasonable to analyse the data based on the value classes of PET obtained by Matzarakis and Mayer (1996). Furthermore, according to ***Fig. 6.1.2 — 6.1.4***, it is worth to point out that the applied value classes have distinguished the HTC conditions at 14 LST obviously, not only from month to month, but also from city to city. Meanwhile, the PET (***Fig. 6.1.2***) can present the HTC perception more sensitively, according to the comparison with T_a (***Fig. 6.1.3***) and T_{mrt} (***Fig. 6.1.4***).

Although PET has been selected as the HTC index for preliminary analysis at present, HTC information can be updated by the improved HTC indices. For instance, the definition of PET is based on a 35-year man with specific clothing and working conditions (Höppe 1999). The improved index may distinguish the people with young group, middle age group, and old group; distinguish the people with clothing conditions in summer, in winter, and in spring/autumn; or distinguish the people with metabolic rate in different levels in the future. At the same time, the suitable value classes of the updated HTC index should be also considered.

Beside the personal conditions, the HTC information is driven by the meteorological parameters. That means, under the fact of the climate change (i.e. the meteorological data would change within years) (IPCC 2007), the information on meso scale should be better updated synchronously. According to the comparison regarding the climate change in Qinghai-Tibet Plateau (Li and Chi 2014), there are obviously difference between the 3 groups of data with 10-year different period. Therefore, the same period, or the shorter period (say 5 years), may be helpful for the accurate information analysing and updating in the future.

The core method regarding frequencies of value classes in this study has been applied in many other studies with the purpose on precisely presenting the HTC conditions, the trend of HTC conditions, or the connection between HTC conditions with specific issues in practices. For example, the connection between weather and cycling has been illustrated by the a bar graph with 9 thermal sensation levels (Brandenburg et al. 2007). It can be found from this research that the warmer thermal conditions indicated by PET are preferred by cyclists in the south of Vienna, Austria. The hourly PET distribution of one year in Freiburg, Germany, has been showed based on the value classes from Matzarakis and Mayer (1996) with the hourly data (Matzarakis 2007b), which revealed the high percentage of points in time with very cold conditions in this city. In other two studies, the monthly frequencies of PET (1961 to 1990, and 1999 to 2009) has been presented in

bar charts showed the background conditions of HTC in Freiburg, which belongs to a cool and moderate climate type (Matzarakis and Endler 2010; Herrmann and Matzarakis 2012). The similar applications of the monthly frequencies of PET values can also be find in other studies (Matzarakis et al. 2009; Endler et al. 2010; Farajzadeh and Matzarakis 2012).

Currently, as the background meteorological information in each selected city, the monthly frequencies have been adopted to present the actual HTC conditions in each month; however, if there would be more precisely requirements, i.e. the temporally downscaling analysis, the monthly frequencies could be replaced by the frequencies within the higher temporal resolution (e.g. 10-day). The applications have been applied in studies related to tourism, or urban structures (Matzarakis 2007a; Zaninović and Matzarakis 2009; Lin et al. 2010b; Lin et al. 2010a; Hwang et al. 2011; Matzarakis et al. 2013).

7.1.1.3 Necessity of analysis of other meteorological parameters

Except the PET, other normal meteorological parameters in this set of information are necessary for indicating HTC information, although they have been involved in the calculation of PET. Actually, several parameters are still applied individually (e.g. T_a, *VP*, *RH* and *v*) in practice. However, regarding to the sort of values in the practice, there are possibilities of improvement.

As a traditionally meteorological parameter, T_a is used to indicate the hot/cold conditions for a long period. However, considering the clothing insulation, the thermal environment indicated by T_a are not as actual as that perceived by human beings. This is also the reason why the subjects in laboratory studies related to HTC might be required to wear the limited clothes, and even to be unclothed (Gagge et al. 1967). Therefore, HTC index, here PET, is more appreciate to indicate the actual thermal environment perceived by human beings. However, monthly average of T_a is still the popular indicator in practice for urban-PDM, and this indicator will be continually used in a period. For instance, ***Table 7.1.1*** is

obtained from the National Bureau Statistics of China, which is on the monthly mean T_a of 2013 in the related 7 Chinese cities involved in current studies. This sort of table has been applied for constructions together with ***Table 7.1.2***. ***Table 7.1.2*** presents monthly mean T_a in January and July, respectively, which is the different climate conditions (not the same as KGC) in China based on the definition in the Design Standard for Civil Buildings in (GB50352-2005). Meanwhile, the location of these values in the value classes in ***Fig. 6.1.3*** for T_a has also been compared in ***Table 7.1.1*** and ***Table 7.1.2***, respectively.

Comparing the ***Table 7.1.1*** and ***Table 7.1.2*** with the respect of the value classes in ***Fig. 6.1.3***, the applied meteorological information (i.e. a single value in each month), currently, seems like rough evaluation. For example, the data in July is simplified as a single value, but there are devise conditions existed according to the quantitative information of T_a in ***Fig. 6.1.3*** in different value classes. The presented values is – 4.7 ℃ in January and 27.7 ℃ in July in Beijing (Dwa); however, there are more than 20 % of days with T_a higher than 4 ℃ at 14 LST in January, and approximate 70 % of days with T_a in 29—41 ℃. The possible results are that the heating consumption in January might be overestimated, and the risk of human health in July might be underestimated. Therefore, the single value cannot present the dynamic changes which combine the information related to the peak value/risk information/highest consumption, as the heat gain and lose is a dynamic process. Through the comparison between the single value in each standard in ***Table 7.1.2*** (i.e. in the different climate conditions and periods, respectively) and the multiple value ranges (e.g. value classes in ***Fig. 6.1.3***), the current approach based on the monthly frequencies of diverse value classes can be considered as an improvement for the information related to T_a, as the figure provide a dynamic value ranges which may be more precise and practical. ***Table 7.1.2*** is from The Design Standard for Civil Buildings (GB50352-2005), and it shows the T_a conditions without *RH* conditions.

Table 7.1.1 Comparison between the mean monthly T_a of 2013 in 7 Chinese cities and the corresponding value class in monthly frequencies of T_a in ***Fig.6.1.3***

City	January*	Value class in ***Fig. 6.1.3***	July*	Value class in ***Fig. 6.1.3***
Beijing (Dwa)	– 4.7 ℃	≤ 4 °C	27.4 ℃	23–29 °C
Hohhot (Dwb)	– 10.9 ℃	≤ 4 °C	21.5 ℃	18–23 °C
Shanghai (Cfa)	4.6 ℃	4–8 °C	32 ℃	29–35 °C
Kunming (Cwb)	8.8 ℃	8–13 °C	20.8 ℃	18–23 °C
Lhasa (Dwc)	– 0.3 ℃	≤ 4 °C	16.8 ℃	13–18 °C
Yinchuan (BWk)	– 5.5 ℃	≤ 4 °C	24.4 ℃	23–29 °C
Urumqi (Dfb)	– 10.3 ℃	≤ 4 °C	23.6 ℃	23–29 °C

* Data is from National Bureau Statistics of China (http://www.stats.gov.cn/tjsj/ndsj/2014/indexch.htm)

Table 7.1.2 Comparison between of the range on T_a in the Design Standard for Civil Buildings and the range on T_a in ***Fig.6.1.3***

Code of Standard	Monthly mean value in January	Value classes in ***Fig. 6.1.3***	Monthly mean value in July	Value classes in ***Fig. 6.1.3***
Ⅰ	$T_a \leq -10$ ℃	≤ 4 °C	$T_a \leq 25$ °C	≤ 29 °C
Ⅱ	T_a: – 10 to 0 ℃	≤ 4 °C	T_a: 18 to 28 ℃	> 18 ℃
Ⅲ	T_a: 0 to 10 ℃	≤ 13 °C	T_a: 25 to 30 ℃	> 23 ℃
Ⅳ	$T_a > 10$ °C	> 8 ℃	T_a: 25 to 29 ℃	> 23 ℃
Ⅴ	T_a: 0 to 13 ℃	≤ 13 °C	T_a: 18 to 25 ℃	> 18 ℃
Ⅵ	T_a: – 22 to 0 ℃	≤ 4 °C	$T_a < 18$ °C	≤ 18 °C
Ⅶ	T_a: – 20 to – 5 ℃	≤ 4 °C	$T_a \geq 18$ °C	> 18 ℃

Air humidity (AH) conditions are another common aspect regarded as the reference on climatic characteristics of a region in China, and the information is involved in the Design Standard for Civil Buildings in standard Ⅰ and standard Ⅶ (GB50352-2005), based on *RH*. However, according to the study from Nicol (2004), *RH* is not as suitable as *VP* to indicate AH conditions. The inefficient aspect can be also found in current study. For instance, the main *RH* conditions in Urumqi (Dfb) are roughly similar with that in

Kunming (Cwb) (please see section 6.1.4.3 and ***Table 6.1.4***). Although there is a huge amount of snowmelt from the Tianshan Mountains as the source of surface water in Urumqi (Dfb), and abundant of vegetation in the Zhungeer Basin (where Urumqi (Dfb) is located in), according to empirical feedback of the tourists, the perception of AH in these two cities are not as similar as that indicated by *RH*. Most of the tourists normally will emphasise the dry conditions in Urumqi (Dfb) in Xinjiang Province. In contrast, the *VP* conditions (please see section 6.1.4.3 and ***Table 6.1.3***) has clearly distinguished the AH conditions between this two cities.

In urban planning and design, wind conditions are usually presented by wind rose, which is necessary information in case analysis. In current study (please see ***Fig. 6.1.7*** and ***Fig. 6.1.8***), the calm wind and light breeze conditions (Beaufort scale) in each city existed with high frequencies; in contrast, the conditions with *v* above 4.5 m/s were not popular. This may present the preference of human beings on the permanent habitat regarding wind conditions. The correlation between strong wind and discomfort in Kassel (in Cfb in KGC) and Sheffield (in Cfb in KGC) inside city during summer (Nikolopoulou and Lykoudis 2006) indicated that the air flow has complex influence in specific thermal environment. However, before performing the downscaling (i.e. local-scale or micro-scale) simulations, measurements and investigation, the background driving force of air flow, i.e. the natural wind conditions of the whole city, are the necessary information.

In traditional practices, mean monthly T_a and mean monthly *RH* together with wind rose are the popular reference information in urban-PDM, however; as the criticism mentioned by architects and urban planners (Ng 2012), these information presents the general information which is weak to indicate the precisely reference values. As the monthly frequencies of parameters with multiple value classes have been regarded as the information depicted on temporal dimension (Matzarakis 2010), the monthly frequencies of multiple value ranges applied in current study can be the possible improvement of the application of meteorological information.

7.1.2 Application in different topics

Considering of the potential on applications, the analysis in Part One are necessary for urban-PDM, in which the urban management connects with tourism, human health and energy consumption, and it possesses feedback to urban planning and management.

From the monthly frequencies of PET and other meteorological parameters at the relative warmest point in time, the month with high heating requirement, high cooling requirement, the risk of human health, or the acceptable tourism situation could be evaluated more precisely with the dynamic information, comparing with the monthly average values. This will be discuss in the applications in different topics.

7.1.2.1 Urban planning and design

The analysis and the evaluations of the thermal environment based on the monthly frequencies are of importance for urban planning and design. Comparing with the UCMap method which can illustrate HTC conditions in the spatial dimension, the method with frequencies of value classes depicted the HTC conditions in the temporal dimension with full-view information. As the benefits of this temporal HTC information have not been taken into the practice, the results in this study is an attempt of this method in the selected Chinese cities. The limitation is that the data is obtained only from one weather station in each city. The study in Strasbourg (Matzarakis et al. 2009) indicated the different HTC conditions between the rural space and the urban area. Similarly, the frequencies of value classes on different sites have been compared in the study on shading effect in Taiwan (Lin et al. 2010a). Thus, if possible, the comparison of the monthly frequencies of PET and other parameters between rural areas and the urban areas is necessary to assist the urban development strategy. The combined information would be a sort of information distinguished both on spatial dimension and temporal dimension.

As the land surface influences the climate (Kabat 2004), how to construct the urban area need to be considered thoughtfully. The urban extension should also be careful on HTC

conditions. The sensitivity of PET is helpful for distinguish the HTC conditions in different location of a city (e.g. rural area vs. urban area). Furthermore, where to locate the suitable stations for monitor, will be the following consideration downscaling, e.g. the study in LCZs (Stewart and Oke 2012).

7.1.2.2 Tourism

Currently, the monthly frequencies of the continued value classes have been depicted as the basic information on meso scale. Due to the sort of the data resource, the long-term observed data in national level weather stations in cities, the information can be understood as the background information of a city, and the quantified regular information for tourists. For Chinese people, the traveling opportunities is highly correlated with the public-holiday; for the international tourists, the tourism period of one terminal may be driven by several reasons, in which the weather conditions should be one of the most important aspect. For both of the tourism groups, the empirical information regarding the HTC conditions is helpful to guarantee the satisfaction of the tourism. Based on the currently monthly frequencies and the popular recommended months (***Table 7.1.3***), the general HTC conditions in the 12 Chinese cities can be preliminarily estimated. Some new parameters are not included in current study precisely, e.g. the solar ultraviolet radiation (UV) conditions and the *RR* conditions. Considering for human health, the ***Fig. 6.1.2*** revealed the clearly thermal-stress grades, which is a reference information for people to take necessary protection, and to select an optimal traveling period, according to the personal situations. For instance, in Sanya (Aw), the most comfortable season for tourists should be in winter; and in Hohhot (Dwb), summer is more suitable for tourists.

Under the idea of the application of frequencies of specific conditions, the Climate Tourism Information Scheme (CTIS) (Zaninović and Matzarakis 2009) can be applied in further study for certain tourism issues in each city. And consequently, the specific HTC conditions will be emphasised in each city. For instance, the thermally comfort period in Sun Moon Lake from June to August with frequent rain (Lin and Matzarakis 2008); the

cooler comfort period in Australia is from January to March, and the warmer period is in November and December (Shiue and Matzarakis 2011); and the suitable (thermal comfort in CTIS) period in Lhasa is summer (Li and Chi 2014). Meanwhile, there is another innovation on the evaluation of tourism, which is called Customized rating assessment of climate suitability (CRACS) (Lin et al. 2015). Based on the CRACS approach, the reference on the planning activities in the city and the future travel plan can be obtained.

Table 7.1.3 Popular period for tourism in the 12 Chinese cities according to the travelling guidelines

Month	Jan.	Feb.	Mar.	Apr.	May	Jun.	Jul.	Aug.	Sep.	Oct.	Nov.	Dec.
Sanya (Aw)	**P**	**P**	**P**	**P**	*UV*	*UV*	*UV*	*UV*	*TY*	*TY*	**P**	**P**
Qionghai (Am)	**P**	**P**	**P**	**P**	*UV*	*UV*	*UV*	*UV*	*TY*	*TY*	**P**	**P**
Shenzhen (Cwa)	**P**	**P**	**P**	**P⁻**	**P⁻**	**P⁻**	**P⁻**	**P**	**P**	**P**	**P**	**P**
Kunming (Cwb)	**P⁻**	**P⁻**	**P**	**P**	**P**	**P**	**P**	**P**	**P**	**P**	**P⁻**	**P⁻**
Lhasa (Dwc)	*C*	*C*	*C*	*C*	*C*	**P**	**P**	**P**	**P**	*C*	*C*	*C*
Shanghai (Cfa)	**P⁻**	**P⁻**	**P**	**P**	**P**	*RR*	*RR*	*RR*	*RR*	**P⁻**	**P⁻**	**P⁻**
Yuncheng (BSk)	*C*	*C*	*C*	*C*	**P**	**P**	**P**	**P**	**P**	**P**	*C*	*C*
Yinchuan (BWk)	*C*	*C*	*C*	*C*	**P**	**P**	**P**	**P**	**P**	**P**	*C*	*C*
Dalian (Dwa)	*C*	*C*	*C*	*C*	**P**	**P**	**P**	**P**	**P**	*C*	*C*	*C*
Beijing (Dwa)	*C*	*C*	*C*	**P**	**P**	**P**	**P**	**P**	**P**	**P**	*C*	*C*
Hohhot (Dwb)	*C*	*C*	*C*	**P⁻**	**P**	**P**	**P**	**P**	**P**	**P⁻**	*C*	*C*
Urumqi (Dfb)	*C*	*C*	*C*	*C*	**P⁻**	**P⁻**	**P⁻**	**P**	**P**	**P⁻**	*C*	*C*

****P** (**P⁻**): the month recommended as the quite suitable (or suitable) period for tourism; ***UV***: the month with strong solar UV radiation; ***TY***: the month with frequent typhoon; ***C***: the month with cold and very cold conditions; ***RR***: excessive precipitation

7.1.2.3 Human health

During the period, in which there are frequent discomfort conditions, human body will be weak to overcome the illness (Omonijo and Matzarakis 2011; Laschewski and Jendritzky 2002). There are a series of studies have been performed in Ondo State, Nigera, which are related to the connection between HTC conditions and human health. For example,

one study (Omonijo et al. 2012) found that the more frequent transmission of measles can be detected during the period with high value of HTC indices. In the study related to the pneumonia (Omonijo and Matzarakis 2015), it has been demonstrated that the meteorological and bio-meteorological parameters modulate pneumonia infection. Ondo State, Nigeria is located in a tropical wet-and-dry climate, and in the Am in KGC type (i.e. the same KGC type in current study as Sanya in). These studies also revealed that meteorological parameters have strong impact on the transmission of the infectious diseases (Omonijo et al. 2012; Omonijo et al. 2011). Therefore, the evaluation of meteorological conditions towards human health are highly recommended to be involved in the public policy.

According the fact that the human health is associated with HTC conditions, the analysis and evaluation in this study could be also regard as the reference for a city. For example, the period with value class above 35 ℃ in PET should be pay more attention in each city, especially in the Sanya (Aw), Qionghai (Am), Shenzhen (Cwa) and Shanghai (Cfa), because the conditions maintain much longer time than other cities in a year. Actually, there is warning value taken into account in Shanghai China (35 ℃ in T_a as the heat warning value) (Tan et al. 2004); however the HTC indices have not been applied broadly. Winter is the period with cold stress, especially in northern cities (in China), and the HTC information below 4 ℃, or even below 0 ℃ will be helpful for the administration, as well as individuals for preventing illness related to cold stress. According to ***Fig. 6.1.2*** and ***Table 6.1.2***, the concentration on the cold stress should be maintained from late autumn until early spring in Lhasa (Dwa), Shanghai (Cfa), Yuncheng (BSk), Yinchuan (BWk), Dalian (Dwa), Beijing (Dwa), Hohhot (Dwb) and Urumqi (Dfb). The possible reference could be obtained from ***Table 7.1.4.***

Table 7.1.4 The recommended period with emphasis for heat & cold stress in each city

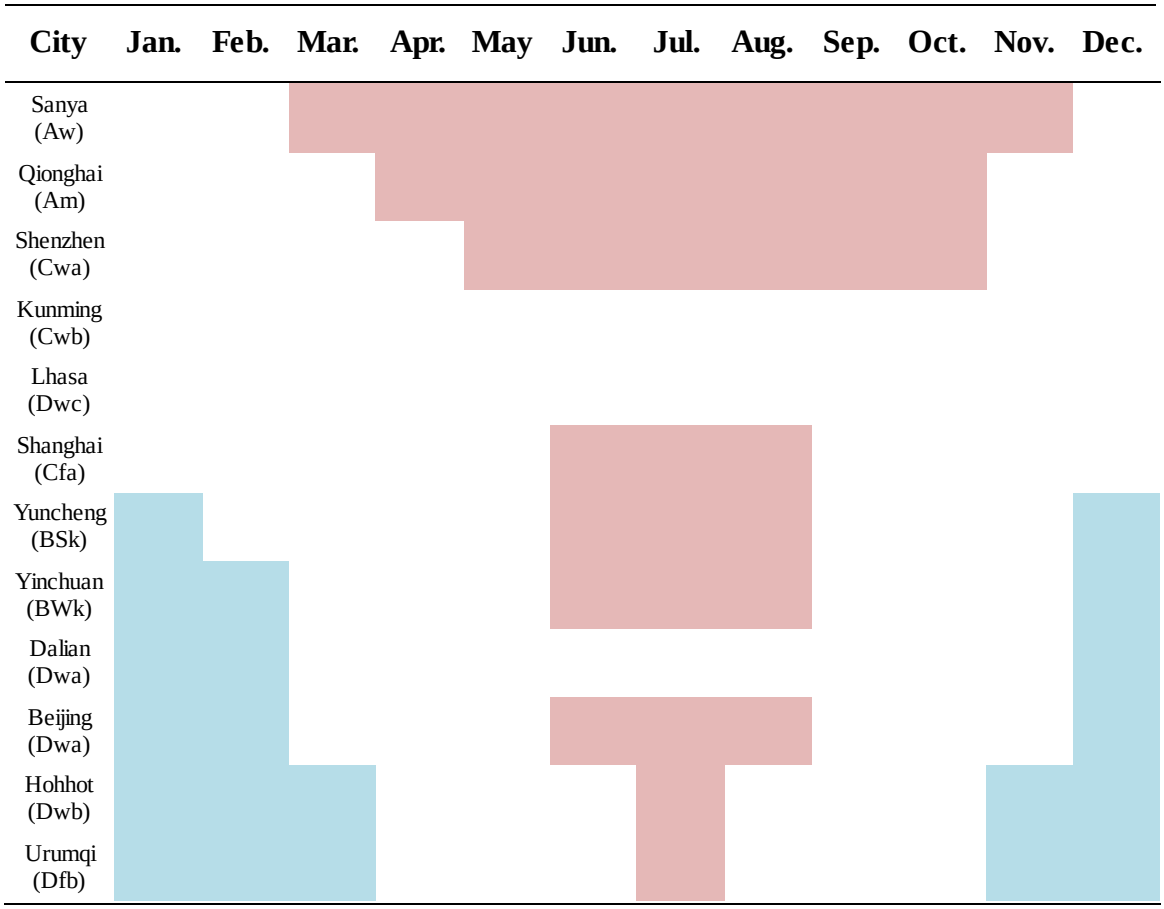

7.1.2.4 Energy consumption

In order to fulfil the thermal comfort requirement, the heating and cooling system are the essential approach, which are based on the energy consumption (e.g. heating/cooling relies on coal, natural gas, water, wind, solar energy; power of vehicle relies on oil or nature gas). Currently, the main energy consumption in China are still the traditional source, rather than the renewable source (Sinton et al. 1992). Therefore, under the strategy of sustainable development, the quantification of the thermal requirements is an optimal way to assessment the potential demand.

In this study, Sanya (Aw), Qionghai (Am), Shenzhen (Cwa), Kunming (Cwb) and Shanghai (Cfa) are the cities normally without the collective civil heating system in the buildings; however, the air conditions are widely considered as the necessary equipment

to maintain the indoor thermal environment, especially when the heat stress appeared in summer. ***Figure 7.1.1*** presents the assumed electricity consumption in Hangzhou (Ouyang et al. 2009), which is a Chinese city located nearby Shanghai (Cfa). Both Shanghai and Hangzhou are in the same climate type Cfa; thus, it could assume there were the similar demands pattern in Shanghai (Cfa). The highest demand of the electricity existed in summer. Comparing with the ***Fig. 6.1.2*** (monthly frequencies of PET) the period of the high demands on cooling matches with the period with heat stress in Shanghai (Cfa). There might be possibility to accurately predict the demands based on the thermal demands indicated by PET value classes. According to ***Fig. 6.1.2*** and ***Fig. 7.1.1***, the demands might last longer than the whole summer.

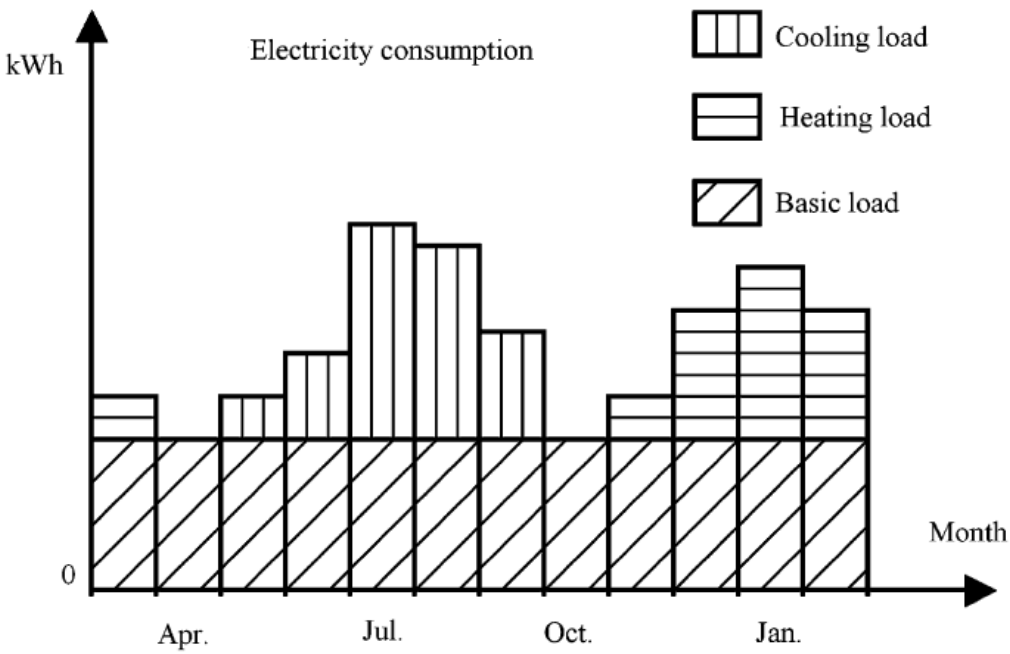

Fig. 7.1.1 The assumption of electricity consumption groups in the 12 months of 1 year in Hang Zhou (from Ouyang et al.2009)

The working time of the collective heating system in other Chinese cities are diverse. For example, the periods in the other 6 cities in this study have been generalised in ***Table 7.1.5***. The similar heating periods can be found in some cities, e.g. Yuncheng (BSk) and Yinchuan (BWk), Hohhot (Dwb) and Urumqi (Dfb). Comparing ***Table 7.1.5*** with the monthly frequencies of the PET and T_a values in ***Fig. 6.1.2*** and ***Fig. 6.1.3***, respectively,

the heating period (frequencies of days per month) is corresponding with period (frequencies of days per month) of the cold stress (value below 4 ℃), although the data in the two figures are at 14 LST. Actually, during the heating period, the running conditions will be controlled based on the actual weather conditions, i.e. there is dynamic heating strength. The meanings of the results in current study indicate that the predicted energy consumption might be estimated, based on the dynamic meteorological and biometeorological information. Regarding to the application in urban-PDM, utilisation of this information would be much helpful for policymaking, especially compared to the single values, with the respect of the sustainable development.

Table 7.1.5 Percentage of heating days in each month in 6 Chinese cities in northern China

City	Yuncheng (BSk)	Yinchuan (BWk)	Dalian (Dwa)	Beijing (Dwa)	Hohhot (Dwb)	Urumqi (Dfb)
Period	15_{th}. 11 – 15_{th}. 03	1_{st}. 11 – 15_{th} 03	5_{th}. 11 – 5_{th} 04	15_{th}. 11 – 15_{th}. 03	15_{th}.10 – 5_{th}.04	10_{th}.10 – 10_{th}.04
Jan.	100%	100%	100%	100%	100%	100%
Feb.	100%	100%	100%	100%	100%	100%
Mar.	48%	48%	100%	48%	100%	100%
Apr.	0%	0%	17%	0%	17%	33%
May	0%	0%	0%	0%	0%	0%
Jun.	0%	0%	0%	0%	0%	0%
Jul.	0%	0%	0%	0%	0%	0%
Aug.	0%	0%	0%	0%	0%	0%
Sep.	0%	0%	0%	0%	0%	0%
Oct.	0%	0%	0%	0%	48%	68%
Nov.	50%	100%	83%	53%	100%	100%
Dec.	100%	100%	100%	100%	100%	100%

7.2 Implementation of HTC in KGC

7.2.1 Preliminary description of HTC information in KGC

Currently, a possible methodology on how to link HTC information together with AH information with the KGC has been developed. The quantification of HTC conditions has been added to 11 climate types based on the data from 12 Chinese cities. The key step of

this methodology is to utilise the frequencies of PET and the frequencies of *VP* in specific time periods: annual period, the hottest month, the coldest month, the wettest month and the driest month.

In order to present the actual HTC conditions with a stable data set, the long-term meteorological data with 3-hour resolution is superior to be included in the current study. Through the utilisation of the frequencies, the variation of data could be presented. Thus, frequencies of PET and *VP* can depict more accurate HTC conditions, compared to, for example, mean PET values and mean *VP* values.

Brief and visual information on HTC conditions could be helpful to readers. For example, people could gain the HTC information of each climate type by scanning simple figures. Therefore, bar graphs can be a possible solution to fulfil this requirement. Meanwhile the data, which will be presented in the bar graphs, needs to be simplified and accurately represented. In the current study, the frequencies of PET and *VP* on an annual scale have been used to show the general HTC conditions. Frequencies of PET and *VP* in the hottest month and the coldest month have been analysed in order to show the extreme hot/cold HTC conditions during a year for each selected climate type. Similarly, frequencies of PET and *VP* in the wettest month and the driest month have been analysed in order to show the extreme wet/dry HTC conditions during the year. Finally, the visual form of HTC conditions together with AH conditions in each climate type has been achieved through the 6 bar graphs.

This methodology can be applied not only in China, but also in other regions. It is of great importance for future research to extend into other sample cities or even worldwide, in order to improve and quantify the current methodological information.

7.2.2 Limitation and orientation in further studies

Due to the similar results that appear in several climate types (please see section result 6.2.4), it is also possible to adjust the value classes of PET and *VP*, in order to obtain

more variant HTC conditions between each climate type.

As there are differences of the HTC conditions between Dwa (Beijing) and Dwa (Dalian), the parameters that were used for the HTC conditions may have more sensitive qualities than T_a and *RR*. Therefore, the variations of PET and *VP* are more obvious than that of T_a and *RR*, respectively. These differences between Dwa (Beijing) and Dwa (Dalian) may also lead to two considerations: (1) How large of differences in HTC conditions should be classified in one climate type? (2) Is it necessary to classify other new biometeorological types in the future?

Additionally, although BSk (Yuncheng) and BWk (Yinchuan) are the arid climate types in KGC (Kottek et al. 2006), the current study shows that the driest HTC conditions exist in Dwc (Lhasa) and Dfb (Urumqi). This can demonstrate that the traditional climate classification cannot indicate the wet/dry HTC conditions for human beings efficiently through *RR*.

7.2.3 Meaning in application

Based on future global human-biometeorological information, more suitable building styles could be selected, more precise energy consumption (heating /cooling) could be budgeted, possible disease periods could be predicted and the most suitable tourism season could be estimated in every climate type. Therefore, the topics of architecture, urban planning, public health, and tourism could benefit from the global human-biometeorological information.

7.3 Application for outdoor design

The HTC conditions of the high-rise building district in 12 Chinese cities (i.e. different climate types) have been presented, based on simulations on micro scale. According to the analysis of the results, the individual HTC conditions can be found in each scenario (i.e. each city), which were driven by the diverse meteorological input, as well as the

adapted design schemes. Based on the meteorological input (i.e. background conditions), the simulated results could be regarded as the "predicted" information of the HTC conditions for community environment design. Meanwhile, the diverse design can be modified according to the comparison between the 1st round simulations (before design) and the 2nd round simulations (after design). Back to the problem statement, the questions can be addressed through these simulations, and could be compared with other studies.

7.3.1 Approach of evaluation on micro scale

What kind of input data is suitable for the simulation?

In order to prepare the input data, the analysis of the long-term data (3-hour data) in Part One (Preliminary analysis) is necessary, as the analysis presented the background conditions of each city on meso scale. This is a key information for the preparation of the simulation in Part Three (Application for outdoor design). The relatively hottest period (i.e. the relatively hottest month) has been concentrated in this study. In order to obtain a set of input data for presenting the generally meteorological conditions in the hottest month, the hourly average values of T_a together with *RH* in one day in the relative hottest month have been calculated and applied as the input data (please see ***Fig. 6.3.2***). Comparing the T_a at 14 LST in each city in ***Fig. 6.3.2*** (i.e. advance input at 14 LST) with the monthly frequencies of T_a in each city in ***Fig. 6.1.3*** (i.e. the preliminary analysis at 14 LST in Part One), the average values are falling inside the main value class at 14 LST in each city. The similar conditions of *RH* can be found in ***Fig. 6.3.2*** and ***Fig. 6.1.6***. In other words, these calculated input data at 14 LST has be regarded as the representative values at 14 LST in the simulations in the short period, i.e. the relative hottest month. Due to the same method of the calculation, the input data at other points in time can also present the main conditions in the hottest month, although the monthly frequencies of other points in time have not been included in the Part One (Preliminary analysis) in current study.

In the previous studies, the actual values in one day (normally with the strongest heat

stress in summer) have been selected as the input data for simulations. In one study, the input data is based on the conditions in a typical summer in the Algerian Sahara (Ali-Toudert and Mayer 2007a). The meteorological data from a neighbour weather station at 21st of July has been selected to present the hottest time of summer in Damascus, Syria (Yahia and Johansson 2013). The simulation in a hot and dry 7-day period in 2003 has been performed by ENVI-met, which facilitated the evaluation of the changes in HTC conditions for an open space in Freiburg, Germany due the redesign project (Fröhlich and Matzarakis 2013). The meteorological data at 22nd of June in 2003 chosen as the input data for ENVI-met simulation, in order to evaluate the thermal comfort conditions of one urban district in Stuttgart, Germany (Ketterer and Matzarakis 2014a). Comparing with the meteorological values applied in the studies mentioned upwards, which supported the assessment of a specific day, the calculated data in current study is an attempt of the simulation, which is based on the treated input data. Therefore, different from the concentrations on the specific day, this set of input data is considered as the representative meteorological conditions in one period (e.g. the hottest month, or even the warmest season); and it is helpful in the urban-PDM for the general evaluation.

Will the HTC conditions in this district be distinguished on micro scale through the simulation?

Although the similarities can be recognised in several scenarios (e.g. please see Appendix A2: ***Fig. A2.1*** and ***Fig. A2.2***; ***Fig. A2.3*** and ***Fig. A2.5***; ***Fig. A2.10*** and ***Fig. A2.12***, respectively); the answer is positive. The HTC conditions are simulated under the regularly physical pattern (i.e. formula system in ENVI-met 3.0), therefore, the difference of the output values for the same district in different scenarios are decided by the input data. First of all, because HTC conditions are influenced by diverse meteorological parameters and the position of the obstacles. Secondly, the value of each parameter are not the same between different cities. Consequently, the HTC conditions cannot be the same. In order to form the thermal comfortable environment in community

environment design, the requirements on locating the specific HTC conditions become prominent in practice. After the analysis of the HTC conditions from the 1st round simulations, the community environment design for each scenario was performed, based on the diverse distribution of the HTC conditions (i.e. mainly the PET distribution in the figures in Appendix A2).

The distributions of the HTC conditions at the hottest point in time are selected in each scenario, which indicate the time with the highest thermal stress in the district in different cities. The same concentration of the positions can be also found in other applications of simulations (Yahia and Johansson 2014; Ketterer and Matzarakis 2014a; Shen et al. 2013). The simulation of the district pointed out the possible positions of the diverse HTC conditions in the district for different meteorological scenarios. For example, the large zone with PET above 54 ℃ would be appear in the street valley in Shenzhen (Cwa) at 15 LST (please see ***Fig. A2.3*** in Appendix A2), and Shanghai (Cfa) at 14 LST (please see ***Fig. A2.5*** in Appendix A2) in the same residential district, thus this street valley in these two city required modification in this large area for mitigation of the heat stress, especially for the pedestrian street. Consequently, more trees have been given in the community environment design in current study as a solution. As the results from the 3D simulation are depicted by a 2D map, the "problem" zone would be more easily located by landscape architectural designers, compared with the traditional reference without spatial description, e.g. seasonal wind roses, monthly mean T_a. Afterwards, the suitable modifications can be chosen, e.g. adding trees, or other design elements in appropriate position.

In the evaluation of the greenery scheme in National University of Singapore campus (Wong and Jusuf 2008), the mitigating effects from green spaces have been depicted through the comparison between the twice simulations which are before and after adding green spaces, respectively. Potential temperature has been used as the indicator to present the thermal environment. The position of different HTC conditions indicated by PET has

been traced for a study area in Szeged, Hungary (Égerházi et al. 2013). Combined with questionnaires, the increase of shade structures in specific positions has been considered as solutions.

7.3.2 The effects of direct short wave radiation

Although the direct short wave acts as the radiant source of the simulated area, all of the radiation in outputs from ENVI-met 3.0 are the values of radiant flux density, instead of the accumulated value of energy. As there is no direct input related to the solar radiation (i.e. the direct short wave radiation in current study), a series of physical formulas should have been involved in ENVI-met 3.0 for the estimation of the direct short wave radiation ($\boldsymbol{K_{di}}$), which is the radiant energy source of the study area. The estimation should be based on the input location and the atmospherically features of each scenario, respectively. From ***Table 6.3.3***, it could be noticed that direct short wave radiation ($\boldsymbol{K_{di}}$) possesses virtually the lowest estimate in the multiple liner regression test, compared with other parameters. The relative low estimate of $\boldsymbol{K_{di}}$ could be explained from two aspects.

The simulated PET values in the district in each scenario are spatially diverse in each hour. However, in the simulated results in one hour of each scenario, the value of $\boldsymbol{K_{di}}$ is the same in all of the grids under the sun or in the shadow, i.e. the $\boldsymbol{K_{di}}$ is almost not a spatial variable in the simulation in one time step, except the difference between the grids under the sun and the grids in the shadow. In contrast, other parameters presented in ***Table 6.3.3*** are absolute spatial variables, i.e. there are devise values in the grids in each hour. Thus, in one hour (i.e. one time step in the simulation), other spatial variables (i.e. other parameters in ***Table 6.3.3***) contribute higher impact on PET than $\boldsymbol{K_{di}}$. Secondly, comparing the values in different time step, the degree of the absolute change of $\boldsymbol{K_{di}}$ is lower than other parameters, e.g. especially than *v*, and SVF. Thus, as one of the predicator variables, there is less variations in $\boldsymbol{K_{di}}$, and weaker impact on PET value, the response variable.

However, the effect of the direct short wave radiation has not been ignored. Based on the

distribution of PET in each scenario (please see Appendix A2), the shading area were clearly presented by the much lower PET value ranges in each scenario. These areas were the same areas of $\boldsymbol{K_{di}}$ = 0 when the distribution of $\boldsymbol{K_{di}}$ in each scenario was individually checked. Hence, the shading effect has been considered in the community environment design, although the influence of $\boldsymbol{K_{di}}$ was lower than that of other parameters, especially lower than that of SVF and *v*.

7.3.3 Analysis and evaluation of the 12 scenarios

Under the application of 12 meteorological scenarios (i.e. meteorological conditions in 12 Chinese cities), there were two rounds of simulations have been completed, which were the simulations before community environment design, and the simulations after community environment design. The 1st round simulations focused on the distributions of specific HTC conditions in the district only with buildings, and the design was assisted by the 1st round simulations. The 2nd round simulations were utilised for the evaluation of the mitigated effects on HTC conditions from the design elements in each scenario. Based on the twice simulations in 12 scenario, a systemic process on how to apply the HTC information in outdoor design has been formed.

7.3.3.1 Before community environment design

For the same building group but located in different cities, and in different climate types, how the HTC conditions outdoors are?

Comparing the 12 simulations before adding design elements (i.e. PET distributions in Appendix A2), the HTC conditions between each scenario were diverse. The variations were determined through the input data (e.g. latitude, longitude, and WD).

In each figure, the distributions of the heat stress (i.e. higher PET value classes in each scenario) were orientation related. Comparing with the input data in ***Table 6.3.2***, the distribution of the higher PET values existed along the WD. However, the value classes of PET do not correlate with the *v* in ***Table 6.3.2***. For example, although the values of *v*

are both 1.7 m/s in Hohhot (Dwb) and Lhasa (Dwc), the heat stress presented by PET was mainly in 47─60 °C in Hohhot (Dwb), in contrast, it fluctuated in 41─54 °C in Lhasa (Dwc).

Meanwhile, the different strength of shading effect of buildings is briefly depicted in each scenario. The shading effects on HTC conditions are determined by the location (please see ***Table 6.3.2***) and the position of the obstacles (e.g. buildings, trees, and hedges). Due to the increase of the latitude, the shading area of the cities located at the higher latitude is larger than that of the cities located at the lower latitude, e.g. the shading area in Qionghai (Am), Yuncheng (BSk) and Hohhot (Dwb) at 15 LST, which are located at the approximate lines of longitude.

The PET distribution in the district in all of the scenarios can be clustered by three main groups, which are the emerged heat stress, the basic conditions, and the shading area, respectively (please see ***Table 7.3.1***). In each main group, the sub-groups have been defined according to the appeared PET value classes (which were the value classes utilised in Part Three on micro scale, instead of the value classes in Part One on meso scale), due to the variation in each scenario.

Table 7.3.1 Group and sub-group for the analysis of the simulated HTC conditions in each district

Group	Emerged heat stress	Basic conditions	Shading areas
Sub-group	above 54 ℃	47─54 °C	29─41 °C
	47─60 °C	41─47 °C (or partly with 35─41 °C)	23─35 °C
	41─54 °C	35─41 °C	18─29 °C (or partly with 29─35 °C)

Regarding to the emerged heat stress in the 1st round simulations of 12 scenarios, ***Table 7.3.2*** are the comparison between (1) the simulated PET value classes indicating the heat stress (results from Part Three), (2) the input T_a at the same point in time with the selected PET conditions from the simulation of each scenario (results from Part Three),

(3) in which PET value classes on meso scale at 14 LST (results from Part One), and (4) in which PET value classes on macro scale based on 3-hour data (results from Part Two). The simulated PET values indicating the heat stress were divided as PET above 54 ℃, PET in 47─60 °C, and PET in 41─54 °C, respectively (please see the emerged heat stress in ***Table 7.3.1***).

As T_a is calculated based on the data in the selected month (please see ***Table 6.3.1***), the T_a is falling in the main value classes on meso-scale analysis (in ***Fig. 6.1.3***), which has been mentioned in 7.3.1. Comparing the PET conditions indicating the heat stress with the input T_a in each scenario, the difference were more than 20 ℃. The great difference between the input T_a and the simulated HTC conditions has been addressed the similar concentration which has been discussed in 7.1.1.2 on meso-scale data analysis, that the PET can indicate the HTC perception more sensitively that T_a. Meanwhile, the simulated PET has contained the impacts from radiation. Three groups of PET conditions indicating the heat stress in each scenario were falling inside the highest PET value classes both on meso scale (i.e. in each city) and macro scale (i.e. in each KGC type), respectively. Although the simulated HCT conditions are in a day regarded as the representative of the hottest month in each scenario, the phenomenon of the PET conditions falling in the highest PET value classes of the biometeorological data analysis predicts a possible fact that there would be the HTC conditions with stronger heat stresses in specific urban area, which has been mentioned frequently in the studies related to urban heat island effects (Oliveira et al. 2011; Krüger et al. 2013; Ketterer and Matzarakis 2014b).

Table 7.3.2 Three kinds of emerged heat stress in 12 scenarios

Mainly with PET above 54 ℃					
Unit: ℃	Sanya (Aw)	Qionghai (Am)	Shenzhen (Cwa)	Shanghai (Cfa)	Yuncheng (BSk)
T_a *	31.6 at 14 LST	31.8 at 15 LST	31 at 15 LST	31.9 at 14 LST	31.2 at 15 LST
PET **			> 41		
PET ***			> 35		

Mainly with PET in 47─60 ℃						
Unit: ℃	Kunming (Cwb)	Beijing (Dwa)	Dalian (Dwa)	Hohhot (Dwb)	Urumqi (Dfb)	Yinchuan (BWk)
T_a *	23.6 at 16 LST	30.8 at 14 LST	26.4 at 14 LST	27.8 at 15 LST	27.7 at 16 LST	28.9 at 15 LST
PET **				> 41		
PET ***				> 35		

Mainly with PET in 41─54 °C	
Unit: ℃	Lhasa (Dwc)
T_a *	21.7 at 17 LST
PET **	> 41
PET ***	> 35

* T_a value in ***Fig. 6.3.2***
** PET value classes in ***Fig. 6.1.2***
*** PET value classes in ***Fig. 6.2.1***

Regarding to the basic conditions in the 1st round simulations of 12 scenarios, ***Table 7.3.3*** are the comparison between (1) the simulated PET value classes indicating the basic conditions (results from Part Three), (2) the input T_a at the same point in time with the selected PET conditions from the simulation of each scenario (results from Part Three), (3) in which PET value classes on meso scale at 14 LST (results from Part One), and (4) in which PET value classes on macro scale based on 3-hour data (results from Part Two). The simulated PET values indicating the basic conditions were divided as PET above 47─54 °C, PET in 41─47 °C (or partly with 35─41 °C), and PET in 35─41 °C, respectively (please see the basic conditions in ***Table 7.3.1***).

The PET values presenting the basic conditions were ─ as the preconditions ─ lower than the PET values presenting the heat stress in each scenario. Meanwhile, the PET values of basic conditions are falling in the highest value classes in Part One on meso scale (i.e. in

each city), as well as on macro scale (i.e. in each KGC type), respectively; except the conditions in Kunming (Cwb) and Lhasa (Dwc), in which the PET values of the basic conditions were falling in the second highest value class in Part One on meso scale (i.e. 35─41 °C). That means the basic HTC conditions of the district in Kunming (Cwb) and Lhasa (Dwc) might possess the similar background HTC conditions in these two cities, in contrast, the basic HTC conditions in other scenarios are warmer than the background HTC conditions in each city on micro scale, respectively.

The situation can extend to two consideration: (1) Due to the limitation (please see section 7.3.4) of the ENVI-met 3.0, these two scenarios (Kunming (Cwb) and Lhasa (Dwc)) were the simulated results with lower value output; (2) the meteorological characteristics in Kunming (Cwb) and Lhasa (Dwc) could maintain the background HTC conditions.

The scenario in Dalian (Dwa) was also special, because the areas with PET in 35─41 ℃ (please see ***Fig. A2.7*** in Appendix A2) were also the basic conditions. Comparing the distribution of PET in ***Fig. A2.7*** and the distribution of *v* in ***Fig. A4.7***, the existence of PET in 35─41 °C is due to high *v* in this scenario. It can be found that the position of the PET in 35─41 °C was cooperated with the position of the *v* greater than 3.0 m/s. That means this cooler conditions of the PET was based on the relative high wind speed (say above 3.0 m/s in this simulation).

Table 7.3.3 Three kinds of basic conditions in 12 scenarios

Mainly with PET in 47─54 °C					
Unit: ℃	Sanya (Aw)	Qionghai (Am)	Shenzhen (Cwa)	Shanghai (Cfa)	Yuncheng (BSk)
T_a *	31.6 at 14 LST	31.8 at 15 LST	31 at 15 LST	31.9 at 14 LST	31.2 at 15 LST
PET **			> 41		
PET ***			> 35		
Mainly with PET in 41─47 °C (35─41 ℃ involved in Dalian (Dwa))					
Unit: ℃	Beijing (Dwa)	Dalian (Dwa)	Hohhot (Dwb)	Urumqi (Dfb)	Yinchuan (BWk)
T_a *	30.8 at 14 LST	26.4 at 14 LST	27.8 at 15 LST	27.7 at 16 LST	28.9 at 15 LST
PET **			> 41		
PET ***			> 35		
Mainly with PET in 35─41 °C					
Unit: ℃		Kunming (Cwb)		Lhasa (Dwc)	
T_a *		23.6 at 16 LST		21.7 at 17 LST	
PET **			35─41		
PET ***			> 35		

* T_a value in ***Fig. 6.3.2***
** PET value classes in ***Fig. 6.1.2***
*** PET value classes in ***Fig. 6.2.1***

Regarding to the shading areas in the 1st round simulations of 12 scenarios, ***Table 7.3.4*** are the comparison between (1) the simulated PET value classes indicating the shading areas (results from Part Three), (2) the input T_a at the same point in time with the selected PET conditions from the simulation of each scenario (results from Part Three), (3) in which PET value classes on meso scale at 14 LST (results from Part One), and (4) in which PET value classes on macro scale based on 3-hour data (results from Part Two). The simulated PET values indicating the shading areas were divided as PET above 29─41 °C, PET in 23─35 °C, and PET in 18─29 °C (or partly with 29─35 °C), respectively (please see the shading areas in ***Table 7.3.1***).

The shading areas provide the coolest HTC conditions in each scenario. The T_a value fell in the value class of the simulated PET in each scenario, e.g. 31.6 °C is in 29─41 °C in Sanya (Aw). Therefore, the thermal environment in shading area indicated by PET is not

dramatically different from that indicated by T_a. The possible reason might be the absence of the direct short wave radiation. Meanwhile, the PET value classes presenting the shading areas fell in the second highest and third highest value classes (29─35 °C, and 35─41 °C) on meso scale, on macro scale they are falling in the value class which are above 8 ℃.

Table 7.3.4 Three kinds of shading areas in 12 scenarios

Mainly with PET in 29─41 °C						
Unit: ℃	Sanya (Aw)	Qionghai (Am)	Shenzhen (Cwa)	Shanghai (Cfa)	Beijing (Dwa)	Yuncheng (BSk)
T_a *	31.6 at 14 LST	31.8 at 15 LST	31 at 15 LST	31.9 at 14 LST	30.8 at 14 LST	31.2 at 15 LST
PET **	29─35, and 35─41					
PET ***	8─35, and > 35					
Mainly with PET in 23─35 °C						
Unit: ℃	Hohhot (Dwb)		Urumqi (Dfb)		Yinchuan (BWk)	
T_a *	27.8 at 15 LST		27.7 at 16 LST		28.9 at 15 LST	
PET **	23─29, and 29─35					
PET ***	8─35					
Mainly with PET in in 18─29 °C, or partly with 29─35 ℃ in Dalian (Dwa)						
Unit: ℃	Dalian (Dwa)		Kunming (Cwb)		Lhasa (Dwc)	
T_a *	26.4 at 14 LST		23.6 at 16 LST		21.7 at 17 LST	
PET **	18─23, and 23─29					
PET ***	8─35					

* T_a value in ***Fig. 6.3.2***
** PET value classes in ***Fig. 6.1.2***
*** PET value classes in ***Fig. 6.2.1***

7.3.3.2 After community environment design

Can the HTC conditions outdoors be modified (i.e. through community environment design) in different climate type?

Comparing the difference between the twice simulations before and after adding design elements (i.e. difference in PET in Appendix A5), three kinds of changes can be summarised according to the current value classes, which are positive changes (difference

in PET > 2 K), negative changes (difference in PET < – 2 K) and slight fluctuation of simulation (difference in PET between – 2─2 K). According to the analysis of the results on the comparison between the distribution of the difference in PET (Appendix A5) and the position of the design elements (Appendix A2), the positive changes were contributed by trees, hedges and water bodies, and the negative changes were caused by hedges and trees. The slight fluctuation of simulations existed frequently in all 12 scenarios included the areas with grassland, since trees and hedges in the 2nd round simulations were not given to everywhere. According to the current value classes, the effects on HTC conditions from the added grass seemed not strong enough to be recognised from the difference in PET (please see Appendix A5), the difference in SVF (please see Appendix A6), or the difference in *v* (please see Appendix A7), respectively.

Trees and hedges can cause the positive changes above 15 K (especially between 15 K and 25 K) in 10 scenarios (i.e. the red areas and the purplish red areas in ***Fig. A5.3─A5.12***, respectively). The weakest positive changes contributed by trees and hedges appeared in Sanya (Aw) and Qionghai (Am), in which the positive changes are between 5─25 K , especially between 5 K and 10 K, (i.e. the partial yellow areas in ***Fig. A5.1*** and ***Fig. A5.2***). Water bodies can drive the positive changes between 5 K and 10 K in most of scenarios, and between 5 K and 15 K in Urumqi (Dfb). Meanwhile, the changes were located exactly at the same position where the water bodies were.

As hedges were the same in all 12 scenarios, the main reason of the weaker positive changes in Sanya (Aw) and Qionghai (Aw) is the type of the tree utilised in the simulations. In Sanya (Aw) and Qionghai (Am), the selected tree was one locally popular palm tree (i.e. *Cocos nucifera* in ***Table 5.3.1***), which possesses the characteristics of smaller canopy, less dense leaves and relative higher trunk, compared with other tree types in ***Table 5.3.1***. Thus the weakest changes on SVF from trees (i.e. the difference between 0.15 and 0.25 in ***Fig. A6.1*** and ***Fig. A6.2***) can be found in Sanya (Aw) and Qionghai (Am), through the comparison with the differences in SVF from trees in other 10 scenario (i.e. the difference

above 0.25 in Hohhot (Dwb) and Lhasa (Dwc) in ***Fig. A6.8*** and ***Fig. A6.9***, respectively; the difference above 0.35 in Beijing (Dwa), Dalian (Dwa), Urumqi (Dfb), Yuncheng (BSk), and Yinchuan (BWk) in ***Fig. A6.6***, ***Fig. A6.7***, ***Fig. A6.10***, ***Fig. A6.11*** and ***Fig. A6.12***, respectively; and the difference above 0.45 in Shenzhen (Cwa), Kunming (Cwb), and Shanghai (Cfa) in ***Fig. A6.3***, ***Fig. A6.4***, ***Fig. A6.5***, respectively.

Due to the weaker impact from trees in Sanya (Aw) and Qionghai (Am), the impact from hedges emerged obviously in these two scenarios (i.e. the positive changes in PET above 15 K). Actually, the impact of hedges added to the individual grid in the simulation was similar in all scenarios, as the definition of the hedge in the simulation was the same, i.e. 2 (m) height with dense leaves. Since the trunk is the main part of trees at the height of 0─6 (m) above ground, hedges can reduce the SVF more efficiently in the height of 0─3 (m) than trees can. Except the trees in Sanya (Aw) and Qionghai (Am), the canopies of other trees in other 10 scenarios have stranger impact in the height of 0─3 (m); therefore, the positive changes from hedges in Sanya (Aw) and Qionghai (Am) were obviously.

As the impacts of water bodies cannot be recognised in the spatial distribution of the difference in SVF (please see Appendix A6), or the spatial distribution of the difference in *v* (please see Appendix A7), the main reason of the positive changes in PET in the areas added with water bodies should be related to other parameters in ***Table 6.3.3***. However, the difference in PET in the areas nearby the water bodies have not presented the visualised positive changes, based on the current value classes. In other words, the mitigating effects from the stable water body (in current simulation model) cannot extend to the neighbour efficiently, according to the simulations in 12 meteorological scenarios.

Comparing the difference in PET (please see Appendix A5) with the difference in *v* (Appendix A7), the negative changes were mainly caused by trees and hedges, which have blocked wind around the zones with the negative changes, and have reduced the relative high *v* values. Thus, it can be found from the comparisons that the PET in certain zones may increase synchronously in the 2nd simulation, when the *v* in the same zones

decreases in the 2nd simulation in each scenario. Meanwhile, the WD was always as same as the input settings, the negative changes always individually appeared at the same position during the whole simulation in each scenario, i.e. the lee side of trees and hedges in each scenario. In Shenzhen (Cwa), Shanghai (Cfa) and Beijing (Dwa), the negative changes are obviously in the street valley, respectively. The first reason of this phenomenon is due to the double lines of the trees (i.e. stronger block effect on wind) in the street valley in these three scenarios. Although there are also double lines of tree in the street valley in Sanya (Aw) and Qionghai (Am), the occupied spaces of the palm tree in the simulations are smaller than that of other trees; thus, the block effect were not as significant as the 3 scenarios mentioned above. The block effects in Sanya (Aw) were mainly caused by the continued trees and hedges, e.g. in the zone of x = (10─100) and y = (110─150) (please see ***Fig. A5.1*** in Appendix A5), and in the zone of x = (10─60) and y = (120─150) (please see ***Fig. A5.2*** in Appendix A5). Furthermore, the double lines of trees narrowed the free space of air flow in the street valley on the height concentrated currently (i.e. 0─3 m).

Comparing the difference in PET with the difference in SVF, it can be found that the position of the positive changes moved a little bit northern or north-eastern to the zones with main changes in SVF (e.g. comparison between the ***Fig. A5.1*** and ***Fig. A6.1***, ***Fig. A5.5*** and ***Fig. A6.5***, or ***Fig. A5.12*** and ***Fig. A6.12***). This is because the shading effect on HTC conditions is related to SVF, but does not equal to the effect of SVF on HTC conditions. Meanwhile, the positive changes presented the pattern on points corresponding, i.e. the position with positive changes is associated with the individual grid, in which trees, hedges or water bodies have been added. Comparing the difference in PET with the difference in v, the position of the negative changes is highly related to the position of the great changes in v (e.g. comparison between the ***Fig. A5.1*** and ***Fig. A7.1***, ***Fig. A5.5*** and ***Fig. A7.5***, or ***Fig. A5.12*** and ***Fig. A7.12***). Therefore, the negative changes depicted the pattern on flat pieces corresponding. These two aspects are

one kind of efficient information for designers in practice for the further modification of the community environment design in each scenario.

7.3.3.3 Advices for community environment design

Are there advices can be obtained from the analysis and evaluation of the HTC conditions on micro scale?

From the evaluation of the impacts of the each design element on HTC conditions in the simulations, the individual tips can be generalised for each design element applied this study.

The utilisation of trees is the main approach in landscape architectural design to form green spaces in vertical and horizontal direction, and the ability on mitigation of heat stress has been confirmed (Akbari 2009). In current study, the positive changes and the negative changes on PET from trees can be both detected in 12 scenarios. Thus, there are two aspects of advices might be worth to be emphasised. Before adding trees to modify the HTC conditions of an exactly position, the displacement of the efficient mitigation should be considered, due to the combined impact of shading and SVF. For example, the position of trees in street valley were roughly added along the lines of y = (52) and y = (70) in Yuncheng (BSk) (please see ***Fig. A2.11***), and the great difference of SVF (above 0.35) formed by these trees (please see ***Fig. A6.11***) roughly appeared along the same lines: y = (52) and y = (70). However, the positive changes in PET (above 15 K in ***Fig. A5.11***) formed by these trees appeared along the lines of y = (55) and y = (73) at 15 LST. With the displacement of 3 units, i.e. y = (55) – y = (52), and y = (73) – y = (70), there are 6 meters changed on the direction of y, between the position with trees and the position with positive changes in PET. This distance is significant in community environment design on micro scale. Furthermore, the mitigation is also influenced by the tree type with the respect of the height of the trunk and the width of the canopy. On the other hand, the density of trees is correlated with the negative changes of PET, due to the block effect on

wind. Therefore, it should be better identified which areas in the district demand the optimal air flow. For example, in the zone of x = (10─100) and y = (110─150) in Sanya (Aw) (please see ***Fig. A5.1*** in Appendix A5, and ***Fig. A7.1*** in Appendix A7), the design should be modified, in order to avoid the strong block effect.

Hedges have been popularly applied for space separation and decoration in community environment design; however, in China, it is customary to utilise the hedges lower than human beings' height. Therefore, the changes in SVF from the default hedges (2.0 m) in ENVI-met 3.0, i.e. the changes of radiant conditions, are not common in practices in China. However, as the horizontal distribution was arranged as the actual method in practice, there is one aspect advice can be obtained from these simulations. Since the negative changes in the simulations were caused through the continued hedges (also trees) in the height of 0─3 (m), the density and the position of hedges should be careful, regarding the fluent air flow in specific spaces (e.g. ventilation corridors of the district) at the height like human beings.

According to the simulations, grassland cannot provide obviously changes in PET (based on the current value classes for the difference in PET). Therefore, the further analysis on how to apply grass with the respect to HTC mitigation is required, which can be performed through, for example, the smaller value classes for analysis the difference in PET, or visualisation of other parameters.

Regarding the scale of the residential district, normally, the water body is constructed as the decoration part but is one kind of necessary element in middle- and high-grade residential district, at least in China. Due to the habitual thinking on the cooling effect from big water bodies (such as oceans, huge nature lakes), the water body is easily expected to optimise the thermal environment. According to the analysis of results in each scenario, the cooling effects (i.e. the positive changes in PET) from water bodies, were limited in the areas which were just covered by water bodies in the simulations. Meanwhile, the water bodies in the simulations (which are stable and deep water bodies)

are not the normal entertainment area, such as the areas for sports and recreational activities. Therefore, in practice, the utilisation of water bodies demands creative method with the regarding on the size, the style and the location. For instance, the cooling effect from the water body ─ a fountain equipped with 1.0 (mm) diameter nozzles ─ have been confirmed (Nishimura et al. 1998).

In landscape architectural design, there are other facilities and equipment for the outdoor environment modification, which are worth to be applied in practice. Considering the requirements of the shading effect and the decrease of SVF, the facilities, such as tensile membrane structures (Zhao et al. 2012; Elseragy and Elnokaly 2006), can form optimal shading effect.

7.3.4 Limitations in current simulations

Although ENVI-met 3.0 can distinguish the HTC conditions in landscape architectural design, the limitation of current study should be listed as the orientation for the further study.

With the respect to the simulation, there are three aspects required to be clarify. The first common issue is related to the insufficient accuracy of the simulated values in current study. The possible reason is mainly due to the process of the heat storage in the wall which leads to the relative high T_{mrt} during daytime and relative low T_{mrt} during night (Toudert 2005; Johansson 2006; Ketterer and Matzarakis 2014a). The second aspect is related to the validation, which is normally combined with the simulation of one real case study. Through the comparison between the measured values and the simulated values, the evaluation of the single value could be justified accurately and reasonably (Huttner 2012). The third aspect is that the input data of wind conditions for the model initialization are two single values (i.e. v and WD). While the real conditions of the wind are diverse. Therefore, the input data should represent the popular conditions of a certain period, which are normally not a single wind condition. In other words, regarding the wind

conditions, the multiple simulations of one meteorological scenario are helpful. Currently, as the application of the microclimatic simulation in this study focuses on the facilitating the community environment design through locating the discomfortable spaces in the district, the spatial distribution of PET has illustrated the possible locations for design elements. However, with the multiple simulations, the location might be limited in more seriously areas which required definitely modification on HTC conditions.

Regarding to the objects considered in the simulations, there are two issues worth to be examined in further studies. Firstly, the effects on HTC conditions from design elements have been analysed; however, the impact form grassland was presented through neither PET, nor other parameters, based on the current value classes at the selected height in the figures. As the cooling effect from grassland have been detected in other studies (Shashua - Bar et al. 2011), the application of grassland for mitigation of heat stress is still acceptable, but as complement. The simulated results might because that the effects from grassland exist nearby ground. The second aspect is related to the buildings. The impact on HTC conditions from buildings has not been examined in current study, while it is worthy to be evaluated, especially on the decision of the land use in urban planning. Thus, the district could be evaluated within a larger scope, e.g. the evaluation the effect from high-rise building group on the vicinity.

8 Conclusion and Outlook

8.1 Conclusion

Under the supports of the meteorological data in each city from 2000 to 2012, as well as the necessary models (such as RayMan model, and ENVI-met model), the Human-biometeorological conditions in each city have been analysed on three scales, which are macro scale, mese scale, and micro scale.

Based on the monthly frequencies of each human-biometeorological parameter, such as PET, T_a, T_{mrt}, *VP*, *RH*, *v*, and WD, on meso scale, the individual HTC conditions in each city have been presented. According to the monthly frequencies of the specific value classes, there are possibility to apply the HTC information in multiple topics, such as human health, energy consumption, and tourism. The heat stress at 14 LST, which was indicated by PET, existed with high frequencies in most of the months through the whole year in Sanya (Aw), Qionghai (Am), and Shenzhen (Cwa). In these cities, the period with the emphasis on heat stress might be relative longer than other cities, in order to guarantee the human health; the diverse tourism production with protection against negative weather might be helpful for the tourism market; the cooling demand from the energy consumption might be relative higher. In contrast, the cold stress at 14 LST happened much frequently in winter in Yuncheng (BSk), Yinchuan (BWk), Dalian (Dwa), Beijing (Dwa), Hohhot (Dwb), and Urumqi (Dfb). The concerns on HTC conditions in these cities focus on the influence from cold stress in longer period. Meanwhile, the data analysis has been regarded as the fundament of the study in Part One and Part Three, respectively.

Based on the analysis of the monthly frequencies of each parameter in Part One, as well as the analysis of KGC, the study on macro scale in Part Two has provide a group of bar graphs as the approach to implement the HTC information in KGC. The significant sections in this level are two aspects. The first one is the conservation of the parameters, which refers to that PET is linked to T_a as a hot/cold indicator especially for human beings,

and *VP* is linked to *RR* as a wet/dry indicator especially for human beings, respectively. The second one is the method on quantification of the information, which is completed through the frequencies of simplified value classes in specific periods. The group of bar graphs consists of the annual frequencies of PET, the frequencies of PET in the hottest month, the frequencies of PET in the coldest month, annual frequencies of *VP*, the frequencies of *VP* in the wettest month, and the frequencies of *VP* in the driest month in each climate type (i.e. each KGC type).

On micro scale in Part Three, the analysis and evaluation of HTC conditions in different cities (i.e. 12 scenarios) have revealed the thermal environment of the hypothetically residential district with high-rise buildings, and the mitigation effects on the heat stress from the community environment design in current study. The analysis and evaluation of HTC conditions in 12 scenarios are based on a unified process. The individual community design scheme has been performed for the district according to the HTC conditions (at the relative hottest point in time) under 12 meteorological scenarios, respectively. The effects of the design elements on HTC conditions in each meteorological scenario have been analysed through the comparison between the HTC conditions from the simulations before design and the HTC conditions from the simulations after design.

The effects from hedges are similar in all 12 scenarios, as the same type has been set in the simulations. However, the strength of the effect from trees are diverse, because the different types have been applied, which is related to the characteristics on height of the tree, the scope of the canopy, and the leaf area density. Both of the trees and the hedges can cause the positive changes (i.e. mitigation of the heat stress), and negative changes on HTC conditions (i.e. the increase of the heat stress), respectively. The reason of the positive changes are mainly due the decrease of the radiation flux in and around the areas with trees and hedges. On the other hand, the negative changes are mainly related to the blocking effects from the continued trees or hedges on the ventilation corridor.

Currently, the mitigation effect from the grassland has not been detected from the height

observed in the simulations, based on the value classes of the difference in PET. The water bodies can drive the positive changes of PET within the limited areas.

Based on the analysis and evaluation of the simulated HTC conditions, there are recommendations for community environment design with the respect to the impacts of the design elements on HTC conditions on micro scale. Firstly, the position of the trees and hedges should be decided according to (1) the requirements of cooling effects formed by the weakly radiant conditions, and (2) the requirements of the air flow. Secondly, the creative style of water bodies are helpful to transform the area with water bodies into the availably entertainment area for residents. Thirdly, the utilisation of grassland could be maintained under the traditional requirements. According to HTC conditions in 12 scenarios, it has been found that the individual site analysis related to the HTC conditions are required, although there is the unified physical laws on the atmosphere activities.

Throughout the analysis and evaluation of the HTC conditions in 12 Chinese cities on three scales, one set of accurately approach on how to describe and estimate the HTC conditions on macro scale, on meso scale , and on micro scale (in local scale) has been presented, respectively. With the respects to urban planning, urban design, urban management on different scales, the application of the HTC information will facilitate the understanding in human health, tourism and the energy consumption.

8.2 Outlook

Based on the scales in meteorology, one kind of innovation on data analysis on each scale has been performed. Although there are limitations of in this study on each scale, the future studies are helpful to perfect the entirely analysis system of the HTC conditions.

With regard to the macro scale, there are four aspects of the modifications and developments required by the implementation of HTC information on KGC. First of all, the more sample cities should be added in each KGC type, in order to describe the HTC

information more precisely (i.e. fluctuation of the frequencies in one KGC type with more sample cites); secondly, the value classes should be adjusted, in order to be more comprehensive of the thermal perception and the humid perception (i.e. the field investigations are required in each KGC type); thirdly, the different kinds of information based on the separation of day and night are worth to be considered (i.e. the HTC information during daytime and the HTC information during night); fourthly, according the truth of the climate change, the predicted HTC information is also necessary for the strategy of sustainable development on macro scale.

On meso scale, the analysis of HTC conditions on other points in time need to be concentrated, for example, the monthly frequencies of HTC conditions at 5 LST which is the relative coolest point in time of one day in all cities, which is worth to be concentrated especially around winter. As the dynamic information, the higher temporal resolution may be applied in the frequencies of different value classes, for example by 10 days. Based on the frequencies of the value classes in certain period, the accurate association of the HTC requirements with the human health conditions, the popular tourism seasons, as well as the energy consumption, are highly recommended to be examined in each city.

With the respect to micro scale, the community environment design can be modified according to the predicted effects of each design elements on HTC conditions in current study. Under the supports of the available numerical models, the microclimatic simulation of the one district can be combined within a larger area, in which the effect of the district of high-rise buildings on the vicinity can be examined; and consequently, the landscape architectural design can be considered in a larger scope, which is helpful, for example, on the mitigation of the urban heat island effects (UHI). The Part Three in current study is performed on micro scale and in a LCZ. Following the development of the numerical simulation model (e.g. SkyHelios), there is possibility, and necessity to complete the evaluation of the HTC conditions of the 12 Chinese cities on the local scale in the future, i.e. the UCMap on local scale of the 12 Chinese cites.

Reference

Ahmed KS (2003) Comfort in urban spaces: defining the boundaries of outdoor thermal comfort for the tropical urban environments. Energy and buildings 35 (1):103–110

Akbari H (2009) Cooling our communities. A guidebook on tree planting and light-colored surfacing. Lawrence Berkeley National Laboratory

Ali-Toudert F (2005) Dependence of outdoor thermal comfort on street design in hot and dry climate. Rep Meteorologisches Institut der Universitat Freiburg, No. 15. Retrieved from http://www.freidok.uni-freiburg.de/volltexte/2078

Ali-Toudert F, Mayer H (2007a) Effects of asymmetry, galleries, overhanging facades and vegetation on thermal comfort in urban street canyons. Solar energy 81 (6):742–754

Ali-Toudert F, Mayer H (2007b) Thermal comfort in an east–west oriented street canyon in Freiburg (Germany) under hot summer conditions. Theoretical and Applied Climatology 87 (1–4):223–237

Amelung B, Viner D (2006) Mediterranean tourism: exploring the future with the tourism climatic index. Journal of sustainable tourism 14 (4):349–366

ASHRAE (2009) Handbook Fundamentals. American society of heating, refrigerating and air-conditioning engineers. Inc: Atlanta, GA, USA

ASHRAE (2013) Standard 55-2013 “Thermal environmental conditions for human occupancy”. American Society of Heating, Refrigerating and Air-Conditioning Engineering. Atlanta, USA

ASHRAE (2004) Standard 55-2004 “Thermal environmental conditions for human occupancy”. American Society of Heating, Refrigerating and Air-Conditioning Engineering. Atlanta, USA

ASHRAE (1992) Standard 55-1992 “Thermal Environmental Conditions for Human Occupancy”. American Society of Heating, Refrigerating and Air-Conditioning Engineers. Atlanta, USA

Atmaca I, Kaynakli O, Yigit A (2007) Effects of radiant temperature on thermal comfort. Building and environment 42 (9):3210–3220

Balaras CA, Dascalaki E, Gaglia A (2007) HVAC and indoor thermal conditions in hospital operating rooms. Energy and buildings 39 (4):454–470

Belda M, Holtanová E, Halenka T, Kalvová J (2014) Climate classification revisited: from Köppen to Trewartha. Climate research 59 (1):1–13

Benzinger TH (1969) Heat regulation: homeostasis of central temperature in man. Physiological Reviews 49 (4):671–759

Berke P, Kaiser EJ (2006) Urban land use planning. University of Illinois Press

Bi P, Williams S, Loughnan M, Lloyd G, Hansen A, Kjellstrom T, Dear K, Saniotis A (2011) The effects of extreme heat on human mortality and morbidity in Australia: implications for public health. Asia-Pacific Journal of Public Health. doi: 10.1177/1010539510391644

Blazejczyk K, Jendritzky G, Bröde P, Fiala D, Havenith G, Epstein Y, Psikuta A, Kampmann B (2013) An introduction to the Universal Thermal Climate Index (UTCI). Geographia

Polonica 86 (1): 5–10

Blennow K (1995) Sky view factors from high-resolution scanned fish-eye lens photographic negatives. Journal of Atmospheric and Oceanic Technology 12 (6):1357–1362

Blocken B, Tominaga Y, Stathopoulos T (2013) CFD simulation of micro-scale pollutant dispersion in the built environment. Building and environment 64:225–230

Booth NK (1989) Basic elements of landscape architectural design. Waveland press

Bröde P, Krüger EL, Fiala D (2013) UTCI validation and the practical application to the assessment of urban outdoor thermal comfort. Geographia Polonica 86 (1):11–20

Brager GS, de Dear R (2001) Climate, comfort, & natural ventilation: a new adaptive comfort standard for ASHRAE standard 55. Proceedings, Moving Thermal Comfort Standards into the 21st Century, Windsor, UK. April.

Brandenburg C, Matzarakis A, Arnberger A (2007) Weather and cycling—a first approach to the effects of weather conditions on cycling. Meteorological applications 14 (1):61–67

Brosy C, Zaninovic K, Matzarakis A (2014) Quantification of climate tourism potential of Croatia based on measured data and regional modeling. International Journal of Biometeorology 58 (6):1369–1381

Bruse M (2004) ENVI-met 3.0: updated model overview. University of Bochum. Retrieved from: http://www.envi-met.com/

Bruse M, Fleer H (1998) Simulating surface–plant–air interactions inside urban environments with a three dimensional numerical model. Environmental Modelling & Software 13 (3):373–384

Bucher K, Wetterdienst D (1993) Ein Verfahren zur objektiven Klassifikation des Wetters unter biosynoptischen Gesichtspunkten. Berichte des Deutschen Wetterdienstes. Deutscher Wetterdienst: Offenbach am Main

Burkhard B, Kroll F, Nedkov S, Müller F (2012) Mapping ecosystem service supply, demand and budgets. Ecological Indicators 21:17-29

Carmona M, Tiesdell S, Heath T, Oc. T (2010) Public places, urban spaces: the dimensions of urban design, vol 2nd Edition. Architectural Press, Amsterdam

Champness SS (1950) Effect of microclimate on the establishment of timothy grass. Nature, Lond. 165, 325. doi:10.1038/165325a0

Chapman L, Thornes J (2004) Real-time sky-view factor calculation and approximation. Journal of Atmospheric and Oceanic Technology 21 (5):730–741

Chen H, Jia B, Lau S (2008) Sustainable urban form for Chinese compact cities: Challenges of a rapid urbanized economy. Habitat International 32 (1):28–40

Chen L, Ng E, An X, Ren C, Lee M, Wang U, He Z (2012) Sky view factor analysis of street canyons and its implications for daytime intra‐urban air temperature differentials in high‐rise, high‐density urban areas of Hong Kong: a GIS‐based simulation approach. International Journal of Climatology 32 (1):121–136

Cheng V, Ng E, Chan C, Givoni B (2012) Outdoor thermal comfort study in a sub-tropical climate: a longitudinal study based in Hong Kong. International Journal of

Biometeorology 56 (1):43–56

Chow WT, Brazel AJ (2012) Assessing xeriscaping as a sustainable heat island mitigation approach for a desert city. Building and environment 47:170–181

Corburn J (2004) Confronting the challenges in reconnecting urban planning and public health. American journal of public health 94 (4):541–546

de Dear R, Brager GS (2001) The adaptive model of thermal comfort and energy conservation in the built environment. International Journal of Biometeorology 45 (2):100–108

de Dear RJ, Brager GS (2002) Thermal comfort in naturally ventilated buildings: revisions to ASHRAE Standard 55. Energy and buildings 34 (6):549–561

Djamila H, Chu C-M, Kumaresan S (2014) Effect of Humidity on Thermal Comfort in the Humid Tropics. Journal of Building Construction and Planning Research 2:109–117

Égerházi LA, Kovács A, Unger J (2013) Application of microclimate modelling and onsite survey in planning practice related to an urban micro-environment. Advances in meteorology 2013: 1–10.

Elseragy A, Elnokaly A (2006) Appropriateness' of the use of tensile membrane structures in hot arid regions. In: The International Conference on Urbanism and Culture, October 28–30, Cairo, Egypt

Emmanuel R, Johansson E (2006) Influence of urban morphology and sea breeze on hot humid microclimate: the case of Colombo, Sri Lanka. Climate research 30 (3):189-200

Endler C, Oehler K, Matzarakis A (2010) Vertical gradient of climate change and climate tourism conditions in the Black Forest. International Journal of Biometeorology 54 (1):45–61

Endy D (2005) Foundations for engineering biology. Nature 438 (7067):449-453

Fang X, Jiang W, Miao S, Zhang N, Xu M, Ji C, Chen X, Wei J, Wang Z, Wang X (2004) The multi-scale numerical modeling system for research on the relationship between urban planning and meteorological environment. Advances in Atmospheric Sciences 21 (1):103–112

Fanger PO (1973) Assessment of man's thermal comfort in practice. British journal of industrial medicine 30 (4):313–324

Fanger PO (1970) Thermal comfort. Analysis and applications in environmental engineering. Danish Technical Press, Copenhagen, Denmark

Fanger PO, Toftum J (2002) Extension of the PMV model to non-air-conditioned buildings in warm climates. Energy and buildings 34 (6):533–536

Farajzadeh H, Matzarakis A (2012) Evaluation of thermal comfort conditions in Ourmieh Lake, Iran. Theoretical and Applied Climatology 107 (3–4):451–459

Fröhlich D, Matzarakis A (2013) Modeling of changes in thermal bioclimate: examples based on urban spaces in Freiburg, Germany. Theoretical and Applied Climatology 111 (3–4):547–558

Fröhlich D, Matzarakis A (2015) A quantitative sensitivity analysis on the behaviour of common thermal indices under hot and windy conditions in Doha, Qatar. Theoretical and Applied Climatology:1–9

Frank L, Engelke P, Schmid T (2003) Health and community design: the impact of the built environment on physical activity. Island Press

Gagge A, Stolwijk J, Saltin B (1969) Comfort and thermal sensations and associated physiological responses during exercise at various ambient temperatures. Environmental research 2 (3):209–229

Gagge AP, Stolwijk J, Hardy J (1967) Comfort and thermal sensations and associated physiological responses at various ambient temperatures. Environmental research 1 (1):1-20

Gan G (1994) Numerical method for a full assessment of indoor thermal comfort. Indoor Air 4 (3):154–168

Gan G (2001) Analysis of mean radiant temperature and thermal comfort. Building Services Engineering Research and Technology 22 (2):95–101

GB50352-2005 The General Principles for the design of civil buildings in China

Gedzelman S, Austin S, Cermak R, Stefano N, Partridge S, Quesenberry S, Robinson D (2003) Mesoscale aspects of the urban heat island around New York City. Theoretical and Applied Climatology 75 (1–2):29–42

Giridharan R, Lau S, Ganesan S, Givoni B (2008) Lowering the outdoor temperature in high-rise high-density residential developments of coastal Hong Kong: The vegetation influence. Building and environment 43 (10):1583–1595

Gosling SN, Bryce EK, Dixon PG, Gabriel KM, Gosling EY, Hanes JM, Hondula DM, Liang L, Mac Lean PAB, Muthers S (2014) A glossary for biometeorology. International Journal of Biometeorology 58 (2):277–308

Gousseau P, Blocken B, Stathopoulos T, Van Heijst G (2011) CFD simulation of near-field pollutant dispersion on a high-resolution grid: a case study by LES and RANS for a building group in downtown Montreal. Atmospheric Environment 45 (2):428–438

Höppe P (1999) The physiological equivalent temperature–a universal index for the biometeorological assessment of the thermal environment. International Journal of Biometeorology 43 (2):71–75

Hamada S, Ohta T (2010) Seasonal variations in the cooling effect of urban green areas on surrounding urban areas. Urban Forestry & Urban Greening 9 (1):15–24

Han-fei L (2002) Discussion on Environmental Land-scape Design of Residential Area. Journal of Chinese Landscape Architecture 2:003

Hardy J, Stolwijk J (1966) Partitional calorimetric studies of man during exposures to thermal transients. Journal of Applied Physiology 21 (6):1799–1806

Havenith G, Holmér I, Parsons K (2002) Personal factors in thermal comfort assessment: clothing properties and metabolic heat production. Energy and buildings 34 (6):581–591

Herrmann J, Matzarakis A (2012) Mean radiant temperature in idealised urban canyons—examples from Freiburg, Germany. International Journal of Biometeorology 56 (1):199–203

Hirsch C (2007) Numerical Computation of Internal and External Flows: The Fundamentals of Computational Fluid Dynamics: The Fundamentals of Computational Fluid

Dynamics. 2nd Edn. Butterworth-Heinemann, Oxford

Howard E (2010) To-morrow: A peaceful path to real reform. Cambridge University Press

Humphreys MA, Nicol JF (2002) The validity of ISO-PMV for predicting comfort votes in every-day thermal environments. Energy and buildings 34 (6):667–684

Huttner S (2012) Further development and application of the 3D microclimate simulation ENVI-met. Johannes Gutenberg-Universität, Mainz

Huttner S, Bruse M, Dostal P (2008) Using ENVI-met to simulate the impact of global warming on the microclimate in central European cities. 5th Japanese-German Meeting on Urban Climatology. Freiburg, Germany: Meteorological Institute, Albert-Ludwigs-University: 307–312

Hwang R-L, Lin T-P, Matzarakis A (2011) Seasonal effects of urban street shading on long-term outdoor thermal comfort. Building and environment 46 (4):863–870

Hyatt OM, Lemke B, Kjellstrom T (2010) Regional maps of occupational heat exposure: past, present, and potential future. Global health action 3. doi:10.3402/gha.v3i0.5715

IPCC (2007) Climate Change 2007: the scientific basis. Contribution of the Working Group I to the Fourth Assessment Report of the Intergovernmental Panel on Climate Change. Solomon S, Qin D et al (eds), Cambridge University Press, Cambridge

ISO7226 (1998) Ergonomics of the Thermal Environment, Instruments for Measuring Physical Quantities. Geneva: International Standard Organization

Jacobs A, Appleyard D (1987) Toward an urban design manifesto. Journal of the American Planning Association 53 (1):112-120

Jarraud M (2008) Guide to Meteorological Instruments and Methods of Observation (WMO-No. 8). World Meteorological Organisation: Geneva, Switzerland

Jendritzky G, de Dear R, Havenith G (2012) UTCI—Why another thermal index? International Journal of Biometeorology 56 (3):421–428

Jim C, Chen WY (2009) Value of scenic views: Hedonic assessment of private housing in Hong Kong. Landscape and urban planning 91 (4):226–234

Johansson E (2006) Urban Design and Outdoor Thermal Comfort in Warm Climates. Studies in Fez and Colombo. Lund University

Johansson E, Emmanuel R (2006) The influence of urban design on outdoor thermal comfort in the hot, humid city of Colombo, Sri Lanka. International Journal of Biometeorology 51 (2):119–133

Kántor N, Unger J (2011) The most problematic variable in the course of human-biometeorological comfort assessment—the mean radiant temperature. Central European Journal of Geosciences 3 (1):90–100

Köppen W (1900) Attempted climate classification in relation to plant distributions. Geographische Zeitschrift 6:657-679

Köppen W (1884) Die Wärmezonen der Erde, nach der Dauer der heissen, gemässigten und kalten Zeit und nach der Wirkung der Wärme auf die organische Welt betrachtet (The thermal zones of the earth according to the duration of hot, moderate and cold periods and to the impact of heat on the organic world). –Meteorologische Zeitschrift 1, 215–226. (translated and edited by Volken, E. and S. Brönnimann (2011) Meteorologische

Zeitschrift 20(3), 351–360)

Kabat P (2004) Vegetation, Water, Humans and the Climate: A New Perspective on an Internactive System. Springer Science & Business Media

Kampstra P (2008) Beanplot: A boxplot alternative for visual comparison of distributions. Journal of statistical software 28(1): 1–9

Ketterer C, Matzarakis A (2014a) Human-biometeorological assessment of heat stress reduction by replanning measures in Stuttgart, Germany. Landscape and urban planning 122:78-88

Ketterer C, Matzarakis A (2014b) Human-biometeorological assessment of the urban heat island in a city with complex topography—The case of Stuttgart, Germany. Urban Climate 10:573–584

Konarska J, Holmer B, Lindberg F, Thorsson S (2015) Influence of vegetation and building geometry on the spatial variations of air temperature and cooling rates in a high - latitude city. International Journal of Climatology. doi: 10.1002/joc.4502

Konopacki S, Akbari H (2002) Energy savings of heat island reduction strategies in Chicago and Houston (including updates for Baton Rouge, Sacramento, and Salt Lake City). Lawrence Berkeley National Laboratory Report LBNL-49638. Berkeley, CA.

Kottek M, Grieser J, Beck C, Rudolf B, Rubel F (2006) World map of the Köppen-Geiger climate classification updated. Meteorologische Zeitschrift 15 (3):259–263

Krüger E, Drach P, Emmanuel R, Corbella O (2013) Urban heat island and differences in outdoor comfort levels in Glasgow, UK. Theoretical and Applied Climatology 112 (1–2):127–141

Lai D, Guo D, Hou Y, Lin C, Chen Q (2014) Studies of outdoor thermal comfort in northern China. Building and environment 77:110–118

Laschewski G, Jendritzky G (2002) Effects of the thermal environment on human health: an investigation of 30 years of daily mortality data from SW Germany. Climate research 21 (1):91-103

Lau KK-L, Lindberg F, Rayner D, Thorsson S (2014) The effect of urban geometry on mean radiant temperature under future climate change: a study of three European cities. International Journal of Biometeorology 59(7): 799–814

Law CM (1993) Urban tourism: attracting visitors to large cities. Mansell Publishing Limited, New York

Li R, Chi X (2014) Thermal comfort and tourism climate changes in the Qinghai–Tibet Plateau in the last 50 years. Theoretical and Applied Climatology 117 (3–4):613–624

Lin T-P, Matzarakis A (2008) Tourism climate and thermal comfort in Sun Moon Lake, Taiwan. International Journal of Biometeorology 52 (4):281–290

Lin T-P, Matzarakis A (2011) Tourism climate information based on human thermal perception in Taiwan and Eastern China. Tourism Management 32 (3):492–500

Lin T-P, Matzarakis A, Hwang R-L (2010a) Shading effect on long-term outdoor thermal comfort. Building and environment 45 (1):213–221

Lin T-P, Matzarakis A, Hwang R-L, Huang Y-C (2010b) Effect of pavements albedo on long-term outdoor thermal comfort. Berichte des Meteorologischen Instituts der Albert-

Ludwigs-Universität Freiburg:497

Lin T-P, Yang S-R, Matzarakis A (2015) Customized rating assessment of climate suitability (CRACS): climate satisfaction evaluation based on subjective perception. International Journal of Biometeorology 59 (12):1825-1837

Lindberg F, Holmer B, Thorsson S (2008) SOLWEIG 1.0–Modelling spatial variations of 3D radiant fluxes and mean radiant temperature in complex urban settings. International Journal of Biometeorology 52 (7):697–713

Madlener R, Sunak Y (2011) Impacts of urbanization on urban structures and energy demand: What can we learn for urban energy planning and urbanization management? Sustainable Cities and Society 1 (1):45–53

Makaremi N, Salleh E, Jaafar MZ, GhaffarianHoseini A (2012) Thermal comfort conditions of shaded outdoor spaces in hot and humid climate of Malaysia. Building and environment 48:7-14

Maller C, Townsend M, Pryor A, Brown P, St Leger L (2006) Healthy nature healthy people:'contact with nature' as an upstream health promotion intervention for populations. Health promotion international 21 (1):45–54

Manobianco J, Taylor GE, Zack JW (1996) Workstation-based real-time mesoscale modeling designed for weather support to operations at the Kennedy Space Center and Cape Canaveral Air Station. Bulletin of the American Meteorological Society 77 (4):653–672

Maslow AH (1943) A theory of human motivation. Psychological review 50 (4):370

Matuschek O, Matzarakis A (2010) Estimation of sky view factor in complex environment as a tool for applied climatological studies. Berichte des Meteorologischen Instituts der Albert-Ludwigs-Universität Freiburg 20:534–539

Matzarakis A (2007a) Assessment method for climate and tourism based on daily data. In: Matzarakis A, de Freitas CR, Scott D (eds) Developments in tourism climatology. Commission Climate, Tourism and Recreation, International Society of Biometeorology, pp 52–58

Matzarakis A (2007b) Climate, human comfort and tourism. In: Amelung, B., Blazejczyk, K., Matzarakis, A., (eds.) Climate Change and Tourism: Assessment and Coping Strategies: 139–154

Matzarakis A (2010) Climate change and adaptation at regional and local scale. Tourism and the implications of climate change: Issues and actions Bingley: Emerald:237-259

Matzarakis A, Amelung B (2008) Physiological equivalent temperature as indicator for impacts of climate change on thermal comfort of humans. In: Seasonal forecasts, climatic change and human health. Springer, pp 161–172

Matzarakis A, De Rocco M, Najjar G (2009) Thermal bioclimate in Strasbourg-the 2003 heat wave. Theoretical and Applied Climatology 98 (3-4):209–220

Matzarakis A, Endler C (2010) Climate change and thermal bioclimate in cities: impacts and options for adaptation in Freiburg, Germany. International Journal of Biometeorology 54 (4):479–483

Matzarakis A, Fröhlich D, Gangwisch M, Ketterer C, Peer A (2015) Developments and applications of thermal indices in urban structures by RayMan and SkyHelios model.

In: ICUC9 9th international conference on the urban climate jointly with the 12th symposium on the urban environment

Matzarakis A, Matuschek O (2011) Sky View Factor as a parameter in applied climatology–Rapid estimation by the SkyHelios Model. Meteorologische Zeitschrift 20 (1):39–45

Matzarakis A, Mayer H (1996) Another kind of environmental stress: thermal stress. WHO Collaborating Centre for Air Quality Management and Air Pollution Control. Newsletters 18:7–10

Matzarakis A, Mayer H, Iziomon MG (1999) Applications of a universal thermal index: physiological equivalent temperature. International Journal of Biometeorology 43 (2):76–84

Matzarakis A, Röckle R, Richter C, Höfl H, Steinicke W, Streifeneder M, Mayer H (2008) Planungsrelevante Bewertung des Stadtklimas — Am Beispiel von Freiburg im Breisgau. Gefahrstoffe —Reinhaltung der Luft 68, 334–340

Matzarakis A, Rammelberg J, Junk J (2013) Assessment of thermal bioclimate and tourism climate potential for central Europe—the example of Luxembourg. Theoretical and Applied Climatology 114 (1–2):193–202

Matzarakis A, Rutz F (2005) Application of RayMan for tourism and climate investigations. Annalen der Meteorologie 41 (2):631-636

Matzarakis A, Rutz F, Mayer H (2006) Modelling the thermal bioclimate in urban areas with the RayMan Model. In: International Conference on Passive and Low Energy Architecture. 449–453

Matzarakis A, Rutz F, Mayer H (2007) Modelling radiation fluxes in simple and complex environments—application of the RayMan model. International Journal of Biometeorology 51 (4):323–334

Matzarakis A, Rutz F, Mayer H (2010) Modelling radiation fluxes in simple and complex environments: basics of the RayMan model. International Journal of Biometeorology 54 (2):131–139

Mayer H, Höppe P (1987) Thermal comfort of man in different urban environments. Theoretical and Applied Climatology 38 (1):43–49

McLeod S (2007) The Expanded Hieraarchy of Needs from Maslow's hierarchy of needs. Retrieved from internet: http://www.simplypsychology.org/maslow.html

Mochida A, Lun IY (2008) Prediction of wind environment and thermal comfort at pedestrian level in urban area. Journal of wind engineering and industrial aerodynamics 96 (10):1498-1527

Muthers S, Matzarakis A (2010) Use of beanplots in applied climatology—A comparison with boxplots. Meteorologische Zeitschrift 19 (6):641–644

Newsham GR (1997) Clothing as a thermal comfort moderator and the effect on energy consumption. Energy and buildings 26 (3):283–291

Ng E (2009) Policies and technical guidelines for urban planning of high-density cities–air ventilation assessment (AVA) of Hong Kong. Building and environment 44 (7):1478–1488

Ng E (2012) Towards planning and practical understanding of the need for meteorological and climatic information in the design of high‐density cities: A case‐based study of

Hong Kong. International Journal of Climatology 32 (4):582–598

Nichol J (2005) Remote sensing of urban heat islands by day and night. Photogrammetric Engineering & Remote Sensing 71 (5):613–621

Nicol JF (2004) Adaptive thermal comfort standards in the hot–humid tropics. Energy and buildings 36 (7):628–637

Nicol JF (1974) An analysis of some observations of thermal comfort in Roorkee, India and Baghdad, Iraq. Annals of human biology 1 (4):411–426

Nicol JF, Humphreys MA (2002) Adaptive thermal comfort and sustainable thermal standards for buildings. Energy and buildings 34 (6):563–572

Nikolopoulou M, Baker N, Steemers K (2001) Thermal comfort in outdoor urban spaces: understanding the human parameter. Solar energy 70 (3):227–235

Nikolopoulou M, Lykoudis S (2006) Thermal comfort in outdoor urban spaces: analysis across different European countries. Building and environment 41 (11):1455–1470

Nishimura N, Nomura T, Iyota H, Kimoto S (1998) Novel water facilities for creation of comfortable urban micrometeorology. Solar energy 64 (4):197-207

Niu J (2004) Some significant environmental issues in high-rise residential building design in urban areas. Energy and buildings 36 (12):1259–1263

Oke TR (2002) Boundary layer climates. Routledge

Oliveira S, Andrade H, Vaz T (2011) The cooling effect of green spaces as a contribution to the mitigation of urban heat: A case study in Lisbon. Building and environment 46 (11):2186–2194

Omonijo A, Matzarakis A, Oguntoke O, Adeofun C (2011) Influence of Weather and Climate on Malaria Occurrence Based on Human-Biometeorological Methods in Ondo State, Nigeria. Journal of Environmental Science and Engineering 5 (9)

Omonijo AG, Adeofun CO, Oguntoke O, Matzarakis A (2013) Relevance of thermal environment to human health: a case study of Ondo State, Nigeria. Theoretical and Applied Climatology 113 (1-2):205–212

Omonijo AG, Matzarakis A (2011) Climate and bioclimate analysis of Ondo State, Nigeria. Meteorologische Zeitschrift 20 (5):531–539

Omonijo AG, Matzarakis A (2015) Pneumonia Occurrence in Relation to Population and Thermal Environment in Ondo State, Nigeria. The African Review of Physics 9

Omonijo AG, Matzarakis A, Oguntoke O, Adeofun CO (2012) Effect of thermal environment on the temporal, spatial and seasonal occurrence of measles in Ondo state, Nigeria. International Journal of Biometeorology 56 (5):873–885

Ouyang J, Ge J, Hokao K (2009) Economic analysis of energy-saving renovation measures for urban existing residential buildings in China based on thermal simulation and site investigation. Energy policy 37 (1):140-149

Pantavou K, Theoharatos G, Mavrakis A, Santamouris M (2011) Evaluating thermal comfort conditions and health responses during an extremely hot summer in Athens. Building and environment 46 (2):339–344

Parsons K (2014) Human thermal environments: the effects of hot, moderate, and cold

environments on human health, comfort, and performance. Crc Press

Parsons K (2002) The effects of gender, acclimation state, the opportunity to adjust clothing and physical disability on requirements for thermal comfort. Energy and buildings 34 (6):593–599

Patz JA, Campbell-Lendrum D, Holloway T, Foley JA (2005) Impact of regional climate change on human health. Nature 438 (7066):310–317

Peel MC, Finlayson BL, McMahon TA (2007) Updated world map of the Köppen-Geiger climate classification. Hydrology and Earth System Sciences, 11 (5): 1633–1644

Picot X (2004) Thermal comfort in urban spaces: impact of vegetation growth: case study: Piazza della Scienza, Milan, Italy. Energy and buildings 36 (4):329–334

Pielke Sr RA (2013) Mesoscale meteorological modeling. (3rd edn.). Academic press

Plumley HJ (1977) Design of outdoor urban spaces for thermal comfort. In: Heisler, Gordon M.; Herrington, Lee P., eds. Proceedings of the conference on metropolitan physical environment; Gen. Tech. Rep. NE-25. Upper Darby, PA: U.S. Department of Agriculture, Forest Service, Northeastern Forest Experiment Station. 152–162

Poston B (2009) Maslow's hierarchy of needs. surgical technologist:348

Röckle R, Richter C, Höfl H, Steinicke W, Streifeneder M, Matzarakis A (2003) Klimaanalyse Stadt Freiburg. Auftraggeber Stadtplanungsamt der Stadt Freiburg

Rakodi C (2001) Forget planning, put politics first? Priorities for urban management in developing countries. International journal of applied earth observation and geoinformation 3 (3):209-223

Reddy KN (1996) Urban redevelopment: a study of high-rise buildings. Concept Publishing Company

Ren C, Ng E, Katzschner L (2011) Urban climatic map studies: a review. International Journal of Climatology 31 (15):2213–2233

Ren C, Spit T, Lenzholzer S, Yim HLS, Heusinkveld B, van Hove B, Chen L, Kupski S, Burghardt R, Katzschner L (2012) Urban climate map system for Dutch spatial planning. International journal of applied earth observation and geoinformation 18:207–221

Rijal HB, Tuohy P, Humphreys MA, Nicol JF, Samuel A, Clarke J (2007) Using results from field surveys to predict the effect of open windows on thermal comfort and energy use in buildings. Energy and buildings 39 (7):823–836

Rizwan AM, Dennis LY, Chunho L (2008) A review on the generation, determination and mitigation of Urban Heat Island. Journal of Environmental Sciences 20 (1):120–128

Robitu M, Musy M, Inard C, Groleau D (2006) Modeling the influence of vegetation and water pond on urban microclimate. Solar energy 80 (4):435–447

Rogers EB (2001) Landscape design: a cultural and architectural history. Harry N. Abrams New York

Rubel F, Kottek M (2010) Observed and projected climate shifts 1901–2100 depicted by world maps of the Köppen-Geiger climate classification. Meteorologische Zeitschrift 19 (2):135–141

Rubel F, Kottek M (2011) Comments on:"The thermal zones of the Earth" by Wladimir Köppen (1884). Meteorologische Zeitschrift 20 (3):361–365

Schmidt S, Buehler R (2007) The planning process in the US and Germany: a comparative analysis. International Planning Studies 12 (1):55–75

Shashua-Bar L, Hoffman M (2000) Vegetation as a climatic component in the design of an urban street: An empirical model for predicting the cooling effect of urban green areas with trees. Energy and buildings 31 (3):221–235

Shashua-Bar L, Pearlmutter D, Erell E (2011) The influence of trees and grass on outdoor thermal comfort in a hot - arid environment. International Journal of Climatology 31 (10):1498–1506

Shen T, Chow D, Darkwa J (2013) Simulating the influence of microclimatic design on mitigating the Urban Heat Island effect in the Hangzhou Metropolitan Area of China. International Journal of Low-Carbon Technologies. http://dx.doi.org/10.1093/ijlct/ctt050

Shiue I, Matzarakis A (2011) Estimation of the tourism climate in the Hunter Region, Australia, in the early twenty-first century. International Journal of Biometeorology 55 (4):565–574

Sinton JE, Levine M, Liu F, Davis W, Zhenping J, Xing Z, Kejun J, Dadi Z (1992) China energy databook. Lawrence Berkeley Lab., CA (United States)

Smagorinsky J (1974) Global atmospheric modeling and the numerical simulation of climate. In Hess WN (ed.). Weather and Climate Modification, Wiley, New York

Solecki WD, Rosenzweig C, Parshall L, Pope G, Clark M, Cox J, Wiencke M (2005) Mitigation of the heat island effect in urban New Jersey. Global Environmental Change Part B: Environmental Hazards 6 (1):39–49

Staiger H, Laschewski G, Grätz A (2012) The perceived temperature – a versatile index for the assessment of the human thermal environment. Part A: scientific basics. International Journal of Biometeorology 56 (1):165–176

Steinacker R, Ratheiser M, Bica B, Chimani B, Dorninger M, Gepp W, Lotteraner C, Schneider S, Tschannett S (2006) A mesoscale data analysis and downscaling method over complex terrain. Monthly Weather Review 134 (10):2758–2771

Stewart ID, Oke TR (2012) Local climate zones for urban temperature studies. Bulletin of the American Meteorological Society 93 (12):1879–1900

Stolwijk J, Hardy J (1966) Partitional calorimetric studies of responses of man to thermal transients. Journal of Applied Physiology 21 (3):967–977

Stone Jr B, Rodgers MO (2001) Urban form and thermal efficiency: how the design of cities influences the urban heat island effect. Journal of the American Planning Association 67 (2):186–198

Svensson MK (2004) Sky view factor analysis–implications for urban air temperature differences. Meteorological applications 11 (03):201–211

Svensson MK, Thorsson S, Lindqvist S (2003) A geographical information system model for creating bioclimatic maps–examples from a high, mid-latitude city. International Journal of Biometeorology 47 (2):102–112

Taleghani M, Kleerekoper L, Tenpierik M, van den Dobbelsteen A (2015) Outdoor thermal

comfort within five different urban forms in the Netherlands. Building and environment 83:65–78

Tan J, Kalkstein L, Huang J, Lin S, Yin H, Shao D (2004) An operational heat/health warning system in Shanghai. International Journal of Biometeorology 48 (3):157–162

Tang Y-Q, Cui Z-D, Wang J-X, Lu C, Yan X-X (2008) Model test study of land subsidence caused by high-rise building group in Shanghai. Bulletin of Engineering Geology and the Environment 67 (2):173–179

Toftum J (2005) Handbook of Human Factors and Ergonomics Methods. CRC Press, Boca Raton, FL, USA

Unger J (2008) Connection between urban heat island and sky view factor approximated by a software tool on a 3D urban database. International Journal of Environment and Pollution 36 (1–3):59–80

Upmanis H, Eliasson I, Lindqvist S (1998) The influence of green areas on nocturnal temperatures in a high latitude city (Göteborg, Sweden). International Journal of Climatology 18 (6):681–700

Vaneckova P, Hart MA, Beggs PJ, de Dear RJ (2008) Synoptic analysis of heat-related mortality in Sydney, Australia, 1993–2001. International Journal of Biometeorology 52 (6):439–451

Vanos JK, Warland JS, Gillespie TJ, Kenny NA (2010) Review of the physiology of human thermal comfort while exercising in urban landscapes and implications for bioclimatic design. International Journal of Biometeorology 54 (4):319–334

VDI (1998) VDI 3787, Part I: Environmental Meteorology, Methods for the human biometeorological evaluation of climate and air quality for the urban and regional planning at regional level. Part I: Climate. Beuth, Berlin, p 29

Wai C-K (1994) Community planning of Shenzhen's residential districts. HKU Theses Online (HKUTO). The University of Hong Kong (Pokfulam, Hong Kong)

Wan J, Yang K, Zhang W, Zhang J (2009) A new method of determination of indoor temperature and relative humidity with consideration of human thermal comfort. Building and environment 44 (2):411–417

Wang Y, Akbari H (2015) Development and application of “thermal radiative power” for urban environmental evaluation. Sustainable Cities and Society 14:316-322

Warner TT, Seaman NL (1990) A real-time, mesoscale numerical weather-prediction system used for research, teaching, and public service at The Pennsylvania State University. Bulletin of the American Meteorological Society 71 (6):792–805

Watson I, Johnson G (1987) Graphical estimation of sky view - factors in urban environments. Journal of Climatology 7 (2):193–197

Webb C (1959) An analysis of some observations of thermal comfort in an equatorial climate. British journal of industrial medicine 16 (4):297–310

Wende W, Huelsmann W, Marty M, Penn-Bressel G, Bobylev N (2010) Climate protection and compact urban structures in spatial planning and local construction plans in Germany. Land Use Policy 27 (3):864–868

WHO (1948) Official records of the World Health Organization, No. 2. Geneva

Wissler EH (1964) A mathematical model of the human thermal system. The Bulletin of mathematical biophysics 26 (2):147–166

Wolkoff P, Kjærgaard SK (2007) The dichotomy of relative humidity on indoor air quality. Environment International 33 (6):850–857

Wong N, Feriadi H, Lim P, Tham K, Sekhar C, Cheong K (2002) Thermal comfort evaluation of naturally ventilated public housing in Singapore. Building and environment 37 (12):1267–1277

Wong N, Jusuf SK, La Win AA, Thu HK, Negara TS, Xuchao W (2007) Environmental study of the impact of greenery in an institutional campus in the tropics. Building and environment 42 (8):2949–2970

Wong NH, Jusuf SK (2008) GIS-based greenery evaluation on campus master plan. Landscape and urban planning 84 (2):166–182

Yahia MW, Johansson E (2013) Influence of urban planning regulations on the microclimate in a hot dry climate: The example of Damascus, Syria. Journal of Housing and the Built Environment 28 (1):51–65

Yahia MW, Johansson E (2014) Landscape interventions in improving thermal comfort in the hot dry city of Damascus, Syria—The example of residential spaces with detached buildings. Landscape and urban planning 125:1–16

Yamashita S, Sekine K, Shoda M, Yamashita K, Hara Y (1986) On relationships between heat island and sky view factor in the cities of Tama River basin, Japan. Atmospheric Environment (1967) 20 (4):681–686

Yang F, Lau SS, Qian F (2010) Summertime heat island intensities in three high-rise housing quarters in inner-city Shanghai China: Building layout, density and greenery. Building and environment 45 (1):115–134

Zaninović K, Matzarakis A (2009) The bioclimatological leaflet as a means conveying climatological information to tourists and the tourism industry. International Journal of Biometeorology 53 (4):369–374

Zhao J, He J, Zhang Y, Zeng Z, Luo Y, Lan C (2012) Study of investigating and improving negative space in an old urban block of Nanning city: Strategies for improving negative space. In: Consumer Electronics, Communications and Networks (CECNet), The 2nd International Conference on. IEEE: 2097–2101

Zhao M, Künzel HM, Antretter F (2015) Parameters influencing the energy performance of residential buildings in different Chinese climate zones. Energy and buildings 96:64–75

Appendices

Appendix A1 Beanplots and boxplots of T_a, T_{mrt} and PET in 12 cities

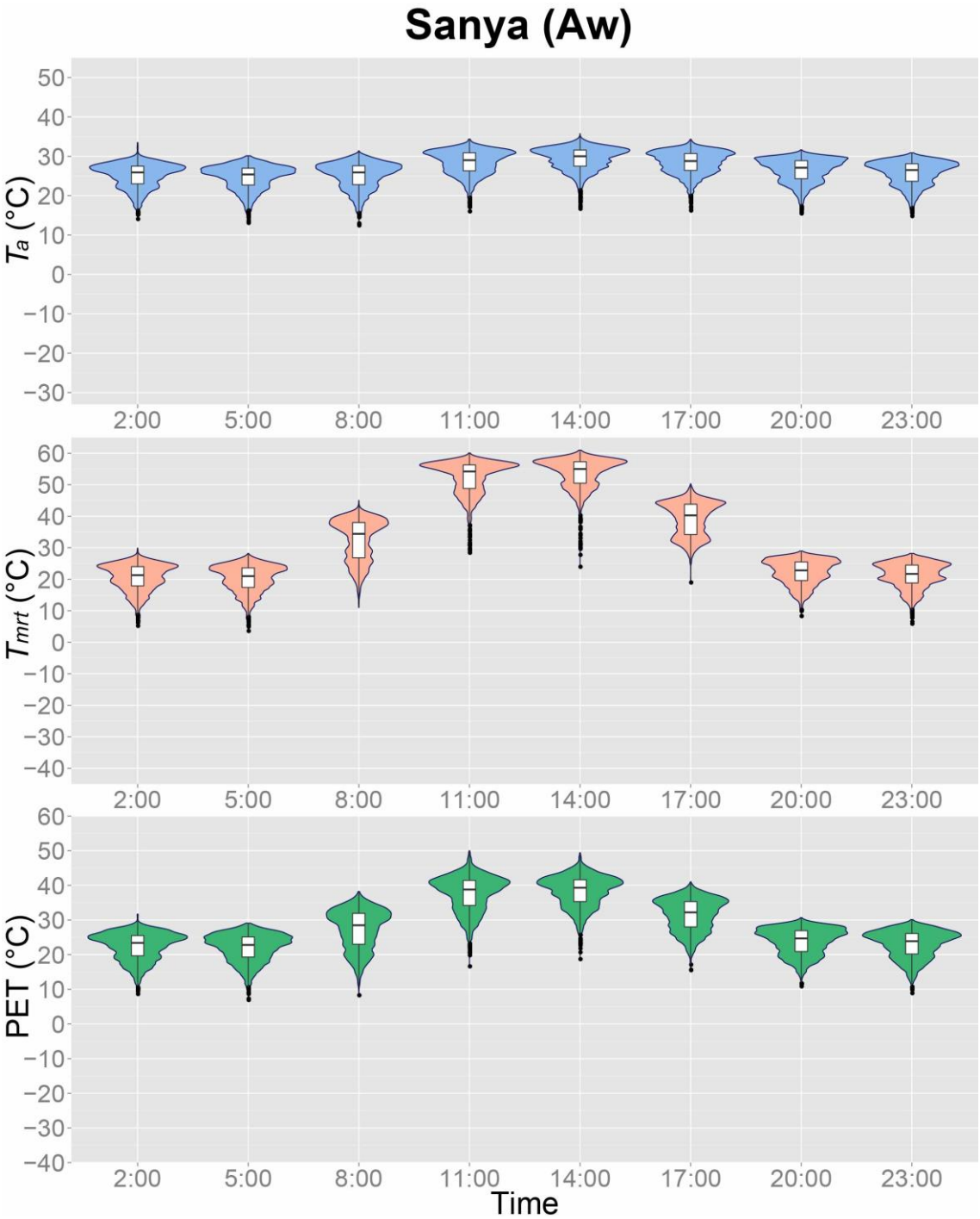

Fig. A1.1 Beanplots and boxplots of T_a, T_{mrt} and PET at 8 points in time in Sanya (Aw), respectively

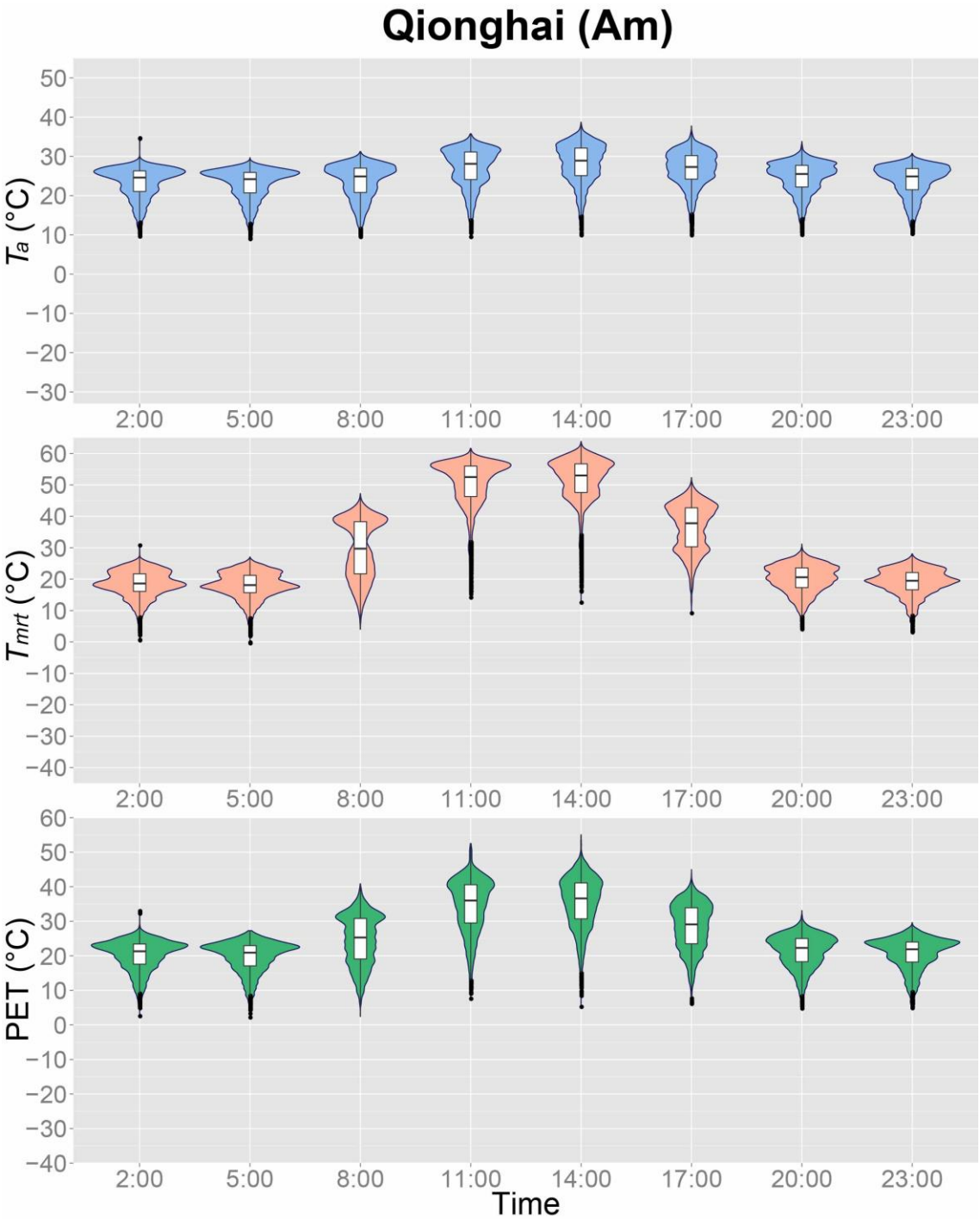

Fig. A1.2 Beanplots and boxplots of T_a, T_{mrt} and PET at 8 points in time in Qionghai (Am), respectively

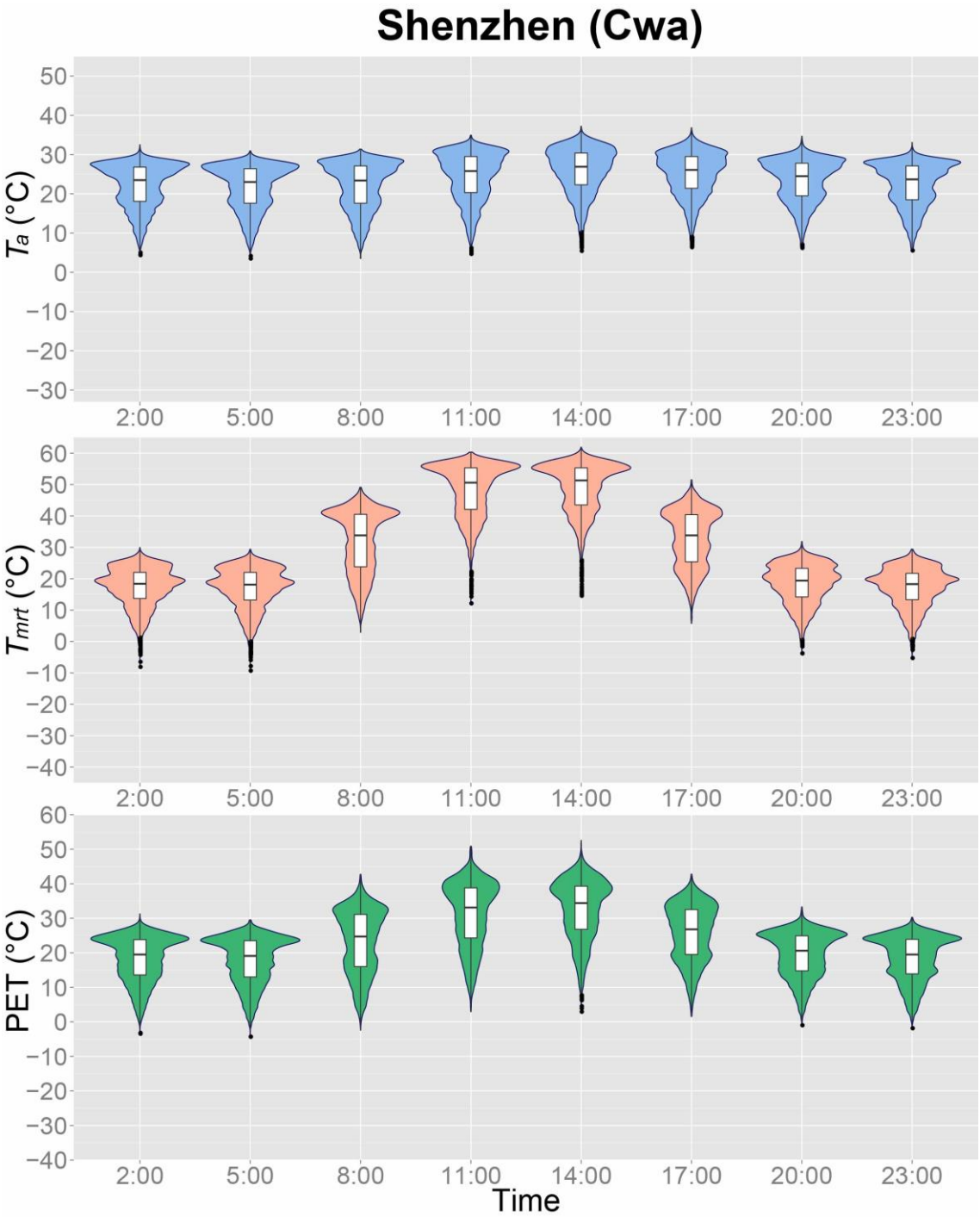

Fig. A1.3 Beanplots and boxplots of T_a, T_{mrt} and PET at 8 points in time in Shenzhen (Cwa), respectively

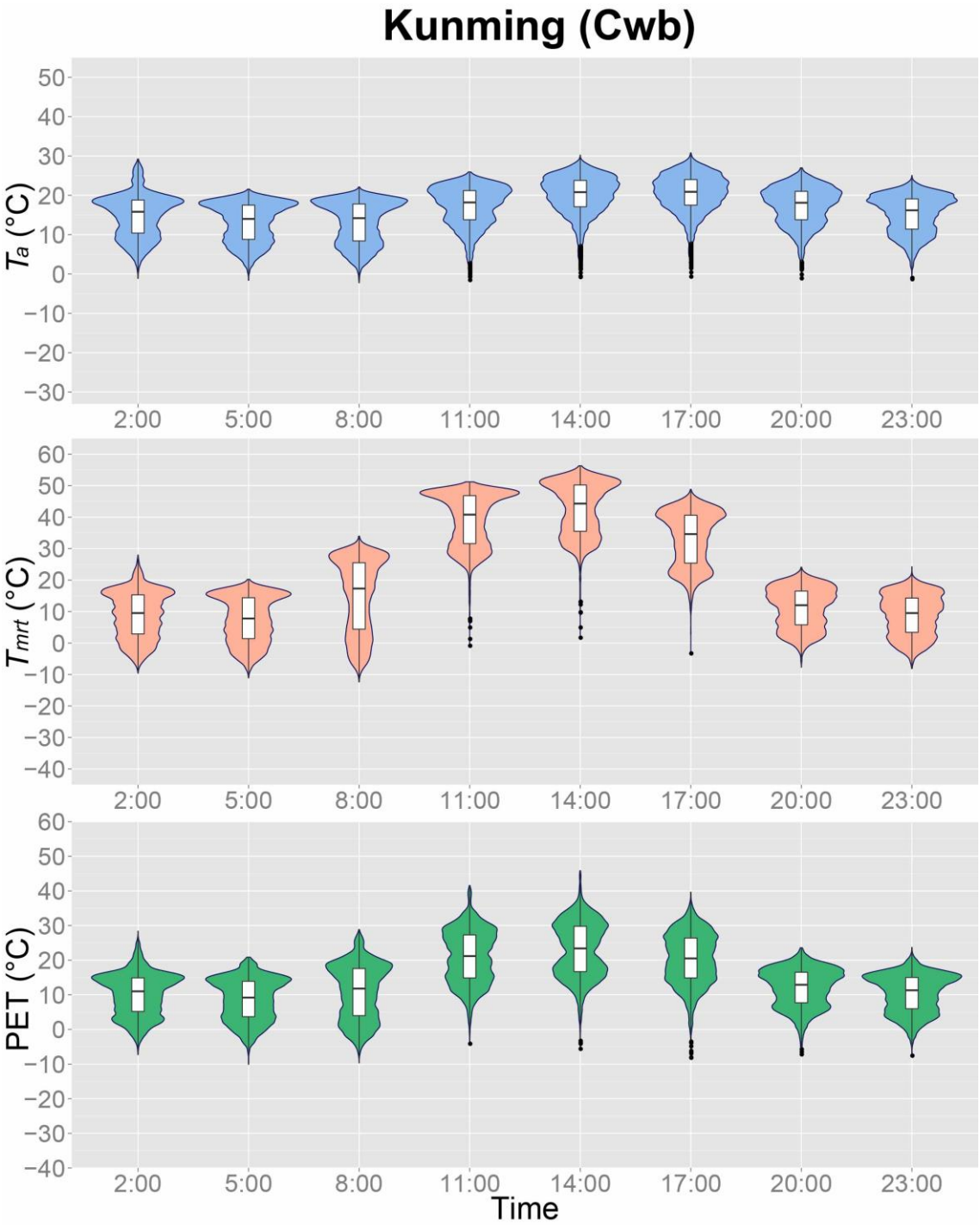

Fig. A1.4 Beanplots and boxplots of T_a, T_{mrt} and PET at 8 points in time in Kunming (Cwa), respectively

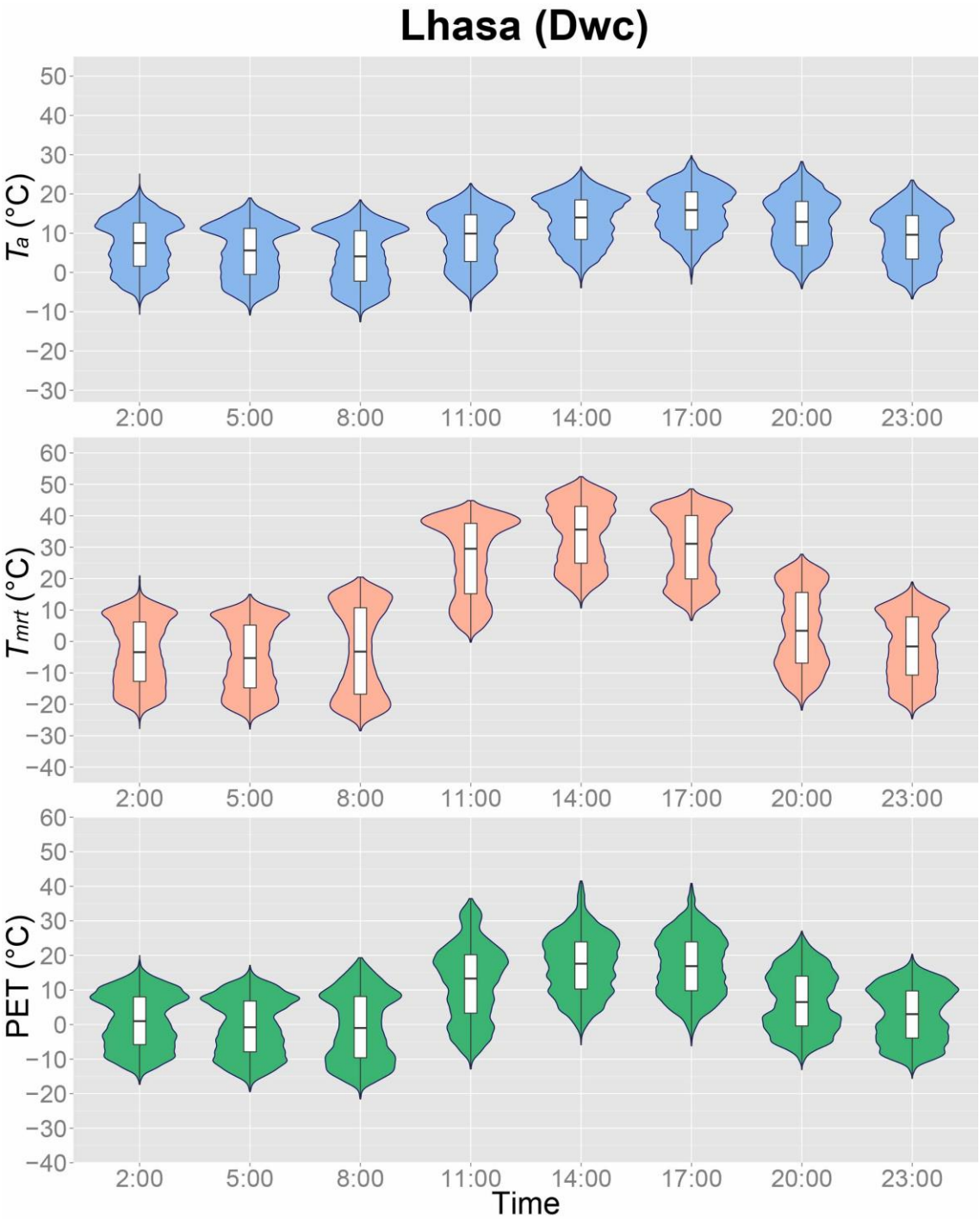

Fig. A1.5 Beanplots and boxplots of T_a, T_{mrt} and PET at 8 points in time in Lhasa (Dwa), respectively

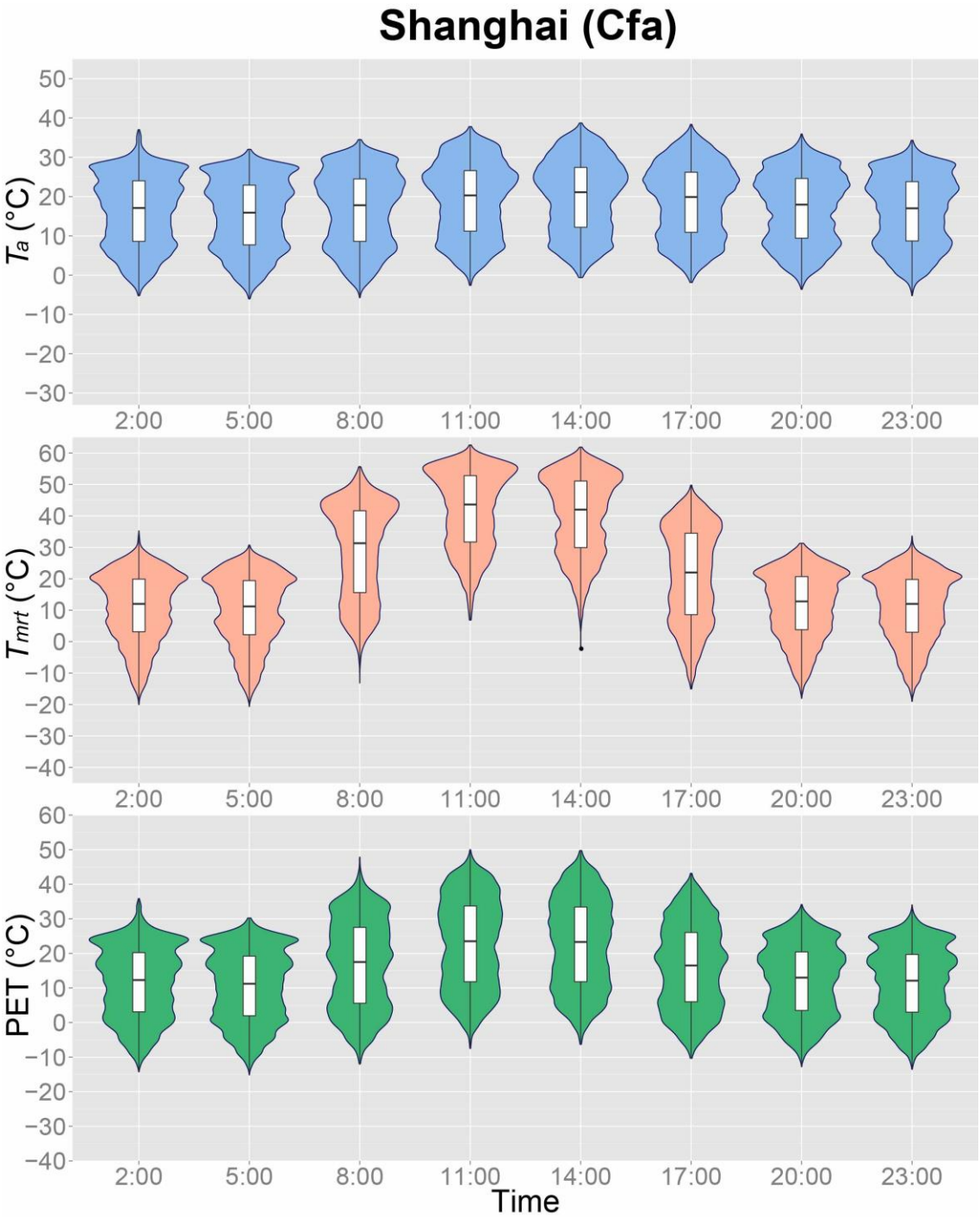

Fig. A1.6 Beanplots and boxplots of T_a, T_{mrt} and PET at 8 points in time in Shanghai (Cfa), respectively

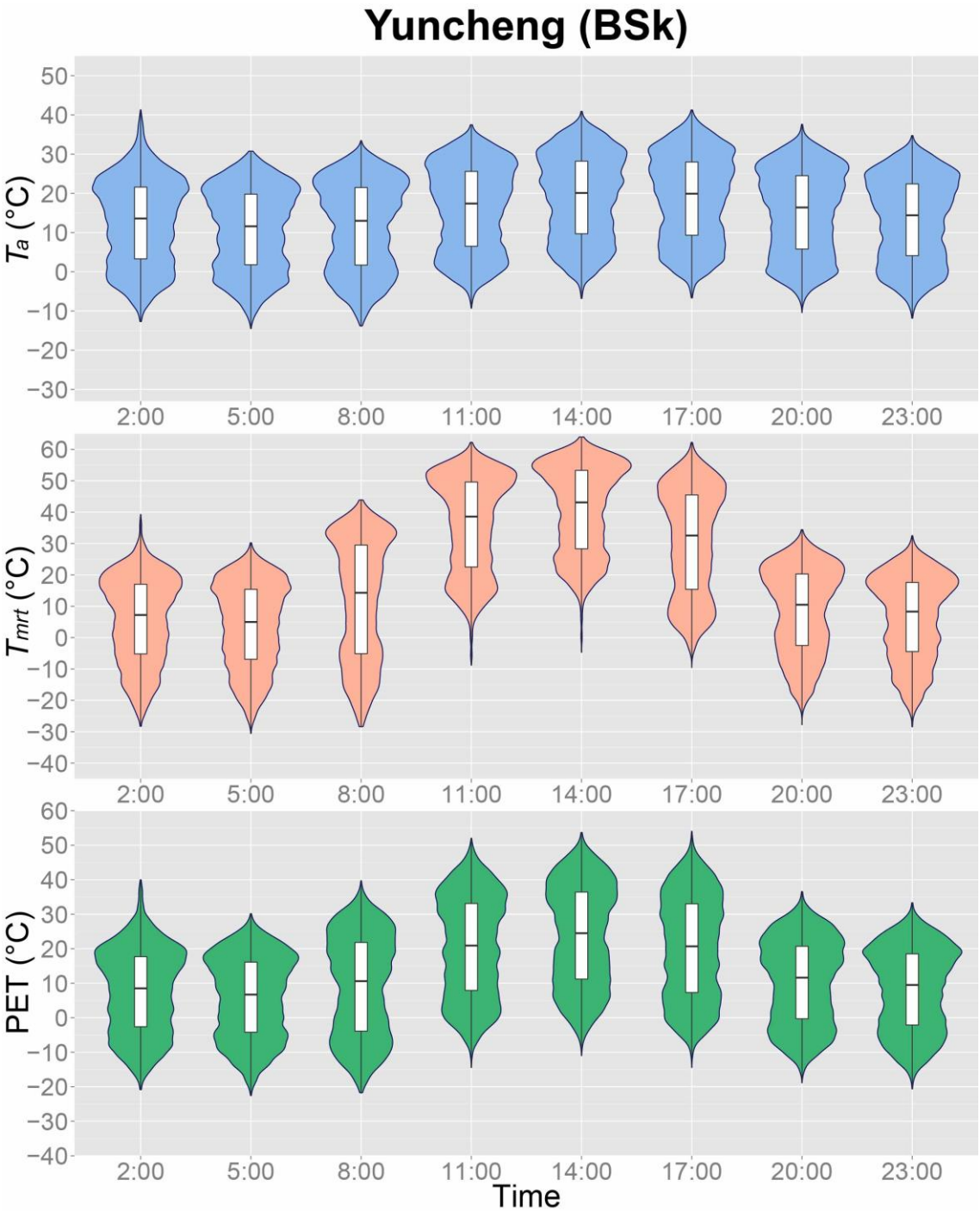

Fig. A1.7 Beanplots and boxplots of T_a, T_{mrt} and PET at 8 points in time in Yuncheng (BSk), respectively

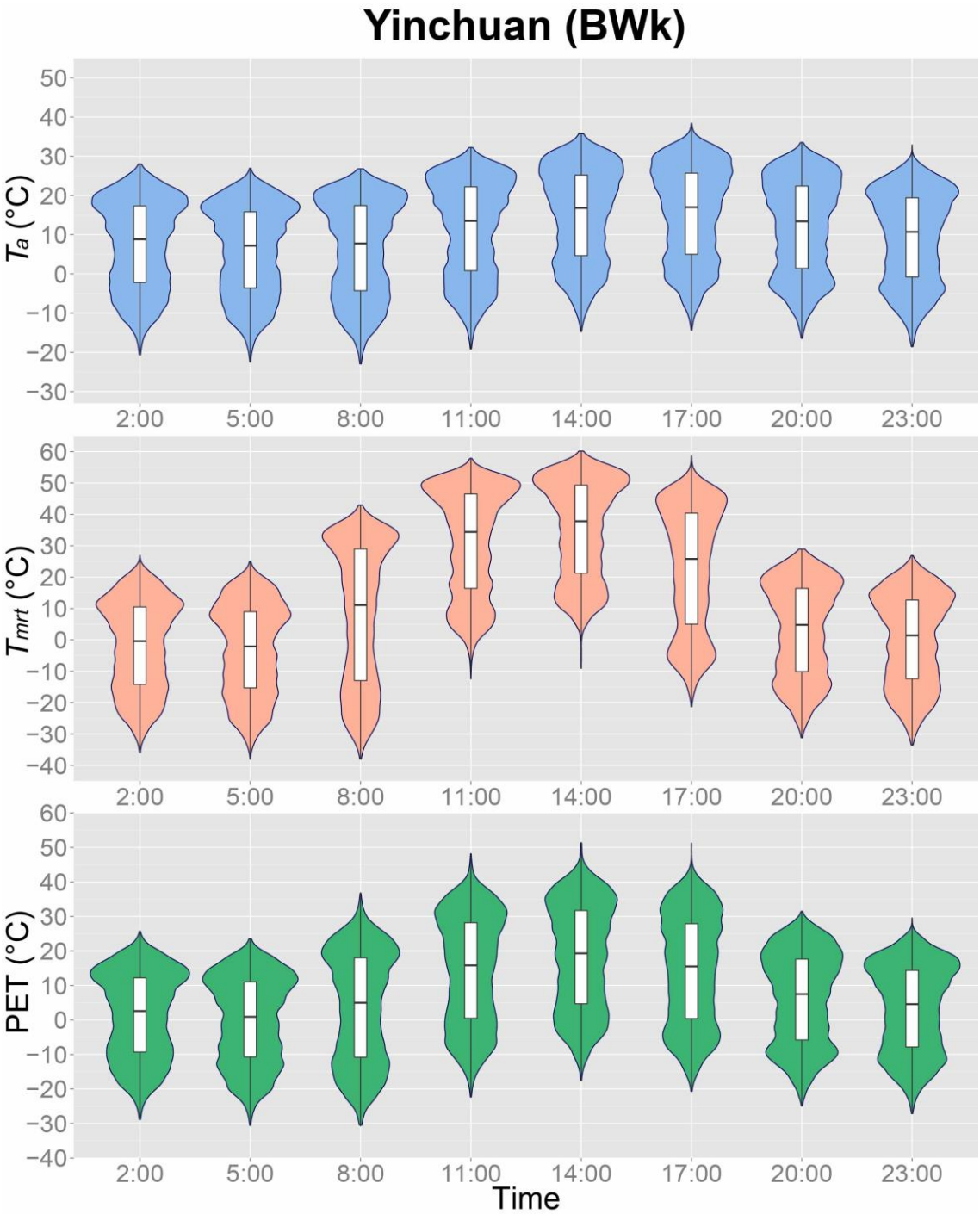

Fig. A1.8 Beanplots and boxplots of T_a, T_{mrt} and PET at 8 points in time in Yinchuan (BWk), respectively

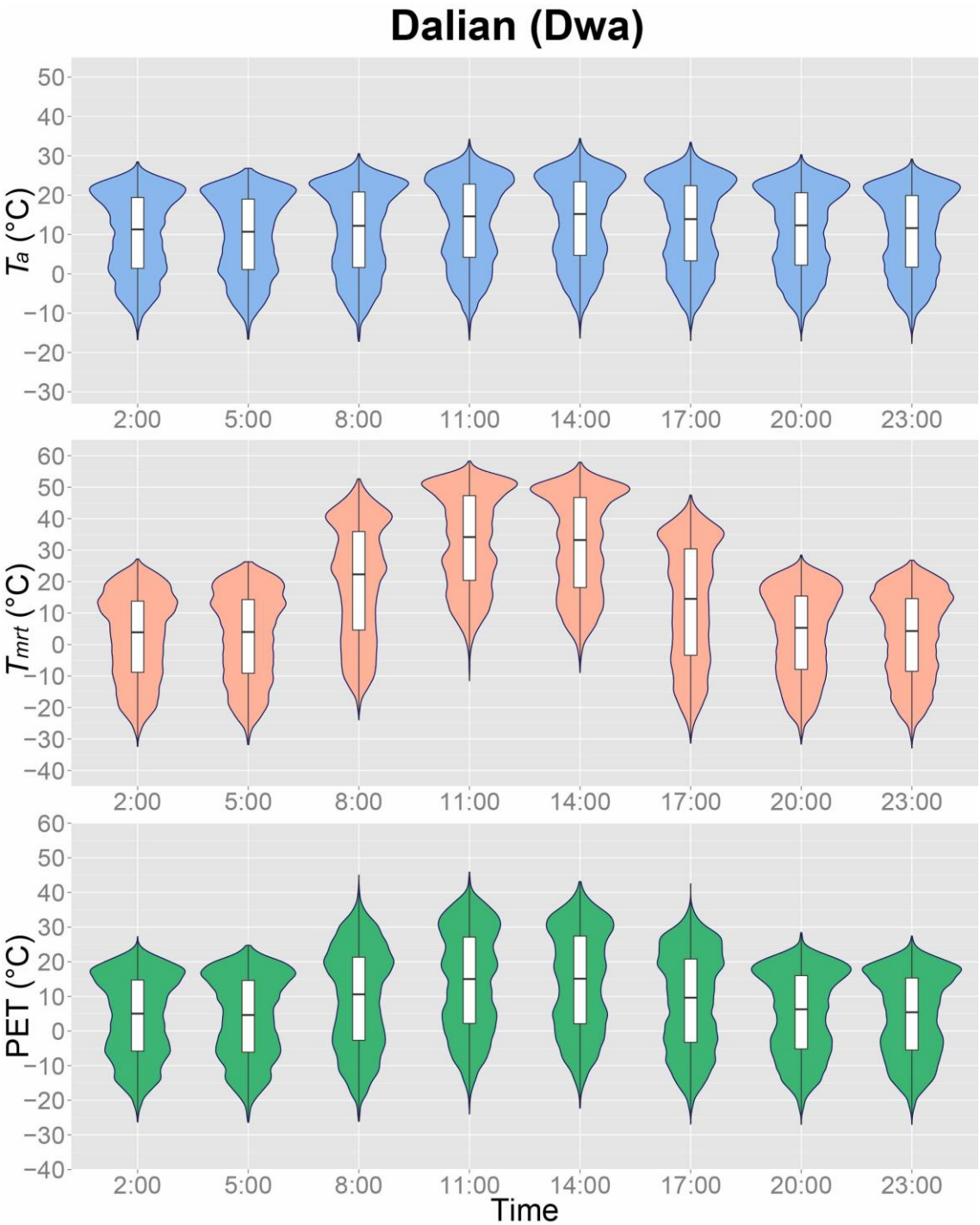

Fig. A1.9 Beanplots and boxplots of T_a, T_{mrt} and PET at 8 points in time in Dalian (Dwa), respectively

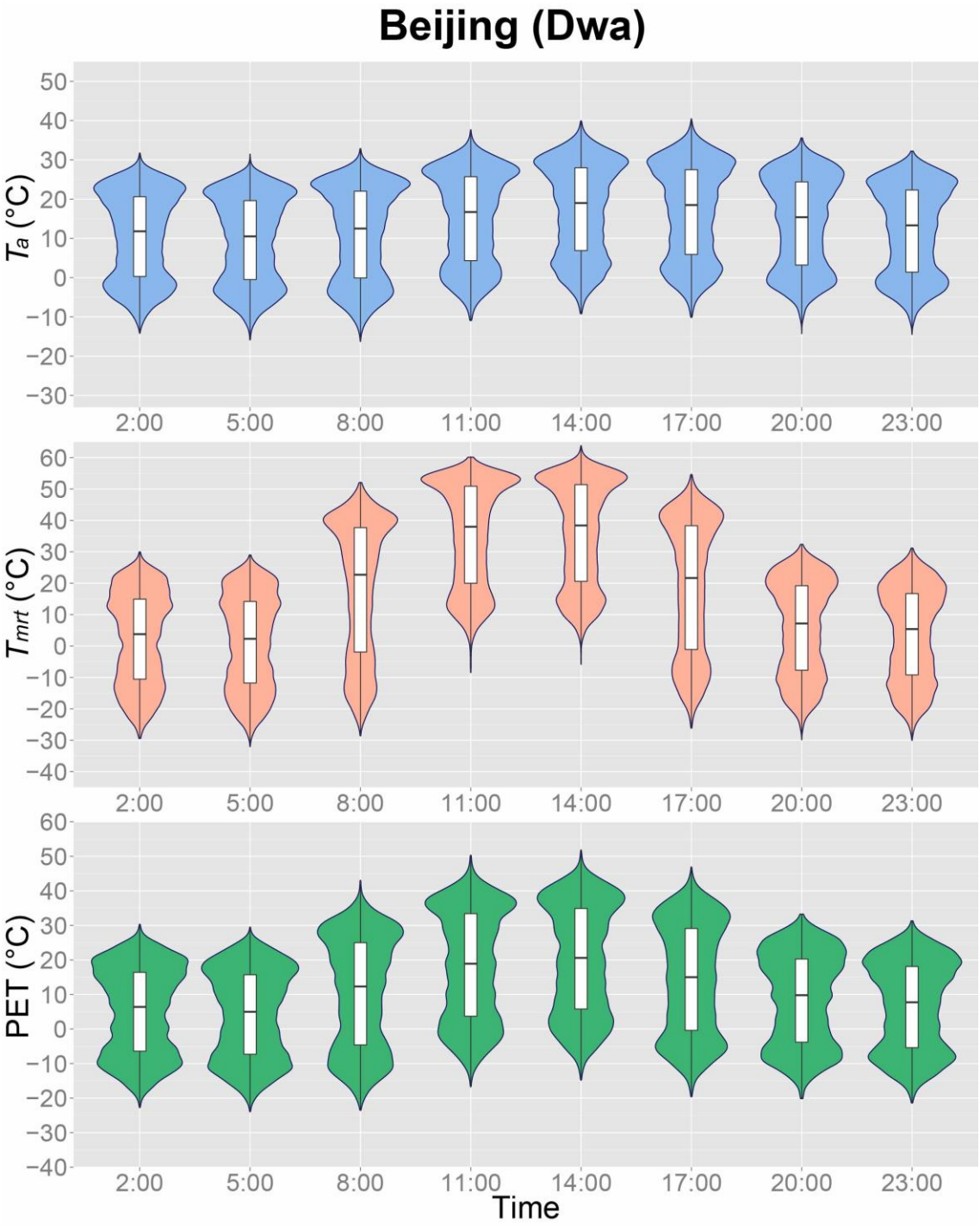

Fig. A1.10 Beanplots and boxplots of T_a, T_{mrt} and PET at 8 points in time in Beijing (Dwa), respectively

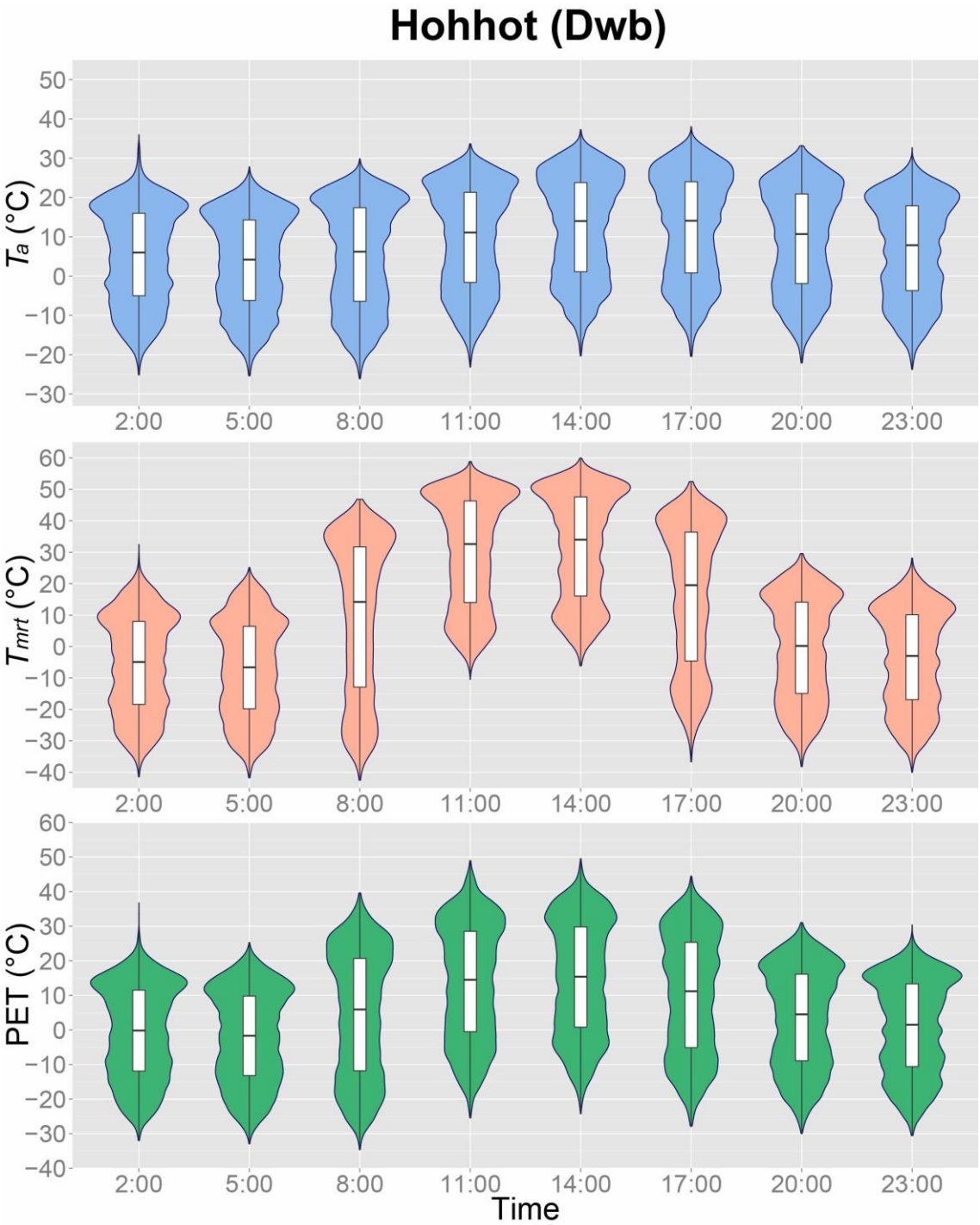

Fig. A1.11 Beanplots and boxplots of T_a, T_{mrt} and PET at 8 points in time in Hohhot (Dwb), respectively

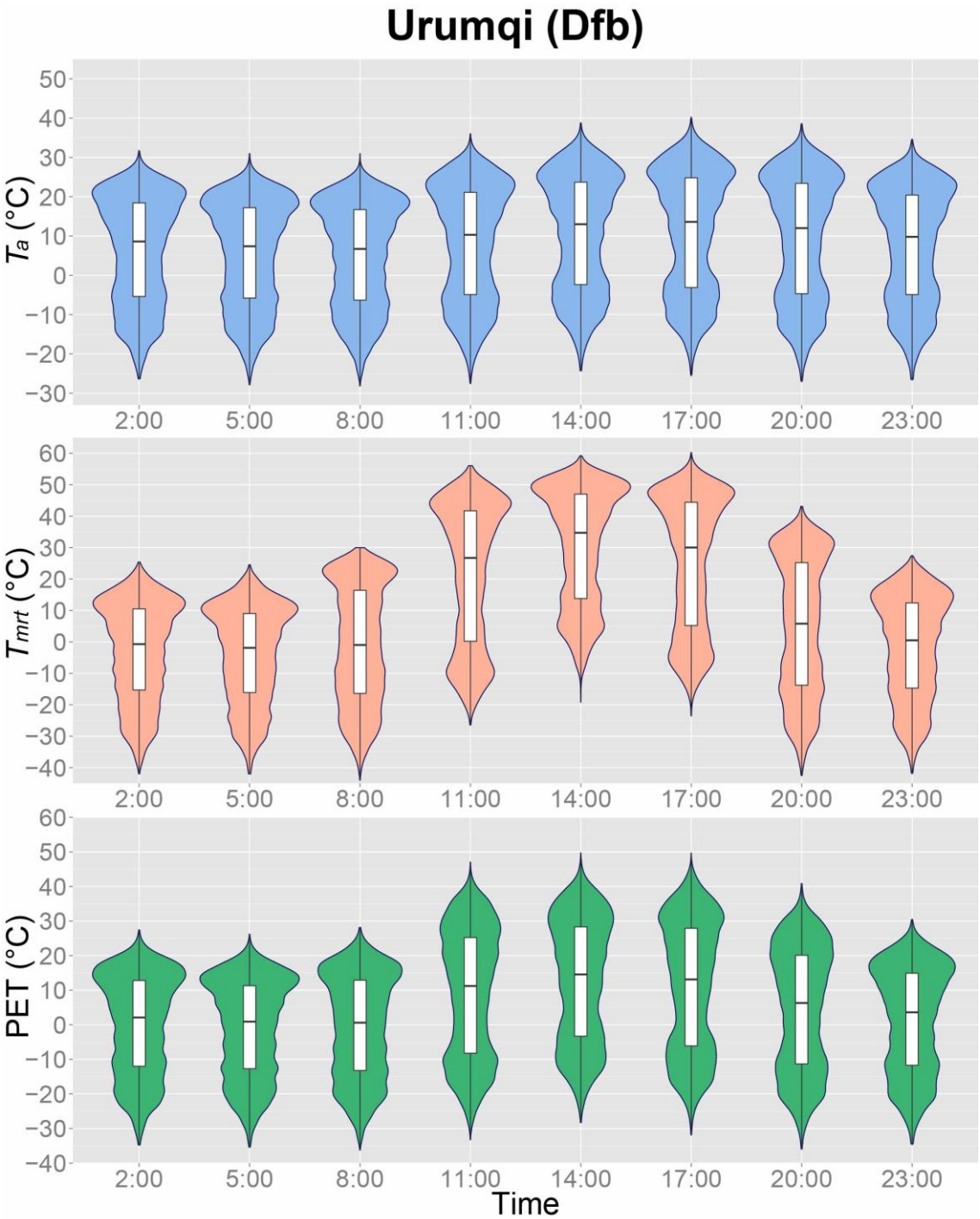

Fig. A1.12 Beanplots and boxplots of T_a, T_{mrt} and PET at 8 points in time in Urumqi (Dfb), respectively

Appendix A2 Distribution of PET in the 1st round simulation and the community environment design for 12 scenarios, respectively

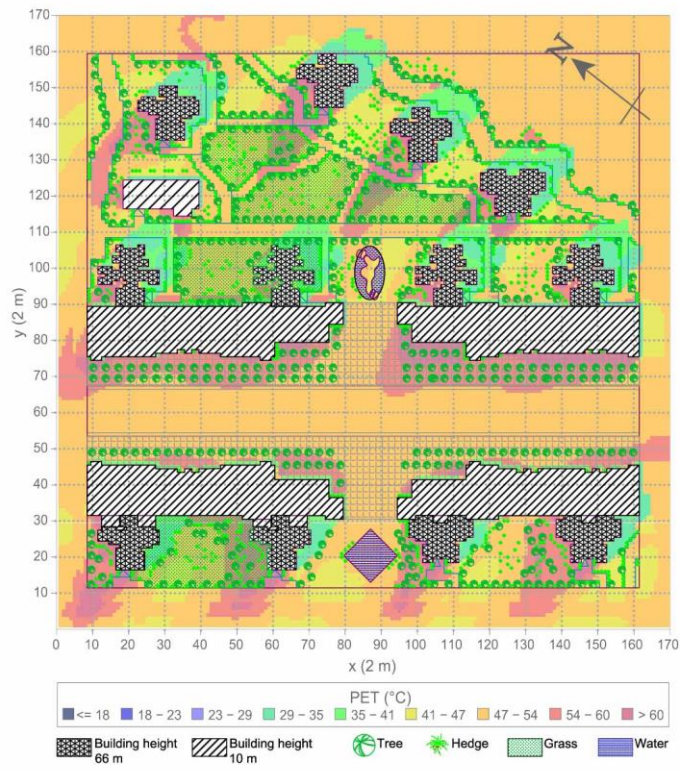

Fig. A2.1 Community environment design, based on PET distribution at 14 LST in the 1st simulation in Sanya (Aw)

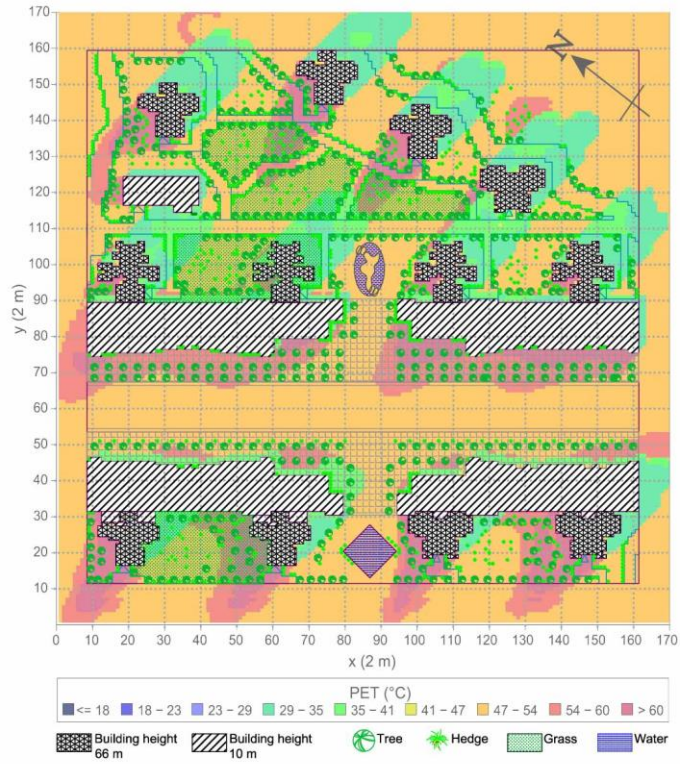

Fig. A2.2 Community environment design, based on PET distribution at 15 LST in the 1st simulation in Qionghai (Am)

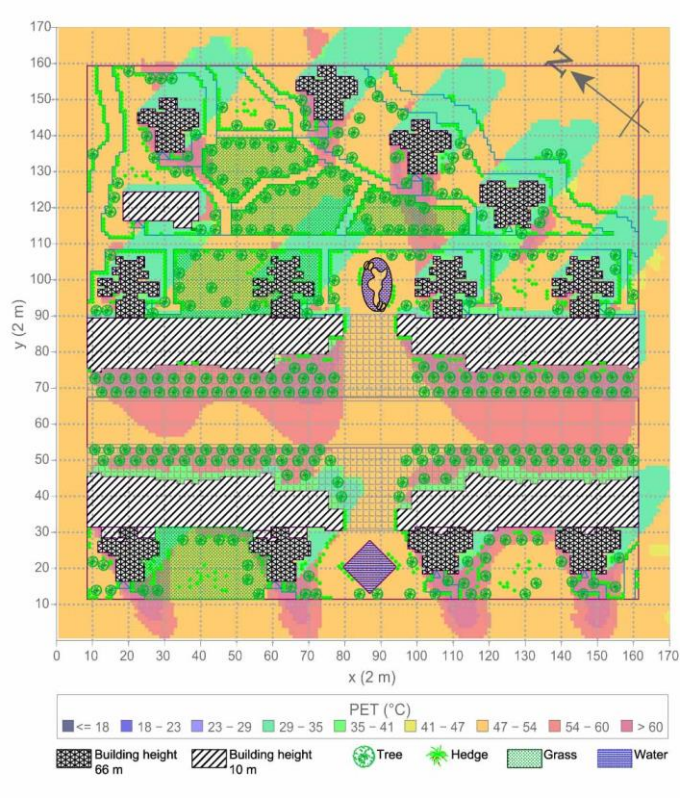

Fig. A2.3 Community environment design, based on PET distribution at 15 LST in the 1st simulation in Shenzhen (Cwa)

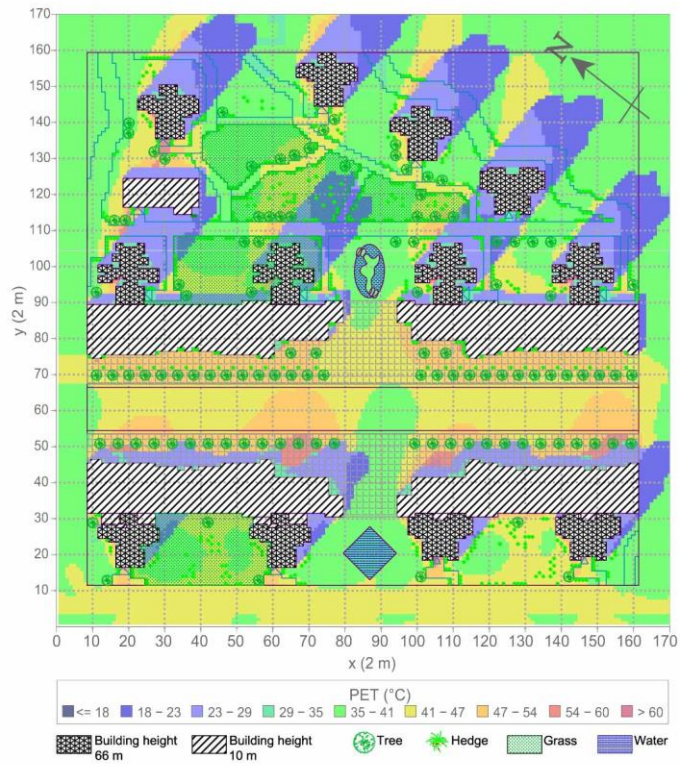

Fig. A2.4 Community environment design, based on PET distribution at 16 LST in the 1st simulation in Kunming (Cwb)

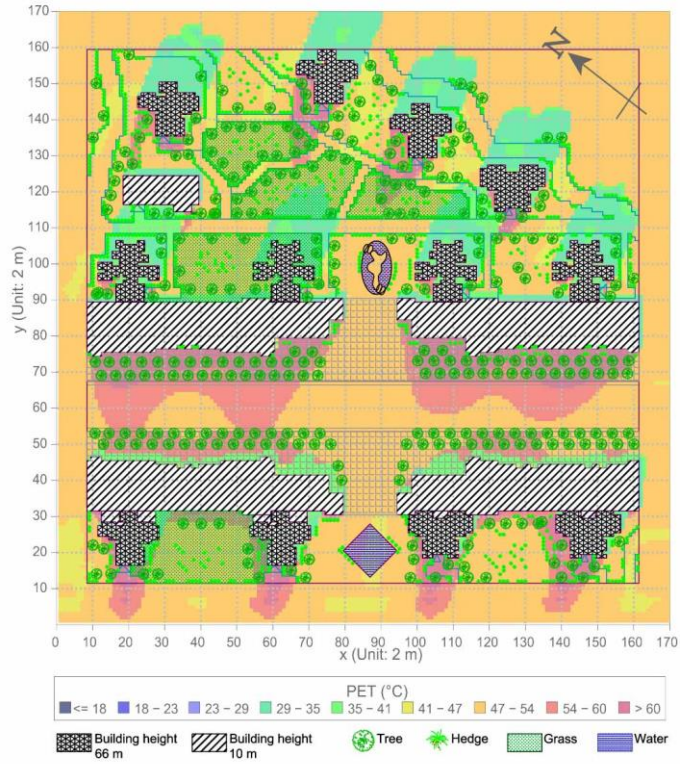

Fig. A2.5 Community environment design, based on PET distribution at 14 LST in the 1st simulation in Shanghai (Cfa)

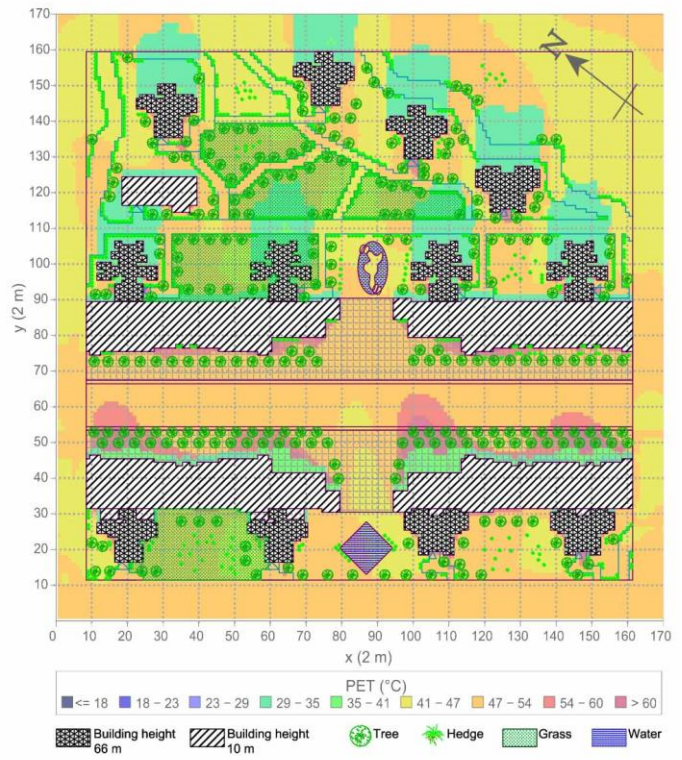

Fig. A2.6 Community environment design, based on PET distribution at 14 LST in the 1st simulation in Beijing (Dwa)

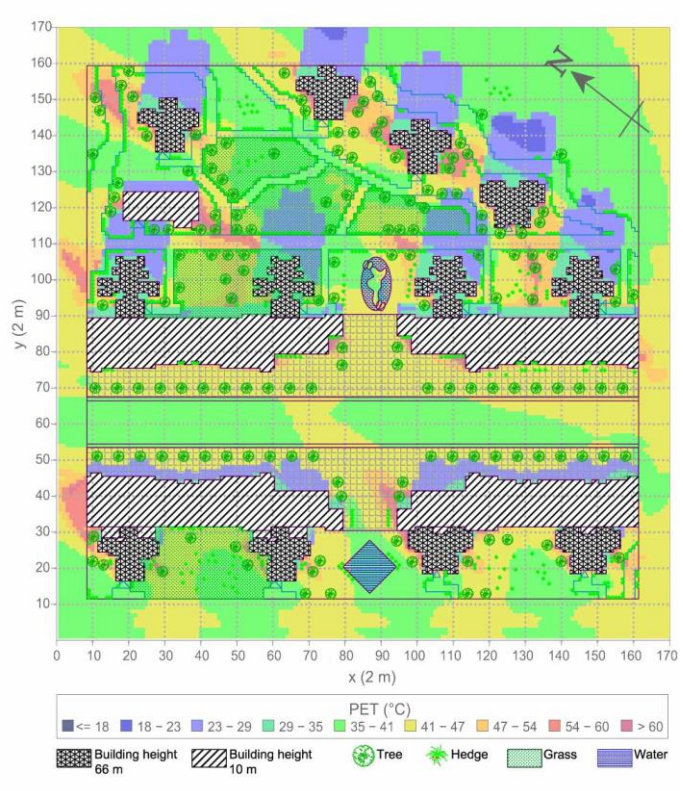

Fig. A2.7 Community environment design, based on PET distribution at 14 LST in the 1st simulation in Dalian (Dwa)

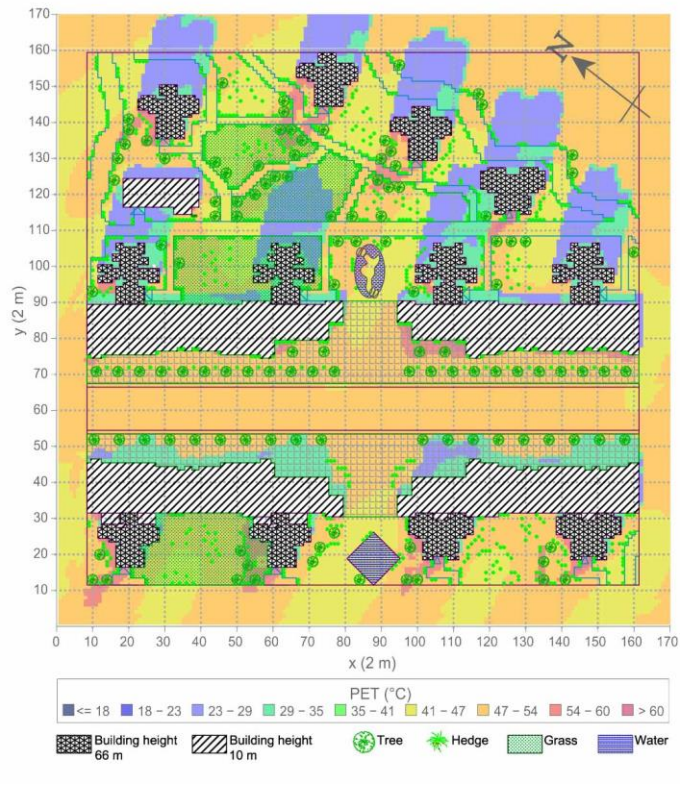

Fig. A2.8 Community environment design, based on PET distribution at 15 LST in the 1st simulation in Hohhot (Dwb)

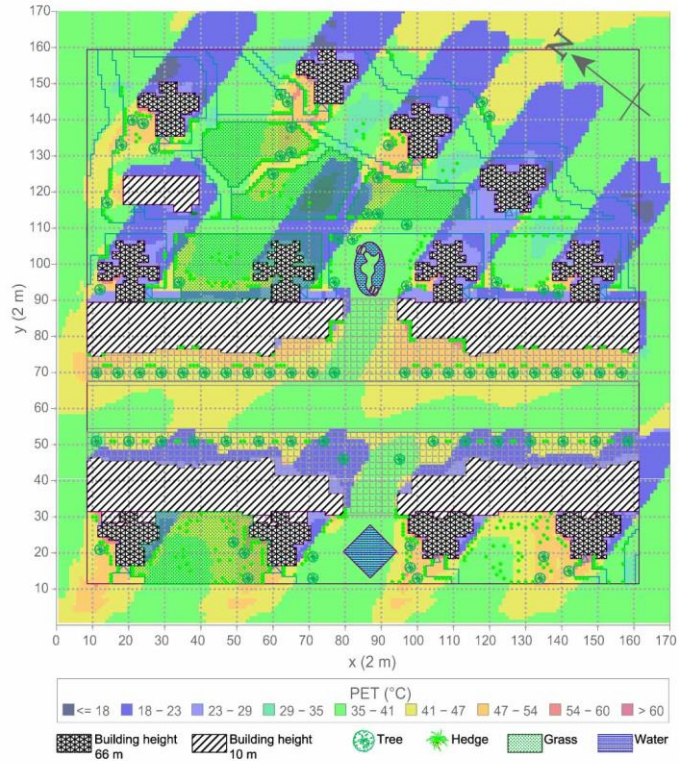

Fig. A2.9 Community environment design, based on PET distribution at 17 LST in the 1st simulation in Lhasa (Dwc)

Fig. A2.10 Community environment design, based on PET distribution at 16 LST in the 1st simulation in Urumqi (Dfb)

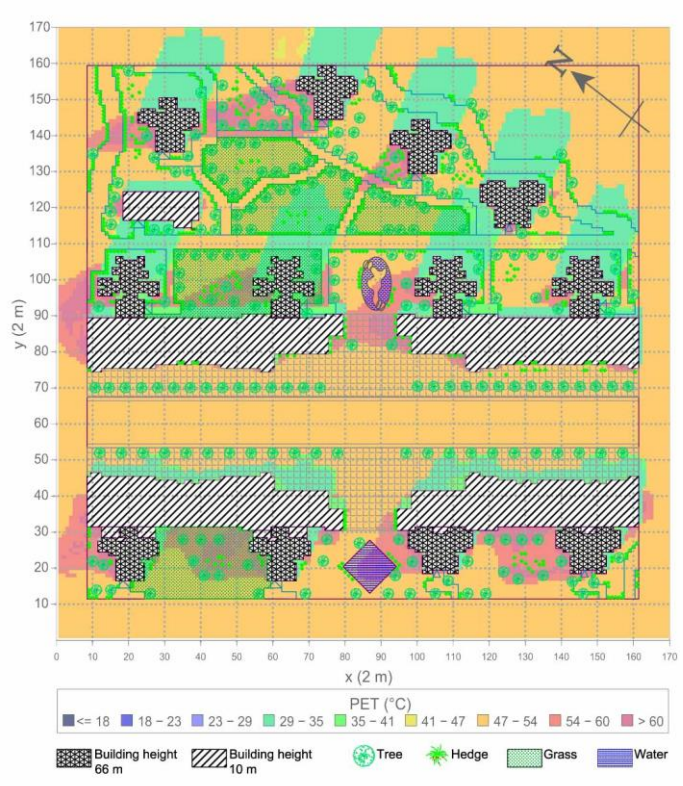

Fig. A2.11 Community environment design, based on PET distribution at 15 LST in the 1st simulation in Yuncheng (BSk)

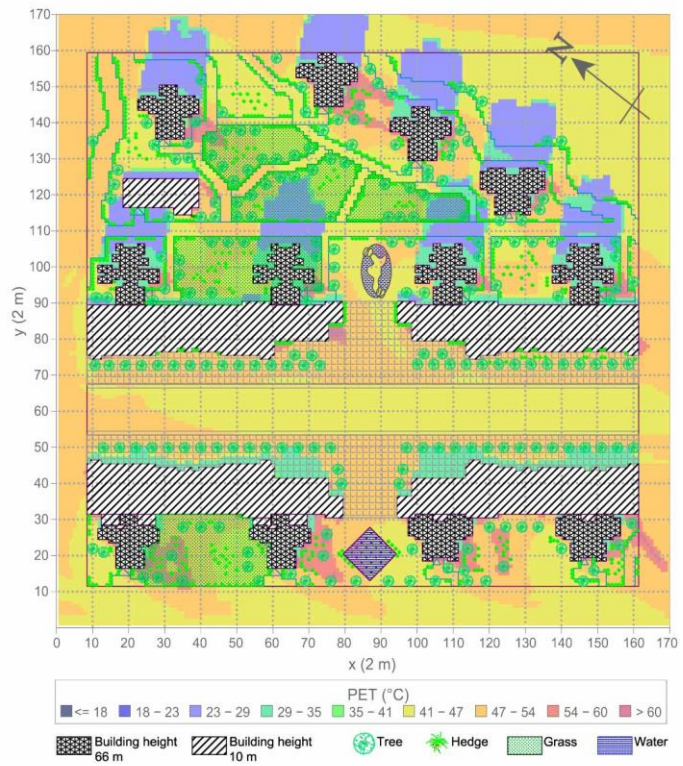

Fig. A2.12 Community environment design, based on PET distribution at 15 LST in the 1st simulation in Yinchuan (BWk)

Appendix A3 Distribution of SVF in the 1st round simulation

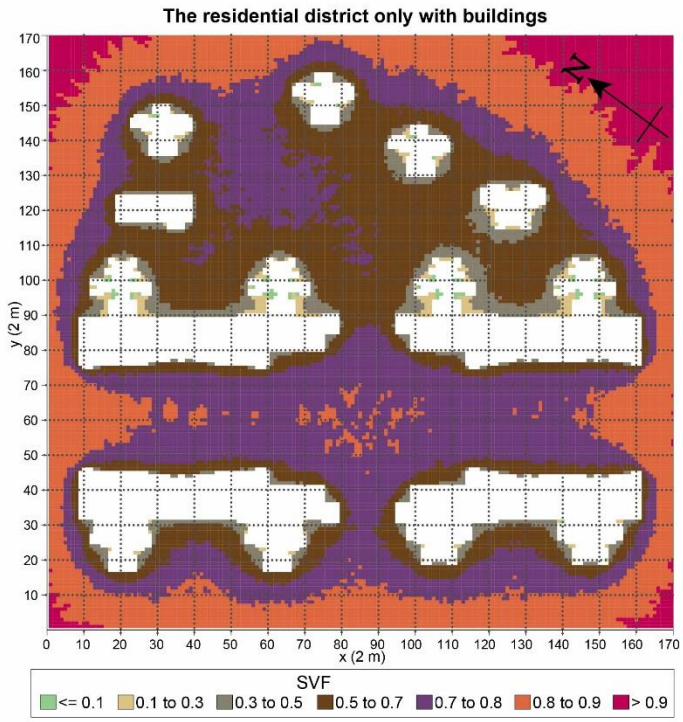

Fig. A3.1 Distribution of SVF in the 1st round simulation (it is the same in 12 scenarios without design elements)

Appendix A4 Distribution of *v* in the 1st round simulation in 12 scenarios, respectively

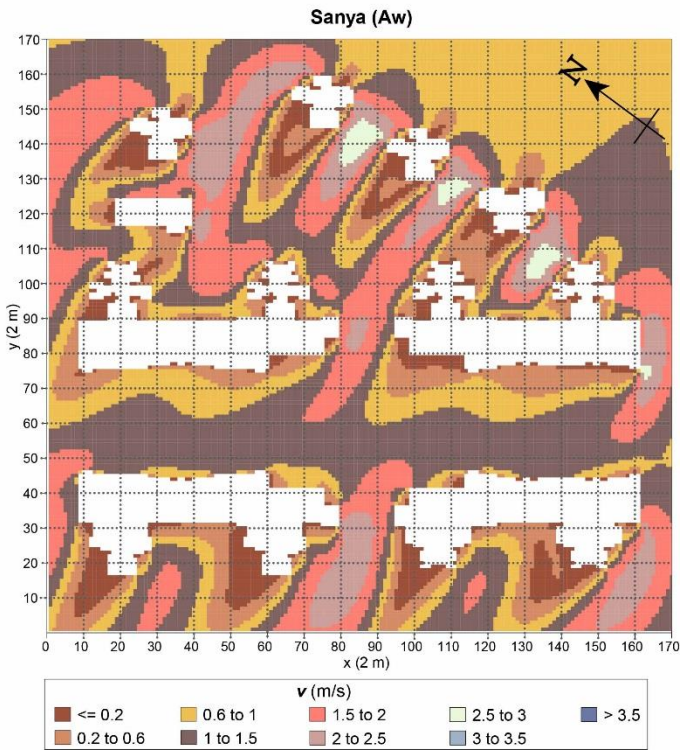

Fig. A4.1 Distribution of *v* at 14 LST in the 1st simulation in Sanya (Aw)

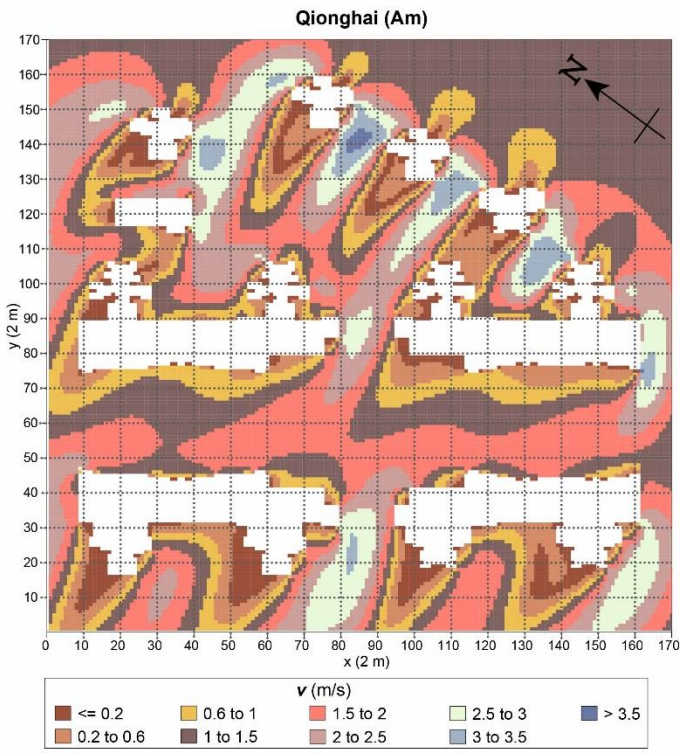

Fig. A4.2 Distribution of *v* at 15 LST in the 1st simulation in Qionghai (Am)

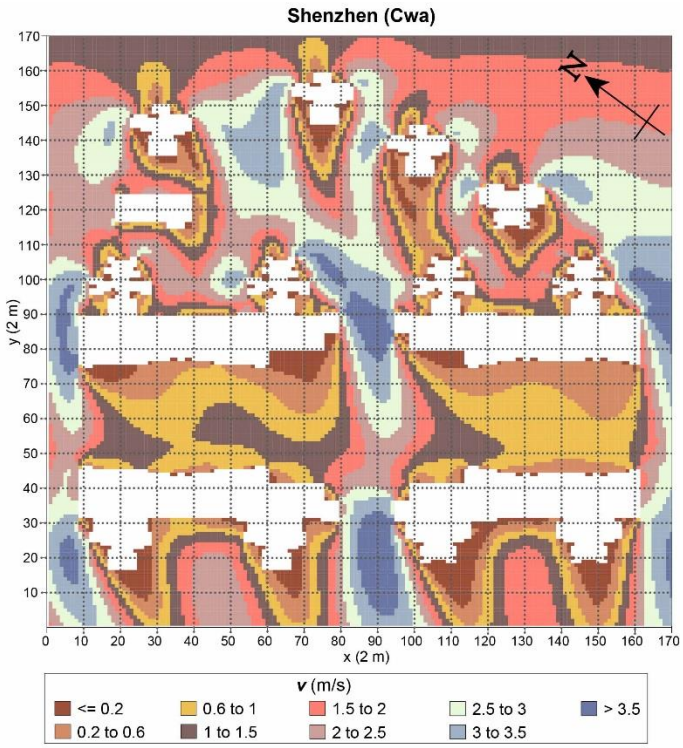

Fig. A4.3 Distribution of *v* at 15 LST in the 1st simulation in Shenzhen (Cwa)

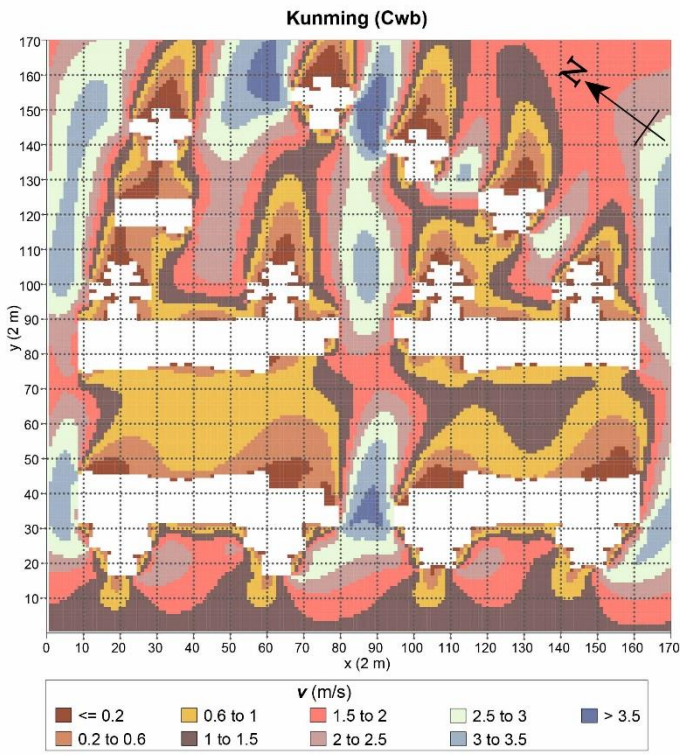

Fig. A4.4 Distribution of *v* at 16 LST in the 1st simulation in Kunming (Cwb)

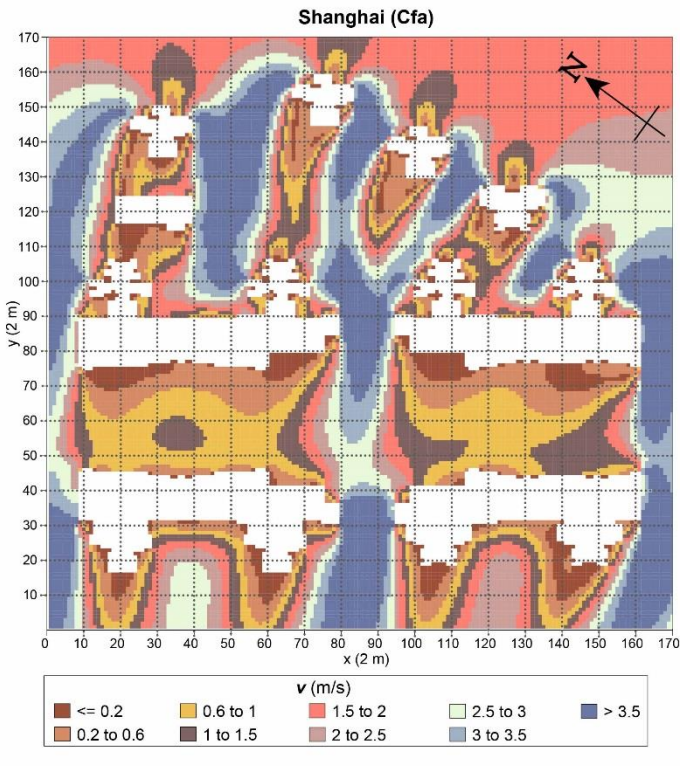

Fig. A4.5 Distribution of *v* at 14 LST in the 1st simulation in Shanghai (Cfa)

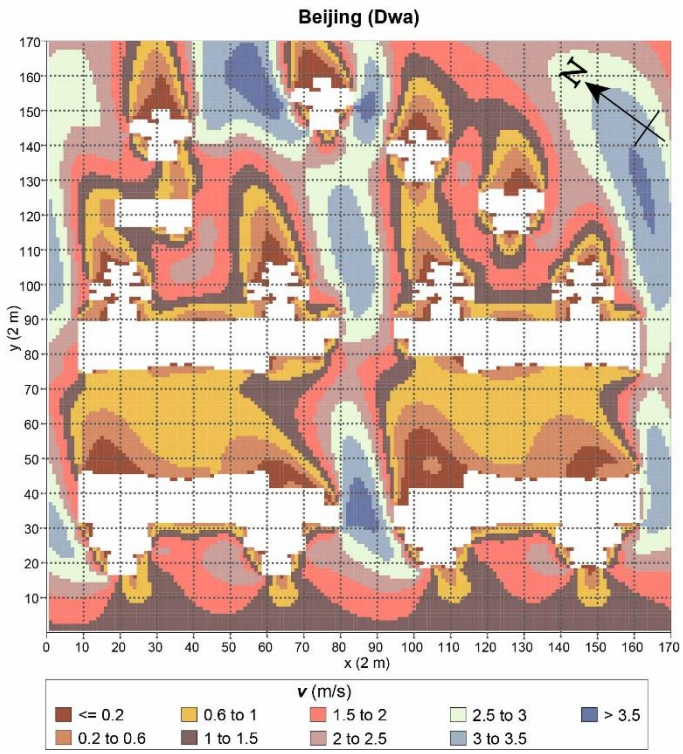

Fig. A4.6 Distribution of *v* at 14 LST in the 1st simulation in Beijing (Dwa)

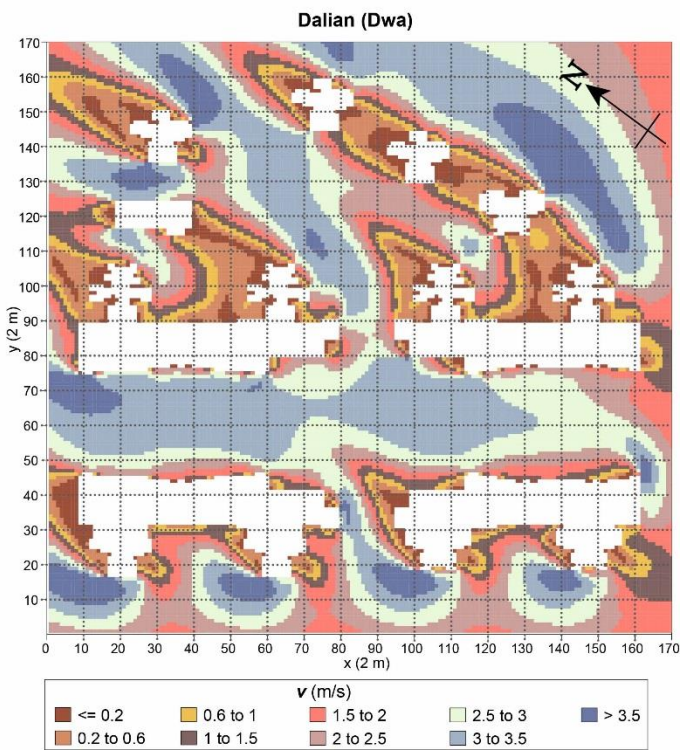

Fig. A4.7 Distribution of *v* at 14 LST in the 1st simulation in Dalian (Dwa)

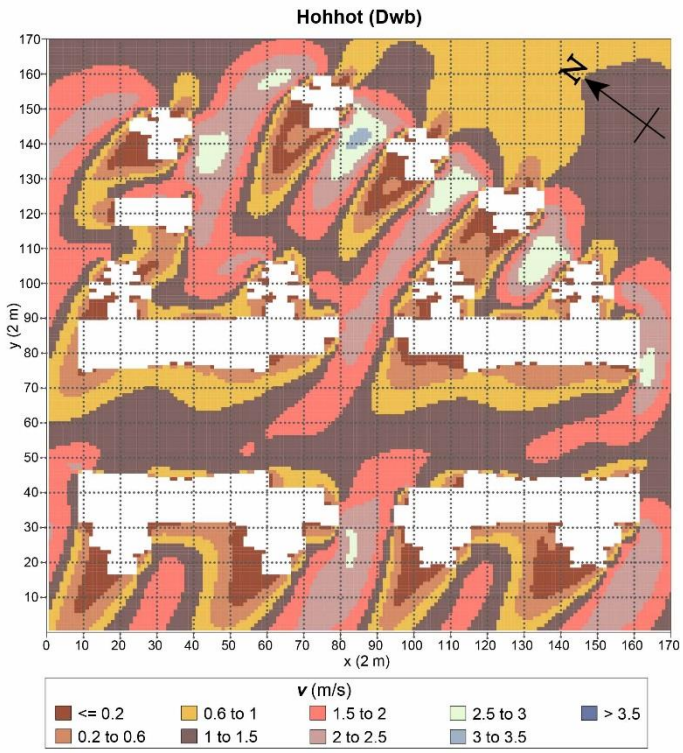

Fig. A4.8 Distribution of *v* at 15 LST in the 1st simulation in Hohhot (Dwb)

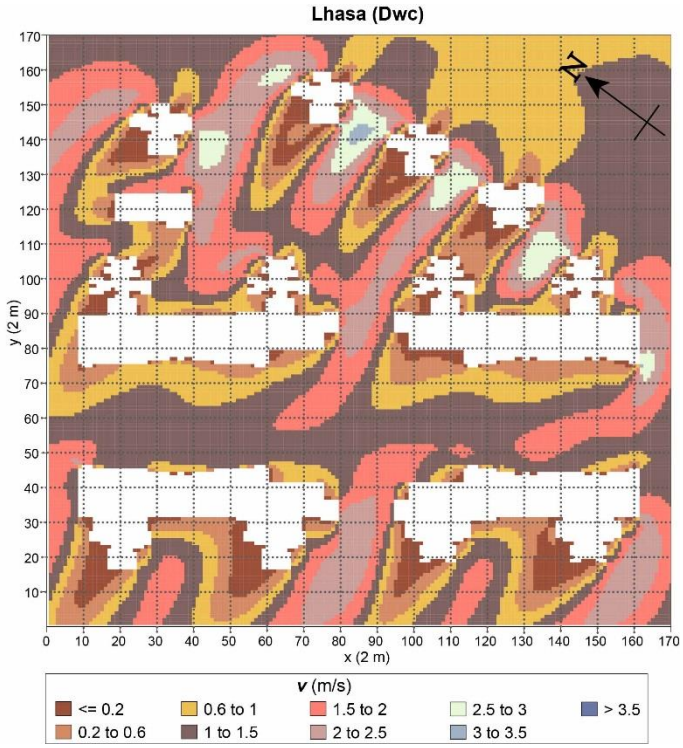

Fig. A4.9 Distribution of *v* at 17 LST in the 1st simulation in Lhasa (Dwc)

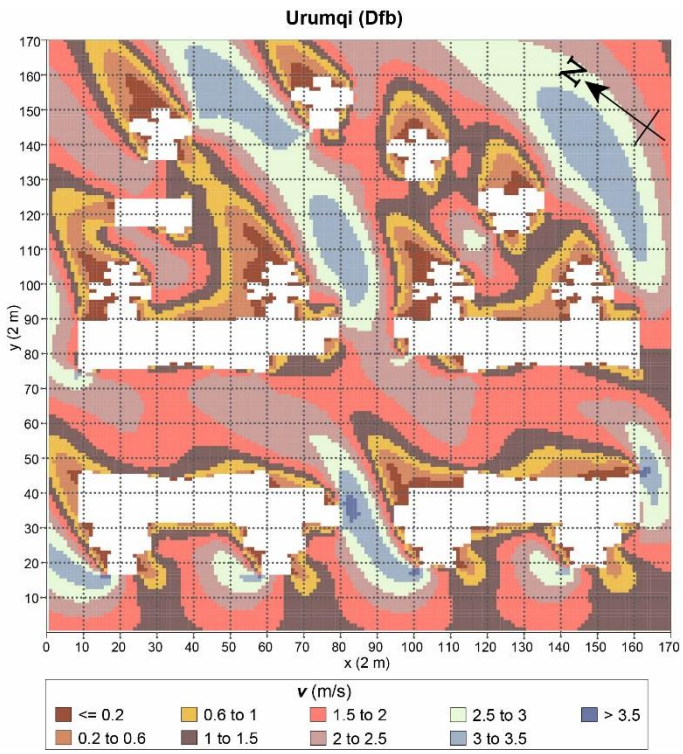

Fig. A4.10 Distribution of *v* at 16 LST in the 1st simulation in Urumqi (Dfb)

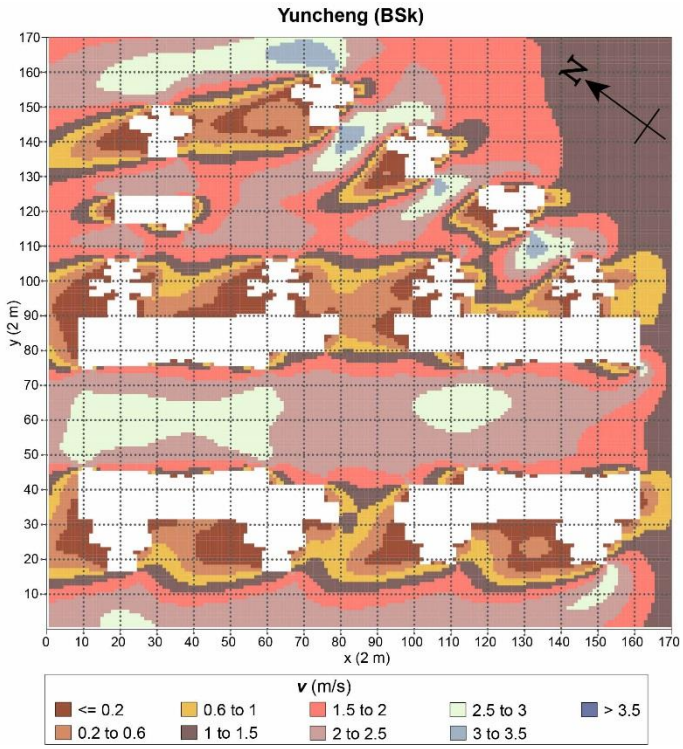

Fig. A4.11 Distribution of *v* at 15 LST in the 1st simulation in Yuncheng (BSk)

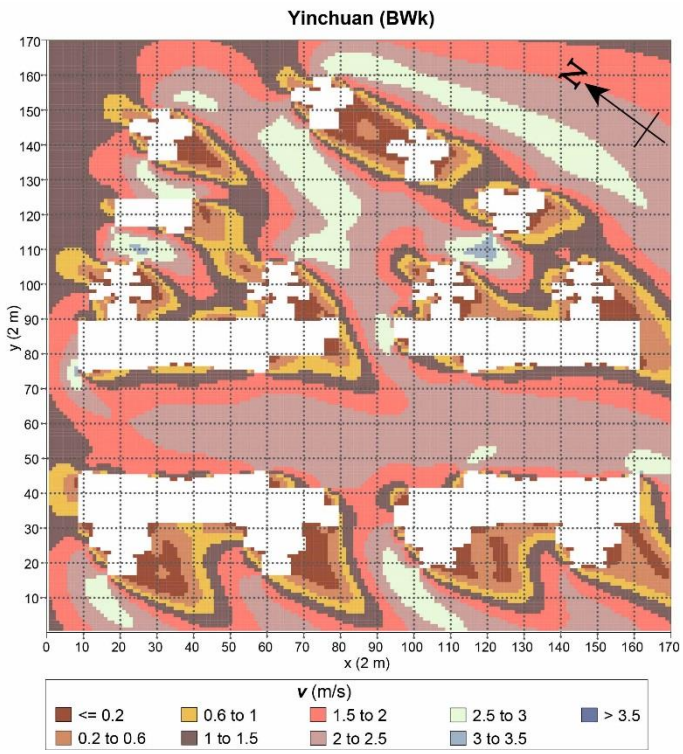

Fig. A4.12 Distribution of *v* at 15 LST in the 1st simulation in Yinchuan (BWk)

Appendix A5 Distribution of the difference between the twice simulations in PET in 12 scenarios, respectively

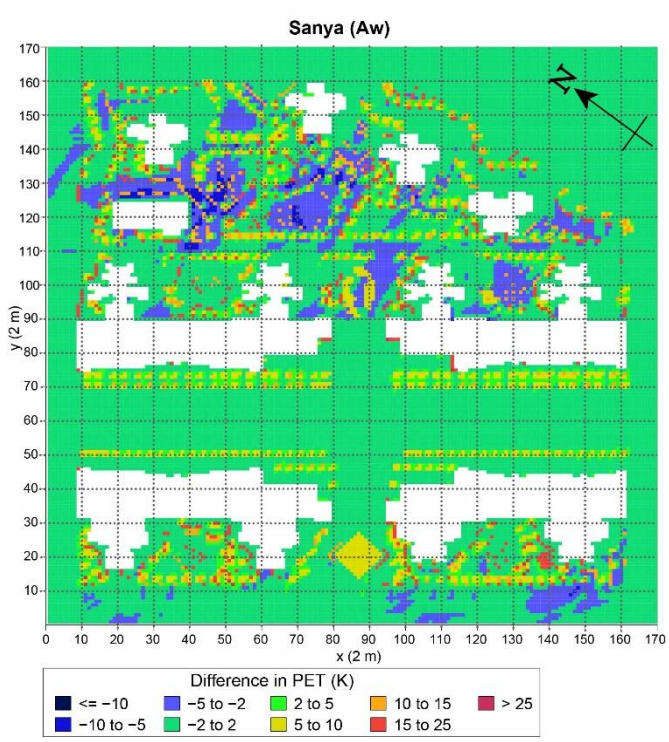

Fig. A5.1 Difference at 14 LST between twice simulations in PET in Sanya (Aw)

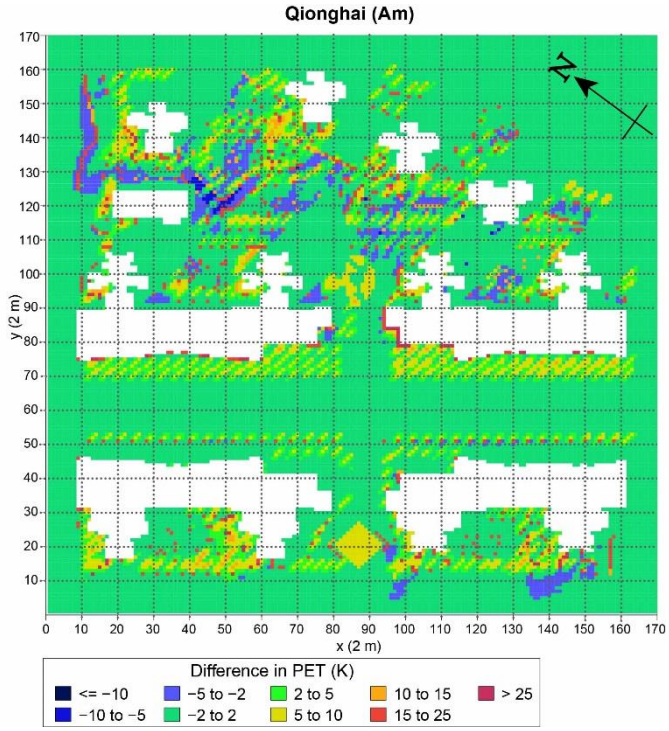

Fig. A5.2 Difference at 15 LST between twice simulations in PET in Qionghai (Am)

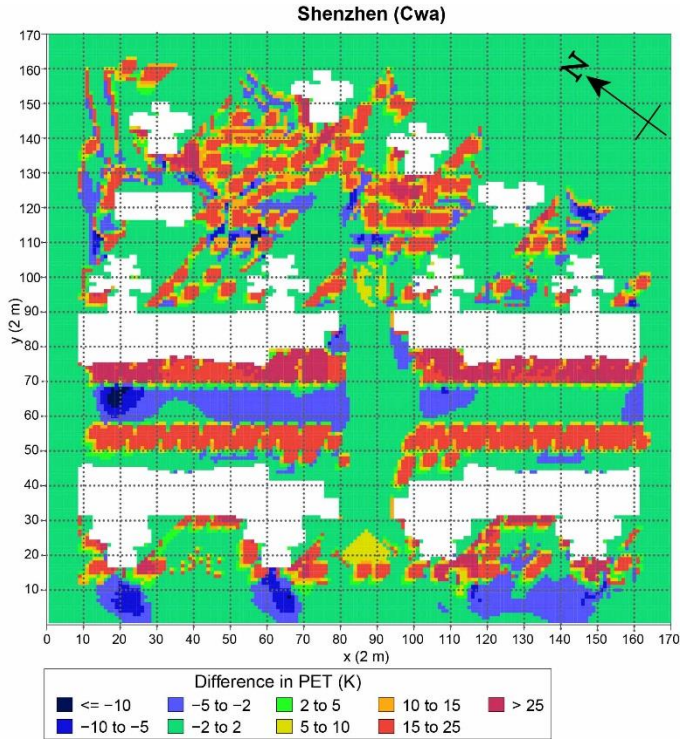

Fig. A5.3 Difference at 15 LST between twice simulations in PET in Shenzhen (Cwa)

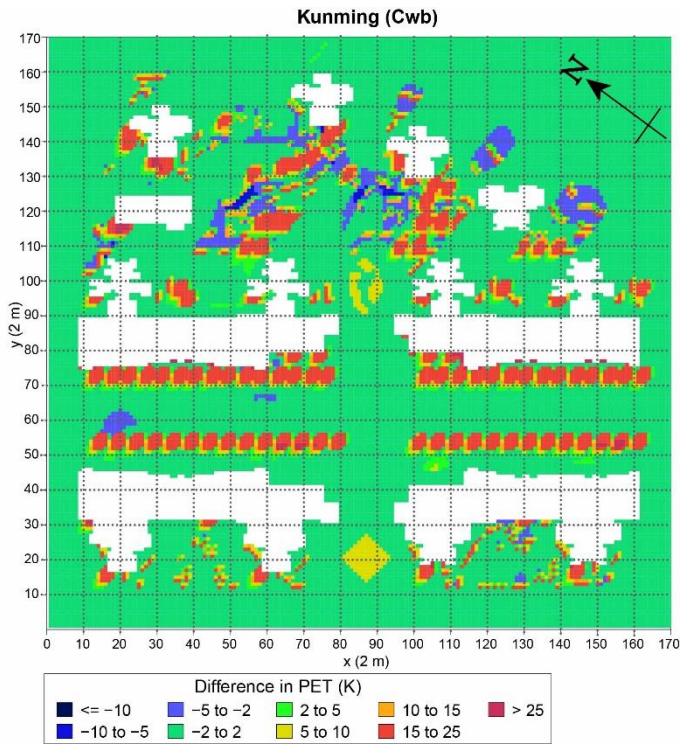

Fig. A5.4 Difference at 16 LST between twice simulations in PET in Kunming (Cwb)

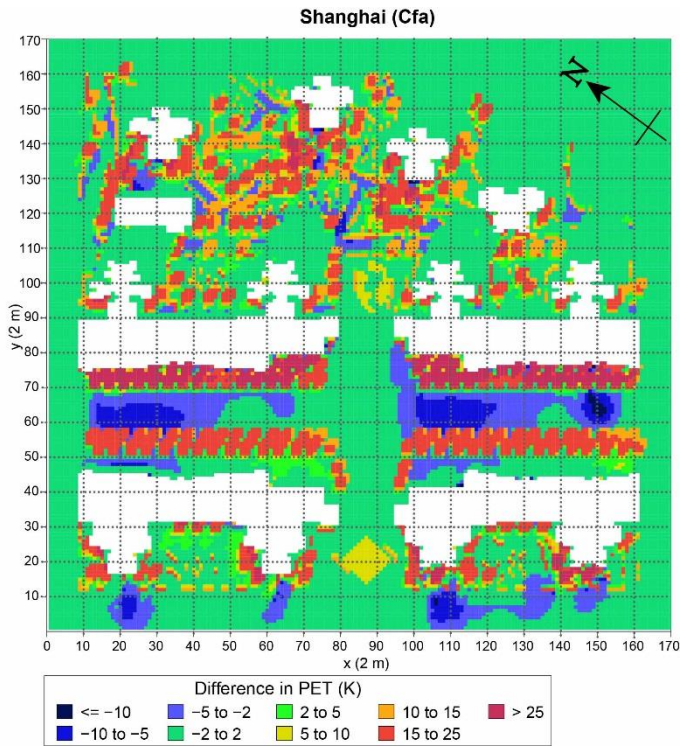

Fig. A5.5 Difference at 14 LST between twice simulations in PET in Shanghai (Cfa)

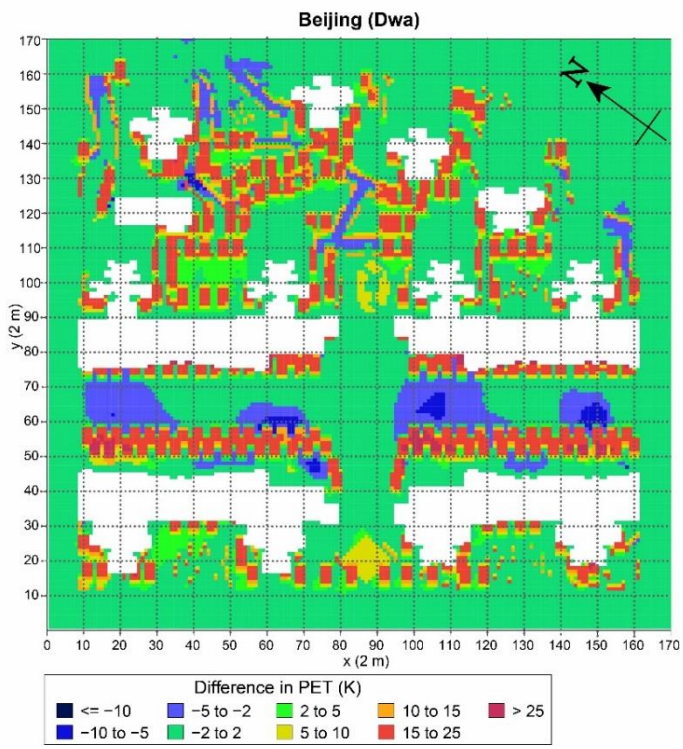

Fig. A5.6 Difference at 14 LST between twice simulations in PET in Beijing (Dwa)

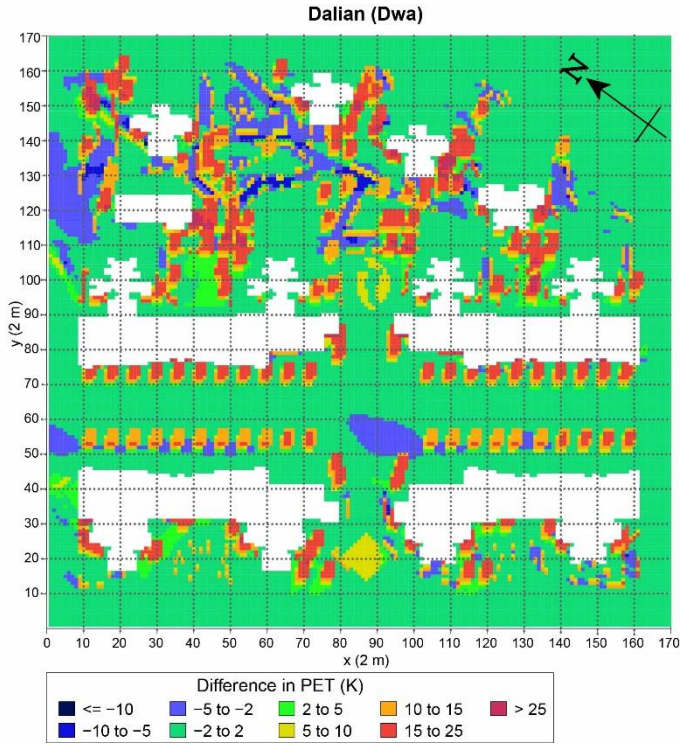

Fig. A5.7 Difference at 14 LST between twice simulations in PET in Dalian (Dwa)

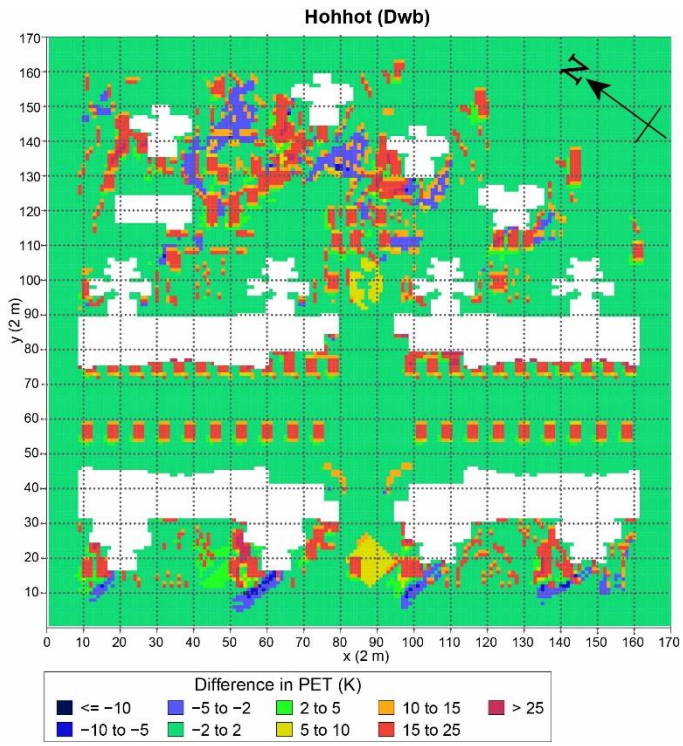

Fig. A5.8 Difference at 15 LST between twice simulations in PET in Hohhot (Dwb)

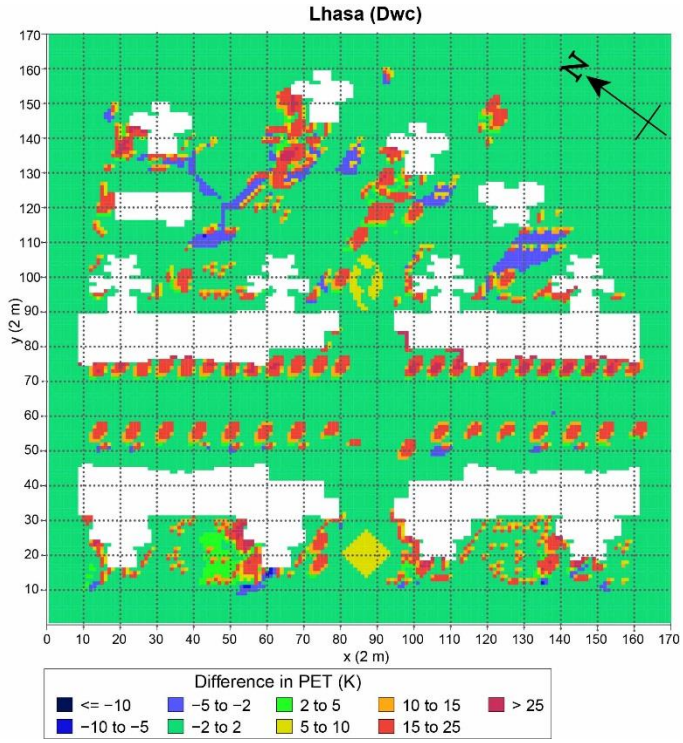

Fig. A5.9 Difference at 17 LST between twice simulations in PET in Lhasa (Dwc)

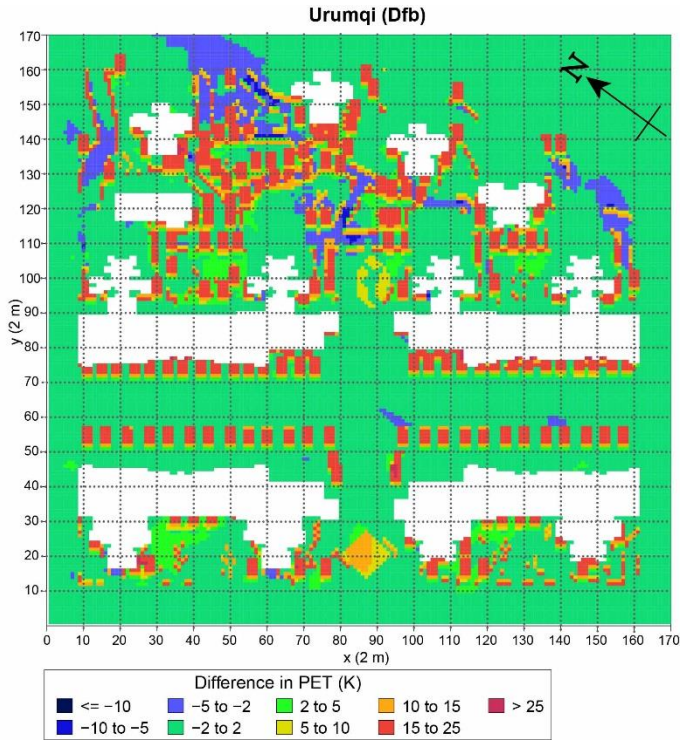

Fig. A5.10 Difference at 16 LST between twice simulations in PET in Urumqi (Dfb)

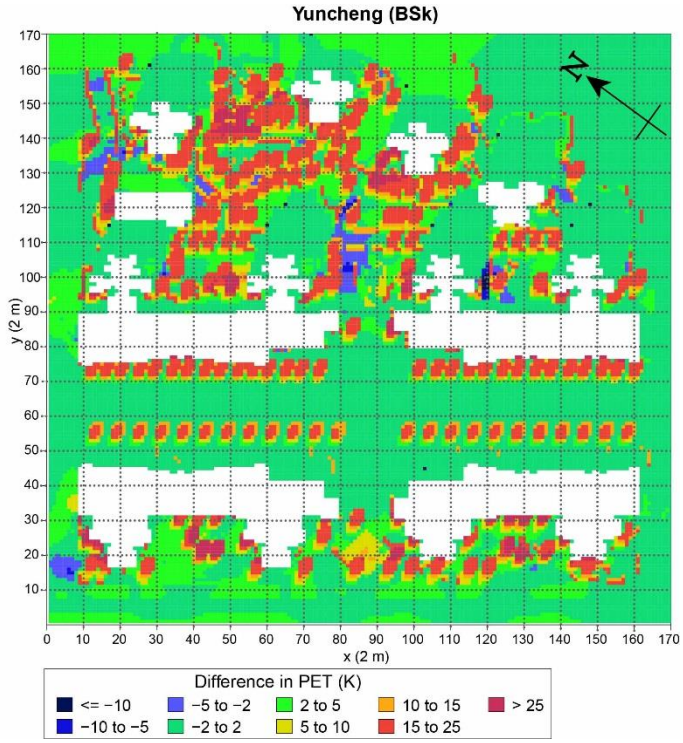

Fig. A5.11 Difference at 15 LST between twice simulations in PET in Yuncheng (BSk)

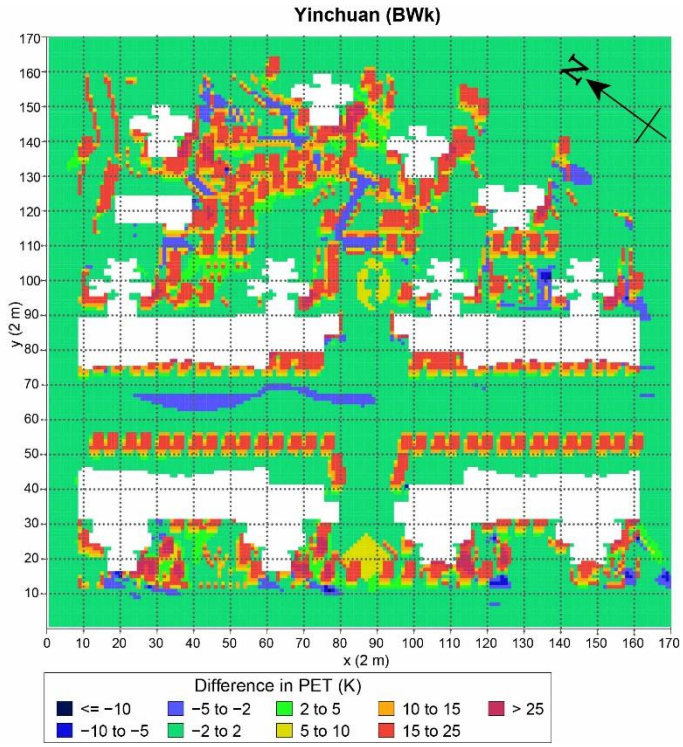

Fig. A5.12 Difference at 15 LST between twice simulations in PET in Yinchuan (BWk)

Appendix A6 Distribution of the difference between the twice simulations in SVF in 12 scenarios, respectively

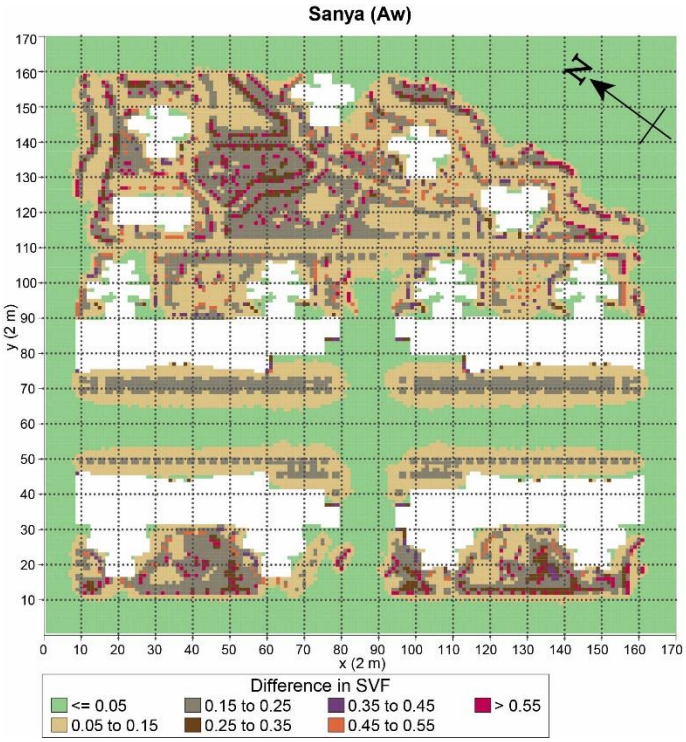

Fig. A6.1 Difference at 14 LST between twice simulations in SVF in Sanya (Aw)

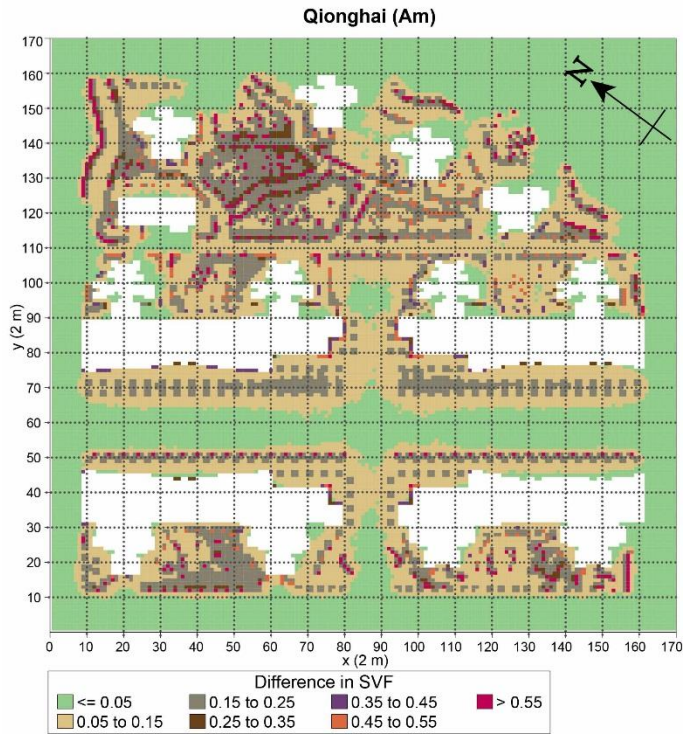

Fig. A6.2 Difference at 15 LST between twice simulations in SVF in Qionghai (Am)

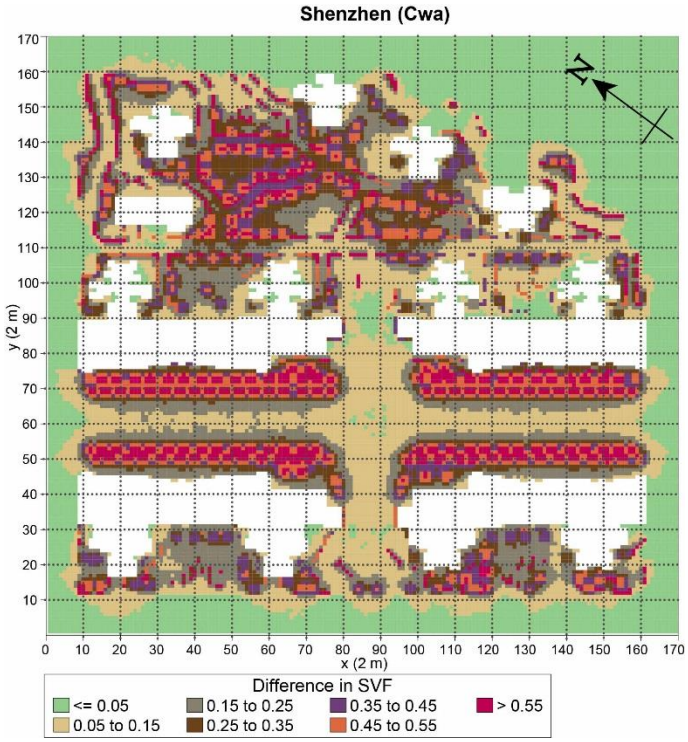

Fig. A6.3 Difference at 15 LST between twice simulations in SVF in Shenzhen (Cwa)

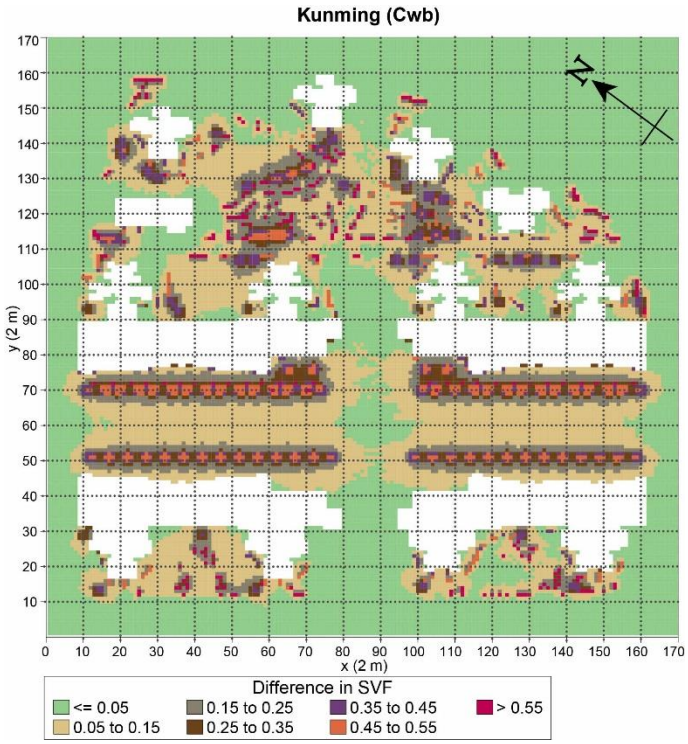

Fig. A6.4 Difference at 16 LST between twice simulations in SVF in Kunming (Cwb)

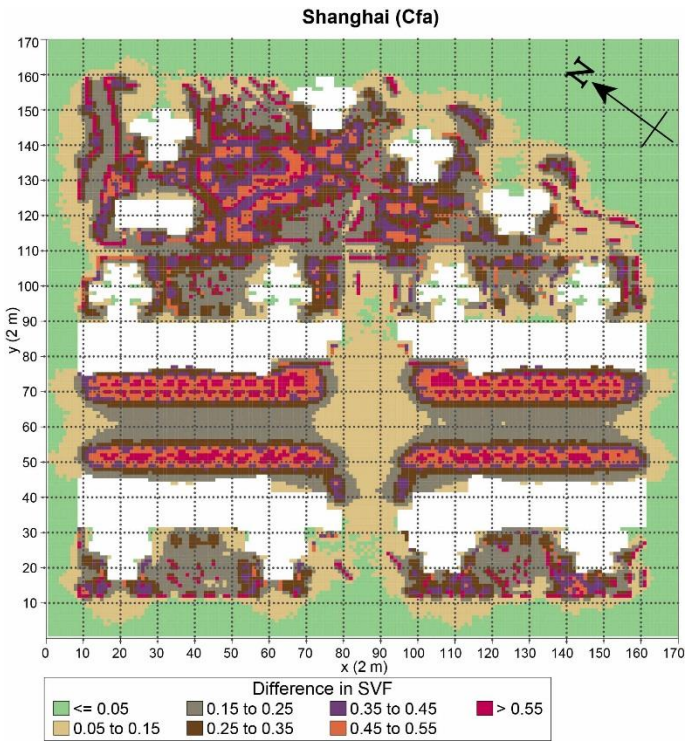

Fig. A6.5 Difference at 14 LST between twice simulations in SVF in Shanghai (Cfa)

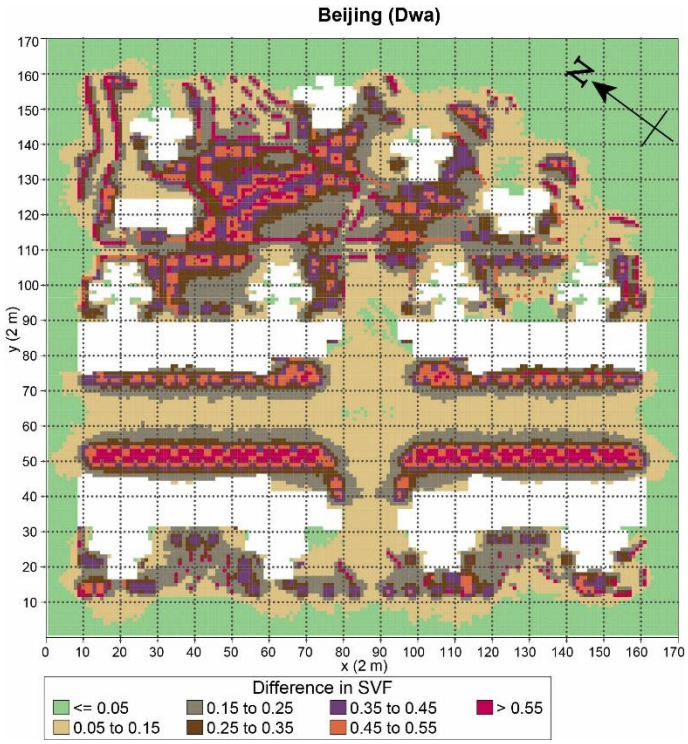

Fig. A6.6 Difference at 14 LST between twice simulations in SVF in Beijing (Dwa)

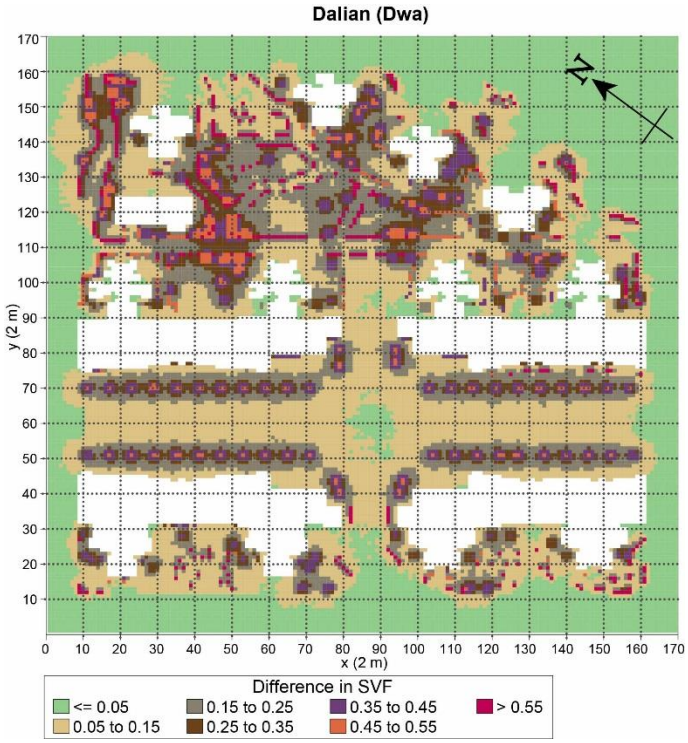

Fig. A6.7 Difference at 14 LST between twice simulations in SVF in Dalian (Dwa)

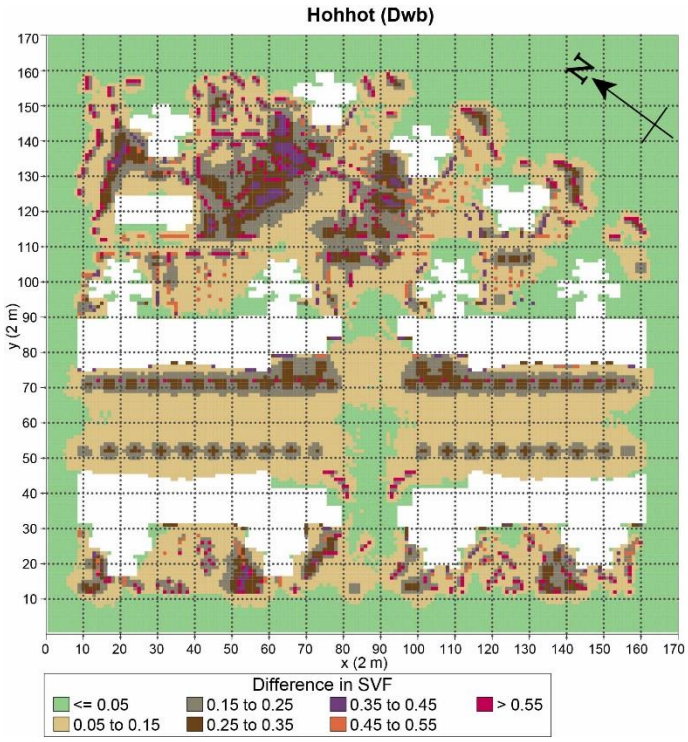

Fig. A6.8 Difference at 15 LST between twice simulations in SVF in Hohhot (Dwb)

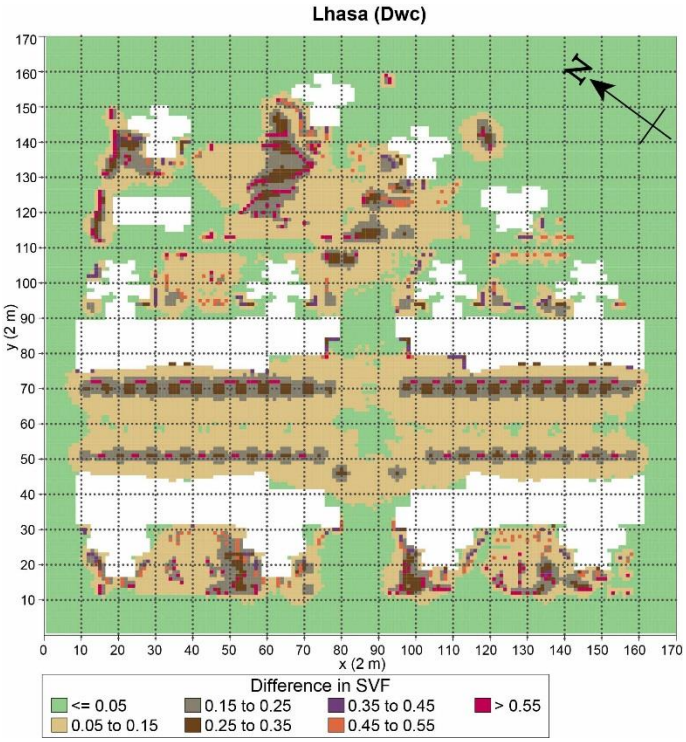

Fig. A6.9 Difference at 17 LST between twice simulations in SVF in Lhasa (Dwc)

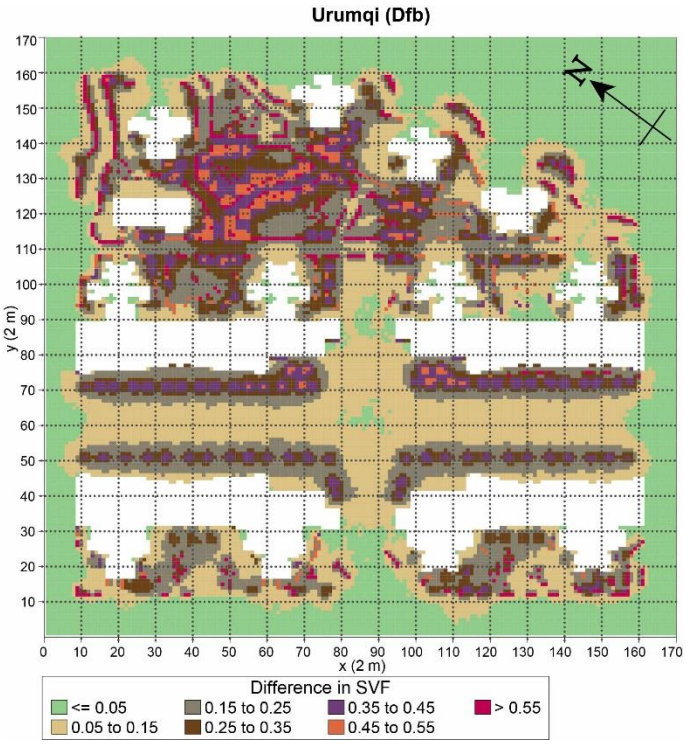

Fig. A6.10 Difference at 16 LST between twice simulations in SVF in Urumqi (Dfb)

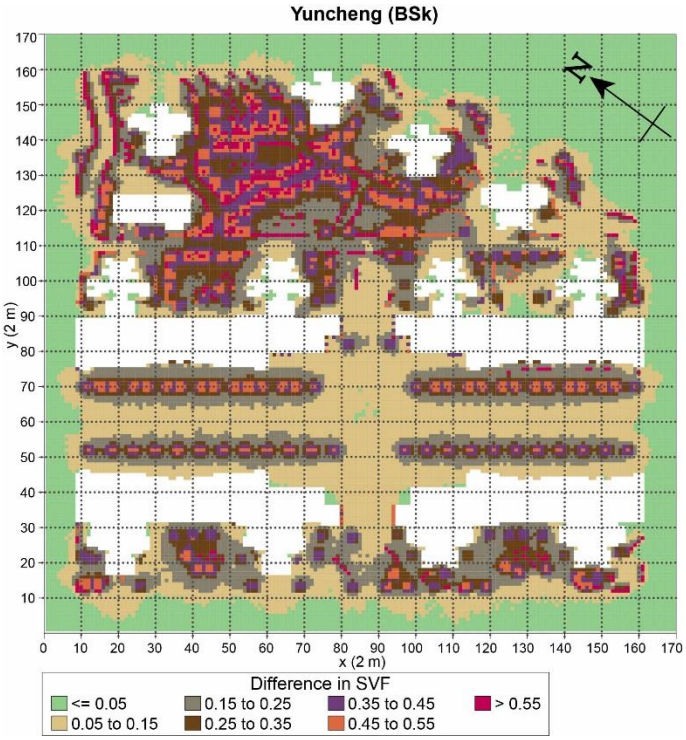

Fig. A6.11 Difference at 15 LST between twice simulations in SVF in Yuncheng (BSk)

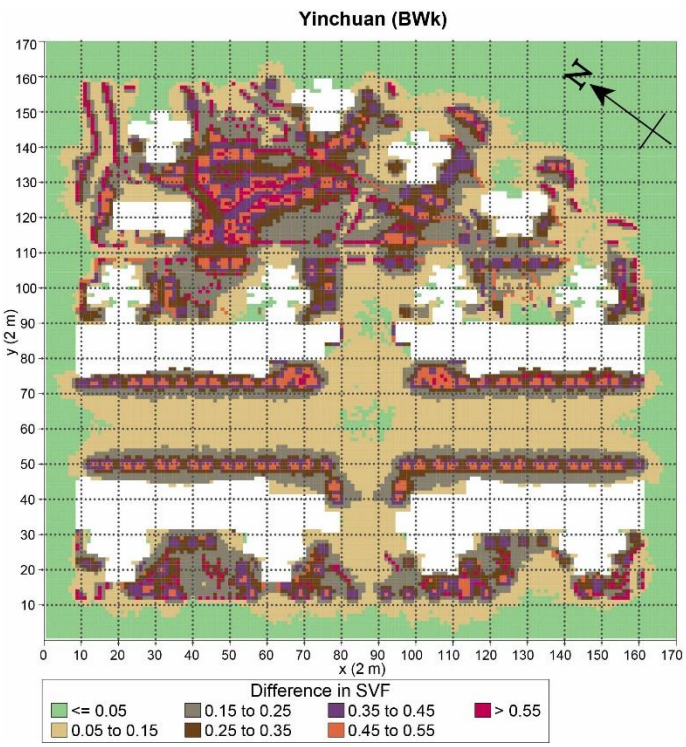

Fig. A6.12 Difference at 15 LST between twice simulations in SVF in Yinchuan (BWk)

Appendix A7 Distribution of the difference between the twice simulations in *v* in 12 scenarios, respectively

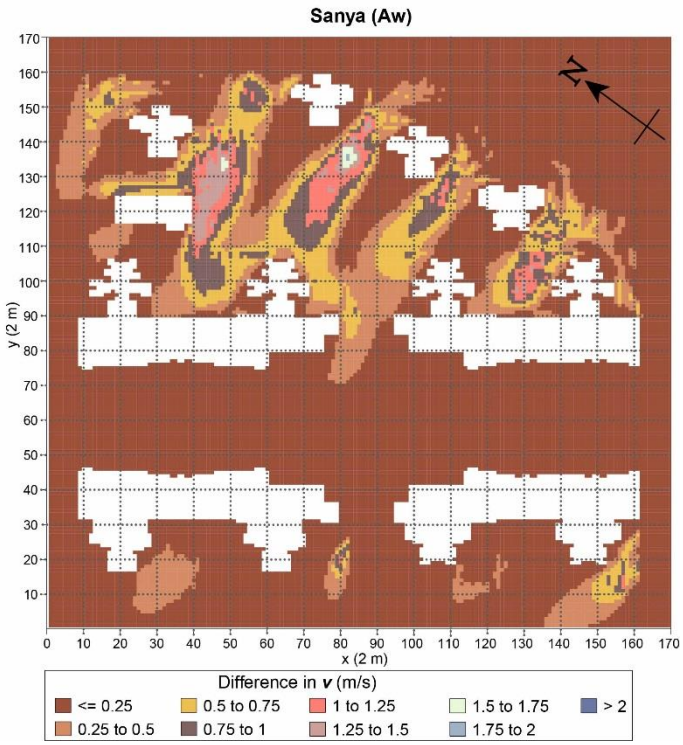

Fig. A7.1 Difference at 14 LST between twice simulations in *v* in Sanya (Aw)

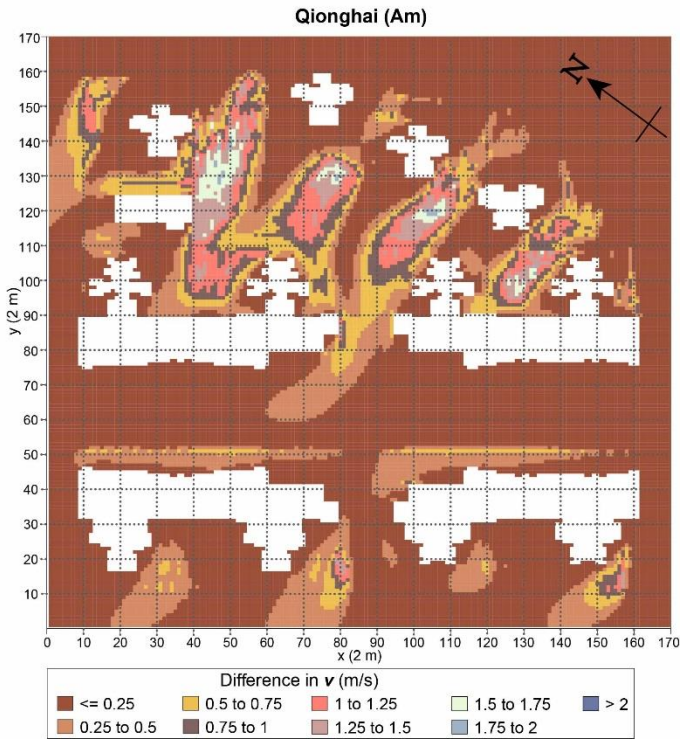

Fig. A7.2 Difference at 15 LST between twice simulations in *v* in Qionghai (Am)

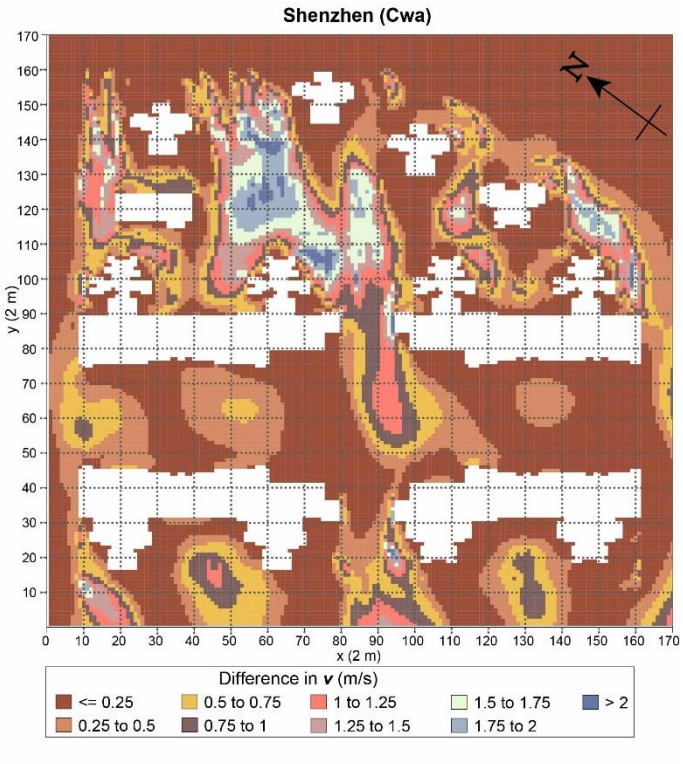

Fig. A7.3 Difference at 15 LST between twice simulations in *v* in Shenzhen (Cwa)

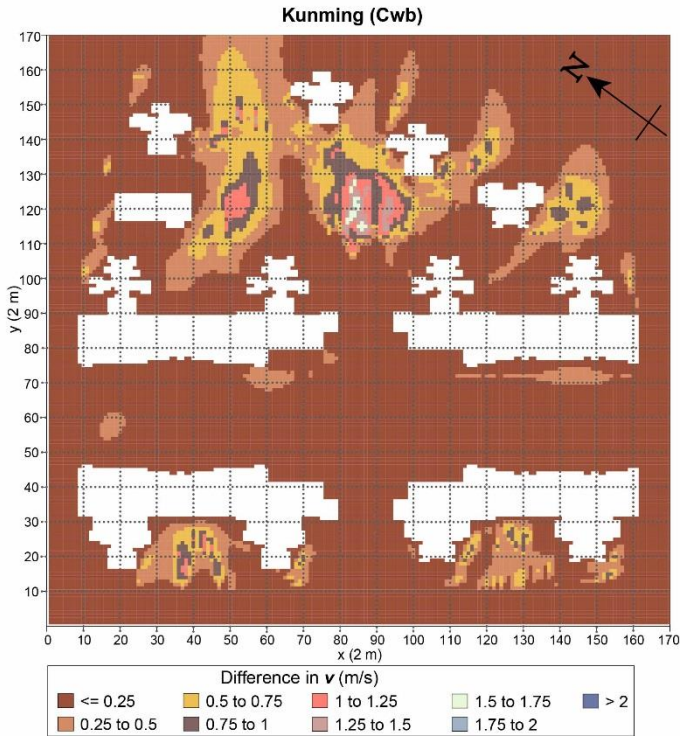

Fig. A7.4 Difference at 16 LST between twice simulations in *v* in Kunming (Cwb)

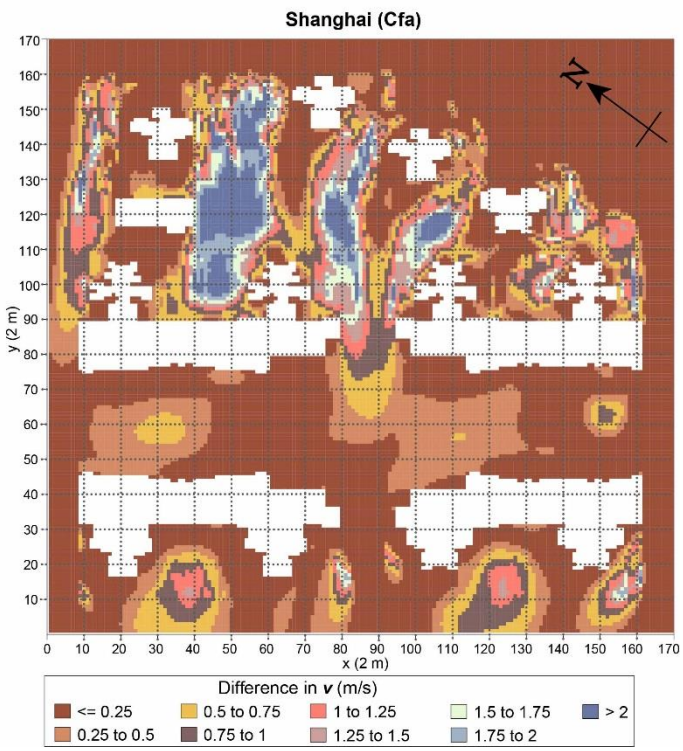

Fig. A7.5 Difference at 14 LST between twice simulations in *v* in Shanghai (Cfa)

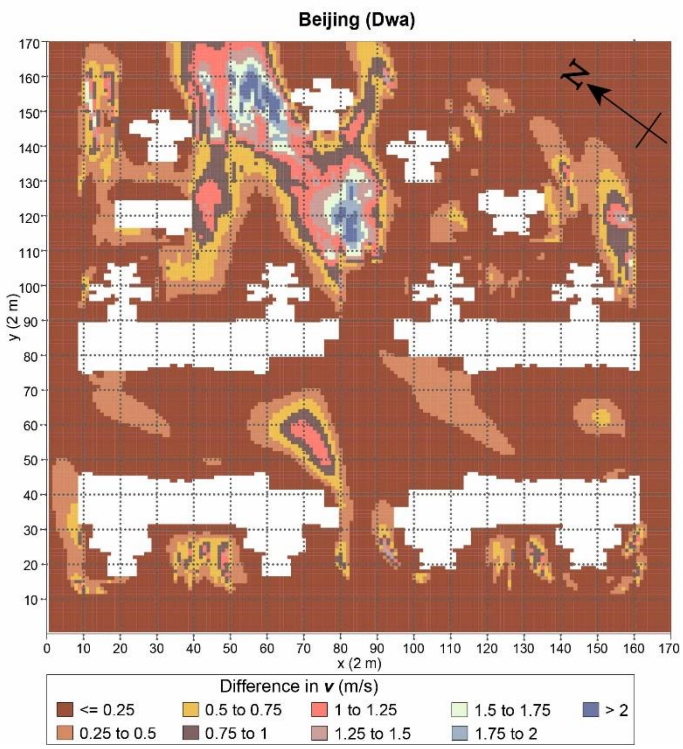

Fig. A7.6 Difference at 14 LST between twice simulations in *v* in Beijing (Dwa)

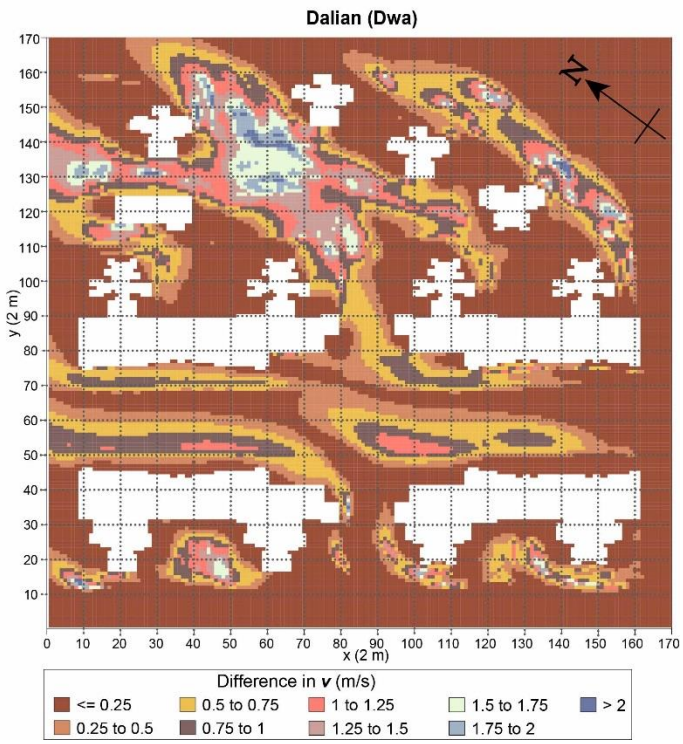

Fig. A7.7 Difference at 14 LST between twice simulations in *v* in Dalian (Dwa)

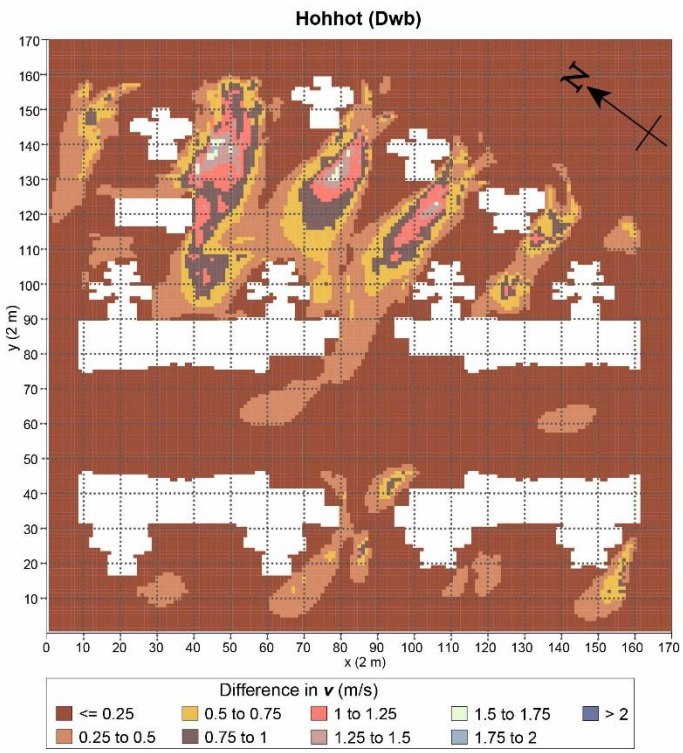

Fig. A7.8 Difference at 15 LST between twice simulations in *v* in Hohhot (Dwb)

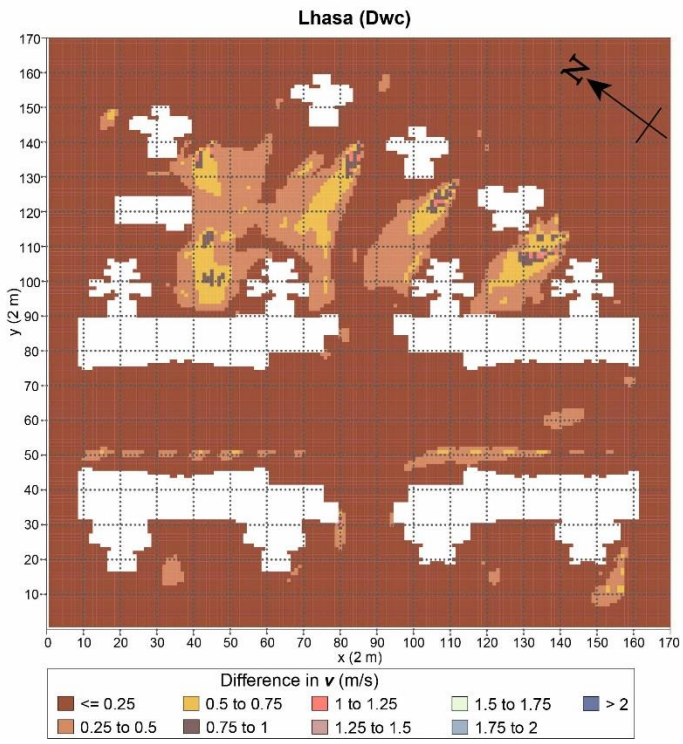

Fig. A7.9 Difference at 17 LST between twice simulations in *v* in Lhasa (Dwc)

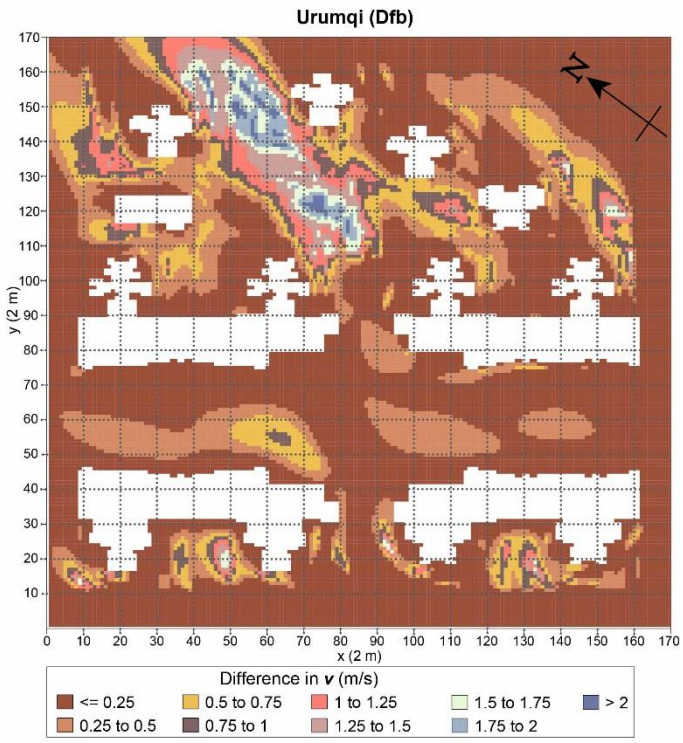

Fig. A7.10 Difference at 16 LST between twice simulations in *v* in Urumqi (Dfb)

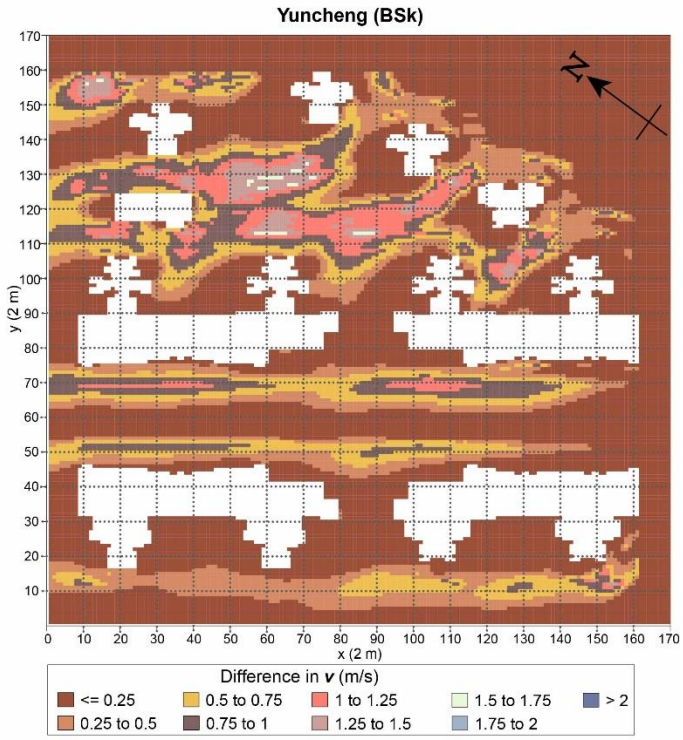

Fig. A7.11 Difference at 15 LST between twice simulations in *v* in Yuncheng (BSk)

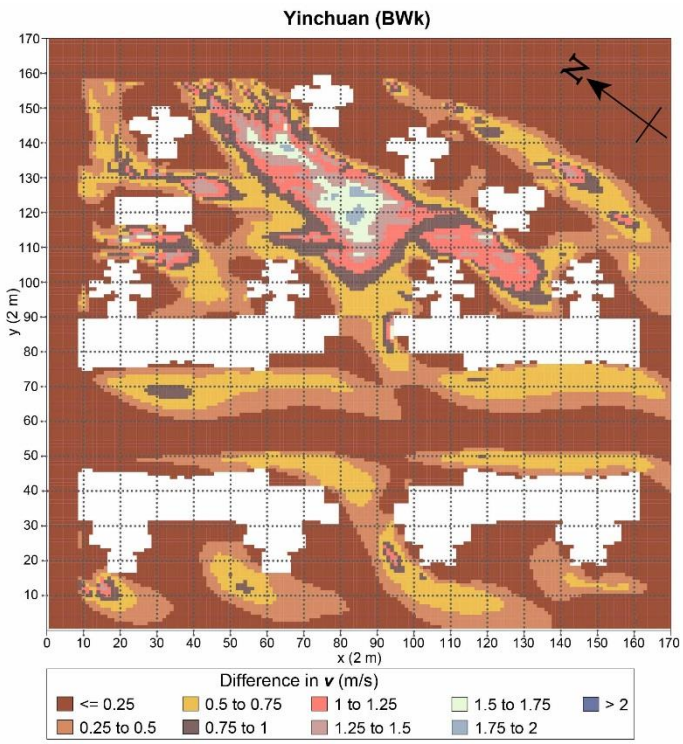

Fig. A7.12 Difference at 15 LST between twice simulations in *v* in Yinchuan (BWk)

List of Figures

Figure 1.1.1 Maslow's hierarchy pyramid (from Poston 2009)

Figure 1.1.2 Time and space scales of various atmospheric phenomena. The shaded area represents the characteristic domain of boundary layer features (from Oke 2002, modified after Smagorinsky 1974)

Figure 1.1.3 World Map of Köppen-Geiger climate classification for the period 1951 to 2000 on a regular 0.5 degree latitude/longitude grid (from Kottek et al. 2006)

Figure 1.1.4 Air temperature frequencies for Sun Moon Lake, Taiwan in 10-day units, based on the hourly data from 1996 to 2005 (from Lin and Matzarakis 2008)

Figure 1.1.5 Map of the physiologically equivalent temperature (PET) during day time in Freiburg, Germany (from Matzarakis et al. 2008)

Figure 1.1.6 Thermal bioclimatic conditions on the redesigned Place of the Old Synagogue as calculated by ENVI-met for the third day of a hot and dry period (from Fröhlich and Matzarakis 2013)

Figure 3.4.1 The thermal zones of the Earth according to the duration of hot, moderate and cold periods (from Köppen 1884, translated in 2011)

Figure 3.9.1 Connection between the evaluation of thermal environment and community environment design

Figure 4.1.1 Location of 12 Chinese cites (Elevation data from China Geospatial Data Cloud)

Figure 5.2.1 The example of the HTC conditions in one climate type (sample city)

Figure 5.3.1 The unified residential district without community environment design in the 1st round simulations

Figure 6.1.1 Location of each city in the map of Köppen–Geiger classification (KGC: 1976─2000) (modified after Rubel and Kottek 2010)

Figure 6.1.2 Monthly frequencies of different PET value classes at 14 LST in 12 cities in 2000─2012 (Sanya: 2000─2008)

Figure 6.1.3 Monthly frequencies of different T_a value classes at 14 LST in 12 cities in 2000─2012 (Sanya: 2000─2008)

Figure 6.1.4 Monthly frequencies of different T_{mrt} value classes at 14 LST in 12 cities in 2000─2012 (Sanya: 2000─2008)

Figure 6.1.5 Monthly frequencies of different *VP* value classes at 14 LST in 12 cities in 2000─2012 (Sanya: 2000─2008)

Figure 6.1.6 Monthly frequencies of different *RH* value classes at 14 LST in 12 cities in 2000─2012 (Sanya: 2000─2008)

Figure 6.1.7 Wind roses of 12 cities based on the data at 8 points in time in 2000─2012 (Sanya: 2000─2008)

Figure 6.1.8 Monthly frequencies of different *v* value classes at 8 points in time in 12 cities in 2000─2012 (Sanya: 2000─2008)

Figure 6.2.1 The quantification of HTC conditions in 11 climate types in KGC in China (**PET_a**: **annual** frequencies of **PET**; **PET_h**: frequencies of **PET** in the **hottest** month; **PET_c**: frequencies of **PET** in the **coldest** month; **VP_a**: **annual** frequencies of ***VP***; **VP_w**: frequencies of ***VP*** in the **wettest** month; **VP_d**: frequencies of ***VP*** in the **driest** month)

Figure 6.3.1 The process of the evaluation on the human thermal comfort for community environment design

Figure 6.3.2 Hourly average values of T_a and *RH* in one day in the hottest month

Figure 6.3.3 The residential district with design elements in Yinchuan (BWk) (example)

Figure 7.1.1 The assumption of electricity consumption groups in the 12 months of 1 year in Hang Zhou (from Ouyang et al.2009)

Figure A1.1 Beanplots and boxplots of T_a, T_{mrt} and PET at 8 points in time in Sanya (Aw), respectively

Figure A1.2 Beanplots and boxplots of T_a, T_{mrt} and PET at 8 points in time in Qionghai (Am), respectively

Figure A1.3 Beanplots and boxplots of T_a, T_{mrt} and PET at 8 points in time in Shenzhen (Cwa), respectively

Figure A1.4 Beanplots and boxplots of T_a, T_{mrt} and PET at 8 points in time in Kunming (Cwa), respectively

Figure A1.5 Beanplots and boxplots of T_a, T_{mrt} and PET at 8 points in time in Lhasa (Dwa), respectively

Figure A1.6 Beanplots and boxplots of T_a, T_{mrt} and PET at 8 points in time in Shanghai (Cfa), respectively

Figure A1.7 Beanplots and boxplots of T_a, T_{mrt} and PET at 8 points in time in Yuncheng (BSk), respectively

Figure A1.8 Beanplots and boxplots of T_a, T_{mrt} and PET at 8 points in time in Yinchuan (BWk), respectively

Figure A1.9 Beanplots and boxplots of T_a, T_{mrt} and PET at 8 points in time in Dalian (Dwa), respectively

Figure A1.10 Beanplots and boxplots of T_a, T_{mrt} and PET at 8 points in time in Beijing (Dwa), respectively

Figure A1.11 Beanplots and boxplots of T_a, T_{mrt} and PET at 8 points in time in Hohhot (Dwb), respectively

Figure A1.12 Beanplots and boxplots of T_a, T_{mrt} and PET at 8 points in time in Urumqi (Dfb), respectively

Figure A2.1 Community environment design, based on PET distribution at 14 LST in the 1st simulation in Sanya (Aw)

Figure A2.2 Community environment design, based on PET distribution at 15 LST in the 1st simulation in Qionghai (Am)

Figure A2.3 Community environment design, based on PET distribution at 15 LST in the 1st simulation in Shenzhen (Cwa)

Figure A2.4 Community environment design, based on PET distribution at 16 LST in the 1st simulation in Kunming (Cwb)

Figure A2.5 Community environment design, based on PET distribution at 14 LST in the 1st simulation in Shanghai (Cfa)

Figure A2.6 Community environment design, based on PET distribution at 14 LST in the 1st simulation in Beijing (Dwa)

Figure A2.7 Community environment design, based on PET distribution at 14 LST in the 1st simulation in Dalian (Dwa)

Figure A2.8 Community environment design, based on PET distribution at 15 LST in the 1st simulation in Hohhot (Dwb)

Figure A2.9 Community environment design, based on PET distribution at 17 LST in the 1st simulation in Lhasa (Dwc)

Figure A2.10 Community environment design, based on PET distribution at 16 LST in the 1st simulation in Urumqi (Dfb)

Figure A2.11 Community environment design, based on PET distribution at 15 LST in the 1st simulation in Yuncheng (BSk)

Figure A2.12 Community environment design, based on PET distribution at 15 LST in the 1st simulation in Yinchuan (BWk)

Figure A3.1 Distribution of SVF in the 1st round simulation (it is the same in 12 scenarios without design elements)

Figure A4.1 Distribution of *v* at 14 LST in the 1st simulation in Sanya (Aw)

Figure A4.2 Distribution of *v* at 15 LST in the 1st simulation in Qionghai (Am)

Figure A4.3 Distribution of *v* at 15 LST in the 1st simulation in Shenzhen (Cwa)

Figure A4.4 Distribution of *v* at 16 LST in the 1st simulation in Kunming (Cwb)

Figure A4.5 Distribution of *v* at 14 LST in the 1st simulation in Shanghai (Cfa)

Figure A4.6 Distribution of *v* at 14 LST in the 1st simulation in Beijing (Dwa)

Figure A4.7 Distribution of *v* at 14 LST in the 1st simulation in Dalian (Dwa)

Figure A4.8 Distribution of *v* at 15 LST in the 1st simulation in Hohhot (Dwb)

Figure A4.9 Distribution of *v* at 17 LST in the 1st simulation in Lhasa (Dwc)

Figure A4.10 Distribution of *v* at 16 LST in the 1st simulation in Urumqi (Dfb)

Figure A4.11 Distribution of *v* at 15 LST in the 1st simulation in Yuncheng (BSk)

Figure A4.12 Distribution of *v* at 15 LST in the 1st simulation in Yinchuan (BWk)

Figure A5.1 Difference at 14 LST between twice simulations in PET in Sanya (Aw)

Figure A5.2 Difference at 15 LST between twice simulations in PET in Qionghai (Am)

Figure A5.3 Difference at 15 LST between twice simulations in PET in Shenzhen (Cwa)

Figure A5.4 Difference at 16 LST between twice simulations in PET in Kunming (Cwb)
Figure A5.5 Difference at 14 LST between twice simulations in PET in Shanghai (Cfa)
Figure A5.6 Difference at 14 LST between twice simulations in PET in Beijing (Dwa)
Figure A5.7 Difference at 14 LST between twice simulations in PET in Dalian (Dwa)
Figure A5.8 Difference at 15 LST between twice simulations in PET in Hohhot (Dwb)
Figure A5.9 Difference at 17 LST between twice simulations in PET in Lhasa (Dwc)
Figure A5.10 Difference at 16 LST between twice simulations in PET in Urumqi (Dfb)
Figure A5.11 Difference at 15 LST between twice simulations in PET in Yuncheng (BSk)
Figure A5.12 Difference at 15 LST between twice simulations in PET in Yinchuan (BWk)
Figure A6.1 Difference at 14 LST between twice simulations in SVF in Sanya (Aw)
Figure A6.2 Difference at 15 LST between twice simulations in SVF in Qionghai (Am)
Figure A6.3 Difference at 15 LST between twice simulations in SVF in Shenzhen (Cwa)
Figure A6.4 Difference at 16 LST between twice simulations in SVF in Kunming (Cwb)
Figure A6.5 Difference at 14 LST between twice simulations in SVF in Shanghai (Cfa)
Figure A6.6 Difference at 14 LST between twice simulations in SVF in Beijing (Dwa)
Figure A6.7 Difference at 14 LST between twice simulations in SVF in Dalian (Dwa)
Figure A6.8 Difference at 15 LST between twice simulations in SVF in Hohhot (Dwb)
Figure A6.9 Difference at 17 LST between twice simulations in SVF in Lhasa (Dwc)
Figure A6.10 Difference at 16 LST between twice simulations in SVF in Urumqi (Dfb)
Figure A6.11 Difference at 15 LST between twice simulations in SVF in Yuncheng (BSk)
Figure A6.12 Difference at 15 LST between twice simulations in SVF in Yinchuan (BWk)
Figure A7.1 Difference at 14 LST between twice simulations in *v* in Sanya (Aw)
Figure A7.2 Difference at 15 LST between twice simulations in *v* in Qionghai (Am)
Figure A7.3 Difference at 15 LST between twice simulations in *v* in Shenzhen (Cwa)
Figure A7.4 Difference at 16 LST between twice simulations in *v* in Kunming (Cwb)
Figure A7.5 Difference at 14 LST between twice simulations in *v* in Shanghai (Cfa)
Figure A7.6 Difference at 14 LST between twice simulations in *v* in Beijing (Dwa)
Figure A7.7 Difference at 14 LST between twice simulations in *v* in Dalian (Dwa)
Figure A7.8 Difference at 15 LST between twice simulations in *v* in Hohhot (Dwb)
Figure A7.9 Difference at 17 LST between twice simulations in *v* in Lhasa (Dwc)
Figure A7.10 Difference at 16 LST between twice simulations in *v* in Urumqi (Dfb)
Figure A7.11 Difference at 15 LST between twice simulations in *v* in Yuncheng (BSk)
Figure A7.12 Difference at 15 LST between twice simulations in *v* in Yinchuan (BWk)

List of Tables

Table 1.1.1 Structure of current study, based on the human-biometeorological data

Table 3.2.1 Thermal sensitivity and Grades of physiological stress based on PET

Table 3.2.2 Classes of three applied human thermal indices, respectively

Table 3.3.1 The significant meaning of HTC information in diverse aspects in urban development

Table 3.4.1 Climate types and subtypes defined by the Köppen-Geiger climate classification updated (KGC) (modified after Kottek et al. 2006)

Table 3.4.2 Climate types and subtypes defined by the Köppen climate classification (KCC) (Köppen 1936, from Belda et al. 2014)

Table 3.4.3 Climate types and subtypes defined by the updated Köppen-Geiger climate classification (KGC_{AU}) (modified from Peel et al. 2007)

Table 3.4.4 Climate types and subtypes defined by Köppen-Trewartha climate classification (KTC) (modified from Belda et al. 2014)

Table 3.4.5 Comparison of each version in five aspects of difference

Table 3.7.1 Concentrated aspects of 5 simulation models/approaches in urban climate

Table 3.9.1 Overview of state of the art in current study

Table 4.1.1 Basic information of 12 Chinese cities

Table 5.1.1 PET value classes and HTC conditions (modified after Matzarakis and Mayer 1996)

Table 5.3.1 Typical tree in each city and the input code of the tree, the hedge and grass, respectively

Table 5.3.2 Adding strength of each design element for the specific areas in each city

Table 5.3.3 The meaning of each value class for the difference in PET (the same for 12 scenarios)

Table 6.1.1 Summarised information from beanplots and boxplots of 12 cities

Table 6.1.2 Days per year with the heat stress (PET > 35 ℃), the cold stress^{+} (PET < 0 ℃) and acceptable conditions (PET in 13─29 °C) in the 12 cities at 14 LST, respectively

Table 6.1.3 Days per year of each *VP* value class in 12 cities at 14 LST in 2000─2012 (Sanya: 2000─2008)

Table 6.1.4 Days per year of each *RH* value class in 12 cities at 14 LST in 2000─2012 (Sanya: 2000─2008)

Table 6.3.1 The hottest month and the wettest month in each city

Table 6.3.2 Basic input settings of twice round simulations for 12 scenarios, based on the long-term data in the hottest month in each city

Table 6.3.3 Partial estimates of 10 parameters on PET values in 12 simulations, based on multiple linier regression function in R language

Table 6.3.4 The point in time with the most frequently heat stress in each scenario

Table 7.1.1 Comparison between the mean monthly T_a of 2013 in 7 Chinese cities and the corresponding value class in monthly frequencies of T_a in ***Fig. 6.1.3***

Table 7.1.2 Comparison between of the range on T_a in the Design Standard for Civil Buildings and the range on T_a ***Fig. 6.1.3***

Table 7.1.3 Popular period for tourism in the 12 Chinese cities according to the travelling guidelines

Table 7.1.4 The recommended period with emphasis for heat & cold stress in each city

Table 7.1.5 Percentage of heating days in each month in 6 Chinese cities in northern China

Table 7.3.1 Group and sub-group for the analysis of the simulated HTC conditions in each district

Table 7.3.2 Three kinds of emerged heat stress in 12 scenarios

Table 7.3.3 Three kinds of basic conditions in 12 scenarios

Table 7.3.4 Three kinds of shading areas in 12 scenarios

List of Abbreviations

2D	2-dimensional
3D	3-dimensional
AH	Air humidity
BFA	Boao Forum for Asia
CET	Central European time
CFD	Computational Fluid Dynamics
CTIS	Climate Tourism Information Scheme
Fig.	Figure
GIS	Geographic Information System
HTC	Human thermal comfort
KCC	Köppen climate classification
KGC	Köppen-Geiger climate classification updated
KGC_{AU}	Updated Köppen-Geiger climate classification
KTC	Köppen-Trewartha climate classification
LCZ	Local climate zone
LST	Local Standard Time
NOAA	National Oceanic and Atmospheric Administration
NYC	New York City
SOLWEIG	Solar Longwave Environmental Irradiance Geometry model
UCMap	Urban Climate Maps
UHI	Urban heat island effects
Urban-PDM	Urban planning, urban design, and urban management
BJB	The 1st simulation of Beijing (Dwa) just with buildings
BJE	The 2nd simulation of Beijing (Dwa) added with design elements
DLB	The 1st simulation of Dalian (Dwa) just with buildings
DLE	The 2nd simulation of Dalian (Dwa) added with design elements
HHB	The 1st simulation of Hohhot (Dwb) just with buildings
HHE	The 2nd simulation of Hohhot (Dwb) added with design elements
KMB	The 1st simulation of Kunming (Cwb) just with buildings
KME	The 2nd simulation of Kunming (Cwb) added with design elements
LSB	The 1st simulation of Lhasa (Dwc) just with buildings
LSE	The 2nd simulation of Lhasa (Dwc) added with design elements
QHB	The 1st simulation of Qionghai (Am) just with buildings
QHE	The 2nd simulation of Qionghai (Am) added with design elements
SYB	The 1st simulation of Sanya (Aw) just with buildings
SYE	The 2nd simulation of Sanya (Aw) added with design elements
SHB	The 1st simulation of Shanghai (Cfa) just with buildings
SHE	The 2nd simulation of Shanghai (Cfa) added with design elements
SZB	The 1st simulation of Shenzhen (Cwa) just with buildings

SZE	The 2nd simulation of Shenzhen (Cwa) added with design elements
URB	The 1st simulation of Urumqi (Dfb) just with buildings
URE	The 2nd simulation of Urumqi (Dfb) added with design elements
YCB	The 1st simulation of Yuncheng (BSk) just with buildings
YCE	The 2nd simulation of Yuncheng (BSk) added with design elements
YCnB	The 1st simulation of Yinchuan (BWk) just with buildings
YCnE	The 2nd simulation of Yinchuan (BWk) added with design elements

x	x-axis in horizon
y	y-axis in horizon
z	z-axis in vertical

List of Symbols

ATM	Atmospheric pressure	hPa
DWPT	Dew point	℃
K_{di}	Direct short wave radiation	W/m^2
K_{fs}	Diffuse short wave radiation	W/m^2
K_{rf}	Reflect short wave radiation	W/m^2
LAD	Leaf area density	
L_{en}	Long wave radiation from environment	W/m^2
PET	Physiologically equivalent temperature	℃
PMV	Predicted mean vote	
PPD	Predicted percentage of dissatisfied	
PT	Perceived temperature	℃
RAD	Root area density	
RH	Relative humidity	%
RR	Precipitation	mm
SH	Specific humidity	g/kg
SVF	Sky view factor	
T_a	Air temperature	℃
T_{mrt}	Mean radiant temperature	℃
T_s	Surface temperature	℃
UTCI	Universal thermal climate index	℃
UV	Ultraviolet radiation	W/m^2
v	Wind velocity	m/s
VP	Vapour pressure	hPa
WD	Wind direction	
*	There are remarks of the contents in ***Tables***	

Units

clo	Unit of clothing insulation
℃	Celsius degree
K	Kelvin
hPa	Hectopascal
h	Hour
min	Minute
s	Second
mm	Millimeter
m	Meter
m^2	Square meter
g	Gram
kg	Kilogram
W	Watt